

**METHODS AND APPLICATIONS FOR FAST-SCAN CYCLIC VOLTAMMETRIC
DETECTION OF *IN VIVO* CATECHOLAMINE DYNAMICS**

Elizabeth Showalter Bucher

A dissertation submitted to the faculty of the University of North Carolina at Chapel Hill in
partial fulfillment of the requirements for the degree of Doctor of Philosophy in the
Department of Chemistry.

Chapel Hill
2014

Approved by:

Mark Wightman

Regina Carelli

Royce Murray

Paul Manis

Matthew Lockett

©2014
Elizabeth Showalter Bucher
ALL RIGHTS RESERVED

ABSTRACT

Elizabeth Showalter Bucher: Methods and Applications for Fast-Scan Cyclic Voltammetric
Detection of In Vivo Catecholamine Dynamics
(Under the direction of R. Mark Wightman)

Fast-scan cyclic voltammetry (FSCV) at carbon-fiber microelectrodes provides the spatial, temporal and chemical resolution required to study rapid catecholamine dynamics in the brain. It is most well-known for its use in dopamine studies, where it has contributed much to our knowledge regarding the presynaptic regulation of dopamine as well as its role reward learning and addiction. Only recently has FSCV been applied to the detection of norepinephrine, the other major catecholamine neurotransmitter in the central nervous system. This is largely due to issues of selectivity; the electrochemistry of dopamine and norepinephrine is indistinguishable with FSCV. For dopamine selectivity is not as much of an issue as there are large regions of the brain innervated by dopamine neurons that lack major noradrenergic input. For norepinephrine, however, there are only a few noradrenergic terminal regions that receive little dopamine innervation and the small size of these regions (typically $\sim 0.5 \text{ mm}^3$) make them difficult, but not impossible, to target.

Five years ago, it was demonstrated through electrochemical, chemical, anatomical and pharmacological assays that norepinephrine could be monitored selectively with FSCV in ventral subregion of the bed nucleus of the stria terminalis (vBNST), a limbic structure that integrates cognitive and sensory information to initiate the physiological and behavioral responses to stress, including glucocorticoid secretion via the HPA axis. Norepinephrine signaling within the BNST is thought to potentiate these processes, and its dysregulation is widely implicated in anxiety-related conditions such as post-traumatic stress disorder (PTSD). Initial recordings within the vBNST have revealed that norepinephrine can release

can be evoked by electrical stimulation of the dorsal and ventral noradrenergic axon pathways, that it is regulated by the norepinephrine autoreceptor and transporter, and have confirmed that, like dopamine, it is modulated by stimulation frequency and pulse number. Additional work has established that BNST norepinephrine dynamics can be recorded in awake, freely-moving rats and that it oppositely responds to administration of aversive and appetitive tastants.

The studies presented in this volume are an extension of this preliminary work and explore several facets of norepinephrine signaling within the BNST with FSCV in anesthetized and behaving animals. Chapter 2 investigates the neural pathways by which electrical stimulation evokes norepinephrine release within the BNST. Chapters 3 and 4 compares the responses of norepinephrine in the BNST and dopamine in the NAc, a related limbic structure, during an aversive sensory stimulation and during reward learning and extinction. Chapter 5 employs combined iontophoresis and FSCV to probe the local mechanisms by which BNST norepinephrine regulates hemodynamic function during neuronal activity. Finally, Chapter 6 and 7 describe and assess new experimental tools for FSCV data collection and analysis. Together the results of these studies demonstrate the utility of FSCV in the detection of rapid norepinephrine signaling *in vivo* and provide new information regarding the dual role of BNST norepinephrine as a neuro- and vaso-modulator.

ACKNOWLEDGEMENTS

There are many individuals I would like to acknowledge for their direct and indirect contributions to this work. First and foremost, I would like to thank my advisor Dr. Mark Wightman for his support and mentorship over the last five years. I greatly appreciate the many opportunities you have presented me to grow as a scientist in a truly exciting field of research. I would also like to thank my undergraduate advisors Dr. Don Jameson and Dr. Stephanie Wetzel, who together inspired me to pursue a degree in Analytical Chemistry as a Tarheel.

I have had the pleasure of working with many talented collaborators during my time at UNC. Meg Fox and Justin Johnson conducted the chromatography and behavioral experiments in Chapter 2. The work presented in Chapters 3 and 4 were led by Dr. Jinwoo Park. Kristy Fontillas, Dr. Nina Owesson-White, Jenny Ariansen and Dr. Gina Carelli also provided data and intellectual contributions to the work of Chapter 4. Meg Fox, Laura Kim, Doug Kirkpatrick, and Nathan Rodeberg performed several of the experiments described in Chapter 5, and Anna Belle provided guidance during the iontophoresis experiments of this study. Chapter 6 was the culmination of many efforts, including those of Ken Brooks, Matthew Verber, Dr. Richard Keithley, Dr. Nina Owesson-White, Dr. Susan Carroll, Dr. Pavel Takmakov, and Collin McKinney. The preliminary results described in Chapter 7 were the efforts of a number of dedicated undergraduate students including Laura Kim, Isaac Studebaker, Preethi Gowrishankar, Marc Gonzalez, and Nathaniel Swofford.

On a more general note, I would like to thank several individuals from the Wightman group who have provided friendship and support over the years. To Richard and Pasha,

thank you both for showing me the ropes when I was a young Wightmanite. To Jinwoo, thank you for recruiting me onto 'Team Norepinephrine,' teaching me how to interpret 'bloody' color plots, and for the late night ghost stories. To Meg, thank you for the many long norepinephrine discussions and for always lending a helping hand, even when you didn't have one to offer. To Laura, thank you for an awesome four years and for dealing with all us weird grad students. I feel extremely lucky to have had you on my team. To Nathan and Justin, thanks for slaving away on Chapters 2 and 5. I eagerly await the first publication in the Johnson-Rodeberg series.

Finally, I would like to thank several people outside of academia who made this work possible. To my parents and grandparents, thank you for all of the emotional (and financial) support over the years, for always believing in me, and for fostering my interest in science throughout my childhood. (Mom, I think our trip to the water treatment plant must be the defining moment in my decision to pursue grad school.) To Laurie, thank you for the many motivational messages. They brought a smile to my face at times when the work seemed to have no end. And to Kevin, thank you for standing by my side throughout this process. I don't know how I would have made it without you.

TABLE OF CONTENTS

LIST OF TABLES.....	xiv
LIST OF FIGURES.....	xv
LIST OF ABBREVIATIONS AND SYMBOLS.....	xviii
CHAPTER 1: ELECTROCHEMICAL ANALYSIS OF NEUROTRANSMITTERS.....	1
Introduction.....	1
Detection of neurotransmitters with electrochemical techniques	2
Constant potential amperometry	3
Fast-scan cyclic voltammetry	4
Electrochemical detection of new neuromodulators	6
Enzyme-modified electrodes	6
Waveform modification strategies	7
Microsensor developments	9
Carbon-nanotube based microelectrodes.....	10
Fused-silica carbon-fiber microelectrodes	11
Microelectrode arrays.....	12
Novel applications.....	14
Challenging the conventions of neurochemical measurements.....	14
Basal level measurements with FSCV	14
‘Ultrafast’ microdialysis	16
Multimodal measurements.....	17
Neurotransmitter detection in non-rodent models.....	20

Drosophila (fruit flies)	21
Non-human primates	22
Humans	25
Conclusions	26
References	28
CHAPTER 2: ELECTRICAL STIMULATION OF THE DORSAL NORADRENERGIC BUNDLE EVOKES NOREPINEPHRINE OVERFLOW IN THE BED NUCLEUS OF THE STRIA TERMINALIS THROUGH A NON-COERULEAN PATHWAY	
Introduction.....	39
Experimental.....	41
Drugs and reagents.....	41
Animals	41
Surgeries	41
Voltammetric measurements.....	42
DSP-4	43
Ibotenic acid infusion.....	43
Histology	43
Tissue content analysis	44
Behavioral assessment	45
Data analysis	46
Results	46
Measurement of norepinephrine in target regions	46
Effects of DSP-4 on catecholamine tissue content in the vBNST and AV	49
Electrically-stimulated norepinephrine release in the AV after DSP-4	49
Electrically-stimulated norepinephrine release in the vBNST after DSP-4	52

Electrically-stimulated norepinephrine release after ibotenic acid into the DNB	54
Behavioral responses elicited by electrical stimulation at the depth of the DNB	55
Discussion	58
LC lesioning attenuates norepinephrine release in the AV but not in the vBNST	59
Midbrain cell body activation supports norepinephrine release in the vBNST but not in the AV	61
Conclusions	63
References	65
CHAPTER 3: NOREPINEPHRINE AND DOPAMINE TRANSMISSION IN TWO LIMBIC REGIONS DIFFERENTIALLY RESPOND TO ACUTE NOXIOUS STIMULATION	75
Introduction.....	75
Experimental.....	77
Animals	77
Surgery	77
Noxious stimulation	78
Voltammetric procedures	78
Histology	79
Chemical and drugs	79
Data analysis	79
Results	80
Rapid extracellular dopamine changes in the NAc shell elicited by tail pinch	80
Effects of dopamine autoreceptor and transporter inhibition on tail pinch induced responses in the NAc shell	84
Rapid extracellular norepinephrine changes in the vBNST elicited by tail pinch	86

Effects of norepinephrine autoreceptor and transporter inhibition on tail-pinch induced responses in the vBNST	89
Discussion	91
Tail-pinch induced dopamine transmission in the NAc shell	92
Tail-pinch induced norepinephrine transmission in the vBNST	94
Conclusions	96
References.....	97
 CHAPTER 4: OPPOSING CATECHOLAMINE CHANGES IN THE BED NUCLEUS OF THE STRIA TERMINALIS DURING INTRACRANIAL SELF-STIMULATION AND ITS EXTINCTION	
Introduction.....	103
Experimental.....	104
Animals	104
Surgery	105
Intracranial self-stimulation training	105
Fast-scan cyclic voltammetry	106
Histology	106
Chemicals and drugs	106
Data analysis	108
Results	110
Cue-evoked dopamine concentration changes in the dIBNST during ICSS	110
Pharmacological effects on dopamine in the dIBNST	112
Norepinephrine responses during maintenance-delay trials	115
Pharmacological effects on norepinephrine in the vBNST	115
Extracellular changes of dopamine and norepinephrine during extinction of ICSS	115
Discussion	110

Different roles for each catecholamine in subregions of the BNST during ICSS	122
Opposing catecholamine changes during extinction of ICSS	125
Conclusions	127
References	128
CHAPTER 5: MEDULLARY NOREPINEPHRINE NEURONS MODULATE LOCAL OXYGEN CONCENTRATIONS IN THE BED NUCLEUS OF THE STRIA TERMINALIS	
	134
Introduction.....	134
Experimental.....	136
Chemical and drugs	136
Electrode fabrication	136
Fast-scan cyclic voltammetry	136
Calibrations	137
Voltammetric data presentation and analysis	137
Surgery	138
<i>In vitro</i> procedure	139
Pharmacological investigations	139
Signal verification	141
Histology	141
Locus coeruleus lesioning with DSP-4	141
Immunohistochemistry	142
Cardiorespiratory measurements	143
Results	143
Immunohistochemistry of recording environment	143
O ₂ response with electrical stimulation	145
Effect of DSP-4 on the electrically-stimulated O ₂ response	151

O ₂ responses with adrenoceptor blockade	151
Local iontophoresis of norepinephrine	156
Local iontophoresis of selective adrenoceptor agonists.....	159
Discussion	162
Conclusions	167
References	169
CHAPTER 6: A FLEXIBLE SOFTWARE PLATFORM FOR FAST-SCAN	
CYCLIC VOLTAMMETRY DATA ACQUISITION AND ANALYSIS	173
Introduction.....	173
Experimental.....	175
Hardware.	175
Software.....	175
HDCV Data Acquisition.....	176
HDCV Data Analysis.....	177
Experimental setup	178
Experimental procedures.	180
Results and discussion	180
Programming techniques.	180
Timing control	181
Active/passive configuration routines.....	181
Setup control structure.....	182
Data storage.....	183
Real-time data analysis and acquisition.	183
Simultaneous detection of neurotransmitter release and single and single unit activity.	185
Two dimensional data filtering.....	188
Analysis of continuous data.....	190

Time bin generation and signal averaging.....	193
Conclusions	196
References	197
CHAPTER 7: EVALUATION OF FUSED-SILICA INSULATED CARBON-FIBER MICROELECTRODES FOR LONGITUDINAL NEUROCHEMICAL STUDIES	200
Introduction.....	200
Experimental.....	202
Chronic electrode construction.....	202
Threading	202
Forming the seal.....	202
Trimming the fiber and adding a connection pin.....	203
Insulating the connection	203
Acute electrode construction.....	203
Electrochemical measurements.....	207
Flow injection analysis	207
<i>In vivo</i> measurements.....	209
Results.....	210
Comparison of acute and chronic type electrode performance	210
Carbon-fiber electrode performance after chronic implantation	214
Discussion.	214
Conclusion.	215
References	216

LIST OF TABLES

Table 2.1: Catecholamine tissue content in the anteroventral thalamus and the ventral bed nucleus of the stria terminalis for untreated and DSP-4 treated animals.....	50
Table 5.1: Average norepinephrine and O ₂ responses to ventral Noradrenergic bundle stimulation	154
Table 7.1: Chronic and acute electrode responses to dopamine with flow Injection analysis	212

LIST OF FIGURES

Figure 2.1: Measurement of norepinephrine in the anteroventral thalamus and the ventral bed nucleus of the stria terminalis	48
Figure 2.2: Effects of DSP-4 on electrically-stimulated norepinephrine release in the anteroventral thalamus	51
Figure 2.3: Effects of DSP-4 on electrically-stimulated norepinephrine release in the ventral bed nucleus of the stria terminalis	53
Figure 2.4: Effects of ibotenic acid infusion into the dorsal noradrenergic bundle on electrically-stimulated norepinephrine release	56
Figure 2.5: Incidence of behavioral responses to dorsal noradrenergic bundle stimulation	57
Figure 3.1: Anatomical mapping of tail pinch induced and electrically evoked dopamine responses in the nucleus accumbens shell	81
Figure 3.2: Dopamine signaling in the nucleus accumbens shell in response to tail pinch	82
Figure 3.3: Dopamine signaling in the nucleus accumbens shell in response to tail pinch after transporter and autoreceptor inhibition	85
Figure 3.4: Anatomical mapping of tail pinch induced and electrically evoked norepinephrine responses in the ventral bed nucleus of the stria terminalis	87
Figure 3.5: Norepinephrine signaling in the ventral bed nucleus of the stria terminalis in response to tail pinch	88
Figure 3.6: Norepinephrine signaling in the ventral bed nucleus of the stria terminalis in response to tail pinch after transporter and autoreceptor inhibition	90
Figure 4.1: Representative histological verification of recording sites in the nucleus accumbens and the bed nucleus of the stria terminalis	107
Figure 4.2: Effects of selective autoreceptor and uptake inhibitors on electrically-evoked catecholamine release and clearance in subregions of the bed nucleus of the stria terminalis	109
Figure 4.3: Dopamine changes in the dorsal lateral bed nucleus of the stria terminalis during maintenance-delay intracranial self-stimulation	111

Figure 4.4: Dopamine increase in the dorsal lateral bed nucleus of the stria terminalis during maintenance-delay intracranial self-stimulation after administration of GBR12909	113
Figure 4.5: Dopamine concentration changes in the dorsal lateral bed nucleus of the stria terminalis and latency to lever-press during maintenance-delay intracranial self-stimulation before and after administration of desipramine	114
Figure 4.6: Norepinephrine changes in the ventral bed nucleus of the stria terminalis during maintenance-delay intracranial self-stimulation	116
Figure 4.7: Average norepinephrine concentrations in the vBNST during phase 2 of intracranial self-stimulation at the 2nd day and the 5th day of training	117
Figure 4.8: Norepinephrine increase in the ventral bed nucleus of the stria terminalis during maintenance-delay intracranial self-stimulation after administration of desipramine	118
Figure 4.9: Norepinephrine concentration change in the ventral bed nucleus of the stria terminalis and latency of the lever-press during maintenance-delay intracranial self-stimulation after administration of GBR 12909.....	120
Figure 4.10: Catecholamine responses in the nucleus accumbens, dorsal lateral bed nucleus of the stria terminalis, and ventral bed nucleus of the stria terminalis during intracranial self-stimulation extinction.....	121
Figure 4.11: Norepinephrine concentration changes during intracranial self-stimulation extinction before and after the administration of the norepinephrine uptake inhibitor DMI	123
Figure 5.1: Confocal laser scanning images of triple-fluorescence labeling in the rat ventral bed nucleus of the stria terminalis	144
Figure 5.2: Simultaneous detection of 250 μ M O ₂ and 8 μ M norepinephrine in an air-impermeable flow injection system	146
Figure 5.3: Variability of the O ₂ response to electrical stimulation of the ventral noradrenergic bundle	147
Figure 5.4: Effect of stimulating and working electrode placements on the recorded O ₂ response	148
Figure 5.5: Characterization of the second O ₂ increase induced by electrical-stimulation of the ventral noradrenergic bundle	150

Figure 5.6: Predominant O ₂ response recorded in the ventral bed nucleus of the stria terminalis with electrical stimulation of the ventral noradrenergic bundle	152
Figure 5.7: The effect of DSP-4 lesioning on dopamine-beta-hydroxylase immunoreactivity	153
Figure 5.8: Cardiorespiratory responses to anesthesia and adrenoceptor antagonists	156
Figure 5.9: Pharmacology of the ventral noradrenergic bundle stimulated O ₂ response recorded in the ventral bed nucleus of the stria terminalis	157
Figure 5.10: O ₂ changes induced by direct delivery of norepinephrine with iontophoresis	158
Figure 5.11: Effect of norepinephrine concentration applied by iontophoresis on the peak time for the second O ₂ event	160
Figure 5.12: O ₂ changes induced by local delivery of adrenoceptor agonists with iontophoresis	161
Figure 5.13: Proposed mechanism underlying the O ₂ responses recorded after electrical stimulation of the ventral noradrenergic bundle	163
Figure 6.1: Block diagram of hardware for combined electrochemical/electrophysiological recordings during behavior	179
Figure 6.2: Results from <i>in vivo</i> recordings with a carbon-fiber electrode implanted in the nucleus accumbens of an anesthetized rat using a waveform designed for simultaneous detection of O ₂ and dopamine.....	184
Figure 6.3: Simultaneous electrochemistry/electrophysiology measurements	187
Figure 6.4: Use of the 2D-FFT filter in HDCV	189
Figure 6.5: Continuous data analysis in HDCV	192
Figure 6.6: Time bin analysis procedure in HDCV	195
Figure 7.1: Schematic of the chronic type microelectrode	204
Figure 7.2: Size comparison between acute and chronic microelectrode types	205
Figure 7.3: Electron micrographs of acute and chronic carbon-fiber microelectrodes	206

Figure 7.4: Example data collected during a flow injection analysis experiment	210
Figure 7.5: Dopamine calibration curves for 150 μm carbon-fiber microelectrodes	211
Figure 7.6: In vivo performance of chronically implanted carbon-fiber microelectrode	213

LIST OF ABBREVIATIONS AND SYMBOLS

*	probability less than 0.05
**	probability less than 0.01
***	probability less than 0.001
[X]	concentration of analyte X
[X] _{max}	maximum concentration of analyte X
°C	degrees Celsius
2D	two-dimensional
4-MC	4-methylcatechol
ABT	1-aminobenotriazole
AC	anterior commissure
aCSF	artificial cerebrospinal fluid
Ag/AgCl	silver/silver chloride
ANOVA	analysis of variance
AP	anterior-posterior
APT	anterior pretectal nucleus
ATP	adenosine triphosphate
AV	anteroventral thalamus
BNST	bed nucleus of the stria terminalis
BOLD	blood oxygen level dependent
CaCl ₂	calcium chloride
CBF	cerebral blood flow
CE	capillary electrophoresis
CNT	carbon nanatube
CO ₂	carbon dioxide

CV	cyclic voltammogram
CYP	cytochrome P450
DA	dopamine
DAQ	data acquisition
DAT	dopamine transporter
DBH	dopamine-beta-hydroxylase
DBS	deep-brain stimulation
DIO	digital input-output
dIBNST	dorsal lateral bed nucleus of the stria terminali
DMI	desipramine
DNB	dorsal noradrenergic bundle
DSP-4	N-(2-chloroethyl)-N-ethyl-2-bromobenzylamine
DV	dorsal-ventral
E _{app}	applied potential
echem	electrochemistry
ephys	electrophysiology
FFT	fast Fourier transform
fMRI	functional magnetic resonance imaging
FR-1	fixed-ratio 1
FSCV	fast-scan cyclic voltammetry
g	grams
GBR	GBR-12909
GFAP	glial fibrillary acidic protein
GnRH	gonadotropin-releasing hormone
H ₂ O ₂	hydrogen peroxide
HDCV	High-Definition Cyclic Voltammetry

HEPES	4-(2-hydroxyethyl)-1-piperazineethanesulfonic acid
HPC	hippocampus
Hz	hertz
i.p.	intraperitoneal injection
I/O	input/output
IBA	ibotenic acid
ICSS	intracranial self-stimulation
IDA	idazoxan
IgG	immunoglobulin
KCl	potassium chloride
kg	kilograms
L	liters
LC	liquid chromatography
LC	locus coeruleus
μ A	microamperes
μ m	micrometer
μ M	micromolar
mA	milliamperes
M-ENK	met-enkephalin
mg	milligrams
MgCl ₂	magnesium chloride
ML	medial-lateral
mL	milliliters
mm	millimeter
mM	millimolar
MPTP	1-methyl-4-phenyl-1,2,3,6-tetrahydropyridine

ms	millisecond
n	number of samples
N ₂	molecular nitrogen
nA	nanoamperes
NAc	nucleus accumbens
NaCl	sodium chloride
NaH ₂ PO ₄	monosodium phosphate
NaHCO ₃	sodium bicarbonate
NaOH	sodium hydroxide
NaSO ₄	sodium sulfate
NE	norepinephrine
NET	norepinephrine transporter
NO	nitric oxide
NOS	nitric oxide synthase
NST	nucleus of the solitary tract
O ₂	molecular oxygen
P	probability
PAG	periaqueductal gray
PCR	principal component regression
PROP	propranolol
r ²	coefficient of determination
Rac	raclopride
Rt	reticular formation
σ	standard deviation
s	second
SC	superior colliculus

S.E.M.	standard error of the mean
SN	substantia nigra
SNR	substantia nigra pars reticulate
STL	solanum tuberosum agglutinin
t	time
TRIS	tris(hydroxymethyl)aminomethane
TTL	transistor-transistor logic
TZ	terazosin
UEI	universal electrochemical instrument
UNC	University of North Carolina
V	volts
vBNST	ventral bed nucleus of the stria terminalis
VI	virtual instrument
VNB	ventral noradrenergic bundle
VTA	ventral tegmental area
VTO	variable time out

CHAPTER 1: ELECTROCHEMICAL ANALYSIS OF NEUROTRANSMITTERS

Introduction

In the brain neuronal communication primarily occurs through the exocytotic release of neurotransmitters into synaptic junctions and the surrounding extracellular fluid. These chemical signaling molecules modulate post-synaptic cell activity in various ways dependent on the identity of the neurotransmitter and the receptors that are recruited. The downstream effects of neurotransmission underlie a wide range of physiological and behavioral processes and its dysregulation can lead to a number of debilitating disorders as broad as Parkinson's disease, Alzheimer's disease, depression and drug addiction (Weinshenker, 2008; Jacobsen *et al.*, 2012; Janezic *et al.*, 2013; Koob, 2013).

Before the 1970's, there was no available technique with the requisite sensitivity other than radioimmunoassays to detect the small chemical concentrations produced by neurotransmission (Adams, 1976). During the latter part of the 1960's, however, Ralph Adams and his colleagues had studied the electrochemistry of a number of easily oxidizable biogenic amines, and quickly realized the potential applications of their knowledge to the field of neurochemistry. Shortly thereafter, Adams implanted a carbon-paste electrode into the brain of an anesthetized rat and, quite boldly, demonstrated that traditional voltammetric techniques could be applied with success to biological tissues (Kissinger *et al.*, 1973). While the signal recorded was likely ascorbic acid and not dopamine as had been hoped, this work importantly suggested that neurotransmitters could escape the confined space of the synaptic cleft and diffuse to the electrode surface—without which *in vivo* electrochemical measurements would be impossible.

The early days of *in vivo* electrochemistry were fraught with issues of selectivity, mainly due to interference from catecholamine metabolites and ascorbic acid (Justice, 1987). However, over the last four decades numerous methods have been developed to increase not only the selectivity of these measurements, but to apply them at a subsecond time scale. As Adams envisioned, *in vivo* electrochemistry now encompasses a matured set of techniques employed by countless neuroscience and psychology laboratories to study the release, uptake and signaling dynamics of rapid neurotransmission. Electrochemical techniques have found use in a wide variety of applications, from resolving single exocytotic events from single cells to monitoring neurochemical fluctuations in awake, behaving animals.

It is impossible to cover the entire scope of electrochemical detection of neurotransmitters in a single review. This review, therefore, has two goals. First, we provide a general understanding of common electrochemical techniques used for neurotransmitter detection. Second we highlight several new applications defining the next generation of *in vivo* electrochemical research.

Detection of Neurotransmitters with Electrochemical Techniques

Several different electrochemical techniques have been applied to monitor neurotransmitter fluctuations in living tissues, including amperometry, various potential pulse methods, and cyclic voltammetry (Justice, 1987; Kawagoe *et al.*, 1992; Robinson *et al.*, 2008). In general, these methods detect target neurotransmitters through their oxidation or reduction at a solid electrode. The currents generated provide a quantitative measure of dynamic chemical fluctuations that can be correlated to pharmacology, behavior and disease pathology. Target molecules are limited to those that are electroactive within the potential window of the interstitial fluid, which include the biogenic amines (dopamine,

norepinephrine and serotonin), their metabolites, and ascorbic acid. Here we briefly overview the most common techniques in current use.

Constant-potential amperometry

In constant-potential amperometry, often referred to simply as amperometry, the electrode is held at a potential sufficient to oxidize or reduce an analyte of interest so that the currents generated are mass transport limited. As the potential is constant throughout the duration of the experiment, no charging currents are generated and direct integration of the currents detected provides the amount of analyte electrolyzed according to Faraday's law ($Q = nNF$). Moreover, the time resolution of the experiments is only limited by the data acquisition rate. However, these measurements provide very little chemical information as any molecule that is electroactive at a given potential will be detected and should only be applied to samples of known content. For example, *ex situ* analyses typically preprocess samples through separation methods, such as liquid chromatography. Indeed, liquid chromatography with amperometric detection was one of the first viable methods for brain tissue content analysis (Adams, 1976) and is still in common use today.

Cell cultures are typically relatively homogenous in their chemical composition and their contents can be predetermined by other analyses, making them suitable for amperometric analysis (Mosharov & Sulzer, 2005). Intracellular communication occurs through exocytosis, by which a neurotransmitter-filled vesicle docks and fuses to the cell membrane and releases its contents into the extracellular space. The high temporal resolution of amperometry has proven highly useful for the study of exocytosis of monoamines from single cells and cell cultures. In such experiments, a small beveled disk electrode is placed near the cell membrane. Chemical stimulation of the cell is used to evoke neurochemical release. Single exocytosis events are resolved as millisecond-wide spikes in oxidative current. While integration of the current response gives the moles of

neurotransmitters release, a number of other quantitative and qualitative information can be determined from the shape of the spike. The rise time (10% - 90%) of the peak correlates to the opening kinetics of fusion pore between the cell membrane and the neurotransmitter-filled vesicle. The half-width of the spike indicates the duration of the release event. Of recent discovery, the presence of post spike plateau currents is indicative of partial-fusion, or “kiss and run,” events (Mellander *et al.*, 2012). Amperometric measurements have been applied to a variety of cell types including adrenal chromaffin cells (Petrovic *et al.*, 2010), pheochromocytoma (PC12) cells (Westerink & Ewing, 2008), mast cells (Manning *et al.*, 2012), and neurons (Pothos, 2002; Borisovska *et al.*, 2013) to probe the pharmacology and biophysics of vesicular release events.

Fast-scan cyclic voltammetry

In fast-scan cyclic voltammetry (FSCV), a triangular waveform is applied to a microelectrode at a high scan rate (>100 V/s) to rapidly oxidize and reduce electroactive species at the electrode surface. Various performance aspects (i.e. sensitivity, selectivity, and temporal resolution) can be optimized by altering the potential limits, scan-rate and application frequency of the waveform. For instance, a commonly used dopamine waveform scans from -0.4 V to $+1.3$ V at 400 V/s, repeated at 100 ms intervals. The rapid scan generates a large background current that arises mainly from the charging of the electrical double layer and is proportional to the capacitance of the electrode. Thus, to resolve the smaller faradaic currents the background current is subtracted, usually by digital means. In the resulting cyclic voltammogram, the peak potentials provide a chemical signature to identify the species detected. Peak currents are usually converted into concentrations using calibration factors obtained from standards of known concentration.

Given its chemical selectivity, FSCV has been widely employed *in vitro* and *in vivo* to detect a number of electroactive species including but not limited to dopamine,

norepinephrine, serotonin, O₂, and pH changes (Bunin *et al.*, 1998; Venton *et al.*, 2003; Park *et al.*, 2011). Many FSCV studies use electrical stimulation to elicit monoamine release in terminal regions. The rising phase of these responses is determined by release (modified by its autoinhibition) and uptake mechanisms, while the falling phase is principally governed by uptake. Both phases are convoluted with diffusion from the site of release to the electrode. Measurement of these parameters therefore can be used to assay the function of these regulatory mechanisms (Wightman *et al.*, 1988; Wightman & Zimmerman, 1990; McElligott *et al.*, 2013).

Of the biogenic amines, dopamine is the most common target of FSCV measurements. Studies in brain slices and anesthetized animals have proven particularly useful in delineating the regulatory mechanisms controlling dopamine release and uptake in subregions of the striatum and how these processes are disturbed in disease states (Bergstrom *et al.*, 2011; Hashemi *et al.*, 2012; Riday *et al.*, 2012; Calipari *et al.*, 2014). A major accomplishment has been the use of voltammetry in freely-moving animals that has contributed much to our understanding of the central dopamine system and how it drives motivated behaviors during reward-based learning (Carelli, 2004; Owesson-White *et al.*, 2008) and drug addiction (Owesson-White *et al.*, 2009; Addy *et al.*, 2010; Ehrich *et al.*, 2014). In contrast, application of FSCV to the detection of norepinephrine and serotonin *in vivo* has only recently been possible due to issues of selectivity and electrode fouling, respectively. Several effective strategies have been identified to overcome these challenges, involving anatomical positioning for norepinephrine and waveform/electrode modifications for serotonin. Subsequent work has successfully investigated the regulation of norepinephrine overflow in the bed nucleus of the stria terminalis (Park *et al.*, 2009; Park *et al.*, 2013) and serotonin overflow in the substantia nigra pars reticulata (Hashemi *et al.*, 2009; Dankoski *et al.*, 2014).

Electrochemical Detection of New Neuromodulators

A number of endeavors have been made to extend the high temporospatial resolution of *in vivo* electrochemical detection to target molecules that are more difficult to electrolyze. These efforts have principally used two approaches. In one approach, the electrode is modified with an enzyme selective for the molecule of interest. Alternatively, the parameters of the applied voltage sweep have been adjusted. These strategies are discussed in more detail below.

Enzyme-modified electrodes

Enzyme-modified electrodes provide the ability to detect a range of non-electroactive species in biological tissue. In such measurements an enzyme with specific activity for an analyte of interest is immobilized to the electrode surface covalently or through film coating. The activity, stability and selectivity of the enzyme in its immobilized form are crucial aspects of sensor performance (Wilson & Johnson, 2008). Analyte detection is accomplished through the formation of an electroactive product, often H_2O_2 formed by an oxidase. For instance the detection of glutamate can be achieved with glutamate oxidase, which converts glutamate into α -ketoglutarate and H_2O_2 (Kiyatkin *et al.*, 2013). Often a secondary enzyme-free electrode is required to account for non-specific currents (Kiyatkin & Lenoir, 2012). As the kinetics of the enzyme can slow the temporal resolution of such measurements, enzyme-based sensors are usually coupled to amperometry. Amperometric enzyme sensors have been developed for many non-electroactive neurotransmitters, including glutamate (Oldenziel & Westerink, 2005; Kiyatkin *et al.*, 2013), acetylcholine (Sarter *et al.*, 2009), its precursor choline (Parikh *et al.*, 2004) and adenosine (Schmitt *et al.*, 2012).

The chemical information provided by FSCV can alleviate many of the selectivity issues experienced with enzyme-based amperometric sensors. In the past, the use of enzyme-based detection schemes with FSCV at carbon-fiber microelectrodes has largely

been limited by the slow electron-transfer kinetics of H_2O_2 . However, Sanford et al. recently demonstrated that over-oxidizing the carbon-fiber surface with an extended +1.4 V anodic scan facilitates the oxidation of H_2O_2 with FSCV (Sanford *et al.*, 2010). As the over-oxidation process occurs near the anodic switching potential with this extended waveform, the oxidation peak for H_2O_2 appears at +1.2 V on the reverse scan. To detect glucose with this waveform, carbon-fiber microelectrodes were coated by electrodeposition of glucose-oxidase in chitosan, a non-toxic polysaccharide (Lugo-Morales *et al.*, 2013). This sensor was shown to have a 13 μM limit of detection for glucose, stable performance over a 4 hr period, and the ability to discriminate against interferents such as dopamine, ascorbic acid and pH. This work establishes the utility of enzyme-based FSCV sensors for the detection of non-electroactive species.

Waveform modification strategies

There are a number of molecules in the brain that are electroactive but are not oxidized by the voltammetric sweep employed for dopamine measurements (-0.4 V to +1.3 V, 400 V/s). Several of these molecules can be detected by modifying the anodic limits of the potential scan to promote electrode-transfer. Adenosine is one such example. Formed from the degradation of ATP, adenosine is a purine signaling molecule that regulates cerebral blood flow, metabolism, and the activity of different neurotransmitters (Cunha, 2001). Detection of adenosine is accomplished by increasing the anodic limits of the traditional dopamine waveform to +1.5 V (Swamy & Venton, 2007b). This generates an initial oxidation peak at the anodic switching potential and a second oxidation peak at +1.0 V on the forward scan. The second oxidation peak arises from sequential oxidation of the initial electroformed product. Both of these oxidation processes are irreversible; hence no reduction peaks are generated. Since the development of this modified waveform, it has been used to monitor adenosine dynamics in preparations as varied as the murine spinal

lamina (Street *et al.*, 2011; Street *et al.*, 2013), brain slices (Pajski & Venton, 2010; 2013), and the striatum of anesthetized rats (Cechova & Venton, 2008). Initial results have found that adenosine release is evoked by mechanical stimulation (Ross *et al.*, 2014) and correlates to local O₂ fluctuations in intact tissue (Cechova & Venton, 2008). More recently, a 'sawhorse' shaped waveform has been developed, which holds at 1.35 V for 1 ms during the anodic scan (Ross & Venton, 2014). The sawhorse waveform provides discrimination between adenosine and two major interferents that oxidize at similar potentials, H₂O₂ and ATP, and may prove useful for *in vivo* experiments. In parallel studies, Dale and coworkers have used an enzyme modified electrode to probe the dynamics of adenosine and its precursors (Schmitt *et al.*, 2012).

Waveform strategies have also been incorporated to target various peptide neurotransmitters. Glanowska et al. detected gonadotropin-releasing hormone (GnRH) release in mouse brain slices (Glanowska *et al.*, 2012) where it plays a major role in fertility (Belchetz *et al.*, 1978) and is also believed to act as a neuromodulator (Chen & Moenter, 2009). GnRH was detectable as it contains the electroactive amino acid tryptophan. Although the oxidation of tryptophan can foul the electrode, stable oxidation currents were obtained for GnRH using a triangular waveform scanning from 0.5 V to 1.45 V at 400 V/s. With this waveform the oxidation peak for GnRH occurs at ~1.25 V, and could be distinguished from tryptophan and another tryptophan-containing peptide, kisspeptin-10. Measurements in brain slices revealed that GnRH release could be chemically evoked in the median eminence and the preoptic area. No signal was detected from mice genetically modified to lack GnRH supporting its detection in wild-type animals.

FSCV has also been applied to the detection of the small opioid peptide, methionine-enkephalin (M-ENK) (Schmidt *et al.*, 2014). M-ENK and other opioid peptides are involved with many physiological and behavioral processes, including reward-processing, drug addiction and pain perception (Bodnar, 2013). The electroactive moiety in M-ENK is

tyrosine, which, similar to tryptophan, can cause electrode fouling. Schmidt et al. demonstrated that M-ENK could be detected reproducibly and selectively with a variant of the sawhorse waveform that varied the scan rate on the anodic sweep. The optimized waveform scanned from -0.2 to +0.6 V at 100 V/s, then to +1.2 V at 400 V/s. This anodic limit was held for 3 ms before scanning back to the -0.2 V holding potential at 100 V/s. The oxidation peak for M-ENK occurs at +1.0 V on this waveform, which exhibited selectivity against other tyrosine-containing peptides. As the oxidation peaks for catecholamines occur at more negative potentials, it was possible to use this waveform to monitor simultaneous norepinephrine and M-ENK release from tissue extracted from the rat adrenal gland.

Microsensor Developments

The need for a miniaturized working electrode compatible with tissue implantation was recognized soon after the advent of *in vivo* electrochemistry (Adams, 1976). Smaller electrodes allow for minimal tissue damage, higher spatial resolution to probe discrete brain regions, and faster sampling rates given their reduced RC properties. Carbon was the intuitive choice for electrode material given its low cost, good electrochemical properties and biological compatibility; however, the conventional carbon-paste electrodes of the 1970's were not amenable to miniaturization (Stamford, 1989). In the late 70's, the field of *in vivo* electrochemistry took a leap forward with the introduction of the carbon-fiber microelectrode by Gonon and coworkers (Ponchon *et al.*, 1979). These electrodes are fabricated by sealing the carbon fiber (5 – 35 μm diameters) in glass and either cutting the protruding fiber to form a cylindrical electrode or treating the seal with epoxy and polishing the tip to form an elliptical surface. Given the ease and reproducibility of their fabrication, carbon-fiber microelectrodes are routinely used in most *in vivo* electrochemical studies today (Huffman & Venton, 2009).

Over the last several decades, there have been a number of efforts to improve the performance of *in vivo* electrochemical sensors through a number of methods. For instance, effort has been spent investigating surface modification techniques to enhance the selectivity, sensitivity, and kinetic properties of carbon-fiber microelectrodes. Broadly speaking, these have included electrochemical (Heien *et al.*, 2003) and chemical pretreatments (Hermans *et al.*, 2006) as well as film coating. Application of the perfluorinated cation-exchange polymer Nafion through electro-deposition or dip-coating has proven particularly effective in repelling negatively-charged interferents during *in vivo* measurements (Hashemi *et al.*, 2009). Here we highlight several more recent developments in *in vivo* electrochemical sensor technology.

Carbon-nanotube based microelectrodes

Carbon-nanotubes (CNTs) are a subject of interest for various electrochemical applications, given their mechanical strength, high aspect ratios, and good electrical conductivities (Jacobs *et al.*, 2010; Putzbach & Ronkainen, 2013). Research exploring modification of carbon-fiber microelectrodes with CNTs for neurotransmitter measurements has shown increased electron-transfer kinetics and sensitivity for adsorption-controlled species such as dopamine. Such electrodes are also less susceptible to common biofouling agents, such as 5-HIAA. Immobilization of CNTs onto carbon-fiber microelectrodes was first achieved by dip-coating the fibers in a CNT-Nafion suspension (Swamy & Venton, 2007a). However, this method was found to suffer from poor reproducibility and the orientation of the CNTs restricted access to electroactive sites at the ends of the tubes. Further work identified chemical self-assembly of single-walled CNTs to be an effective method to form uniformly aligned CNT layers on carbon-fiber disk electrodes (Xiao & Venton, 2012). Application of these CNT-modified electrodes *in vivo* and *in vitro* demonstrated a 36-fold increase in

sensitivity for dopamine without decreasing response time, a problem that often occurs with other pretreatment methods.

Continuous fibers, or 'yarns', can be formed from carbon-nanotubes through liquid-state and dry-state spinning methods (Zhao *et al.*, 2010; De Volder *et al.*, 2013). By adjusting the size of the nanotubes and the spinning angle, yarns with diameters on the micrometer scale can be prepared. Disk microelectrodes (5 – 30 μm diameters) fabricated from multi-walled CNT yarns exhibit a number of interesting electrochemical properties including lower background currents and faster apparent electron-transfer kinetics, which allows enhanced chemical discrimination (Schmidt *et al.*, 2013; Jacobs *et al.*, 2014). While the time spent at negative holding potentials is a critical factor determining the sensitivity to dopamine at bare electrodes, the dopamine response at yarn microelectrodes is independent of waveform application frequency—believed to be due to slower desorption kinetics for dopamine-*o*-quinone. Jacobs *et al.* demonstrated that dopamine could be detected at a 2 ms timescale while maintaining sensitivity, simply by increasing the scan-rate and application frequency of the waveform. Other work found that sensitivity for dopamine is enhanced even further when the yarns are made in polyethyleneimine, instead of poly(vinyl alcohol) (Zestos *et al.*, 2014). Together CNT-based microelectrodes present the opportunity for sensitive, selective FSCV measurements at unprecedented speeds. However, it is not yet clear whether these advantages of CNT-microelectrodes are of great enough significance to result in their widespread use.

Fused-silica carbon-fiber microelectrodes

Traditionally, carbon-fiber microelectrodes are insulated within borosilicate glass capillaries. While easy to fabricate, glass-sealed microelectrodes are fragile and often break during routine experimental procedures. For a more robust electrode construction several groups have investigated use of fused-silica capillaries (Plotsky, 1987; Swiergiel *et al.*, 1997;

Gerhardt *et al.*, 1999). Fused-silica offers good insulating properties and increased flexibility at low cost. During fabrication, a seal is formed at the carbon fiber by an epoxy droplet. As fused-silica is less prone to breakage smaller diameter (100 vs 600 μm) electrodes are possible, which allows for less tissue damage during implantation.

Several years ago, Phillips and coworkers found that naturally-evoked dopamine release could be measured at polyamide-coated fused-silica electrodes several months after *in vivo* implantation (Clark *et al.*, 2010). Incredibly, measurements were obtainable for up to 25 successive days without any apparent loss in sensitivity—though there was a noted loss in temporal response. Given the heterogeneity of brain microenvironments, the ability to conduct FSCV measure from the same terminal population over multiple days is an exciting prospect for studies of disease and behavioral learning. Indeed, others have attempted to develop such a sensor (Duff & O'Neill, 1994; Kruk *et al.*, 1998), albeit with little success. The performance of the fused-silica electrode design is attributed to its size, which is believed to be small enough to bypass the immune response.

There is still question as to how these sensors can be used. While post-calibration of the sensors revealed no changes in electrode sensitivity after chronic implantation, it is unclear whether the performance of the sensor remains stable after several days of *in vivo* use. Unforeseen issues such as new tissue damage or degradation of the carbon-fiber could change the electrode's response with continued use. In such cases, it would be impossible to determine whether a signal decrease is a biologically relevant change or merely a change in electrode sensitivity. These concerns are the subject of ongoing studies.

Microelectrode arrays

The release of neurotransmitters has been found to vary not only within discrete substructures of the brain (Wightman *et al.*, 2007) but across individual cells (Schroeder *et al.*, 1994). This in turn has spurred the development of microelectrode arrays (MEAs)

compatible with neurochemical measurements for a variety of *in vitro* and *in vivo* purposes. Consolidation of multiple sensing elements onto a single device opens not only the potential for spatially-resolved profiling of neurochemical dynamics but for the simultaneous detection of different analytes by optimizing the potentials applied to each electrode.

To capture exocytotic variation on a subcellular level, the MEA size and electrode spacing must be smaller than the cell itself (~10-20 μm for a neuron). For single cell measurements, carbon-disk MEAs have been fabricated from carbon-fibers inserted into multibarrel glass and from the deposition of carbon through pyrolysis onto a fused assembly of quartz capillaries to form up to 7 and 15 electrodes respectively (Zhang *et al.*, 2011; Lin *et al.*, 2012). In addition, a variety of microfabrication approaches have been employed to create MEA devices with increased electrode number for single cell and cell cluster applications (Cui *et al.*, 2006; Berberian *et al.*, 2009; Carabelli *et al.*, 2010). Recently, Ewing and coworkers have developed platinum MEA platforms that are modified with collagen IV coatings to promote cell adhesion and growth (Wang *et al.*, 2013; Wang *et al.*, 2014). The newest version of their design confines 36 microelectrodes within a 40 μm x 40 μm microwell to position a cultured PC12 cell directly above the sensor surface.

The majority of MEAs developed for *in vivo* neurochemical applications have been carbon-based given its compatibility with FSCV. These have been used to probe neurotransmitter heterogeneity across multiple brain regions and within brain microenvironments. It is possible to achieve multielectrode recordings *in vivo* by simply implanting several individual carbon-fiber microelectrodes (Clark *et al.*, 2010; Zachek *et al.*, 2010b). However, such methodologies can suffer from irreproducibility and are difficult to implement when targeting a single brain structure. Hence, recent efforts have focused on the microfabrication of carbon-based MEAs. Successful devices containing 4 and 16 band microelectrodes have been created from pyrolyzed photoresist (PPF), which is amenable to photolithography and has properties similar to glassy-carbon (Zachek *et al.*, 2010a).

Strategies to construct MEAs from grown carbon nanofibers are also under investigation, but the viability of such devices *in vivo* has yet to be demonstrated (Zhang *et al.*, 2013).

Novel Applications

Challenging the conventions of neurochemical measurements

Microdialysis and FSCV are the two most common *in vivo* neurochemical techniques in use today. Though initially viewed as rival methods early in their development, microdialysis and FSCV are now recognized to provide complementary information. The millisecond temporal resolution of FSCV has made it superior for fast neurochemical measurement of electroactive molecules; however, the need for background-subtract limits detection to rapid concentration changes. With microdialysis, neurotransmitters and other small biomolecules in the brain extracellular fluid are extracted into dialysate driven slowly through a tubular semi-permeable membrane. As the dialysate is collected and analyzed externally, microdialysis affords the ability to detect a wider range of molecules with better chemical selectivity. However, sampling times are typically on the order of minutes, the time required to collect sufficient dialysate for analysis. Here we describe several novel strategies that are currently being developed to redefine the current conventions of FSCV and microdialysis measurements.

Basal level measurements with FSCV

Given its relevance to disorders such as Parkinson's disease, determining the basal level of dopamine has been a goal of microdialysis and FSCV alike. As FSCV is a differential technique, it has required indirect approaches to approximate local extracellular concentrations. For instance, studies have employed pharmacological methods to silence rapidly dopamine signaling in the striatum (Kulagina *et al.*, 2001; Borland & Michael, 2004; Owesson-White *et al.*, 2012). The subsequent decrease in extracellular dopamine detected

at the electrode is assumed to represent the original baseline concentration. Others have used kinetic and diffusion modeling to extrapolate the basal level from the transient dopamine responses elicited by electrical stimulation (Kawagoe *et al.*, 1992; Chen & Budygin, 2007). While many of these studies predict the basal concentration of dopamine to be in the lower nanomolar range others have reported values over a micromolar. Therefore the results of these experiments remain the subject of debate.

Other measurement strategies have taken advantage of the predisposition of dopamine to adsorb to carbon-fiber surfaces via electrostatic and pi-pi stacking interactions (Bath *et al.*, 2000; Heien *et al.*, 2003). These techniques use the signals generated after preconcentration of dopamine at the sensors as a measure of extracellular concentrations, similar to methods employed during anodic stripping voltammetry. One such approach involves a collector-generator-like system on a microfabricated platform (Dengler & McCarty, 2013). When operated, the potential of the outer-generator electrodes are held at ≤ 0 V to promote the adsorption of dopamine, and are then pulsed to a positive potential to desorb the accumulated dopamine at the surface. This repulsion creates a transient wave of dopamine that is detected at the inner-collector electrode with FSCV, and is used to determine the concentration of dopamine surrounding the device. Though detection of 200 nM dopamine was the lowest concentration demonstrated, the spacing of electrodes in future generations can be decreased for improved capture efficiency.

A similar approach has been developed for use with a single carbon-fiber microelectrode (Atcherley *et al.*, 2013). In this technique, termed fast-scan controlled adsorption voltammetry or 'FSCAV,' the holding time between voltammetric scans is altered to promote the adsorption of dopamine in a controlled manner. There are three steps to this process. First a high-speed (1200 V/s) version of the dopamine waveform is applied at 100 Hz to reduce the amount of dopamine adsorbed to the electrode. This is followed by a defined holding period where the potential of the electrode remains constant (typically at -

0.4 V) to allow for new dopamine adsorption to occur. The waveform is then reapplied to oxidize the dopamine accumulated on the surface. Non-faradaic current generated during this step is removed through deconvolution techniques using an electrode response function determined in a buffer solution. Subsequent integration of peak oxidation currents is used to calculate the concentration of dopamine in the solution. Initial characterization reported limits of detection under 10 nM for dopamine, well within the expected *in vivo* concentration range. While performance of this sensor in the complex extracellular environment of the brain has yet to be demonstrated, this strategy has the potential benefit of altering between normal FSCV and FSCAV modes to measure rapid and slow dopamine changes at a single microelectrode.

'Ultrafast' microdialysis

Recent work by the Kennedy group has led to the realization of the first 'ultrafast' microdialysis techniques. The temporal resolution of microdialysis is largely determined by the mass limits of the detection method, with high limits requiring a larger volume of dialysate to be collected for analysis and, in turn, longer sampling times. Therefore, coupling microdialysis to analysis techniques with high mass sensitivity, such as capillary electrophoresis with laser-induced fluorescence detection, greatly increases the sampling speed (Hogan *et al.*, 1994; Lada *et al.*, 1997; Thompson *et al.*, 1999). Further improvements in temporal resolution are limited by band broadening of the sample by Taylor dispersion during transport. Kennedy and coworkers have demonstrated that a segmented flow system can significantly reduce the effects of Taylor dispersion (Wang *et al.*, 2008). In their setup, segmented flow is accomplished on an integrated PDMS chip positioned at the probe outlet, which mixes the dialysate with fluorogenic reagents for derivatization and introduces immiscible oil droplet to partition the dialysate into discrete nanoliter fractions. This partitioning prevents the fractions from mixing thereby preserving temporal information, even

when samples are stored for offline analysis. Online analysis with a microfluidic capillary electrophoresis chip demonstrated that this system can provide a temporal resolution of 2 s and that it is suitable for *in vivo* amino acid measurements (Wang *et al.*, 2010).

The segmented flow strategy has also been coupled to low-flow push-pull perfusion to provide fast neurochemical sampling with higher spatial resolution as sampling occurs only at the tips of two adjoined capillaries (Slaney *et al.*, 2011). During sampling physiological buffer is infused through one capillary (“push”) while fluid is withdrawn through the second capillary (“pull”) at an equal flow rate. Given the low-flow rates (~50 nL/min), which are used to prevent tissue damage, the sampling of this technique is typically very slow. However, endeavors to couple push-pull perfusion to the segmented flow system have produced results suggesting that sub-second time resolution may be possible. Application of this device in the rat striatum established that this sampling technique could follow glutamate changes with 7 s time resolution and with an 80 fold increase in spatial resolution over conventional microdialysis probes.

Multimodal measurements

Millar and colleagues realized soon after the introduction of *in vivo* electrochemical techniques that a complete understanding of neuronal communication requires knowledge of neurochemical release dynamics and the resulting post-synaptic cell responses. In turn they developed a method where catecholamine release and the firing rates of single neurons or “units” could be monitored at a carbon-fiber microelectrode by floating the potential of the electrode between FSCV scans to detect changes in the extracellular potential caused by cell firing (Armstrong-James *et al.*, 1981; Millar & Barnett, 1988; Stamford *et al.*, 1993).

When the combined electrochemical/electrophysiological (echem/ephys) method is coupled to iontophoresis, it is possible to identify the receptors linking pre- and post-synaptic

activity through pharmacological manipulation (Belle *et al.*, 2013). Iontophoresis is a classic drug delivery tool where an applied current induces the flow of solution through a pulled glass capillary via electrophoretic and electroosmotic forces (Herr & Wightman, 2013). During echem/ephys measurements the carbon-fiber microelectrode is housed in one capillary of a pulled multi-barrel glass assembly. The other barrels contain drug solutions whose dispersion are controlled by a constant-current source. Iontophoresis of electroactive species, such as dopamine, is voltammetrically detected at the carbon-fiber to determine the ejected concentration. Iontophoresis of non-electroactive drugs is indirectly monitored through the addition of a biologically-inert, electroactive marker (Herr *et al.*, 2008). To obtain an approximation of the drug introduced, the relative transport of the drug to the marker is determined by capillary electrophoresis.

While this powerful set of tools was first employed over 30 years ago, it has only recently been miniaturized for application in awake animals (Takmakov *et al.*, 2011). On the miniaturized headstage a surface mounted dual operational amplifier chip provides voltage-follower (electrophysiological) and current transducer (electrochemical) modes, which are controlled by a CMOS switch. During combined echem/ephys experiments, a triangular waveform scanning between -0.4 V and +1.3 V at 400 V/s is used to detect dopamine changes. This waveform is applied at 5 Hz, half the normal frequency, to provide ~180 ms of electrophysiological recording between scans. Digital time stamps are used to align these measurements with behavioral and iontophoretic events during data analysis. Detailed descriptions of the hardware and software components of the combined technique have been published elsewhere (Takmakov *et al.*, 2011; Bucher *et al.*, 2013).

Recent work with this setup has provided new insight into the role of dopamine signaling in the nucleus accumbens (NAc), a brain region mediating motivated behaviors. Operant paradigms such as self-administration and intracranial self-stimulation (ICSS) are used to investigate the physiological and psychological mechanisms guiding reward-seeking

behaviors. During such paradigms the animal learns to complete a task such as pressing a lever to receive a reinforcer (i.e. a reward). In the case of self-administration the reinforcer is a drug of abuse. In ICSS the animal receives a rewarding electrical stimulation of its brain, typically targeting dopaminergic processes. Dopamine is widely implicated in the reinforcing components of psychostimulants and ICSS, but extent of its neuromodulatory role during such behaviors has been debated (Murray & Shizgal, 1994; Wise, 1996; Hernandez *et al.*, 2006; Sunsay & Rebec, 2014).

With the combined echem/ephys technique it was found that the medium spiny neurons (MSNs) of the NAc show patterned responses to reward prediction and presentation during ICSS and cocaine self-administration (Cheer *et al.*, 2007; Owesson-White *et al.*, 2009). The magnitude of these phasic firing activities tracked with the amount of dopamine release detected, whereas locations with unresponsive cells exhibited no measurable dopamine release. While this data provided strong correlation between reward-evoked dopamine and unit responsivity, initial pharmacological investigations conducted systemically found that dopamine receptor activation played little part in generating the MSN firing responses observed during ICSS (Cheer *et al.*, 2005). In a subsequent study dopamine receptors were blocked by drug application directly into the NAc through microinfusion and iontophoresis (Cheer *et al.*, 2007). The dopamine D1 receptor antagonist SCH23390 was found to block lever-pressing during ICSS with both methods of drug delivery. However, unlike microinfusion the smaller drug volumes introduced by iontophoresis (Kirkpatrick *et al.*, 2014) did not affect the animals' performance during the task, thereby allowing the neurochemical basis of the behavior to be investigated without influencing the behavior itself.

A more recent study found intriguing differences in the immediate and long term effects of dopamine receptor modulation in conscious animals at rest (Belle *et al.*, 2013). Dopamine D1 (SCH 23390) and D2 (raclopride) receptor inhibitors were introduced into the

NAc as 15 s ejections, during which only a small number of MSNs were found to be effected. In contrast, long term analysis found that the baseline firing rates of most cells were either inhibited by D1 or excited by D2 antagonism, consistent with previous literature findings from brain slices. Interestingly, dopamine itself could evoke immediate cell responses during electrical stimulation, where non-electroactive species such as glutamate are also released. This highlights the role of dopamine as a neuromodulator as opposed to a classical neurotransmitter. While not directly inhibitory or excitatory itself, dopamine can have various effects on the overall excitability of MSNs in the NAc and can regulate the immediate actions of glutamate in a receptor-dependent manner.

The use of the combined echem/ephys technique in awake animals is only in its infancy; however, these early results clearly demonstrate the utility of such measurements in delineating the post-synaptic consequences of rapid neurotransmission. The addition of iontophoresis to this setup in future experiments will provide the unique opportunity to probe the receptor-based underpinnings of behavior at a local circuit level.

Neurotransmitter detection in non-rodent models

The majority of *in vivo* electrochemical studies have been conducted in rats, mice and, to a lesser extent, guinea pigs. Though this work has provided a great deal of our current knowledge regarding dopamine regulation in the striatum, the translatability of this information to other species, importantly humans, is unfortunately tentative. This limitation has spurred attempts to expand electrochemical techniques to non-rodent species. However, these endeavors have had varying degrees of success due to several technological and anatomical challenges. Here we discuss efforts to apply electrochemical neurotransmitter detection in the fly nervous system and in the primate brain.

Drosophila (Fruit Flies)

Drosophila melanogaster, more commonly known as the fruit fly, is a valuable model organism given its short life span, rapid reproduction cycle, and the ease of its genetic manipulability (Sang, 2001). These characteristics provide the ability to produce and screen genetic mutations in a matter of months, whereas similar manipulations would require years in the rat. Although the nervous system of *Drosophila* is only composed of 100,000 neurons (Ito *et al.*), it exhibits a notable degree of genetic homology to vertebrates and supports learning and memory (Sokolowski, 2001). Additionally, *Drosophila* employs many of the same monoamine neurotransmitters as vertebrates, including dopamine and serotonin (Monastirioti, 1999). Together its simplicity and genetic flexibility make *Drosophila* an ideal platform to investigate genetic foundations of neurotransmission.

The study of neurotransmitter release in *Drosophila* has largely been hindered by the size of its central nervous system (~100 μ M across), which is smaller than conventional microdialysis probes. As a result most neurotransmitter work has involved content analysis of homogenized tissue preparations. Although microelectrodes are well-suited to probe biological microenvironments, voltammetric detection of neurotransmission in *Drosophila* presented additional challenges. First, the size of the tissue provides very little opportunity to target discrete structures containing only a single, known electroactive neurotransmitter, as is possible in the rat brain. A larger question was how to elicit selective neurotransmitter release when the *Drosophila* nervous system is smaller than commercially available stimulating electrodes.

Due to such issues, many FSCV measurements conducted in *Drosophila* have involved the application of exogenous dopamine to study the function of the dopamine transporter (Makos *et al.*, 2009; Makos *et al.*, 2010; Berglund *et al.*, 2013). In these experiments a live fly is immobilized in physiological buffer and dissected to expose the central nervous system. Electrode placement is subsequently guided by the fluorescent

signals produced by GFP-transfected dopamine neurons. Dopamine is then introduced by pressure ejection through a capillary positioned next the microelectrode, and the decay of the signal is related the rate of removal by the dopamine transporter. This work has demonstrated that uptake of dopamine from the extracellular space is regulated by similar mechanisms in *Drosophila* and mammalian species and moreover, described an initial protocol for electrochemical measurements in fly preparations.

Study of endogenous monoamine release in *Drosophila* has been accomplished through optogenetic stimulation strategies. Venton and coworkers transfected selected groups of monoamine neurons in *Drosophila* to express Channelrhodopsin-2 (ChR2), a blue-light sensitive ion channel. The ion fluxes generated by blue light exposure cause electrical excitation only in ChR2-expressing cells and therefore can be used as a means of selective neuronal activation. Preliminary FSCV studies have proven that blue light stimulation of ChR2-expressing serotonin and dopamine neurons can elicit measurable release in the ventral nerve cord of *Drosophila* larva and that these monoamine systems have comparable regulatory and frequency-response characteristics to those of the rat brain (Borue *et al.*, 2009; Vickrey *et al.*, 2009; Vickrey & Venton, 2011; Xiao *et al.*, 2014).

Non-human primates

Non-human primates are the most clinically relevant animal models given their genetic semblance to humans and sophisticated cognitive abilities. Though most rodent studies are conducted to gain insight into human behavior and disease, there is substantial reason to believe that the complexities of primate neurochemistry cannot be fully appreciated through such work. For instance, only in primates is the striatum, a dopamine-dense brain region, anatomically separated into the caudate and putamen by the internal capsule. Along with this distinction, primates are more susceptible than rodents to

Parkinsonian-like disorders (Johannessen *et al.*, 1985; Schober, 2004), which is mediated in part by dopamine signaling in striatal regions (Cragg *et al.*, 2000).

Given these anatomical and physiological differences, it is not surprising that FSCV recordings in primate brain slices have discovered greater complexity in dopamine release and regulation (Cragg *et al.*, 2000; 2002; Cragg, 2003). Using marmoset striatal slices, Cragg and coworkers observed that dopamine overflow and tissue content was 2-3 fold larger than the concentrations found in rodents, which was attributed a differences in innervation density. Moreover, the magnitude of dopamine release and the rate of its uptake were found to vary significantly among striatal subregions, a characteristic that is not apparent the striatum of rodents. Interestingly, the rate of dopamine uptake was highest in the dorsal lateral putamen, the area of the striatum most affected by Parkinson's disease. The uptake rate in this region was also 2 times faster than reported for rodents, suggesting that the dopamine transporter may contribute to the susceptibility of primates to Parkinson's disease.

In contrast to the success of brain slice experiments, the application of electrochemical techniques to the brains of intact primates has progressed slowly since the first attempt in 1981 (Lindsay *et al.*, 1981). A handful of studies using amperometric measurements have recorded increased oxidation signals in the monkey striatum with local chemical stimulation, electrical stimulation of dopamine axons, natural reward and reward prediction (Lindsay *et al.*, 1981; Gerhardt *et al.*, 1996; Yoshimi *et al.*, 2011). These data are in accordance with recorded dopamine responses in the rodent brain during such stimuli. However, as amperometry provides very little chemical information none of studies were able to verify that the signal was dopaminergic in origin.

The first study clearly demonstrating electrochemical detection of dopamine release in the primate striatum was an anesthetized experiment conducted by Earl and coworkers in 1998 (Earl *et al.*, 1998). Using FSCV at a conventional carbon-fiber microelectrode they

were able to measure electrically stimulated dopamine release in the striatum of untreated and MPTP-treated marmosets. MPTP is a neurotoxin that generates Parkinsonian-like degeneration of dopamine neurons. This study demonstrated that, as in rodents, dopamine release in the monkey striatum is dependent on stimulation frequency and is regulated by its autoreceptor and transporter. Moreover, they found that dopamine release in MPTP marmosets did not respond to transporter inhibition, consistent with the later work of Cragg proposing its involvement in Parkinson's disease.

However, the marmoset is among the smallest primates used in research, only weighing 400 g at adulthood similar to the rat (Hearn, 1983). Thus, endeavors to employ FSCV in the rhesus monkey, which reaches over 5000 g at adulthood (Grand, 1977), are more relevant to the human brain. To probe the rhesus striatum the electrode must be long enough to hit target regions centimeters, rather than millimeters beneath the skull. This generates issues regarding not only electrode durability but fiber resistance, and requires that the conducting wire form a connection to the carbon fiber near the tip of the electrode. Another set of concerns arises from the more diffuse distribution of dopamine cells, projections and terminals in larger animals. Positioning the microelectrode near striatal dopamine terminals therefore becomes much more of a challenge.

Accordingly, a FSCV study by our group in collaboration with the lab of Wolfram Schultz detected little dopamine release during recordings in the brain of an awake rhesus monkey (Ariansen *et al.*, 2012). The animals were trained in a Pavlovian task where a visual cue predicted the availability of a sweetened liquid, a behavior that involves dopamine neurotransmission. During the behavior extracellular oxygen and pH fluctuations, which are hemodynamic and metabolic markers of neuronal activity (Heales, 1999; Venton *et al.*, 2003), were detected electrochemically. Dopamine-like cyclic voltammograms were also detected at some recording locations, but they were difficult to resolve from the larger oxygen and pH signals.

A more recent FSCV study by Schluter and coworkers, explored the use of electrical stimulation to evoke dopamine release in the rhesus striatum (Schluter *et al.*, 2014). Electrical stimulation of midbrain dopamine neurons in the substantia nigra/ventral tegmental area (SN/VTA) is widely used in rodent studies to aid in electrode positioning and to study the regulation of dopamine overflow. However, electrical stimulation of the SN/VTA was not found to be an effective means to evoke dopamine release in the rhesus striatum, as the area activated by conventionally sized stimulating electrodes comprises only a small portion of SN/VTA neurons. Increasing the current in attempt to recruit a larger population of neurons resulted in undesirable motor responses that interfered with the recordings. However, local terminal stimulation, a technique regularly used in brain slice studies, elicited dopamine release in 10 out of 14 attempts, and aided in recording dopamine release during an unexpected juice reward. Thus, in agreement with our published work in monkeys, they concluded that dopamine release is more difficult to detect in the primate brain than in rodents.

Humans

To date, endeavors to apply FSCV to the human brain have been made in parallel to deep brain stimulation (DBS) treatment, a type of functional brain surgery that can ameliorate the symptoms of Parkinson's and other neurological diseases (Stefurak *et al.*, 2003; Laxpati *et al.*, 2014; Sachdev *et al.*, 2014). The neuronal mechanisms underlying the efficacy of DBS are still largely unknown, though a range of neurotransmitters, including dopamine, serotonin and adenosine, have been implicated in producing its effects (van Dijk *et al.*, 2012; Figuee *et al.*, 2014). Thus, electrochemical detection of these species during DBS surgery may provide valuable information in the development of new and more effective therapeutics.

Voltammetric recordings from the human brain have employed single fused-silica based microelectrode assemblies (Kishida *et al.*, 2011), housing both the reference and working electrodes to confine the damage incurred during implantation. In practice, these probes are positioned near the target of DBS stimulation to eliminate the need for additional surgery. The first recording from a human was accomplished in 2011 with a microelectrode assembly positioned within the striatum. During the procedure, the patient was asked to perform a decision-making task involving monetary investment during which dopamine fluctuations were successfully recorded with FSCV. Thereafter, separate efforts at the Mayo Clinic have created an electrochemical telemetry system called WINCS (Wireless Instantaneous Neurotransmitter Concentration Sensing) that is compatible with FSCV or amperometric measurements in humans (Kasasbeh *et al.*, 2013). With the WINCS system cyclic voltammograms consistent with adenosine release have been recorded in the human thalamus during a treatment for essential tremor (Chang *et al.*, 2012). Notably, the both of these reports found no adverse effects in the health of the patients or the efficacy of DBS treatment. The demonstrated safety of electrochemical recordings is a crucial precedent for future clinical studies.

Conclusions

Since Adams' pioneering work of over forty years ago, the field of *in vivo* electrochemistry has undergone a great deal of development and standardization. Today electrochemical techniques are used routinely for high-speed, spatially-resolved neurochemical measurements in a number of biological preparations. While current methods are robust, versatile, and suitable for use by nonelectrochemists, ongoing innovations in sensor design and experimental methodology present exciting new avenues for electrochemical measurements in neuroscience. Future research may provide unprecedented insight into the neurochemical basis of behavior and disease.

REFERENCES

- Adams, R.N. (1976) Probing brain chemistry with electroanalytical techniques. *Anal Chem*, **48**, 1126A-1138A.
- Addy, N.A., Daberkow, D.P., Ford, J.N., Garriss, P.A. & Wightman, R.M. (2010) Sensitization of rapid dopamine signaling in the nucleus accumbens core and shell after repeated cocaine in rats. *J Neurophysiol*, **104**, 922-931.
- Ariansen, J.L., Heien, M.L., Hermans, A., Phillips, P.E., Hernadi, I., Bermudez, M.A., Schultz, W. & Wightman, R.M. (2012) Monitoring extracellular pH, oxygen, and dopamine during reward delivery in the striatum of primates. *Front Behav Neurosci*, **6**, 36.
- Armstrong-James, M., Fox, K., Kruk, Z.L. & Millar, J. (1981) Quantitative iontophoresis of catecholamines using multibarrel carbon fibre microelectrodes. *Journal of Neuroscience Methods*, **4**, 385-406.
- Atcherley, C.W., Laude, N.D., Parent, K.L. & Heien, M.L. (2013) Fast-scan controlled-adsorption voltammetry for the quantification of absolute concentrations and adsorption dynamics. *Langmuir*, **29**, 14885-14892.
- Bath, B.D., Michael, D.J., Trafton, B.J., Joseph, J.D., Runnels, P.L. & Wightman, R.M. (2000) Subsecond adsorption and desorption of dopamine at carbon-fiber microelectrodes. *Anal Chem*, **72**, 5994-6002.
- Belchetz, P.E., Plant, T.M., Nakai, Y., Keogh, E.J. & Knobil, E. (1978) Hypophysial responses to continuous and intermittent delivery of hypophyseal gonadotropin-releasing hormone. *Science*, **202**, 631-633.
- Belle, A.M., Owesson-White, C., Herr, N.R., Carelli, R.M. & Wightman, R.M. (2013) Controlled iontophoresis coupled with fast-scan cyclic voltammetry/electrophysiology in awake, freely moving animals. *ACS Chem Neurosci*, **4**, 761-771.
- Berberian, K., Kisler, K., Fang, Q. & Lindau, M. (2009) Improved surface-patterned platinum microelectrodes for the study of exocytotic events. *Anal Chem*, **81**, 8734-8740.
- Berglund, E.C., Makos, M.A., Keighron, J.D., Phan, N., Heien, M.L. & Ewing, A.G. (2013) Oral administration of methylphenidate blocks the effect of cocaine on uptake at the *Drosophila* dopamine transporter. *ACS Chem Neurosci*, **4**, 566-574.
- Bergstrom, B.P., Sanberg, S.G., Andersson, M., Mithyantha, J., Carroll, F.I. & Garriss, P.A. (2011) Functional reorganization of the presynaptic dopaminergic terminal in parkinsonism. *Neuroscience*, **193**, 310-322.
- Bodnar, R.J. (2013) Endogenous opiates and behavior: 2012. *Peptides*, **50**, 55-95.
- Borisovska, M., Bensen, A.L., Chong, G. & Westbrook, G.L. (2013) Distinct modes of dopamine and GABA release in a dual transmitter neuron. *J Neurosci*, **33**, 1790-1796.

- Borland, L.M. & Michael, A.C. (2004) Voltammetric study of the control of striatal dopamine release by glutamate. *J Neurochem*, **91**, 220-229.
- Borue, X., Cooper, S., Hirsh, J., Condrón, B. & Venton, B.J. (2009) Quantitative evaluation of serotonin release and clearance in *Drosophila*. *J Neurosci Methods*, **179**, 300-308.
- Bucher, E.S., Brooks, K., Verber, M.D., Keithley, R.B., Owesson-White, C., Carroll, S., Takmakov, P., McKinney, C.J. & Wightman, R.M. (2013) Flexible software platform for fast-scan cyclic voltammetry data acquisition and analysis. *Anal Chem*, **85**, 10344-10353.
- Bunin, M.A., Prioleau, C., Mailman, R.B. & Wightman, R.M. (1998) Release and uptake rates of 5-hydroxytryptamine in the dorsal raphe and substantia nigra reticulata of the rat brain. *J Neurochem*, **70**, 1077-1087.
- Calipari, E.S., Ferris, M.J. & Jones, S.R. (2014) Extended access of cocaine self-administration results in tolerance to the dopamine-elevating and locomotor-stimulating effects of cocaine. *J Neurochem*, **128**, 224-232.
- Carabelli, V., Gosso, S., Marcantoni, A., Xu, Y., Colombo, E., Gao, Z., Vittone, E., Kohn, E., Pasquarelli, A. & Carbone, E. (2010) Nanocrystalline diamond microelectrode arrays fabricated on sapphire technology for high-time resolution of quantal catecholamine secretion from chromaffin cells. *Biosens Bioelectron*, **26**, 92-98.
- Carelli, R.M. (2004) Nucleus accumbens cell firing and rapid dopamine signaling during goal-directed behaviors in rats. *Neuropharmacology*, **47 Suppl 1**, 180-189.
- Cechova, S. & Venton, B.J. (2008) Transient adenosine efflux in the rat caudate-putamen. *J Neurochem*, **105**, 1253-1263.
- Chang, S.Y., Kim, I., Marsh, M.P., Jang, D.P., Hwang, S.C., Van Gompel, J.J., Goerss, S.J., Kimble, C.J., Bennet, K.E., Garriss, P.A., Blaha, C.D. & Lee, K.H. (2012) Wireless fast-scan cyclic voltammetry to monitor adenosine in patients with essential tremor during deep brain stimulation. *Mayo Clin Proc*, **87**, 760-765.
- Cheer, J.F., Aragona, B.J., Heien, M.L., Seipel, A.T., Carelli, R.M. & Wightman, R.M. (2007) Coordinated accumbal dopamine release and neural activity drive goal-directed behavior. *Neuron*, **54**, 237-244.
- Cheer, J.F., Heien, M.L., Garriss, P.A., Carelli, R.M. & Wightman, R.M. (2005) Simultaneous dopamine and single-unit recordings reveal accumbens GABAergic responses: implications for intracranial self-stimulation. *Proc Natl Acad Sci U S A*, **102**, 19150-19155.
- Chen, K.C. & Budygin, E.A. (2007) Extracting the basal extracellular dopamine concentrations from the evoked responses: re-analysis of the dopamine kinetics. *J Neurosci Methods*, **164**, 27-42.
- Chen, P. & Moenter, S.M. (2009) GABAergic transmission to gonadotropin-releasing hormone (GnRH) neurons is regulated by GnRH in a concentration-dependent manner engaging multiple signaling pathways. *J Neurosci*, **29**, 9809-9818.

- Clark, J.J., Sandberg, S.G., Wanat, M.J., Gan, J.O., Horne, E.A., Hart, A.S., Akers, C.A., Parker, J.G., Willuhn, I., Martinez, V., Evans, S.B., Stella, N. & Phillips, P.E. (2010) Chronic microsenors for longitudinal, subsecond dopamine detection in behaving animals. *Nat Methods*, **7**, 126-129.
- Cragg, S.J. (2003) Variable dopamine release probability and short-term plasticity between functional domains of the primate striatum. *J Neurosci*, **23**, 4378-4385.
- Cragg, S.J., Hille, C.J. & Greenfield, S.A. (2000) Dopamine release and uptake dynamics within nonhuman primate striatum in vitro. *J Neurosci*, **20**, 8209-8217.
- Cragg, S.J., Hille, C.J. & Greenfield, S.A. (2002) Functional domains in dorsal striatum of the nonhuman primate are defined by the dynamic behavior of dopamine. *J Neurosci*, **22**, 5705-5712.
- Cui, H.F., Ye, J.S., Chen, Y., Chong, S.C. & Sheu, F.S. (2006) Microelectrode array biochip: tool for in vitro drug screening based on the detection of a drug effect on dopamine release from PC12 cells. *Anal Chem*, **78**, 6347-6355.
- Cunha, R.A. (2001) Adenosine as a neuromodulator and as a homeostatic regulator in the nervous system: different roles, different sources and different receptors. *Neurochem Int*, **38**, 107-125.
- Dankoski, E.C., Agster, K.L., Fox, M.E., Moy, S.S. & Wightman, R.M. (2014) Facilitation of Serotonin Signaling by SSRIs is Attenuated by Social Isolation. *Neuropsychopharmacology*.
- De Volder, M.F., Tawfick, S.H., Baughman, R.H. & Hart, A.J. (2013) Carbon nanotubes: present and future commercial applications. *Science*, **339**, 535-539.
- Dengler, A.K. & McCarty, G.S. (2013) Microfabricated Microelectrode Sensor for Measuring Background and Slowly Changing Dopamine Concentrations. *J Electroanal Chem (Lausanne Switz)*, **693**, 28-33.
- Duff, A. & O'Neill, R.D. (1994) Effect of probe size on the concentration of brain extracellular uric acid monitored with carbon paste electrodes. *J Neurochem*, **62**, 1496-1502.
- Earl, C.D., Sautter, J., Xie, J., Kruk, Z.L., Kupsch, A. & Oertel, W.H. (1998) Pharmacological characterisation of dopamine overflow in the striatum of the normal and MPTP-treated common marmoset, studied in vivo using fast cyclic voltammetry, nomifensine and sulpiride. *J Neurosci Methods*, **85**, 201-209.
- Ehrich, J.M., Phillips, P.E. & Chavkin, C. (2014) Kappa Opioid Receptor Activation Potentiates the Cocaine-Induced Increase in Evoked Dopamine Release Recorded In Vivo in the Mouse Nucleus Accumbens. *Neuropsychopharmacology*.
- Figuee, M., de Koning, P., Klaassen, S., Vulink, N., Mantione, M., van den Munckhof, P., Schuurman, R., van Wingen, G., van Amelsvoort, T., Booij, J. & Denys, D. (2014) Deep Brain Stimulation Induces Striatal Dopamine Release in Obsessive-Compulsive Disorder. *Biological Psychiatry*, **75**, 647-652.

- Gerhardt, G.A., Cass, W.A., Hudson, J., Henson, M., Zhang, Z., Ovadia, A., Hoffer, B.J. & Gash, D.M. (1996) In vivo electrochemical studies of dopamine overflow and clearance in the striatum of normal and MPTP-treated rhesus monkeys. *J Neurochem*, **66**, 579-588.
- Gerhardt, G.A., Ksir, C., Pivik, C., Dickinson, S.D., Sabeti, J. & Zahniser, N.R. (1999) Methodology for coupling local application of dopamine and other chemicals with rapid in vivo electrochemical recordings in freely-moving rats. *J Neurosci Methods*, **87**, 67-76.
- Glanowska, K.M., Venton, B.J. & Moenter, S.M. (2012) Fast scan cyclic voltammetry as a novel method for detection of real-time gonadotropin-releasing hormone release in mouse brain slices. *J Neurosci*, **32**, 14664-14669.
- Grand, T.I. (1977) Body weight: Its relation to tissue composition, segment distribution, and motor function II. Development of *Macaca mulatta*. *American Journal of Physical Anthropology*, **47**, 241-248.
- Hashemi, P., Dankoski, E.C., Lama, R., Wood, K.M., Takmakov, P. & Wightman, R.M. (2012) Brain dopamine and serotonin differ in regulation and its consequences. *Proc Natl Acad Sci U S A*, **109**, 11510-11515.
- Hashemi, P., Dankoski, E.C., Petrovic, J., Keithley, R.B. & Wightman, R.M. (2009) Voltammetric detection of 5-hydroxytryptamine release in the rat brain. *Anal Chem*, **81**, 9462-9471.
- Heales, D.S. (1999) pH AND BRAIN FUNCTION. *Brain*, **122**, 1794-1796.
- Hearn, J. (1983) The Common Marmoset (*Callithrix jacchus*). In Hearn, J. (ed) *Reproduction in New World Primates*. Springer Netherlands, pp. 181-215.
- Heien, M.L., Phillips, P.E., Stuber, G.D., Seipel, A.T. & Wightman, R.M. (2003) Overoxidation of carbon-fiber microelectrodes enhances dopamine adsorption and increases sensitivity. *Analyst*, **128**, 1413-1419.
- Hermans, A., Seipel, A.T., Miller, C.E. & Wightman, R.M. (2006) Carbon-fiber microelectrodes modified with 4-sulfobenzene have increased sensitivity and selectivity for catecholamines. *Langmuir*, **22**, 1964-1969.
- Hernandez, G., Hamdani, S., Rajabi, H., Conover, K., Stewart, J., Arvanitogiannis, A. & Shizgal, P. (2006) Prolonged rewarding stimulation of the rat medial forebrain bundle: neurochemical and behavioral consequences. *Behav Neurosci*, **120**, 888-904.
- Herr, N.R., Kile, B.M., Carelli, R.M. & Wightman, R.M. (2008) Electroosmotic flow and its contribution to iontophoretic delivery. *Anal Chem*, **80**, 8635-8641.
- Herr, N.R. & Wightman, R.M. (2013) Improved techniques for examining rapid dopamine signaling with iontophoresis. *Front Biosci (Elite Ed)*, **5**, 249-257.

- Hogan, B.L., Lunte, S.M., Stobaugh, J.F. & Lunte, C.E. (1994) On-line coupling of in vivo microdialysis sampling with capillary electrophoresis. *Anal Chem*, **66**, 596-602.
- Huffman, M.L. & Venton, B.J. (2009) Carbon-fiber microelectrodes for in vivo applications. *Analyst*, **134**, 18-24.
- Ito, M., Masuda, N., Shinomiya, K., Endo, K. & Ito, K. Systematic Analysis of Neural Projections Reveals Clonal Composition of the Drosophila Brain. *Current Biology*, **23**, 644-655.
- Jacobs, C.B., Ivanov, I.N., Nguyen, M.D., Zestos, A.G. & Venton, B.J. (2014) High temporal resolution measurements of dopamine with carbon nanotube yarn microelectrodes. *Anal Chem*, **86**, 5721-5727.
- Jacobs, C.B., Peairs, M.J. & Venton, B.J. (2010) Review: Carbon nanotube based electrochemical sensors for biomolecules. *Anal Chim Acta*, **662**, 105-127.
- Jacobsen, J.P., Medvedev, I.O. & Caron, M.G. (2012) The 5-HT deficiency theory of depression: perspectives from a naturalistic 5-HT deficiency model, the tryptophan hydroxylase 2Arg439His knockin mouse. *Philos Trans R Soc Lond B Biol Sci*, **367**, 2444-2459.
- Janezic, S., Threlfell, S., Dodson, P.D., Dowie, M.J., Taylor, T.N., Potgieter, D., Parkkinen, L., Senior, S.L., Anwar, S., Ryan, B., Deltheil, T., Kosillo, P., Cioroch, M., Wagner, K., Ansorge, O., Bannerman, D.M., Bolam, J.P., Magill, P.J., Cragg, S.J. & Wade-Martins, R. (2013) Deficits in dopaminergic transmission precede neuron loss and dysfunction in a new Parkinson model. *Proc Natl Acad Sci U S A*, **110**, E4016-4025.
- Johannessen, J.N., Chiueh, C.C., Burns, R.S. & Markey, S.P. (1985) IV. Differences in the metabolism of MPTP in the rodent and primate parallel differences in sensitivity to its neurotoxic effects. *Life Sciences*, **36**, 219-224.
- Justice, J.B. (ed) (1987) *Voltammetry in the Neurosciences*. The Humana Press, Inc. , Clifton.
- Kasasbeh, A., Lee, K., Bieber, A., Bennet, K. & Chang, S.Y. (2013) Wireless neurochemical monitoring in humans. *Stereotact Funct Neurosurg*, **91**, 141-147.
- Kawagoe, K.T., Garris, P.A., Wiedemann, D.J. & Wightman, R.M. (1992) Regulation of transient dopamine concentration gradients in the microenvironment surrounding nerve terminals in the rat striatum. *Neuroscience*, **51**, 55-64.
- Kirkpatrick, D.C., Edwards, M.A., Flowers, P.A. & Wightman, R.M. (2014) Characterization of Solute Distribution Following Iontophoresis from a Micropipet. *Anal Chem*.
- Kishida, K.T., Sandberg, S.G., Lohrenz, T., Comair, Y.G., Saez, I., Phillips, P.E. & Montague, P.R. (2011) Sub-second dopamine detection in human striatum. *PLoS One*, **6**, e23291.
- Kissinger, P.T., Hart, J.B. & Adams, R.N. (1973) Voltammetry in brain tissue--a new neurophysiological measurement. *Brain research*, **55**, 209-213.

- Kiyatkin, E.A. & Lenoir, M. (2012) Rapid fluctuations in extracellular brain glucose levels induced by natural arousing stimuli and intravenous cocaine: fueling the brain during neural activation. *J Neurophysiol*, **108**, 1669-1684.
- Kiyatkin, E.A., Wakabayashi, K.T. & Lenoir, M. (2013) Physiological fluctuations in brain temperature as a factor affecting electrochemical evaluations of extracellular glutamate and glucose in behavioral experiments. *ACS Chem Neurosci*, **4**, 652-665.
- Koob, G.F. (2013) Addiction is a Reward Deficit and Stress Surfeit Disorder. *Front Psychiatry*, **4**, 72.
- Kruk, Z.L., Cheeta, S., Milla, J., Muscat, R., Williams, J.E. & Willner, P. (1998) Real time measurement of stimulated dopamine release in the conscious rat using fast cyclic voltammetry: dopamine release is not observed during intracranial self stimulation. *J Neurosci Methods*, **79**, 9-19.
- Kulagina, N.V., Zigmond, M.J. & Michael, A.C. (2001) Glutamate regulates the spontaneous and evoked release of dopamine in the rat striatum. *Neuroscience*, **102**, 121-128.
- Lada, M.W., Vickroy, T.W. & Kennedy, R.T. (1997) High temporal resolution monitoring of glutamate and aspartate in vivo using microdialysis on-line with capillary electrophoresis with laser-induced fluorescence detection. *Anal Chem*, **69**, 4560-4565.
- Laxpati, N.G., Kasoff, W.S. & Gross, R.E. (2014) Deep brain stimulation for the treatment of epilepsy: circuits, targets, and trials. *Neurotherapeutics*, **11**, 508-526.
- Lin, Y., Trouillon, R., Svensson, M.I., Keighron, J.D., Cans, A.S. & Ewing, A.G. (2012) Carbon-ring microelectrode arrays for electrochemical imaging of single cell exocytosis: fabrication and characterization. *Anal Chem*, **84**, 2949-2954.
- Lindsay, W.S., Herndon, J.G., Jr., Blakely, R.D., Justice, J.B., Jr. & Neill, D.B. (1981) Voltammetric recording from neostriatum of behaving rhesus monkey. *Brain research*, **220**, 391-396.
- Lugo-Morales, L.Z., Loziuk, P.L., Corder, A.K., Toups, J.V., Roberts, J.G., McCaffrey, K.A. & Sombers, L.A. (2013) Enzyme-modified carbon-fiber microelectrode for the quantification of dynamic fluctuations of nonelectroactive analytes using fast-scan cyclic voltammetry. *Anal Chem*, **85**, 8780-8786.
- Makos, M.A., Han, K.A., Heien, M.L. & Ewing, A.G. (2010) Using In Vivo Electrochemistry to Study the Physiological Effects of Cocaine and Other Stimulants on the *Drosophila melanogaster* Dopamine Transporter. *ACS Chem Neurosci*, **1**, 74-83.
- Makos, M.A., Kim, Y.C., Han, K.A., Heien, M.L. & Ewing, A.G. (2009) In vivo electrochemical measurements of exogenously applied dopamine in *Drosophila melanogaster*. *Anal Chem*, **81**, 1848-1854.

- Manning, B.M., Hebbel, R.P., Gupta, K. & Haynes, C.L. (2012) Carbon-fiber microelectrode amperometry reveals sickle-cell-induced inflammation and chronic morphine effects on single mast cells. *ACS Chem Biol*, **7**, 543-551.
- McElligott, Z.A., Fox, M.E., Walsh, P.L., Urban, D.J., Ferrel, M.S., Roth, B.L. & Wightman, R.M. (2013) Noradrenergic synaptic function in the bed nucleus of the stria terminalis varies in animal models of anxiety and addiction. *Neuropsychopharmacology*, **38**, 1665-1673.
- Mellander, L.J., Trouillon, R., Svensson, M.I. & Ewing, A.G. (2012) Amperometric post spike feet reveal most exocytosis is via extended kiss-and-run fusion. *Sci Rep*, **2**, 907.
- Millar, J. & Barnett, T.G. (1988) Basic instrumentation for fast cyclic voltammetry. *Journal of Neuroscience Methods*, **25**, 91-95.
- Monastirioti, M. (1999) Biogenic amine systems in the fruit fly *Drosophila melanogaster*. *Microsc Res Tech*, **45**, 106-121.
- Mosharov, E.V. & Sulzer, D. (2005) Analysis of exocytotic events recorded by amperometry. *Nat Methods*, **2**, 651-658.
- Murray, B. & Shizgal, P. (1994) Evidence implicating both slow- and fast-conducting fibers in the rewarding effect of medial forebrain bundle stimulation. *Behav Brain Res*, **63**, 47-60.
- Oldenziel, W.H. & Westerink, B.H. (2005) Improving glutamate microsensors by optimizing the composition of the redox hydrogel. *Anal Chem*, **77**, 5520-5528.
- Owesson-White, C.A., Ariansen, J., Stuber, G.D., Cleaveland, N.A., Cheer, J.F., Wightman, R.M. & Carelli, R.M. (2009) Neural encoding of cocaine-seeking behavior is coincident with phasic dopamine release in the accumbens core and shell. *Eur J Neurosci*, **30**, 1117-1127.
- Owesson-White, C.A., Cheer, J.F., Beyene, M., Carelli, R.M. & Wightman, R.M. (2008) Dynamic changes in accumbens dopamine correlate with learning during intracranial self-stimulation. *Proc Natl Acad Sci U S A*, **105**, 11957-11962.
- Owesson-White, C.A., Roitman, M.F., Sombers, L.A., Belle, A.M., Keithley, R.B., Peele, J.L., Carelli, R.M. & Wightman, R.M. (2012) Sources contributing to the average extracellular concentration of dopamine in the nucleus accumbens. *J Neurochem*, **121**, 252-262.
- Pajski, M.L. & Venton, B.J. (2010) Adenosine Release Evoked by Short Electrical Stimulations in Striatal Brain Slices is Primarily Activity Dependent. *ACS Chem Neurosci*, **1**, 775-787.
- Pajski, M.L. & Venton, B.J. (2013) The mechanism of electrically stimulated adenosine release varies by brain region. *Purinergic Signal*, **9**, 167-174.

- Parikh, V., Pomerleau, F., Huettl, P., Gerhardt, G.A., Sarter, M. & Bruno, J.P. (2004) Rapid assessment of in vivo cholinergic transmission by amperometric detection of changes in extracellular choline levels. *Eur J Neurosci*, **20**, 1545-1554.
- Park, J., Bucher, E.S., Fontillas, K., Owesson-White, C., Ariansen, J.L., Carelli, R.M. & Wightman, R.M. (2013) Opposing catecholamine changes in the bed nucleus of the stria terminalis during intracranial self-stimulation and its extinction. *Biol Psychiatry*, **74**, 69-76.
- Park, J., Kile, B.M. & Wightman, R.M. (2009) *In vivo* voltammetric monitoring of norepinephrine release in the rat ventral bed nucleus of the stria terminalis and anteroventral thalamic nucleus. *Eur J Neurosci*, **30**, 2121-2133.
- Park, J., Takmakov, P. & Wightman, R.M. (2011) In vivo comparison of norepinephrine and dopamine release in rat brain by simultaneous measurements with fast-scan cyclic voltammetry. *J Neurochem*, **119**, 932-944.
- Petrovic, J., Walsh, P.L., Thornley, K.T., Miller, C.E. & Wightman, R.M. (2010) Real-time monitoring of chemical transmission in slices of the murine adrenal gland. *Endocrinology*, **151**, 1773-1783.
- Plotsky, P. (1987) Probing Pathways of Neuroendocrine Regulation With Voltammetric Microelectrodes. In Justice, J., Jr. (ed) *Voltammetry in the Neurosciences*. Humana Press, pp. 273-309.
- Ponchon, J.L., Cespuglio, R., Gonon, F., Jouvet, M. & Pujol, J.F. (1979) Normal pulse polarography with carbon fiber electrodes for in vitro and in vivo determination of catecholamines. *Anal Chem*, **51**, 1483-1486.
- Pothos, E.N. (2002) Regulation of dopamine quantal size in midbrain and hippocampal neurons. *Behav Brain Res*, **130**, 203-207.
- Putzbach, W. & Ronkainen, N.J. (2013) Immobilization techniques in the fabrication of nanomaterial-based electrochemical biosensors: a review. *Sensors (Basel)*, **13**, 4811-4840.
- Riday, T.T., Dankoski, E.C., Krouse, M.C., Fish, E.W., Walsh, P.L., Han, J.E., Hodge, C.W., Wightman, R.M., Philpot, B.D. & Malanga, C.J. (2012) Pathway-specific dopaminergic deficits in a mouse model of Angelman syndrome. *J Clin Invest*, **122**, 4544-4554.
- Robinson, D.L., Hermans, A., Seipel, A.T. & Wightman, R.M. (2008) Monitoring rapid chemical communication in the brain. *Chem Rev*, **108**, 2554-2584.
- Ross, A.E., Nguyen, M.D., Privman, E. & Venton, B.J. (2014) Mechanical stimulation evokes rapid increases in extracellular adenosine concentration in the prefrontal cortex. *J Neurochem*, **130**, 50-60.
- Ross, A.E. & Venton, B.J. (2014) Sawhorse waveform voltammetry for selective detection of adenosine, ATP, and hydrogen peroxide. *Anal Chem*, **86**, 7486-7493.

- Sachdev, P.S., Mohan, A., Cannon, E., Crawford, J.D., Silberstein, P., Cook, R., Coyne, T. & Silburn, P.A. (2014) Deep Brain Stimulation of the Antero-Medial Globus Pallidus Interna for Tourette Syndrome. *PLoS One*, **9**, e104926.
- Sanford, A.L., Morton, S.W., Whitehouse, K.L., Oara, H.M., Lugo-Morales, L.Z., Roberts, J.G. & Sombers, L.A. (2010) Voltammetric detection of hydrogen peroxide at carbon fiber microelectrodes. *Anal Chem*, **82**, 5205-5210.
- Sang, J.H. (2001) *Drosophila Melanogaster: The Fruit Fly*. In Reeve, C.R. (ed) *Encyclopedia of Genetics*. Fitzroy Dearborn Publishers, London, pp. 157-162.
- Sarter, M., Parikh, V. & Howe, W.M. (2009) Phasic acetylcholine release and the volume transmission hypothesis: time to move on. *Nat Rev Neurosci*, **10**, 383-390.
- Schluter, E.W., Mitz, A.R., Cheer, J.F. & Aeverbeck, B.B. (2014) Real-time dopamine measurement in awake monkeys. *PLoS One*, **9**, e98692.
- Schmidt, A.C., Dunaway, L.E., Roberts, J.G., McCarty, G.S. & Sombers, L.A. (2014) Multiple scan rate voltammetry for selective quantification of real-time enkephalin dynamics. *Anal Chem*, **86**, 7806-7812.
- Schmidt, A.C., Wang, X., Zhu, Y. & Sombers, L.A. (2013) Carbon nanotube yarn electrodes for enhanced detection of neurotransmitter dynamics in live brain tissue. *ACS Nano*, **7**, 7864-7873.
- Schmitt, L.I., Sims, R.E., Dale, N. & Haydon, P.G. (2012) Wakefulness affects synaptic and network activity by increasing extracellular astrocyte-derived adenosine. *J Neurosci*, **32**, 4417-4425.
- Schober, A. (2004) Classic toxin-induced animal models of Parkinson's disease: 6-OHDA and MPTP. *Cell and Tissue Research*, **318**, 215-224.
- Schroeder, T.J., Jankowski, J.A., Senyshyn, J., Holz, R.W. & Wightman, R.M. (1994) Zones of exocytotic release on bovine adrenal medullary cells in culture. *J Biol Chem*, **269**, 17215-17220.
- Slaney, T.R., Nie, J., Hershey, N.D., Thwar, P.K., Linderman, J., Burns, M.A. & Kennedy, R.T. (2011) Push-pull perfusion sampling with segmented flow for high temporal and spatial resolution in vivo chemical monitoring. *Anal Chem*, **83**, 5207-5213.
- Sokolowski, M.B. (2001) *Drosophila*: genetics meets behaviour. *Nat Rev Genet*, **2**, 879-890.
- Stamford, J.A. (1989) In vivo voltammetry--prospects for the next decade. *Trends Neurosci*, **12**, 407-412.
- Stamford, J.A., Palij, P., Davidson, C., Jorm, C.M. & Millar, J. (1993) Simultaneous "real-time" electrochemical and electrophysiological recording in brain slices with a single carbon-fibre microelectrode. *J Neurosci Methods*, **50**, 279-290.

- Stefurak, T., Mikulis, D., Mayberg, H., Lang, A.E., Hevenor, S., Pahapill, P., Saint-Cyr, J. & Lozano, A. (2003) Deep brain stimulation for Parkinson's disease dissociates mood and motor circuits: a functional MRI case study. *Mov Disord*, **18**, 1508-1516.
- Street, S.E., Kramer, N.J., Walsh, P.L., Taylor-Blake, B., Yadav, M.C., King, I.F., Vihko, P., Wightman, R.M., Millan, J.L. & Zylka, M.J. (2013) Tissue-nonspecific alkaline phosphatase acts redundantly with PAP and NT5E to generate adenosine in the dorsal spinal cord. *J Neurosci*, **33**, 11314-11322.
- Street, S.E., Walsh, P.L., Sowa, N.A., Taylor-Blake, B., Guillot, T.S., Vihko, P., Wightman, R.M. & Zylka, M.J. (2011) PAP and NT5E inhibit nociceptive neurotransmission by rapidly hydrolyzing nucleotides to adenosine. *Mol Pain*, **7**, 80.
- Sunsay, C. & Rebec, G.V. (2014) Extinction and Reinstatement of Phasic Dopamine Signals in the Nucleus Accumbens Core During Pavlovian Conditioning. *Behav Neurosci*.
- Swamy, B.E. & Venton, B.J. (2007a) Carbon nanotube-modified microelectrodes for simultaneous detection of dopamine and serotonin in vivo. *Analyst*, **132**, 876-884.
- Swamy, B.E. & Venton, B.J. (2007b) Subsecond detection of physiological adenosine concentrations using fast-scan cyclic voltammetry. *Anal Chem*, **79**, 744-750.
- Swiergiel, A.H., Palamarchouk, V.S. & Dunn, A.J. (1997) A new design of carbon fiber microelectrode for in vivo voltammetry using fused silica. *J Neurosci Methods*, **73**, 29-33.
- Takmakov, P., McKinney, C.J., Carelli, R.M. & Wightman, R.M. (2011) Instrumentation for fast-scan cyclic voltammetry combined with electrophysiology for behavioral experiments in freely moving animals. *Rev Sci Instrum*, **82**, 074302.
- Thompson, J.E., Vickroy, T.W. & Kennedy, R.T. (1999) Rapid determination of aspartate enantiomers in tissue samples by microdialysis coupled on-line with capillary electrophoresis. *Anal Chem*, **71**, 2379-2384.
- van Dijk, A., Klomp makers, A.A., Feenstra, M.G. & Denys, D. (2012) Deep brain stimulation of the accumbens increases dopamine, serotonin, and noradrenaline in the prefrontal cortex. *J Neurochem*, **123**, 897-903.
- Venton, B.J., Michael, D.J. & Wightman, R.M. (2003) Correlation of local changes in extracellular oxygen and pH that accompany dopaminergic terminal activity in the rat caudate-putamen. *J Neurochem*, **84**, 373-381.
- Vickrey, T.L., Condrón, B. & Venton, B.J. (2009) Detection of endogenous dopamine changes in *Drosophila melanogaster* using fast-scan cyclic voltammetry. *Anal Chem*, **81**, 9306-9313.
- Vickrey, T.L. & Venton, B.J. (2011) *Drosophila* Dopamine₂-like receptors function as autoreceptors. *ACS Chem Neurosci*, **2**, 723-729.

- Wang, J., Trouillon, R., Dunevall, J. & Ewing, A.G. (2014) Spatial resolution of single-cell exocytosis by microwell-based individually addressable thin film ultramicroelectrode arrays. *Anal Chem*, **86**, 4515-4520.
- Wang, J., Trouillon, R., Lin, Y., Svensson, M.I. & Ewing, A.G. (2013) Individually addressable thin-film ultramicroelectrode array for spatial measurements of single vesicle release. *Anal Chem*, **85**, 5600-5608.
- Wang, M., Roman, G.T., Schultz, K., Jennings, C. & Kennedy, R.T. (2008) Improved temporal resolution for in vivo microdialysis by using segmented flow. *Anal Chem*, **80**, 5607-5615.
- Wang, M., Slaney, T., Mabrouk, O. & Kennedy, R.T. (2010) Collection of nanoliter microdialysate fractions in plugs for off-line in vivo chemical monitoring with up to 2 s temporal resolution. *J Neurosci Methods*, **190**, 39-48.
- Weinshenker, D. (2008) Functional consequences of locus coeruleus degeneration in Alzheimer's disease. *Curr Alzheimer Res*, **5**, 342-345.
- Westerink, R.H. & Ewing, A.G. (2008) The PC12 cell as model for neurosecretion. *Acta Physiol (Oxf)*, **192**, 273-285.
- Wightman, R.M., Amatore, C., Engstrom, R.C., Hale, P.D., Kristensen, E.W., Kuhr, W.G. & May, L.J. (1988) Real-time characterization of dopamine overflow and uptake in the rat striatum. *Neuroscience*, **25**, 513-523.
- Wightman, R.M., Heien, M.L., Wassum, K.M., Sombers, L.A., Aragona, B.J., Khan, A.S., Ariansen, J.L., Cheer, J.F., Phillips, P.E. & Carelli, R.M. (2007) Dopamine release is heterogeneous within microenvironments of the rat nucleus accumbens. *Eur J Neurosci*, **26**, 2046-2054.
- Wightman, R.M. & Zimmerman, J.B. (1990) Control of dopamine extracellular concentration in rat striatum by impulse flow and uptake. *Brain Res Brain Res Rev*, **15**, 135-144.
- Wilson, G.S. & Johnson, M.A. (2008) In-vivo electrochemistry: what can we learn about living systems? *Chem Rev*, **108**, 2462-2481.
- Wise, R.A. (1996) Addictive drugs and brain stimulation reward. *Annu Rev Neurosci*, **19**, 319-340.
- Xiao, N., Privman, E. & Venton, B.J. (2014) Optogenetic control of serotonin and dopamine release in *Drosophila* larvae. *ACS Chem Neurosci*.
- Xiao, N. & Venton, B.J. (2012) Rapid, sensitive detection of neurotransmitters at microelectrodes modified with self-assembled SWCNT forests. *Anal Chem*, **84**, 7816-7822.
- Yoshimi, K., Naya, Y., Mitani, N., Kato, T., Inoue, M., Natori, S., Takahashi, T., Weitemier, A., Nishikawa, N., McHugh, T., Einaga, Y. & Kitazawa, S. (2011) Phasic reward responses in the monkey striatum as detected by voltammetry with diamond microelectrodes. *Neurosci Res*, **71**, 49-62.

- Zachek, M.K., Park, J., Takmakov, P., Wightman, R.M. & McCarty, G.S. (2010a) Microfabricated FSCV-compatible microelectrode array for real-time monitoring of heterogeneous dopamine release. *Analyst*, **135**, 1556-1563.
- Zachek, M.K., Takmakov, P., Park, J., Wightman, R.M. & McCarty, G.S. (2010b) Simultaneous monitoring of dopamine concentration at spatially different brain locations in vivo. *Biosens Bioelectron*, **25**, 1179-1185.
- Zestos, A.G., Jacobs, C.B., Trikantopoulos, E., Ross, A.E. & Venton, B.J. (2014) Polyethyleneimine Carbon Nanotube Fiber Electrodes For Enhanced Detection of Neurotransmitters. *Anal Chem*.
- Zhang, B., Heien, M.L., Santillo, M.F., Mellander, L. & Ewing, A.G. (2011) Temporal resolution in electrochemical imaging on single PC12 cells using amperometry and voltammetry at microelectrode arrays. *Anal Chem*, **83**, 571-577.
- Zhang, D.A., Rand, E., Marsh, M., Andrews, R.J., Lee, K.H., Meyyappan, M. & Koehne, J.E. (2013) Carbon nanofiber electrode for neurochemical monitoring. *Mol Neurobiol*, **48**, 380-385.
- Zhao, J., Zhang, X., Di, J., Xu, G., Yang, X., Liu, X., Yong, Z., Chen, M. & Li, Q. (2010) Double-peak mechanical properties of carbon-nanotube fibers. *Small*, **6**, 2612-2617.

CHAPTER 2: ELECTRICAL STIMULATION OF THE DORSAL NORADRENERGIC BUNDLE EVOKES NOREPINEPHRINE OVERFLOW IN THE BED NUCLEUS OF THE STRIA TERMINALIS THROUGH A NON-COERULEAN PATHWAY

Introduction

The central noradrenergic system, composed of seven cell populations seated in the pons and medulla oblongata, broadly innervates most cerebral structures to influence processes as diverse as arousal, nociception, and addiction (Berridge & Waterhouse, 2003; Weinshenker & Schroeder, 2007; Pertovaara, 2013). In general the projections of this system terminate as diffuse varicosities (Szabadi, 2013), making the study of noradrenergic neurotransmission analytically challenging. However, there are several structures that receive dense noradrenergic input, one of these being the bed nucleus of the stria terminalis (BNST), a limbic region that mediates behavioral and physiological responses to stress (Forray & Gysling, 2004; Crestani *et al.*, 2013). This innervation is most concentrated in the ventral (v) portion of this structure, which notably contains the highest norepinephrine terminal density within the entire brain (Kilts & Anderson, 1986; Phelix *et al.*, 1992).

Noradrenergic innervation of the brain is provided via two anatomically and functionally distinct ascending pathways, the dorsal noradrenergic bundle (DNB) and the ventral noradrenergic bundle (VNB) (Szabadi, 2013). The BNST is primarily targeted by medullary neurons coursing through the VNB (Terenzi & Ingram, 1995; Forray *et al.*, 2000), though a small norepinephrine contribution does arise from the locus coeruleus (LC, A6) (Lindvall & Stenevi, 1978; Moore, 1978; Phelix *et al.*, 1992), the source of the DNB. In past work, we targeted these pathways by electrical stimulation to study vBNST norepinephrine dynamics with fast-scan cyclic voltammetry (FSCV) (Park *et al.*, 2009). At the coordinates

employed, the ~ 2 mm dorsal-ventral spacing of the DNB and VNB allowed each to be targeted independently with stimulation (Ungerstedt, 1971). Accordingly, norepinephrine release in the vBNST was found to peak at stimulation depths consistent with anatomical reports for the DNB and VNB. In the anteroventral thalamus (AV), a region receiving heavy input from the LC, norepinephrine release could be evoked by stimulation at the depth of the DNB but not the VNB, further supporting discrete activation of these pathways.

More notably, we found that DNB and VNB stimulation produced similar norepinephrine overflow in the vBNST despite the difference between their respective inputs—suggesting the DNB may play a larger role in BNST noradrenergic transmission than originally thought. The possibility of a significant DNB-BNST connection was further substantiated by LC stimulation, which also induced norepinephrine release in this terminal region. However, electrical stimulation is a relatively non-selective means of neuronal activation and can simultaneously depolarize cell bodies, afferent terminals, and fibers of passage—such as the DNB—within the vicinity of the electrode (Ranck, 1975; McIntyre & Grill, 2002; Histed *et al.*, 2009). It is therefore possible that norepinephrine release in the vBNST is caused by stimulation of surrounding neuronal elements or even by antidromic activation of the DNB (Pinault, 1995; Waters *et al.*, 2005).

Here we employ FSCV and selective lesioning strategies to investigate the origins of DNB-stimulated norepinephrine release within the vBNST. DSP-4, which causes degradation of DNB axons, was administered to assess whether release could be evoked in the BNST when the LC norepinephrine system was compromised. In a separate set of animals, the excitotoxic agent ibotenic acid was applied at the stimulation coordinates to ascertain the contribution of local cell body activation. These treatments were repeated for norepinephrine measurements in the AV as a control. Electrochemical results are considered in the context of behavioral observations to suggest potential pathways by which BNST norepinephrine release occurs with electrical stimulation of the DNB.

Experimental

Drugs and reagents

All drugs and reagents were used as received from Sigma-Aldrich (St Louis, MO, USA), unless otherwise noted.

Animals

Sprague-Dawley rats (300 – 400g, Charles River, Wilmington, MA, USA) were pair-housed in a 12-h light cycle, temperature- and humidity-controlled environment with food and water available ad libitum. Care was taken to minimize the number of animals used in this study (47 total) and their suffering. All procedures were conducted according to the NIH Guide for Care and Use of Laboratory Animals and were approved by the Institutional Animal Care and Use Committee of the University of North Carolina at Chapel Hill.

Surgeries

For non-recovery experiments, rats were anesthetized with urethane (1.5 mg/kg) and immobilized in a stereotaxic frame (Kopf, Tujunga, CA, USA). The skull was exposed, and holes were drilled for electrode placements based on coordinates referenced from bregma (Paxinos & Watson, 2007). In each animal a carbon-fiber microelectrode (75–100 μ m exposed tip length, 5 μ m diameter, T-650; Amoco, Greenville, SC, USA) (Cahill *et al.*, 1996) was lowered into the vBNST (anterior-posterior (AP) +0.0 mm, medial-lateral (ML) +1.2 mm, dorsal-ventral (DV) -7.2 to -7.8 mm) or the AV (AP -2.1, ML +1.4, and DV 5.0 to -6.0 mm). In the contralateral hemisphere, a Ag/AgCl reference electrode was implanted and secured to the skull with a jeweler's screw.

Ipsilaterally to the carbon-fiber microelectrode, a stainless steel, bipolar stimulating electrode (Plastics One, West Lafayette, IN, USA) was positioned within a dorsal-ventral tract (AP -5.2 mm, ML +1.2 mm) targeting the DNB (DV -5.5 to -6.5 mm) and the VNB (DV -

8.0 to -8.5 mm). In select animals, a stimulating electrode was also implanted into the LC (AP -9.8 mm, ML +1.4 mm, DV -6.5 to -7.5 mm). The prongs of the stimulating electrodes were positioned 1.0 mm apart and were insulated to the tips. Electrical stimulations ($\pm 300 \mu\text{A}$, 60 biphasic pulses, 2 ms per pulse, 60 Hz) were generated through a pair of commercial stimulators (NL 800A, Neurolog, Digitimer, Hertfordshire, UK) optically isolated from the electrochemical system.

Recovery surgeries followed a similar protocol. Rats were maintained under anesthesia with constant flow of isoflurane (1.5–2.0%) during surgical procedures, where a single stimulating electrode was implanted into the DNB (DV -6.0 mm). The stimulating electrode was secured in place with screws and dental cement. Post-operation rats were provided Tylenol (15 mg/kg) and closely monitored. Animals were allowed a 3 day recovery period before behavioral experiments commenced.

Voltammetric measurements

Fast-scan cyclic voltammetry was computer controlled using HDCV (UNC-Chapel Hill, NC, USA) (Bucher *et al.*, 2013) a data acquisition program based in LabVIEW (National Instruments, Austin, TX, USA), and the electrochemical signals were transduced with a locally constructed UEI potentiostat (UNC Department of Chemistry Electronics Design Facility). Norepinephrine detection was performed using a triangular waveform scanning between -0.4 V to 1.3 V at 400 V/s. The carbon-fiber microelectrode was preconditioned with the waveform (15 min at 60 Hz followed by 15 min at 10 Hz) before recordings were made at a 10 Hz application frequency.

The waveform used in this study cannot distinguish norepinephrine from dopamine, another catecholamine prevalent in the brain (Park *et al.*, 2011). To confirm that the recorded signal was not due to dopamine, animals were given raclopride (2 mg/kg, i.p., dopamine D2 autoreceptor antagonist), and, if not already administered, idazoxan (5 mg/kg,

i.p., α_2 autoreceptor antagonist) at the end of each experiment. In animals where the signal was abolished with ibotenic acid, the stimulating electrode was repositioned within the VNB to obtain a new baseline for release before this pharmacological procedure commenced. Only data from locations that selectively increased to idazoxan were included in this study.

DSP-4

Juvenile rats (150 – 200 g) were administered DSP-4 (N-(2-chloroethyl)-N-ethyl-2-bromobenzylamine) in two doses (0.5 mL, 50 mg/kg, i.p.) provided 3 days apart (Bucher *et al.*, 2014). As DSP-4 is unstable in solution (Ross *et al.*, 1973) it was dissolved in sterile saline immediately before its use. Voltammetric and tissue content experiments were conducted 10 to 15 days after the last dose.

Ibotenic acid infusion

Electrical stimulation of the DNB was repeated every 3 min over a 1 h period to establish a baseline for norepinephrine release. Thereafter the stimulating electrode was removed and the tip of a 2 μ L Hamilton syringe containing sterile saline was positioned 500 μ m dorsal to the original stimulation depth. The saline was infused manually with a microinjection unit (Model 500, Kopf, Tujunga, CA, USA) over a 20 min period and the syringe was removed for reinsertion of the stimulating electrode. Stimulations commenced for another 1 h period before the infusion procedure was repeated with 2 μ L ibotenic acid (130 mM in 2% Chicago Sky Blue prepared in sterile saline, Abcam, Cambridge, MA, USA). The last 15 min of data collected for baseline, post-saline and post-IBA were used in analysis.

Histology

At the end of voltammetric experiments, recording locations were lesioned by

applying a DC voltage (10 V, 30 s) to the carbon-fiber microelectrodes. Animals were then euthanized with an overdose of urethane and decapitated. Brains were quickly removed and stored in a 10% formalin solution for at least 3 days before sectioned into 50 µm slices with a cryostat (Leica, Wetzlar, Germany). To locate the lesions slices were mounted onto glass slides and viewed under a light microscope.

Tissue content analysis

Urethane (1.5 mg/kg) anesthetized rats separate from those used in the voltammetry experiments were decapitated and their brains were rapidly removed and placed on ice. Coronal sections (300 µm thick) containing the BNST or AV were collected with a VF-200 Compresstome (Precisionary Instruments Greenville, NC) in ice cold artificial cerebral spinal fluid (aCSF). The aCSF contained (in mM) 126 NaCl, 25 NaHCO₃, 2.45 KCl, 12 NaH₂PO₄, 1.2 MgCl₂, 2.4 CaCl₂, 20 HEPES, and 11 glucose, and was adjusted to pH 7.4 and saturated with 95% O₂ /5% CO₂. Tissue containing the vBNST or AV was excised bilaterally with a 1 mm punch, and collected into pre-weighed tubes. The samples were mixed with 200 µL of 0.1 N HClO₄ containing 1 µM hydroquinone, the internal standard, and subsequently homogenized using a sonic dismembrator (Fisher Scientific, Model 60, Pittsburgh, PA, USA). The homogenate was spun down at 6000 rpm for 10 minutes, and the supernatant was removed and filtered using a 0.2 µm syringe filter. High performance liquid chromatography was performed using the methods of Mefford and Lähdesmäki *et al* (Mefford, 1981; Lahdesmaki *et al.*, 2002). Briefly, 20 µL injections were made onto a reversed-phase column (5 µm, 4.6 x 5 mm, Waters Atlantis, Milford, MA, USA). The mobile phase consisted of 0.1 M citric acid, 1 mM sodium hexylsulfate, 0.1 mM EDTA (pH = 3), and 10% methanol organic modifier at a flow rate of 1.0 mL/min. Norepinephrine and dopamine were detected with a thin layer radial electrochemical cell (BASi, West Lafayette, IN, USA) at a potential of +800 mV vs Ag/AgCl. Data were collected at 60 Hz using a LabVIEW stripchart recorder program

(Jorgenson Lab, UNC) and homebuilt electronics. Concentration was determined by a ratio of analyte peak area to internal standard peak area, and normalized to wet tissue weight.

Behavioral assessment

Behavioral tests were conducted in a 43 x 43 x 43 cm Plexiglas chamber housed in a sound-attenuated cubicle (Med Associates, St. Albans, Vermont). During testing, a house light mounted 48 cm above the floor was used to illuminate the box for video recording during all trials. After an initial habituation period (15 min), calibration of the stimulation intensity was performed for each rat by increasing the stimulation current (60 Hz, 40 biphasic pulses, 2 ms per pulse) until robust escape behaviors (i.e. scurrying and/or jumping) were elicited by the stimulation. Next, analogous to the generation of 'response rate-frequency' functions in intracranial self-stimulation paradigms, the frequency of the stimulation was varied over a range of values (3, 9, 15, 30, 45, 60 Hz) in order of increasing frequency (Gallistel & Freyd, 1987; Carlezon & Chartoff, 2007). The number of pulses delivered was adjusted to maintain the same total duration of stimulation for all frequencies studied. Trials did not begin until the rat was exhibiting or had resumed exploratory behavior. During the trials, ultrasonic vocalizations were recorded using an omnidirectional electret microphone (Challenge Electronics, Deer Park, NY) and homebuilt electronics. Vocalization data were collected at 100 kHz using HDCV and were analyzed using LabView. Behavioral responses to the stimulation were classified as scurrying, jumping, or neither. Behavioral scoring for the two minutes following stimulation was performed using a time-sampling approach, where the rat was scored for freezing or scanning behavior during 5 second bins for their entirety ('whole interval sampling')(Tyler, 1979). The results from the individual bins were then aggregated to provide an overall 'one-zero' score for the entire two-minute period, with the presence of the behavior during any individual bin being counted as a positive result.

Data analysis

Electrochemical data were processed with the companion HDCV data analysis program. Each data set was digitally filtered (4th order low pass Bessel, 20 KHz cutoff) and background subtracted from baseline currents. Principal component regression, a multivariate chemometric algorithm (Heien *et al.*, 2004; Keithley & Wightman, 2011), was used to determine concentrations based on averaged post-calibration factors obtained in a flow injection analysis system. Cyclic voltammograms for a range of norepinephrine and pH concentrations were obtained at the end of each experiment by pharmacological manipulation (IDA or DMI) and by varying the strength of the stimulation (10-120 p). Training sets were generated from at least 5 cyclic voltammograms for each analyte, and their statistical soundness was assessed by tools provided in HDCV data analysis (Keithley & Wightman, 2011; Bucher *et al.*, 2013).

Peak amplitude and half-life ($t_{1/2}$) were calculated using Clampfit 10.2, a component of the pCLAMP 10.2 software package (Axon Instruments, Foster City, CA, USA). Results are presented as mean \pm SEM with 'n' values indicating the number of animals unless otherwise noted. Statistical significances were determined in GraphPad Prism 4.0 (GraphPad Software, San Diego, CA, USA) using 2-way analysis of variance (ANOVA) with post-hoc Bonferroni tests and unpaired student's t-tests. Differences were considered significant when $P < 0.05$. Behavioral data were analyzed in R using a Firth's biased-reduced logistic regression.

Results

Measurement of norepinephrine in target regions

In this study norepinephrine release and uptake were measured in the anteroventral thalamus (AV) and the ventral bed nucleus of the stria terminalis (vBNST), brain regions receiving significant input from coerulean and medullary noradrenergic cell groups

respectively. The left panels in Figure 2.1 provide histological images of the areas probed in these two terminal structures, where electrical stimulation of the DNB elicits a transient increase in extracellular norepinephrine that is measurable with FSCV (Park *et al.*, 2009). Example recordings capturing these rapid release events are shown in the right panels of Figure 2.1. Color plots are used to map voltammetric data over time, with the voltage scan plotted on the y-axis, the time of acquisition on the x-axis, and currents in false color. Shortly after electrical stimulation, current features appear at 0.65 V and -0.2 V due to the oxidation of norepinephrine and the subsequent reduction of its *o*-quinone form. Cyclic voltammograms representing these redox processes are provided as insets for the times of peak release. Additional current features are also apparent after the electrical stimulation in Figure 2.1B. These arise from an alkaline pH shift believed to occur from increased local perfusion (Venton *et al.*, 2003; Bucher *et al.*, 2014). To remove pH contributions, all norepinephrine concentration changes were determined with principal component regression (see *Methods*). The extracted concentration traces above the color plots show a quick rise and decay in extracellular norepinephrine after the electrical stimulations. The rising phase is controlled by release/uptake dynamics and the falling phase principally by uptake (Wightman *et al.*, 1988; Wightman & Zimmerman, 1990; Park *et al.*, 2009). As uptake is mediated by the norepinephrine transporter, clearance half-life ($t_{1/2}$), defined as the time it takes for peak norepinephrine levels to fall to 50%, is a measure of transporter function (Yorgason *et al.*, 2011). With DNB stimulation the average peak release recorded in the vBNST was $0.276 \pm 0.014 \mu\text{M}$ with an average $t_{1/2}$ of $2.4 \pm 0.3 \text{ s}$ ($n=10$). Release in the AV ($n=5$) was on average smaller ($0.216 \pm 0.035 \mu\text{M}$) and cleared faster ($t_{1/2} = 1.7 \pm 0.5 \text{ s}$) than in the BNST ($n=10$), but not to a significant extent (unpaired student's t-test, $[\text{NE}]_{\text{max}}$: $t(13)=0.609$, $P=0.553$; $t_{1/2}$: $t(13)=1.566$, $P=0.141$). DSP-4 is a neurotoxin that selectively degrades the noradrenergic fibers coursing from the LC via the DNB (Fritschy & Grzanna, 1989; Wolfman *et al.*, 1994; Toussay *et al.*, 2013).

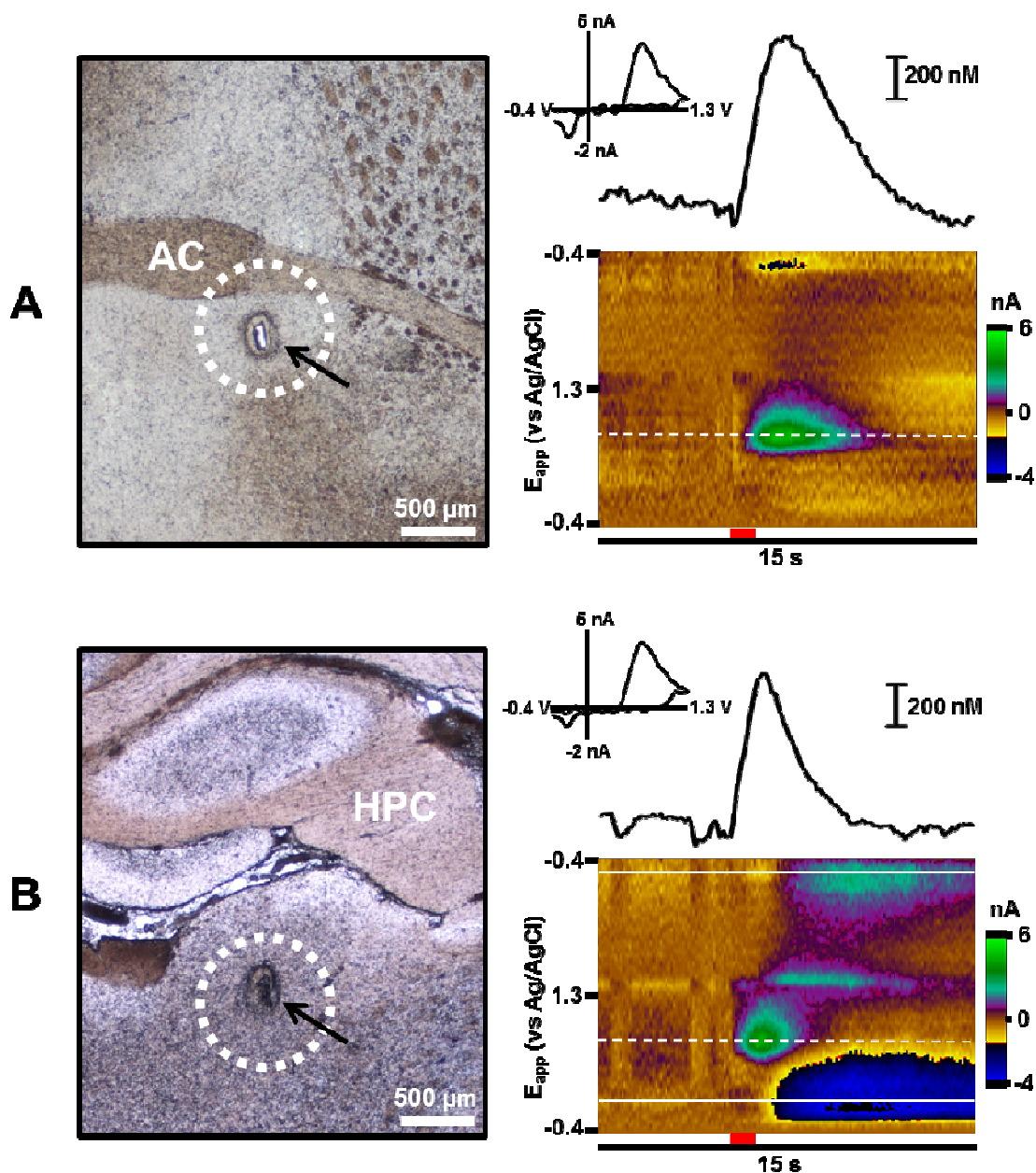


Figure 2.1. Measurement of norepinephrine in the AV and the vBNST. Left panels: histology of the vBNST (A) and the AV (B). Electrode lesions are indicated by black arrows, and the areas sampled for tissue content analysis are marked by the white dashed circles. Right panels: examples of voltammetric data obtained for norepinephrine release in the vBNST (A) and the AV (B) with electrical stimulation of the DNB. Timing of electrical stimulation is denoted by the red bars on the time axes. The potential for norepinephrine oxidation is indicated by the white-dashed lines in the color plots. Features due to shifts in pH are indicated by the solid white lines. Norepinephrine concentrations over time and cyclic voltammograms extracted from the time of peak release are shown above the color plots. Abbreviations: AC, anterior commissure; HPC, hippocampus.

Effects of DSP-4 on catecholamine tissue content in the vBNST and AV

To assess the regional effects of DSP-4 neurotoxicity, tissue content analysis was performed by HPLC to determine the amounts of norepinephrine and its metabolic precursor, dopamine, present in the vBNST and the AV (Table 1). Tissue was excised, as demonstrated in Figure 2.1 (left panels), from freshly dissected brains taken from untreated rats and rats treated with DSP-4. Control values for the vBNST and the AV are similar to those previously reported from our lab (Park *et al.*, 2009; McElligott *et al.*, 2013) and others (Oke *et al.*, 1983; Kilts & Anderson, 1986). DSP-4 treatment significantly reduced norepinephrine and dopamine in the AV (unpaired student's t-test, NE: $t(9)=3.579$, $P=0.006$; DA: $t(9)=2.586$, $P=0.029$), but did not exhibit an effect on the catecholamine content of the vBNST (NE: $t(9)=0.959$, $P=0.363$; DA: $t(9)=0.371$, $P=0.719$).

Electrically-stimulated norepinephrine release in the AV after DSP-4

The effects of DSP-4 lesioning on norepinephrine overflow in the AV were assayed with FSCV (Figure 2.2). In these experiments, the depths of the carbon-fiber and stimulating electrodes were adjusted to maximize the amount of norepinephrine release observed with electrical stimulation of the DNB. Once electrode positions were optimized, stimulations were repeated every 3 min to record a baseline for release. This was followed by administration of the norepinephrine α_2 autoreceptor antagonist, idazoxan, and the norepinephrine transporter (NET) blocker, desipramine (injected 30 min later). In control animals, the respective actions of these drugs increase the amount and duration of electrically-stimulated release (Figure 2.2A).

With DSP-4-treatment, baseline norepinephrine release was significantly attenuated ($[NE]_{\max} = 0.095 \pm 0.038 \mu\text{M}$, unpaired student's t-test, $t(8)=2.363$, $P=0.046$, $n=5$ for each group) compared to control (Figure 2.2B). When comparing the effects of the norepinephrine drugs on maximal release in untreated and DSP-4 treated rats, there was a main effect of

Region	NE ($\mu\text{g/g}$ Tissue)		DA ($\mu\text{g/g}$ Tissue)	
	Untreated	DSP-4	Untreated	DSP-4
vBNST	2.98 ± 0.80	2.14 ± 0.58	0.82 ± 0.25	0.84 ± 0.17
AV	1.82 ± 0.50	$0.18 \pm 0.10^{**}$	1.62 ± 0.52	$0.34 \pm 0.20^*$

Table 2.1. Catecholamine tissue content in the AV and the vBNST for untreated and DSP-4-treated animals. Values are shown as mean \pm SEM. *P < 0.05, **P < 0.01, compared to untreated values. Abbreviations: NE, norepinephrine; DA, dopamine.

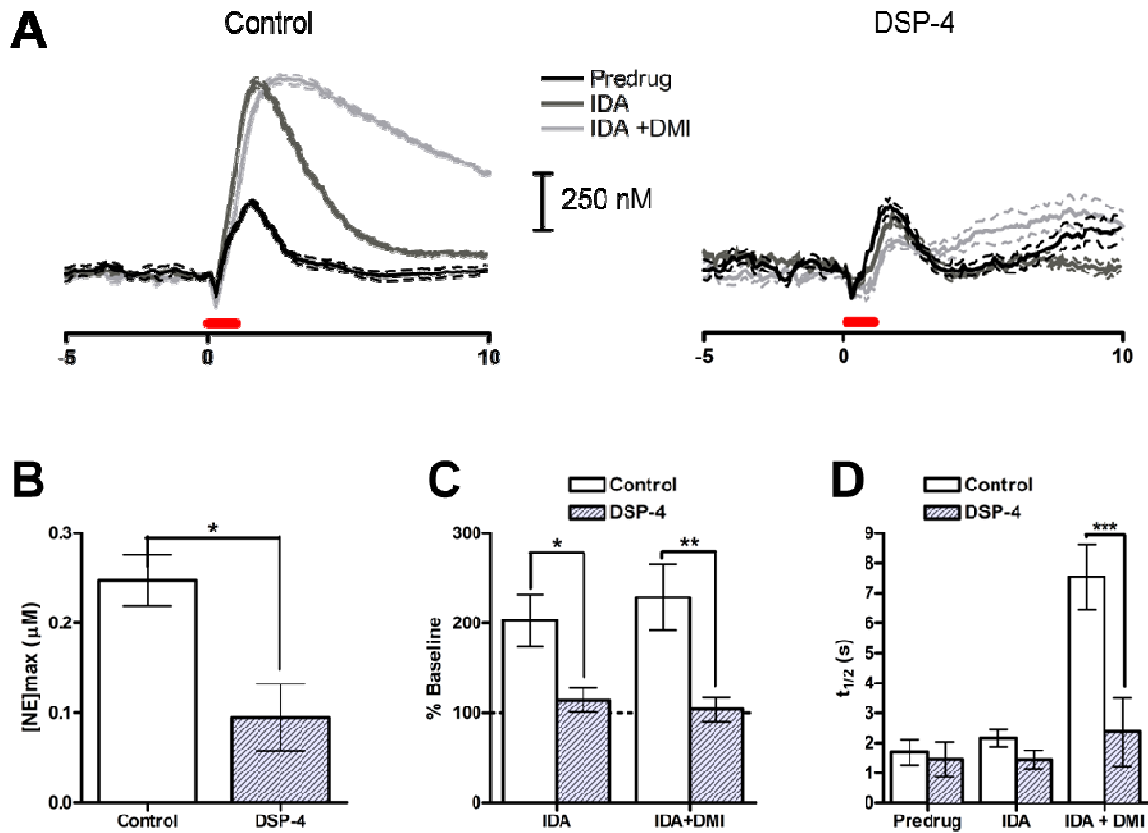


Figure 2.2. Effects of DSP-4 on electrically-stimulated norepinephrine release in the AV. (A) Representative norepinephrine release profiles before and after administration of norepinephrine autoreceptor (IDA, idaxozan, 5 mg/kg, i.p.) and uptake inhibitors (DMI, desipramine, 15 mg/kg, i.p.). Stimulation timing is denoted by the bars along the time axes. $n = 4$ trials, error bars provided as SEM. (B) Maximum release in control and DSP-4-treated animals. (C) Change in release amplitudes after administration of noradrenergic drugs. (D) Clearance half-life after administration of noradrenergic drugs. (B-D) $n = 5$ for control and DSP-4 groups. * $P < 0.05$, ** $P < 0.01$, *** $P < 0.001$.

DSP-4 (2-way ANOVA, $F_{1,16}=17.80$, $P=0.0007$) but no effect of drug ($F_{1,16}=0.939$, $P=0.763$) or interaction ($F_{1,16}=0.514$, $P=0.484$). Post-hoc analysis revealed significant differences between untreated and DSP-4 treated animals in maximal release amplitudes with idazoxan ($203 \pm 29\%$ vs $115 \pm 13\%$, $n=5$ respectively, $P<0.05$) and idazoxan/desipramine ($229 \pm 37\%$ vs $104 \pm 14\%$, $n=5$ respectively, $P<0.01$) on board. There were also significant differences in the effects of the drugs on clearance half-life in untreated and DSP-4 treated animals (2-way ANOVA). Main effects were found for the drugs administered ($F_{2,24}=13.44$, $P=0.0001$) and for DSP-4-treatment ($F_{2,24}=11.78$, $P=0.002$), and these were found to have a significant interaction ($F_{2,24}=6.962$, $P=0.004$). In post-hoc analysis, no significant differences were found in clearance half-life in pre-drug (1.7 ± 0.4 s vs 1.5 ± 0.6 s, $n=5$ respectively, $P>0.05$) or post-idazoxan values (2.2 ± 0.3 s vs 1.5 ± 0.6 s, $n=5$ respectively, $P>0.05$), but a significant difference was found after administration of both idazoxan and desipramine (7.5 ± 1.1 s vs 2.4 ± 1.2 s, $n=5$ respectively, $P<0.001$).

Electrically-stimulated norepinephrine release in the vBNST after DSP-4

The effects of DSP-4 lesioning on norepinephrine overflow in the vBNST were also investigated with FSCV (Figure 2.3). In this set of experiments, the depth of the carbon-fiber microelectrode was optimized with the stimulating electrode positioned in the VNB. As in past work (Park *et al.*, 2009), maximum norepinephrine released was observed when the carbon-fiber was positioned just under the anterior commissure (Figure 2.1A). Thereafter, the position of the carbon-fiber microelectrode was kept constant as the placement of the stimulating electrode was adjusted dorsally to determine the maximum amount of norepinephrine release elicited by stimulation of the DNB (Figure 2.3A). In some animals the stimulating electrode was then removed and lowered into the LC, the origin of DNB fibers, to find the maximum amount of release evoked by direct cell body stimulation.

In untreated and DSP-4 treated animals, maximal norepinephrine concentrations

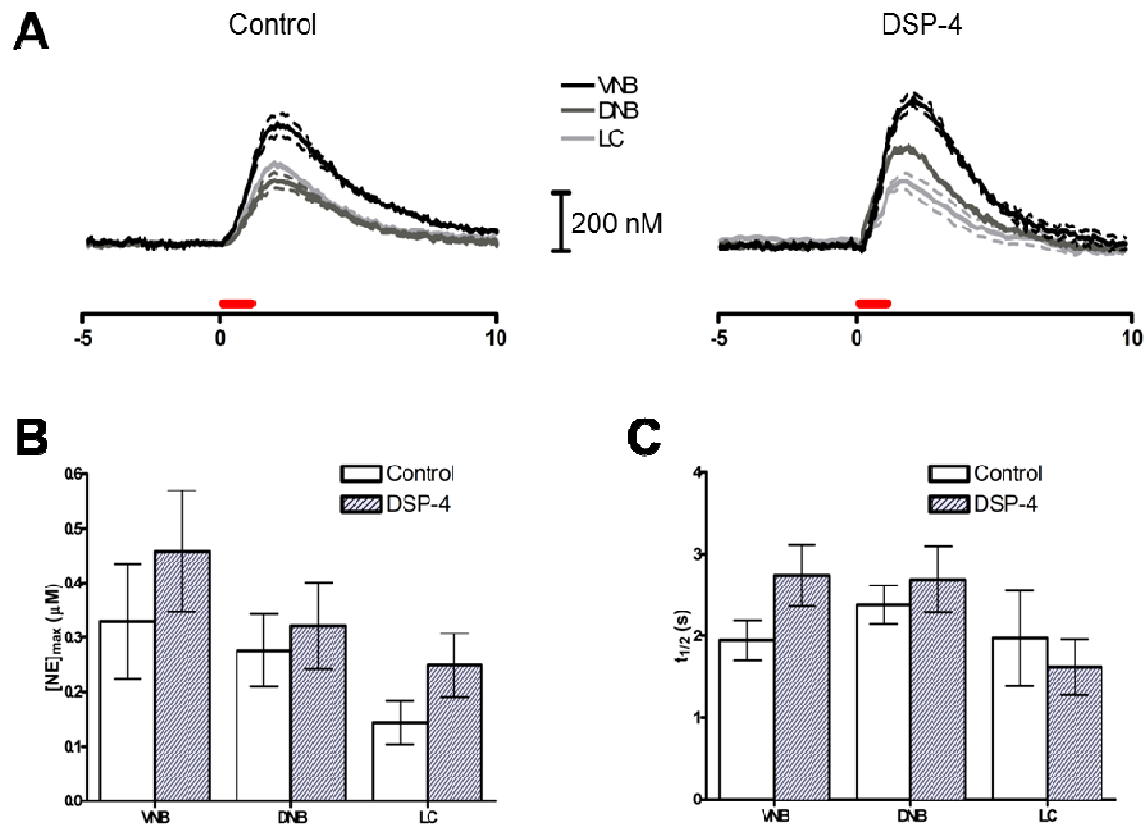


Figure 2.3. Effects of DSP-4 on electrically-stimulated norepinephrine release in the vBNST. (A) Representative norepinephrine release profiles for a single recording location with the stimulating electrode placed within the VNB, DNB or the LC. Stimulation timing is denoted by the bars along the time axes. $n = 4$ trials, error bars provided as SEM. (B) Maximum release in control and DSP-4-treated animals for different stimulation placements. (C) Clearance half-life in control and DSP-4-treated animals for different stimulation placements. (B-D) $n = 9$ and 10 respectively for VNB control/DSP-4, $n = 10$ for DNB control/DSP-4, $n=5$ and 6 respectively for LC control/DSP-4.

were similar with VNB ($0.329 \pm 0.105 \mu\text{M}$ vs $0.458 \pm 0.117 \mu\text{M}$, $n=9$ and 11 respectively) and DNB ($0.380 \pm 0.133 \mu\text{M}$ vs $0.322 \pm 0.083 \mu\text{M}$, $n=11$ and 10 respectively) stimulation, while release with LC stimulation was slightly lower on average ($0.144 \pm 0.040 \mu\text{M}$ vs $0.249 \pm 0.058 \mu\text{M}$, $n=5$ and 6 , respectively). However, comparison of release amplitudes with these stimulations in these treatment groups found no significant effect for stimulation placement (2-way ANOVA, $F_{2,44}=2.00$, $P=0.147$) and DSP-4 treatment ($F_{1,44}=1.46$, $P=0.233$), nor a significant interaction between these two factors ($F_{2,44}=0.13$, $P=0.880$). The half-lives of norepinephrine clearance between untreated and DSP-4 treated animals were also similar for stimulation of the VNB ($1.9 \pm 0.2 \text{ s}$ vs $2.7 \pm 0.4 \text{ s}$, $n=8$ and 10 respectively), DNB ($2.4 \pm 0.3 \text{ s}$ vs $2.7 \pm 0.4 \text{ s}$, $n=10$ respectively), and LC ($2.0 \pm 0.6 \text{ s}$ vs $1.6 \pm 0.3 \text{ s}$, $n=5$ and 4 respectively). Similar to the results obtained for release amplitudes, comparison of $t_{1/2}$ values by 2-way ANOVA found no effect for stimulation placement ($F_{2,41}=1.60$, $P=0.214$) and DSP-4 treatment ($F_{1,41}=0.61$, $P=0.439$), nor a significant interaction between these two factors ($F_{2,41}=0.94$, $P=0.400$).

Electrically-stimulated norepinephrine release after ibotenic acid infusion into the DNB

At the coordinates used in this study, the DNB courses by several midbrain structures, including the reticular formation, superior colliculus, periaqueductal gray, and pretectal nucleus. To explore the possibility that activation of these cells contributed to norepinephrine release in the vBNST, the area of DNB stimulation was lesioned with ibotenic acid (Figure 2.4). Ibotenic acid is a glutamate analog that selectively kills cell bodies while leaving other neuronal elements, such as fibers of passage, intact (Jarrard, 1989). The effects of this neurotoxin are long lasting and can be seen within an hour of infusion (Randich *et al.*, 1990; Zhuang *et al.*, 2008; Liu *et al.*, 2012).

In these experiments, the stimulating electrode was positioned in the DNB to evoke release in the vBNST and AV. Baseline amplitudes were then compared to release after

infusion of saline or ibotenic acid into the area targeted by the stimulation (Figure 2.4A). Both saline and ibotenic acid decreased the amount of norepinephrine release observed with stimulation of the DNB (Figure 2.4B). Analysis of these results by 2-way ANOVA revealed main effects of brain region ($F_{1,17}=7.89$, $P=0.012$) and of ibotenic acid treatment ($F_{1,17}=15.37$, $P=0.001$), which exhibited a significant interaction ($F_{1,17}=18.93$, $P=0.004$). Post-hoc analysis found a significant difference in the degree of attenuation seen for BNST release after infusion of saline and ibotenic acid ($78.0 \pm 3.3\%$ vs $23.6 \pm 6.6\%$, $n=5$ and 6 respectively, $P<0.001$), but no significant difference was found for AV release ($68.0 \pm 4.3\%$ vs $73 \pm 12\%$, $n=5$ respectively, $P>0.05$).

Post-experiment, histology was conducted to locate lesioned areas (Figure 2.4C). Damage along the tracts of the infusion cannulas was readily visible in fixed tissue preparations (Figure 2.4C, left). The tissues penetrated by ibotenic acid are stained by Chicago Sky Blue, which was co-infused during lesioning. The spread of this staining varied between 0.5 – 2 mm in diameter, covering an area similar to the spacing between the prongs of the stimulating electrodes. Representative examples of lesion placements are shown schematically in Figure 2.4C.

Behavioral responses elicited by electrical stimulation at the depth of the DNB

To determine the effects of stimulation at the coordinates of the DNB in freely-moving animals, behavioral testing was conducted (Figure 2.5). To investigate a defined neuronal population across the experiment, the stimulation current was first calibrated for each rat until a robust escape behavior was seen ($108 \pm 33 \mu\text{A}$), and this current was then held constant while the frequency and pulse number were varied (Carlezon & Chartoff, 2007). Each stimulation during testing was only applied after the rat had resumed exploratory

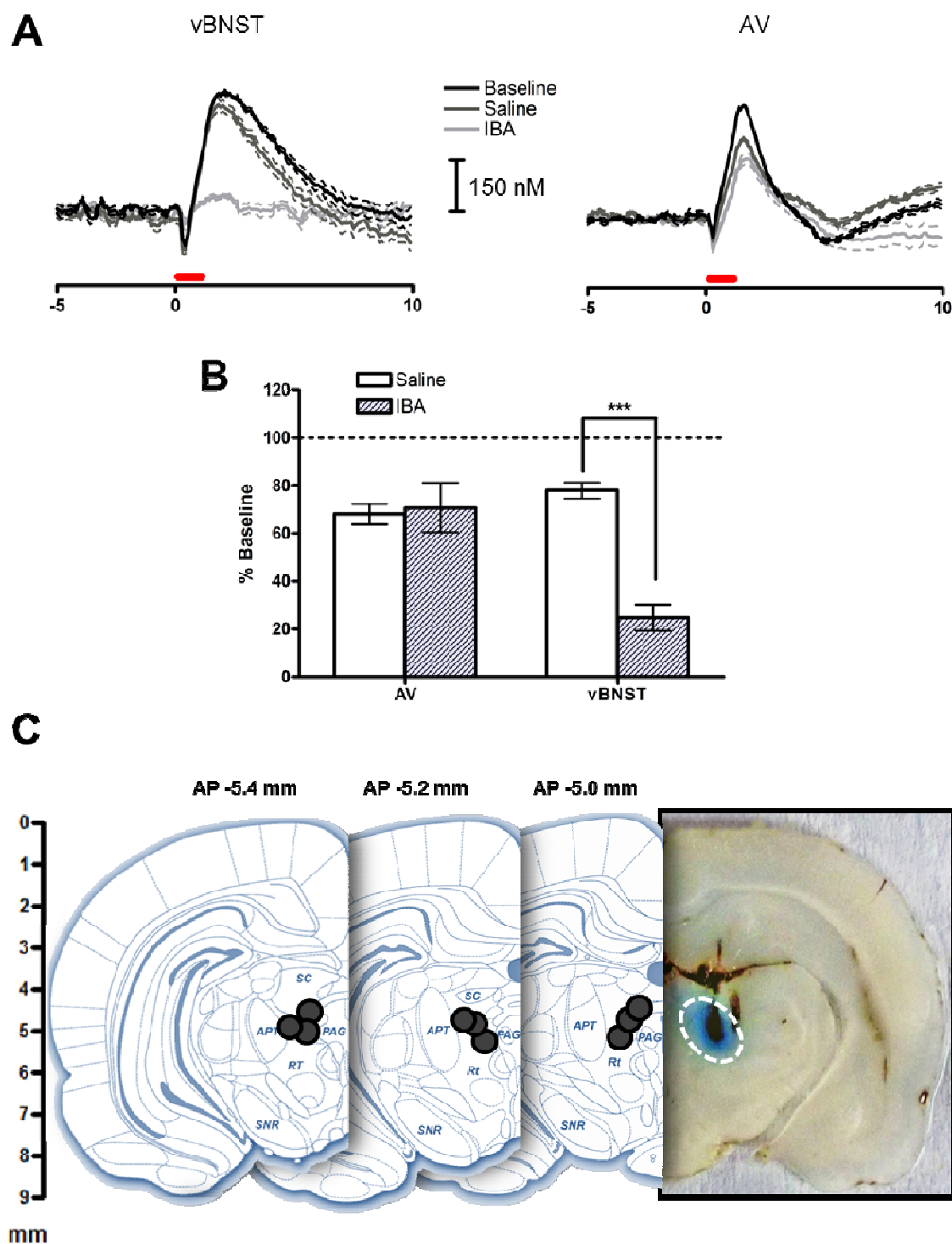


Figure 2.4. Effects of IBA infusion into the DNB on electrically-stimulated norepinephrine release. (A) Representative norepinephrine release profiles in vBNST and AV after infusion of IBA. $n = 5$ trials, error bars provided as SEM. (B) Change in release amplitudes in target regions after IBA. $n = 5$ animals for AV and BNST, *** $P < 0.001$. (C) Representative histology of IBA lesioned areas (right, solid black dots) marked by Chicago Sky Blue (left, dashed oval). Abbreviations: APT, anterior pretectal nucleus; SC, superior colliculus; Rt, reticular formation; PAG, periaqueductal gray; SNR, substantia nigra pars reticulata.

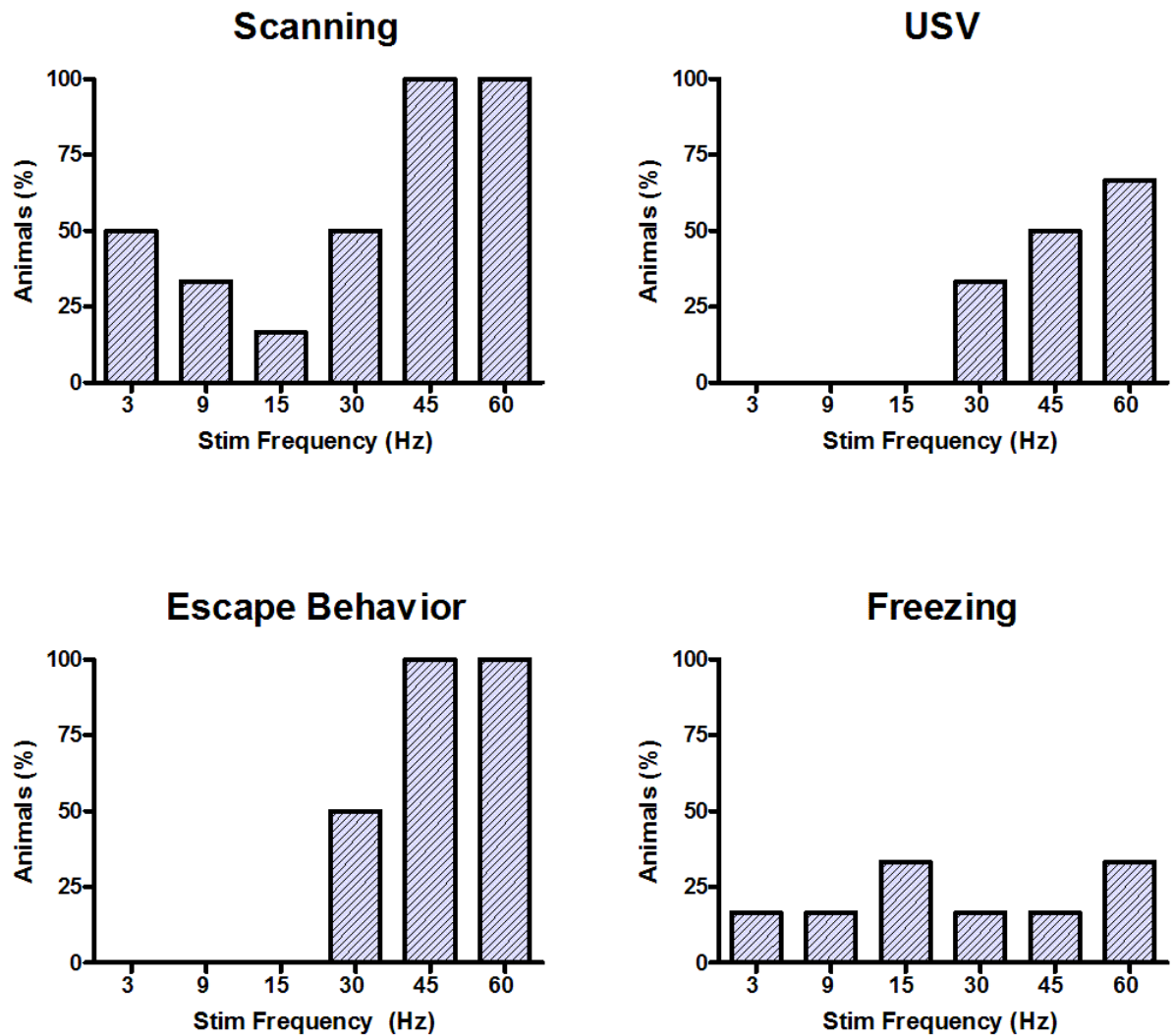


Figure 2.5. Incidence of behavioral responses to DNB stimulation (stim). Values are shown as the percentage of animals (n=6) exhibiting each behavioral reaction. The number of current pulses applied was adjusted to maintain constant stimulation duration as follows: 60 Hz, 40 pulses; 45 Hz, 30 pulses; 30 Hz, 30 pulses; 15 Hz, 10 pulses; 9 Hz, 6 pulses; 3 Hz, 2 pulses.

behavior in order to maintain independence between trials. Additionally, the stimulations were applied in order of increasing frequency, as long-duration responses were typically seen at higher frequencies.

Stimulation at the coordinates of the DNB elicited the expression of aversive behaviors in all rats tested (n=6). Scurrying was the most common escape behavior elicited directly by the stimulation (5 out of 6 rats), while stationary scanning was the dominant aversive behavior exhibited in the post-stimulation period, with $76 \pm 19\%$ of time bins marked positive for its expression at the highest stimulation frequency (60 Hz, 40 pulses). Out of the measured indices of aversion, there was a significant dependence on stimulation frequency for the expression of scanning, vocalization, and active escape behaviors ($P < 0.001$ for each); however, freezing behavior showed no clear frequency dependence and was seen in no more than two animals at any given stimulation frequency. Of note, in three out of six animals, the stimulation directly provoked an unnatural motor response, typically involving the head and forward limbs, prior to or during the expression of any aversive behaviors.

Discussion

The DNB and VNB, the ascending pathways of the central noradrenergic system, are distinct in their connectivity and in the processes in which they modulate (Rinaman, 2011; Szabadi, 2013). Indeed the nuclei forming these projections are differentially activated during physiological challenge (Lightman *et al.*, 1984; Soulier *et al.*, 1992; Pertovaara, 2006), drug exposure (Mitchell *et al.*, 1990; Delfs *et al.*, 2000; Beveridge *et al.*, 2005; Buffalari & Rinaman, 2014) and affective state (Cole & Robbins, 1987; Cryan *et al.*, 2002; Itoi & Sugimoto, 2010; Ku *et al.*, 2012). Medullary cell populations, including the nucleus of the solitary tract (A2) as well as the A1, A5 and A7 groups, produce the projections of the VNB (Ungerstedt, 1971; Johnston *et al.*, 1987). These cells are positioned to intercept visceral

sensory inputs and terminate in the hypothalamus and basal forebrain regions. Neurons of the DNB arise primarily from the LC (A6) and the A4 pontine nucleus, and project to cortical, hippocampal, and thalamic areas (Foote *et al.*, 1983; Szabadi, 2013).

FSCV is a useful technique to monitor norepinephrine release dynamics in the terminal regions of these pathways (Herr *et al.*, 2012; McElligott *et al.*, 2013; Park *et al.*, 2013), though selective measurements are limited to areas with low dopamine innervation (Park *et al.*, 2009). The vBNST, a key modulator of the central stress response, and the AV, a nucleus involved in spatial learning and memory (Warburton *et al.*, 2000; van Groen *et al.*, 2002; Wolff *et al.*, 2008), are two such areas. Here we specifically employed FSCV to consider the relative capacities of VNB and DNB electrical stimulation to evoke norepinephrine overflow in the vBNST. This was accomplished with selective lesioning agents targeting the LC and the cell populations proximal to the location of stimulation. The effects of these treatments were compared for DNB-stimulated norepinephrine release in the vBNST and the AV, a major target of DNB projections. Our results provide evidence to suggest that the DNB is activated with the electrical stimulation, but that norepinephrine release in the vBNST occurs at least in part from concurrent activation of a non-coerulean pathway.

LC lesioning attenuates norepinephrine release in the AV but not in the vBNST

In our first set of experiments, DNB fibers were damaged with DSP-4 to evaluate the extent of its role in producing norepinephrine overflow in the vBNST during electrical stimulation. DSP-4 is a neurotoxin that has been widely used to study the behavioral and physiological consequences of compromised LC activity (Ross & Stenfors, 2014). Within a week of administration DSP-4 causes decreased norepinephrine tissue content (Grzanna *et al.*, 1989; Kudo *et al.*, 2010; Szot *et al.*, 2010), terminal density (Fritschy & Grzanna, 1989; Toussay *et al.*, 2013; Bucher *et al.*, 2014), and receptor expression (Johnson *et al.*, 1987;

Heal *et al.*, 1993; Wolfman *et al.*, 1994) in areas innervated by the LC, but not in areas innervated by the medullary cell populations. It is unclear why only norepinephrine neurons of the LC are targeted; however, uptake of DSP-4 is believed to be mediated by the norepinephrine transporter (Landa *et al.*, 1984; Zaczek *et al.*, 1990), causing first fiber degradation and then cell death at later times (Fritschy & Grzanna, 1991; 1992). These effects are dose-dependent, and the 50 mg/kg treatment we employed has been shown to reproducibly induce widespread LC toxicity (Kudo *et al.*, 2010; Ross & Stenfors, 2014).

In this study, measurements were made in the AV, a major terminal region of the DNB, to assess the efficacy of DSP-4 treatment. Consistent with a loss of noradrenergic terminals, both norepinephrine and dopamine, its metabolic precursor, were significantly reduced in this region in DSP-4 treated animals. In evoked release experiments norepinephrine release in the AV was also found to be attenuated with DSP-4. Moreover, administration of α_2 autoreceptor and NET inhibitors exhibited blunted responses, revealing that presynaptic regulatory mechanisms were significantly compromised. Overall the reduction in AV norepinephrine content and release confirmed that DSP-4 treatment effectively damaged fibers of the DNB.

In contrast to the AV, no significant changes in vBNST catecholamine content were found with DSP-4 treatment. While this is consistent with previous observations, it is somewhat surprising that loss of DNB innervation—which is reported to account for as much as 30% of its noradrenergic input in this region (Phelix *et al.*, 1992; Myers *et al.*, 2005)—did not lead to a measurable attenuation of catecholamine levels. It is quite possible that VNB terminals surviving DSP-4 treatment in the vBNST compensate for DNB denervation. Indeed, compensatory effects including increased extracellular concentrations and turnover have been reported in forebrain regions with attenuated norepinephrine content (Hallman & Jonsson, 1984; Logue *et al.*, 1985; Hughes & Stanford, 1998). Given that the majority of terminals in the BNST are resilient to DSP-4 they may be able to better account for the loss

of LC input. Supporting this possibility, a separate study reported a net increase in BNST norepinephrine with DSP-4 (Szot *et al.*, 2010), though we did not observe this effect in our work.

Regardless of whether or not VNB transmission was enhanced as a result of DSP-4 treatment, recordings in the AV supported that DNB functionality was damaged. Surprisingly however, DSP-4 did not alter the capacity of VNB, DNB, or even LC stimulation to elicit norepinephrine release in the vBNST. In fact, the norepinephrine release with each of these stimulations was on average higher in treated animals—though not to a significant extent. These results suggest that electrical stimulation at the coordinates of LC cell bodies and axons depolarizes fibers of the VNB, which then give rise to the norepinephrine release observed in the vBNST. There are a number of reciprocal connections coursing between the regions of the medullar and pontine norepinephrine cell groups (Van Bockstaele & Aston-Jones, 1992; Van Bockstaele *et al.*, 1999; Mello-Carpes & Izquierdo, 2013); however, antidromic signaling along such a pathway would likely be reduced with DNB damage. As DSP-4 did not attenuate BNST norepinephrine release with DNB stimulation, it is more likely that VNB activation is mediated by some other neuronal substrate.

Midbrain cell body activation supports norepinephrine release in the vBNST but not in the AV

The DNB courses through the midbrain reticular formation, a diffuse network of neurons forming the core of the brainstem (Ungerstedt, 1971; ten Donkelaar, 2011). Surrounding the reticular formation at our coordinates of stimulation are the periaqueductal gray (PAG), superior colliculus, and anterior pretectal nucleus (Paxinos & Watson, 2007), areas important to visual processing, motor-control, nociception, respiration, and arousal (Rees & Roberts, 1993; Johansen *et al.*, 2010; Krauzlis *et al.*, 2013). Of these structures

only those in the midbrain tectum, which include the superior colliculus and the PAG, receive significant noradrenergic input (Swanson & Hartman, 1975). Noradrenergic innervation of the superior colliculus and the dorsal PAG is primarily coerulean (Morrison & Foote, 1986), whereas the lateral and ventral portions of the PAG receive input from the nucleus of the solitary tract, A1 and A5 groups (Byrum & Guyenet, 1987; Herbert & Saper, 1992; Clement *et al.*, 1998).

Despite the differences between their afferent input, each of these midbrain nuclei produce descending efferent projections terminating within or near medullary areas housing noradrenergic cells (Bandler & Tork, 1987; Chiang *et al.*, 1992; Yasui *et al.*, 1994; ten Donkelaar, 2011), and therefore may be able to modulate norepinephrine overflow in the vBNST. We tested this theory with ibotenic acid, an excitotoxic agent that causes cell loss within an area closely confined to the locus of its injection. In the protocol employed in this study, ibotenic acid was infused at the depth of DNB stimulation and changes in stimulated norepinephrine release were observed for the AV and the vBNST. Ibotenic acid does not target afferent terminals or fibers of passage (Jarrard, 1989); therefore its neurotoxicity is not expected to have impacted the axons of the DNB. Interestingly, this treatment did not significantly alter norepinephrine release in the AV—supporting that NE release in this region is mediated by direct activation of the DNB at the stimulation coordinates. Conversely, DNB-stimulated norepinephrine release in the vBNST was significantly reduced after ibotenic acid. This confirms a role for midbrain cells in producing vBNST norepinephrine release with electrical stimulation of the DNB. It is important to note that it is not possible to assess the degree in which these cells contribute to norepinephrine release as there is likely some variability between lesions and the areas of stimulation.

Histology confirmed that many of the lesions covered portions of the superior colliculus and the PAG, areas crucial to producing behavioral and autonomic responses to threatening stimuli. Chemical and electrical activation of this region produces characteristic

defense reactions that are dependent on stimulation intensity (Schenberg *et al.*, 1993; Brandao *et al.*, 1999; Schenberg *et al.*, 2005). When DNB stimulation was administered to awake animals, similar intensity-dependent aversive responses were observed, including scanning, freezing, 20 KHz ultrasonic vocalizations, and escape behaviors. It is therefore likely that stimulation of the DNB recruited the neurons of the superior colliculus and the PAG during anesthetized experiments.

Of the two tectum structures, there is strong anatomical evidence to believe that the PAG could facilitate norepinephrine transmission in the BNST. Descending projections from the PAG terminate within the norepinephrine-containing homeostatic fields of the brainstem to generate cardiorespiratory responses during stress (Sessle *et al.*, 1981; van der Plas *et al.*, 1995; Huang *et al.*, 2000; Boscan & Paton, 2005). Though many of these reported connections are not noradrenergic, a smaller number of studies have argued that the PAG can indirectly and directly signal to the neurons of the VNB noradrenergic system (Bajic & Proudfit, 1999; Bajic *et al.*, 2012), and the lesioning effects observed in our study support this claim. As the BNST and the PAG are both major components of the central stress system, regulation of the VNB by the PAG could be important to the pathology of stress-associated illnesses such as anxiety and panic disorders (Graeff *et al.*, 1993; Walker *et al.*, 2003; McElligott *et al.*, 2013).

Conclusions

The results of this study demonstrate that vBNST norepinephrine overflow is mediated by activation of midbrain structures surrounding the path of the DNB, possibly including the periaqueductal gray. As DSP-4 did not exert an effect on vBNST norepinephrine dynamics, the off-target effects of DNB stimulation likely causes release from VNB fibers terminating in the vBNST. This provides an explanation for the discrepancy between reported inputs to the vBNST and the similarities between norepinephrine release

elicited by DNB and VNB stimulation. Importantly, our data does not preclude the possibility of LC-mediated release in the vBNST. Rather, it suggests that the contribution of the LC to vBNST norepinephrine overflow is much smaller than that of the off-target activations induced by electrical stimulation of its processes.

REFERENCES

- Bajic, D. & Proudfit, H.K. (1999) Projections of neurons in the periaqueductal gray to pontine and medullary catecholamine cell groups involved in the modulation of nociception. *J Comp Neurol*, **405**, 359-379.
- Bajic, D., Van Bockstaele, E.J. & Proudfit, H.K. (2012) Ultrastructural analysis of rat ventrolateral periaqueductal gray projections to the A5 cell group. *Neuroscience*, **224**, 145-159.
- Bandler, R. & Tork, I. (1987) Midbrain periaqueductal grey region in the cat has afferent and efferent connections with solitary tract nuclei. *Neurosci Lett*, **74**, 1-6.
- Berridge, C.W. & Waterhouse, B.D. (2003) The locus coeruleus-noradrenergic system: modulation of behavioral state and state-dependent cognitive processes. *Brain Res Brain Res Rev*, **42**, 33-84.
- Beveridge, T.J., Smith, H.R., Nader, M.A. & Porrino, L.J. (2005) Effects of chronic cocaine self-administration on norepinephrine transporters in the nonhuman primate brain. *Psychopharmacology (Berl)*, **180**, 781-788.
- Boscan, P. & Paton, J.F. (2005) Excitatory convergence of periaqueductal gray and somatic afferents in the solitary tract nucleus: role for neurokinin 1 receptors. *Am J Physiol Regul Integr Comp Physiol*, **288**, R262-269.
- Brandao, M.L., Anseloni, V.Z., Pandossio, J.E., De Araujo, J.E. & Castilho, V.M. (1999) Neurochemical mechanisms of the defensive behavior in the dorsal midbrain. *Neurosci Biobehav Rev*, **23**, 863-875.
- Bucher, E.S., Brooks, K., Verber, M.D., Keithley, R.B., Owesson-White, C., Carroll, S., Takmakov, P., McKinney, C.J. & Wightman, R.M. (2013) Flexible software platform for fast-scan cyclic voltammetry data acquisition and analysis. *Anal Chem*, **85**, 10344-10353.
- Bucher, E.S., Fox, M.E., Kim, L., Kirkpatrick, D.C., Rodeberg, N.T., Belle, A.M. & Wightman, R.M. (2014) Medullary norepinephrine neurons modulate local oxygen concentrations in the bed nucleus of the stria terminalis. *J Cereb Blood Flow Metab*, **34**, 1128-1137.
- Buffalari, D.M. & Rinaman, L. (2014) Cocaine self-administration and extinction alter medullary noradrenergic and limbic forebrain cFos responses to acute, noncontingent cocaine injections in adult rats. *Neuroscience*.

- Byrum, C.E. & Guyenet, P.G. (1987) Afferent and efferent connections of the A5 noradrenergic cell group in the rat. *J Comp Neurol*, **261**, 529-542.
- Cahill, P.S., Walker, Q.D., Finnegan, J.M., Mickelson, G.E., Travis, E.R. & Wightman, R.M. (1996) Microelectrodes for the measurement of catecholamines in biological systems. *Anal Chem.*, **68**, 3180-3186.
- Carlezon, W.A., Jr. & Chartoff, E.H. (2007) Intracranial self-stimulation (ICSS) in rodents to study the neurobiology of motivation. *Nat Protoc*, **2**, 2987-2995.
- Chiang, C.Y., Chen, I.C., Dostrovsky, J.O. & Sessle, B.J. (1992) Anterior pretectal nucleus-induced modulatory effects on trigeminal brainstem somatosensory neurons. *Neurosci Lett*, **134**, 233-237.
- Clement, C.I., Keay, K.A. & Bandler, R. (1998) Medullary catecholaminergic projections to the ventrolateral periaqueductal gray region activated by halothane anaesthesia. *Neuroscience*, **86**, 1273-1284.
- Cole, B.J. & Robbins, T.W. (1987) Dissociable effects of lesions to the dorsal or ventral noradrenergic bundle on the acquisition, performance, and extinction of aversive conditioning. *Behav Neurosci*, **101**, 476-488.
- Crestani, C.C., Alves, F.H., Gomes, F.V., Resstel, L.B., Correa, F.M. & Herman, J.P. (2013) Mechanisms in the bed nucleus of the stria terminalis involved in control of autonomic and neuroendocrine functions: a review. *Curr Neuroparmacol*, **11**, 141-159.
- Cryan, J.F., Page, M.E. & Lucki, I. (2002) Noradrenergic lesions differentially alter the antidepressant-like effects of reboxetine in a modified forced swim test. *Eur J Pharmacol*, **436**, 197-205.
- Delfs, J.M., Zhu, Y., Druhan, J.P. & Aston-Jones, G. (2000) Noradrenaline in the ventral forebrain is critical for opiate withdrawal-induced aversion. *Nature*, **403**, 430-434.
- Foote, S.L., Bloom, F.E. & Aston-Jones, G. (1983) Nucleus locus ceruleus: new evidence of anatomical and physiological specificity. *Physiol Rev.*, **63**, 844-914.
- Forray, M.I. & Gysling, K. (2004) Role of noradrenergic projections to the bed nucleus of the stria terminalis in the regulation of the hypothalamic-pituitary-adrenal axis. *Brain Res Brain Res Rev*, **47**, 145-160.

- Forray, M.I., Gysling, K., Andres, M.E., Bustos, G. & Araneda, S. (2000) Medullary noradrenergic neurons projecting to the bed nucleus of the stria terminalis express mRNA for the NMDA-NR1 receptor. *Brain Res Bull*, **52**, 163-169.
- Fritschy, J.M. & Grzanna, R. (1989) Immunohistochemical analysis of the neurotoxic effects of DSP-4 identifies two populations of noradrenergic axon terminals. *Neuroscience*, **30**, 181-197.
- Fritschy, J.M. & Grzanna, R. (1991) Experimentally-induced neuron loss in the locus coeruleus of adult rats. *Exp Neurol*, **111**, 123-127.
- Fritschy, J.M. & Grzanna, R. (1992) Restoration of ascending noradrenergic projections by residual locus coeruleus neurons: compensatory response to neurotoxin-induced cell death in the adult rat brain. *J Comp Neurol*, **321**, 421-441.
- Gallistel, C.R. & Freyd, G. (1987) Quantitative determination of the effects of catecholaminergic agonists and antagonists on the rewarding efficacy of brain stimulation. *Pharmacol Biochem Behav*, **26**, 731-741.
- Graeff, F.G., Silveira, M.C., Nogueira, R.L., Audi, E.A. & Oliveira, R.M. (1993) Role of the amygdala and periaqueductal gray in anxiety and panic. *Behav Brain Res*, **58**, 123-131.
- Grzanna, R., Berger, U., Fritschy, J.M. & Geffard, M. (1989) Acute action of DSP-4 on central norepinephrine axons: biochemical and immunohistochemical evidence for differential effects. *J Histochem Cytochem*, **37**, 1435-1442.
- Hallman, H. & Jonsson, G. (1984) Pharmacological modifications of the neurotoxic action of the noradrenaline neurotoxin DSP4 on central noradrenaline neurons. *Eur J Pharmacol*, **103**, 269-278.
- Heal, D.J., Butler, S.A., Prow, M.R. & Buckett, W.R. (1993) Quantification of presynaptic alpha 2-adrenoceptors in rat brain after short-term DSP-4 lesioning. *Eur J Pharmacol*, **249**, 37-41.
- Heien, M.L., Johnson, M.A. & Wightman, R.M. (2004) Resolving neurotransmitters detected by fast-scan cyclic voltammetry. *Anal Chem*, **76**, 5697-5704.
- Herbert, H. & Saper, C.B. (1992) Organization of medullary adrenergic and noradrenergic projections to the periaqueductal gray matter in the rat. *J Comp Neurol*, **315**, 34-52.

- Herr, N.R., Park, J., McElligott, Z.A., Belle, A.M., Carelli, R.M. & Wightman, R.M. (2012) In Vivo Voltammetry Monitoring of Electrically Evoked Extracellular Norepinephrine in Subregions of the Bed Nucleus of the Stria Terminalis. *J Neurophysiol*, **107**, 1731-1737.
- Histed, M.H., Bonin, V. & Reid, R.C. (2009) Direct activation of sparse, distributed populations of cortical neurons by electrical microstimulation. *Neuron*, **63**, 508-522.
- Huang, Z.G., Subramanian, S.H., Balnave, R.J., Turman, A.B. & Moi Chow, C. (2000) Roles of periaqueductal gray and nucleus tractus solitarius in cardiorespiratory function in the rat brainstem. *Respir Physiol*, **120**, 185-195.
- Hughes, Z.A. & Stanford, S.C. (1998) A partial noradrenergic lesion induced by DSP-4 increases extracellular noradrenaline concentration in rat frontal cortex: a microdialysis study in vivo. *Psychopharmacology (Berl)*, **136**, 299-303.
- Itoi, K. & Sugimoto, N. (2010) The brainstem noradrenergic systems in stress, anxiety and depression. *J Neuroendocrinol*, **22**, 355-361.
- Jarrard, L.E. (1989) On the use of ibotenic acid to lesion selectively different components of the hippocampal formation. *J Neurosci Methods*, **29**, 251-259.
- Johansen, J.P., Tarpley, J.W., LeDoux, J.E. & Blair, H.T. (2010) Neural substrates for expectation-modulated fear learning in the amygdala and periaqueductal gray. *Nat Neurosci*, **13**, 979-986.
- Johnson, R.D., Iuvone, P.M. & Minneman, K.P. (1987) Regulation of alpha-1 adrenergic receptor density and functional responsiveness in rat brain. *J Pharmacol Exp Ther*, **242**, 842-849.
- Johnston, C.A., Mattiace, L.A. & Negro-Vilar, A. (1987) Effect of ventral noradrenergic bundle lesions on concentrations of monoamine neurotransmitters and metabolites in several discrete areas of the rat brain. *Cell Mol Neurobiol*, **7**, 403-411.
- Keithley, R.B. & Wightman, R.M. (2011) Assessing principal component regression prediction of neurochemicals detected with fast-scan cyclic voltammetry. *ACS Chem Neurosci*, doi: 10.1021/cn200035u.
- Kilts, C.D. & Anderson, C.M. (1986) The simultaneous quantification of dopamine, norepinephrine and epinephrine in micropunched rat brain nuclei by on-line trace enrichment HPLC with electrochemical detection: Distribution of catecholamines in the limbic system. *Neurochem Int*, **9**, 437-445.

- Krauzlis, R.J., Lovejoy, L.P. & Zenon, A. (2013) Superior colliculus and visual spatial attention. *Annu Rev Neurosci*, **36**, 165-182.
- Ku, Y.C., Tsai, Y.J., Tung, C.S., Fang, T.H., Lo, S.M. & Liu, Y.P. (2012) Different involvement of ventral and dorsal norepinephrine pathways on norepinephrine reuptake inhibitor-induced locomotion and antidepressant-like effects in rats. *Neurosci Lett*, **514**, 179-184.
- Kudo, T., Kushikata, T., Kudo, M. & Hirota, K. (2010) A central neuropathic pain model by DSP-4 induced lesion of noradrenergic neurons: preliminary report. *Neurosci Lett*, **481**, 102-104.
- Lahdesmaki, J., Sallinen, J., MacDonald, E., Kobilka, B.K., Fagerholm, V. & Scheinin, M. (2002) Behavioral and neurochemical characterization of alpha(2A)-adrenergic receptor knockout mice. *Neuroscience*, **113**, 289-299.
- Landa, M.E., Rubio, M.C. & Jaim-Etcheverry, G. (1984) The neurotoxic compound N-(2-chloroethyl)-N-ethyl-2-bromobenzylamine hydrochloride (DSP4) depletes endogenous norepinephrine and enhances release of [3H]norepinephrine from rat cortical slices. *J Pharmacol Exp Ther*, **231**, 131-136.
- Lightman, S.L., Todd, K. & Everitt, B.J. (1984) Ascending noradrenergic projections from the brainstem: evidence for a major role in the regulation of blood pressure and vasopressin secretion. *Exp Brain Res*, **55**, 145-151.
- Lindvall, O. & Stenevi, U. (1978) Dopamine and noradrenaline neurons projecting to the septal area in the rat. *Cell Tissue Res*, **190**, 383-407.
- Liu, X.H., Sun, N., Du, J.Q., Tang, J.S., Han, M., Zhu, J.X. & Huo, F.Q. (2012) Chemical lesioning and glutamate administration reveal a major role for the nucleus tractus solitarius in the cardiac-somatic reflex in rats. *Neuroscience*, **207**, 326-332.
- Logue, M.P., Growdon, J.H., Coviella, I.L. & Wurtman, R.J. (1985) Differential effects of DSP-4 administration on regional brain norepinephrine turnover in rats. *Life Sci*, **37**, 403-409.
- McElligott, Z.A., Fox, M.E., Walsh, P.L., Urban, D.J., Ferrel, M.S., Roth, B.L. & Wightman, R.M. (2013) Noradrenergic synaptic function in the bed nucleus of the stria terminalis varies in animal models of anxiety and addiction. *Neuropsychopharmacology*, **38**, 1665-1673.

- McIntyre, C.C. & Grill, W.M. (2002) Extracellular stimulation of central neurons: influence of stimulus waveform and frequency on neuronal output. *J Neurophysiol*, **88**, 1592-1604.
- Mefford, I.N. (1981) Application of high performance liquid chromatography with electrochemical detection to neurochemical analysis: measurement of catecholamines, serotonin and metabolites in rat brain. *Journal of neuroscience methods*, **3**, 207-224.
- Mello-Carpes, P.B. & Izquierdo, I. (2013) The Nucleus of the Solitary Tract --> Nucleus Paragigantocellularis --> Locus Coeruleus --> CA1 region of dorsal hippocampus pathway is important for consolidation of object recognition memory. *Neurobiol Learn Mem*, **100**, 56-63.
- Mitchell, S.N., Brazell, M.P., Schugens, M.M. & Gray, J.A. (1990) Nicotine-induced catecholamine synthesis after lesions to the dorsal or ventral noradrenergic bundle. *Eur J Pharmacol*, **179**, 383-391.
- Moore, R.Y. (1978) Catecholamin innervation of the basal forebrain. I. The septal area. *J Comp Neurol*, **177**, 665-684.
- Morrison, J.H. & Foote, S.L. (1986) Noradrenergic and serotonergic innervation of cortical, thalamic, and tectal visual structures in Old and New World monkeys. *J Comp Neurol*, **243**, 117-138.
- Myers, E.A., Banihashemi, L. & Rinaman, L. (2005) The anxiogenic drug yohimbine activates central viscerosensory circuits in rats. *J Comp Neurol*, **492**, 426-441.
- Oke, A., Solnick, J. & Adams, R.N. (1983) Catecholamine distribution patterns in rat thalamus. *Brain research*, **269**, 180-183.
- Park, J., Bucher, E.S., Fontillas, K., Owesson-White, C., Ariansen, J.L., Carelli, R.M. & Wightman, R.M. (2013) Opposing catecholamine changes in the bed nucleus of the stria terminalis during intracranial self-stimulation and its extinction. *Biol Psychiatry*, **74**, 69-76.
- Park, J., Kile, B.M. & Wightman, R.M. (2009) *In vivo* voltammetric monitoring of norepinephrine release in the rat ventral bed nucleus of the stria terminalis and anteroventral thalamic nucleus. *Eur J Neurosci.*, **30**, 2121-2133.
- Park, J., Takmakov, P. & Wightman, R.M. (2011) In vivo comparison of norepinephrine and dopamine release in rat brain by simultaneous measurements with fast-scan cyclic voltammetry. *J Neurochem*, **119**, 932-944.

- Paxinos, G. & Watson, C. (2007) *The Rat Brain in Stereotaxic Coordinates*. Elsevier Inc., Burlington.
- Pertovaara, A. (2006) Noradrenergic pain modulation. *Prog Neurobiol.*, **80**, 53-83.
- Pertovaara, A. (2013) The noradrenergic pain regulation system: a potential target for pain therapy. *Eur J Pharmacol*, **716**, 2-7.
- Phelix, C.F., Liposits, Z. & Paull, W.K. (1992) Monoamine innervation of bed nucleus of stria terminalis: an electron microscopic investigation. *Brain Res Bull*, **28**, 949-965.
- Pinault, D. (1995) Backpropagation of action potentials generated at ectopic axonal loci: hypothesis that axon terminals integrate local environmental signals. *Brain Res Brain Res Rev*, **21**, 42-92.
- Ranck, J.B., Jr. (1975) Which elements are excited in electrical stimulation of mammalian central nervous system: a review. *Brain research*, **98**, 417-440.
- Randich, A., Ren, K. & Gebhart, G.F. (1990) Electrical stimulation of cervical vagal afferents. II. Central relays for behavioral antinociception and arterial blood pressure decreases. *J Neurophysiol*, **64**, 1115-1124.
- Rees, H. & Roberts, M.H. (1993) The anterior pretectal nucleus: a proposed role in sensory processing. *Pain*, **53**, 121-135.
- Rinaman, L. (2011) Hindbrain noradrenergic A2 neurons: diverse roles in autonomic, endocrine, cognitive, and behavioral functions. *Am J Physiol Regul Integr Comp Physiol*, **300**, R222-235.
- Ross, S.B., Johansson, J.G., Lindborg, B. & Dahlbom, R. (1973) Cyclizing compounds. I. Tertiary N-(2-bromobenzyl)-N-haloalkylamines with adrenergic blocking action. *Acta Pharm Suec*, **10**, 29-42.
- Ross, S.B. & Stenfors, C. (2014) DSP4, a Selective Neurotoxin for the Locus Coeruleus Noradrenergic System. A Review of Its Mode of Action. *Neurotox Res*.
- Schenberg, L.C., Pova, R.M., Costa, A.L., Caldellas, A.V., Tufik, S. & Bittencourt, A.S. (2005) Functional specializations within the tectum defense systems of the rat. *Neurosci Biobehav Rev*, **29**, 1279-1298.

- Schenberg, L.C., Vasquez, E.C. & da Costa, M.B. (1993) Cardiac baroreflex dynamics during the defence reaction in freely moving rats. *Brain research*, **621**, 50-58.
- Sessle, B.J., Ball, G.J. & Lucier, G.E. (1981) Suppressive influences from periaqueductal gray and nucleus raphe magnus on respiration and related reflex activities and on solitary tract neurons, and effect of naloxone. *Brain research*, **216**, 145-161.
- Soulier, V., Cottet-Emard, J.M., Pequignot, J., Hanchin, F., Peyrin, L. & Pequignot, J.M. (1992) Differential effects of long-term hypoxia on norepinephrine turnover in brain stem cell groups. *J Appl Physiol* (1985), **73**, 1810-1814.
- Swanson, L.W. & Hartman, B.K. (1975) The central adrenergic system. An immunofluorescence study of the location of cell bodies and their efferent connections in the rat utilizing dopamine-beta-hydroxylase as a marker. *J Comp Neurol*, **163**, 467-505.
- Szabadi, E. (2013) Functional neuroanatomy of the central noradrenergic system. *J Psychopharmacol*, **27**, 659-693.
- Szot, P., Miguelez, C., White, S.S., Franklin, A., Sikkema, C., Wilkinson, C.W., Ugedo, L. & Raskind, M.A. (2010) A comprehensive analysis of the effect of DSP4 on the locus coeruleus noradrenergic system in the rat. *Neuroscience*, **166**, 279-291.
- ten Donkelaar, H. (2011) The Reticular Formation and Some Related Nuclei *Clinical Neuroanatomy*. Springer Berlin Heidelberg, pp. 211-247.
- Terenzi, M.G. & Ingram, C.D. (1995) A combined immunocytochemical and retrograde tracing study of noradrenergic connections between the caudal medulla and bed nuclei of the stria terminalis. *Brain research*, **672**, 289-297.
- Toussay, X., Basu, K., Lacoste, B. & Hamel, E. (2013) Locus coeruleus stimulation recruits a broad cortical neuronal network and increases cortical perfusion. *J Neurosci*, **33**, 3390-3401.
- Tyler, S. (1979) Time-sampling: A matter of convention. *Animal Behaviour*, **27, Part 3**, 801-810.
- Ungerstedt, U. (1971) Stereotaxic mapping of the monoamine pathways in the rat brain. *Acta Physiol Scand Suppl*, **367**, 1-48.

- Van Bockstaele, E.J. & Aston-Jones, G. (1992) Collateralized projections from neurons in the rostral medulla to the nucleus locus coeruleus, the nucleus of the solitary tract and the periaqueductal gray. *Neuroscience*, **49**, 653-668.
- Van Bockstaele, E.J., Peoples, J. & Telegan, P. (1999) Efferent projections of the nucleus of the solitary tract to peri-locus coeruleus dendrites in rat brain: evidence for a monosynaptic pathway. *J Comp Neurol*, **412**, 410-428.
- van der Plas, J., Maes, F.W. & Bohus, B. (1995) Electrophysiological analysis of midbrain periaqueductal gray influence on cardiovascular neurons in the ventrolateral medulla oblongata. *Brain Res Bull*, **38**, 447-456.
- Venton, B.J., Michael, D.J. & Wightman, R.M. (2003) Correlation of local changes in extracellular oxygen and pH that accompany dopaminergic terminal activity in the rat caudate-putamen. *J Neurochem*, **84**, 373-381.
- Walker, D.L., Toufexis, D.J. & Davis, M. (2003) Role of the bed nucleus of the stria terminalis versus the amygdala in fear, stress, and anxiety. *Eur J Pharmacol*, **463**, 199-216.
- Waters, J., Schaefer, A. & Sakmann, B. (2005) Backpropagating action potentials in neurones: measurement, mechanisms and potential functions. *Prog Biophys Mol Biol*, **87**, 145-170.
- Weinshenker, D. & Schroeder, J.P. (2007) There and back again: a tale of norepinephrine and drug addiction. *Neuropsychopharmacology*, **32**, 1433-1451.
- Wightman, R.M., Amatore, C., Engstrom, R.C., Hale, P.D., Kristensen, E.W., Kuhr, W.G. & May, L.J. (1988) Real-time characterization of dopamine overflow and uptake in the rat striatum. *Neuroscience*, **25**, 513-523.
- Wightman, R.M. & Zimmerman, J.B. (1990) Control of dopamine extracellular concentration in rat striatum by impulse flow and uptake. *Brain Res Brain Res Rev*, **15**, 135-144.
- Wolfman, C., Abo, V., Calvo, D., Medina, J., Dajas, F. & Silveira, R. (1994) Recovery of central noradrenergic neurons one year after the administration of the neurotoxin DSP4. *Neurochem Int*, **25**, 395-400.
- Yasui, Y., Tsumori, T., Ando, A., Domoto, T., Kayahara, T. & Nakano, K. (1994) Descending projections from the superior colliculus to the reticular formation around the motor trigeminal nucleus and the parvocellular reticular formation of the medulla oblongata in the rat. *Brain research*, **656**, 420-426.

Yorgason, J.T., Espana, R.A. & Jones, S.R. (2011) Demon voltammetry and analysis software: analysis of cocaine-induced alterations in dopamine signaling using multiple kinetic measures. *J Neurosci Methods*, **202**, 158-164.

Zaczek, R., Fritschy, J.M., Culp, S., De Souza, E.B. & Grzanna, R. (1990) Differential effects of DSP-4 on noradrenaline axons in cerebral cortex and hypothalamus may reflect heterogeneity of noradrenaline uptake sites. *Brain research*, **522**, 308-314.

Zhuang, J., Xu, F. & Frazier, D.T. (2008) Hyperventilation evoked by activation of the vicinity of the caudal inferior olivary nucleus depends on the fastigial nucleus in anesthetized rats. *J Appl Physiol (1985)*, **104**, 1351-1358.

CHAPTER 3: NOREPINEPHRINE AND DOPAMINE TRANSMISSION IN TWO LIMBIC REGIONS DIFFERENTIALLY RESPOND TO ACUTE NOXIOUS STIMULATION

Introduction

The motivational, hedonic and associative aspects of pain are encoded by the brain's limbic system, a heterogeneous collection of structures positioned at the interface of the hindbrain and cortex. Limbic function is supported by catecholamine innervation from the dopaminergic cells of the ventral tegmental area (VTA) and periaqueductal gray (PAG) (Swanson, 1982; Hasue & Shammah-Lagnado, 2002), as well as the noradrenergic cells of the locus coeruleus (LC), nucleus of the solitary tract (NST, A2) and A1 group (Forray *et al.*, 2000; Park *et al.*, 2009). Indeed, a number of animal studies have demonstrated that these cells respond to noxious stimuli (Grant *et al.*, 1988; Ungless *et al.*, 2004; Brischoux *et al.*, 2009). The modulatory actions of catecholamine neurotransmission are moreover implicated in the physiological and behavioral reactions to pain (Altier & Stewart, 1999; Pertovaara, 2006), and are associated with disorders often comorbid with pain dysregulation such as drug addiction and depression (Delgado, 2004; Zhang *et al.*, 2008; Elman *et al.*, 2013).

Measuring the neurochemical changes induced by acute pain is challenging due to the temporo-spatial dynamics of rapid neurotransmitter release. Unsurprisingly, past studies have produced controversial results (Abercrombie *et al.*, 1989; Pei *et al.*, 1990; Kalivas & Duffy, 1995; Amato *et al.*, 2011). *In vivo* fast-scan cyclic voltammetry (FSCV) at carbon-fiber microelectrodes can capture real-time changes in extracellular catecholamines within the substructures of the brain (Robinson *et al.*, 2008; Park *et al.*, 2012). Recently we employed this methodology in anesthetized animals to observe striatal dopamine responses during a noxious 3 s tail-pinch (Budygin *et al.*, 2011). We found that tail-pinch elevated

extracellular dopamine throughout the nucleus accumbens (NAc), a VTA-innervated limbic structure involved in motivational salience and reward processing. The temporal aspects of this response, however, were subregion-dependent. Dopamine increased during the stimulation in the NAc core but only at the stimulus termination in the NAc shell, demonstrating that accumbal dopamine release differentially encodes information regarding the presence and cessation of a noxious stimulus.

Interestingly, we failed to identify a striatal region where dopamine activity decreased with tail-pinch. This is unexpected as electrophysiological recordings have identified a subset of VTA dopamine neurons that are inhibited by pain (Ungless *et al.*, 2004; Brischoux *et al.*, 2009; Zweifel *et al.*, 2011). The absence of this response pattern in our previous data prompted this reinvestigation of the NAc shell, where no discernable dopamine change was observed during the tail-pinch. We furthermore extend our study to consider norepinephrine responses in the ventral bed nucleus of the stria terminalis (vBNST), a spatially contiguous limbic structure. Norepinephrine release in this region, arising primarily from NST and A1 cell groups, is involved in the affective component of pain and facilitates stress responses through upregulation of HPA axis activity (Forray *et al.*, 2000; Forray & Gysling, 2004; Deyama *et al.*, 2009).

Using pharmacological agents to enhance catecholamine signaling, we found that tail-pinch has diverse effects on dopamine concentrations in the NAc shell and that, in most locations, dopamine release is inhibited during the noxious stimulus. In the vBNST norepinephrine release increased with tail-pinch but, unlike dopamine responses in the NAc shell, did not respond to the termination of the stimulus in a time-locked manner. These results demonstrate that dopamine in the NAc shell and norepinephrine in the vBNST process noxious stimulation via disparate, and in the case of dopamine in the NAc shell non-uniform, signaling patterns. The integration of these responses may act to initiate survival behaviors.

Experimental

Animals

Male Sprague-Dawley rats (300 – 400 g, Charles River Laboratories, Wilmington, MA) were used for these studies. Animals were housed in a controlled humidity and temperature environment with a 12:12 hour light:dark cycle. Food and water were available *ad libitum*. Experiments were conducted between 9:00 am and 5:00 pm. All procedures for handling and caring for the laboratory animals were in accordance with the NIH Guide for Care and Use of Laboratory Animals and were approved by the Institutional Animal Care and Use Committee of the University of North Carolina and Wake Forest University.

Surgery

Rats were anesthetized with urethane (1.5 g/kg, i.p.), immobilized in a stereotaxic frame (David Kopf Instruments, Tujunga, CA) and maintained at a body temperature of 37°C with a heating pad (Harvard Apparatus, Holliston, MA). Holes on the skull were drilled for the stimulating and carbon-fiber working electrodes using coordinates relative to bregma from the atlas of Paxinos and Watson (Paxinos & Watson, 2007). A Ag/AgCl reference electrode was implanted in the contralateral hemisphere and secured to the skull with a jeweler's screw.

In each experiment a carbon-fiber microelectrode was lowered into the NAc shell (anteroposterior [AP] +1.8 mm, mediolateral [ML] +0.8 mm) or vBNST (AP 0.0 mm, ML +1.2 mm). Electrical stimulation (24-60 biphasic pulses, 300 μ A, 2 ms/phase, 60 Hz) was applied through a pair of optically-isolated stimulators (NL 800A, Neurolog, Digitimer Ltd, Hertfordshire, UK) to a bipolar, stainless-steel electrode (0.2 mm in diameter, Plastics One, Roanoke, VA) placed into the VTA/ventral noradrenergic bundle (VNB, AP -5.2 mm, ML +1.2 mm, dorsoventral [DV] -8.0 to -9.0 mm). The VNB is the axon pathway formed mainly

by the noradrenergic neurons of the NST and A1 cell group, and passes directly through the VTA region.

Noxious stimulation

As described in our previous study (Budygin *et al.*, 2011) tail pinch was conducted with soft rubber gloves to avoid tissue damage and electrical noise artifacts. During each stimulus, the tail of the rat was pressed between the thumb and the index finger for 3 s with maximal pressure (P) of 3.12 ± 0.62 MPa. P was calculated by measuring the contact area between the fingers and the tail of the rat and by a measurement of the applied force using a Pasco CI-6537 Force Sensor (Roseville, CA). The stimulus was repeated at least three times at each recording location in the NAc shell or vBNST with rest interval of 2–3 min. Reactions such as ear or whisker twitches to the tail pinch were tested to ensure the animals were fully anesthetized before this procedure commenced.

Voltammetric procedures

A fresh, glass-sealed carbon-fiber microelectrode (75–100 μm exposed tip length, 7 μm diameter, T-650; Amoco, Greenville, SC) (Cahill *et al.*, 1996) was lowered into the NAc shell (DV -5.8 to -7.4 mm) or the vBNST (DV -7.2 to -7.7 mm). Fast-scan cyclic voltammetry was computer-controlled as described in detail previously (Heien *et al.*, 2003). A triangular scan (-0.4 to +1.3 V, 400V/s) was repeated every 100 ms to electrochemically detect catecholamine changes. Background-subtracted cyclic voltammograms were obtained by digitally-subtracting voltammograms collected during stimulation from those collected during baseline recording. Voltammetric responses were viewed as color plots with the abscissa as voltage, the ordinate as acquisition time, and the current encoded in color (Michael *et al.*, 1998). At the end of experiments the carbon-fiber was electrolyzed to create a lesion (see *below*). Currents were converted to concentration based on averaged *in vitro* calibration

factors (6.9 ± 0.3 pA/($\mu\text{M}\cdot\mu\text{m}^2$) for dopamine, 4.5 ± 0.2 pA/($\mu\text{M}\cdot\mu\text{m}^2$) for norepinephrine) obtained from a separate set of electrodes previously used *in vivo*.

Histology

At the end of the experiment, rats were euthanized with an overdose of urethane (2.0 g/kg) and electrode placements were verified by electrolytic lesions made by applying constant current (20 μA for 10 s) to the carbon-fiber microelectrodes (Park *et al.*, 2009). Brains were removed and stored in 10 % formalin solution for at least a week before being coronally sectioned into 50 μm thick slices on a cryostat. The sections were then mounted on slides and examined under a light microscope to verify carbon-fiber placements within the NAc shell or vBNST.

Chemical and drugs

All chemicals and drugs were obtained from Sigma-Aldrich (St. Louis, MO, USA) and were used without further purification. Calibration of the carbon-fiber microelectrodes with pH, dopamine, and norepinephrine were made after *in vivo* recordings in a buffer (pH 7.4 containing 15 mM Tris, 140 mM NaCl, 3.25 mM KCl, 1.2 mM CaCl_2 , 1.25 mM NaH_2PO_4 , 1.2 mM MgCl_2 , and 2.0 mM Na_2SO_4 in double distilled water (Mega Pure System, Corning Glasswork, Corning, NY). Desipramine-HCl, raclopride-HCl, and idazoxan-HCl were dissolved in sterile saline. GBR 12909 was dissolved in water and diluted in saline. Injected volumes were ~ 0.6 mL and were given intraperitoneally (i.p.).

Data analysis

Catecholamine concentration changes in response to tail pinch were quantified using a locally-written principal component regression algorithm (Keithley & Wightman, 2011). A residual analysis procedure was used to validate the predicted concentrations, and any trials

containing uncharacteristic variance larger than 95% of the noise of the training set were discarded. Data from each trial were background subtracted from the time point of lowest concentration. Significant changes of catecholamine concentration in response to tail pinch were evaluated using average baseline (-5.0 to 0 s) before the noxious stimuli. Mean values were compared by using the two-tailed Student's *t*-test to calculate the level of significance. Statistical analysis employed GraphPad Software version 4.0 (San Diego, CA, USA). $P < 0.05$ was regarded as statistically significant. Data are represented as mean \pm S.E.M. and 'n' values indicating the number of rats.

Results

Rapid extracellular dopamine changes in the NAc shell elicited by tail pinch

A fresh carbon-fiber microelectrode was lowered into the NAc shell by 0.2-0.3 mm increments beginning at -5.7 mm from the skull to evaluate changes in extracellular dopamine concentration in response to the noxious stimuli (tail pinch). Figure 3.1A (left panel) shows the coronal plane in which measurements were made (AP \sim +2.0 mm) in the NAc shell with the approximate electrode track marked by the solid line. Our previous study showed that maximal dopamine release is not observed until the electrode is positioned within the depths of the NAc shell (- 6.0 mm to - 7.0 mm below the skull) (Park *et al.*, 2010). Recording location was verified by electrolytic lesion at the end of the experiment (Fig. 3.1A, dashed white circle). Only dopamine signals recorded in the NAc shell were used in this study. To characterize the distribution of dopamine release sites in the NAc shell, dopamine release evoked by a bipolar electrical stimulation (60Hz, 24 pulses, 300 μ A) of the VTA and the VNB was measured at different depths with fast-scan cyclic voltammetry.

Once the electrode was positioned in the NAc shell, changes in extracellular dopamine concentration in response to tail pinch were measured at multiple recording depths (Fig. 3.1B, single animal data). The time course of dopamine concentration changes

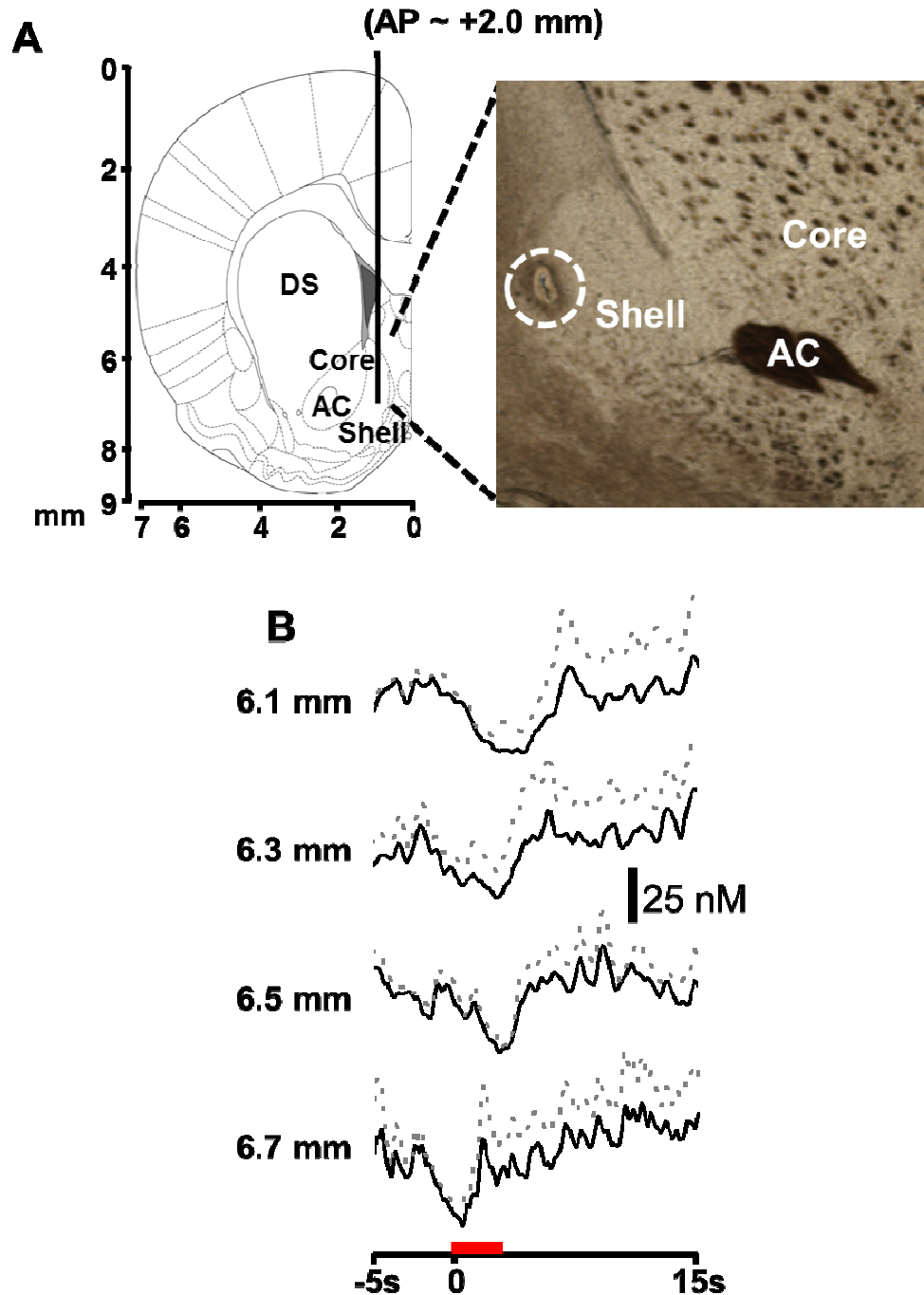


Figure 3.1. Anatomical mapping of tail pinch induced and electrically evoked dopamine responses in the NAc shell. (A) Solid line in the schematic diagram illustrates the approximate path of the carbon-fiber microelectrodes in the NAc shell (left). The coronal section was modified from the atlas of Paxinos and Watson [43]. The placement of the carbon-fiber microelectrode tip is indicated by the dashed white circle, which provides histological evidence that the electrode was positioned in the NAc shell (right). AP, anterior-posterior; AC, anterior commissure. (B) Average dopamine concentration changes to tail-pinch as a function of recording depth ($n = 3$ trials each). The time of tail pinch is indicated by the red bar. The dashed lines represent error as S.E.M.

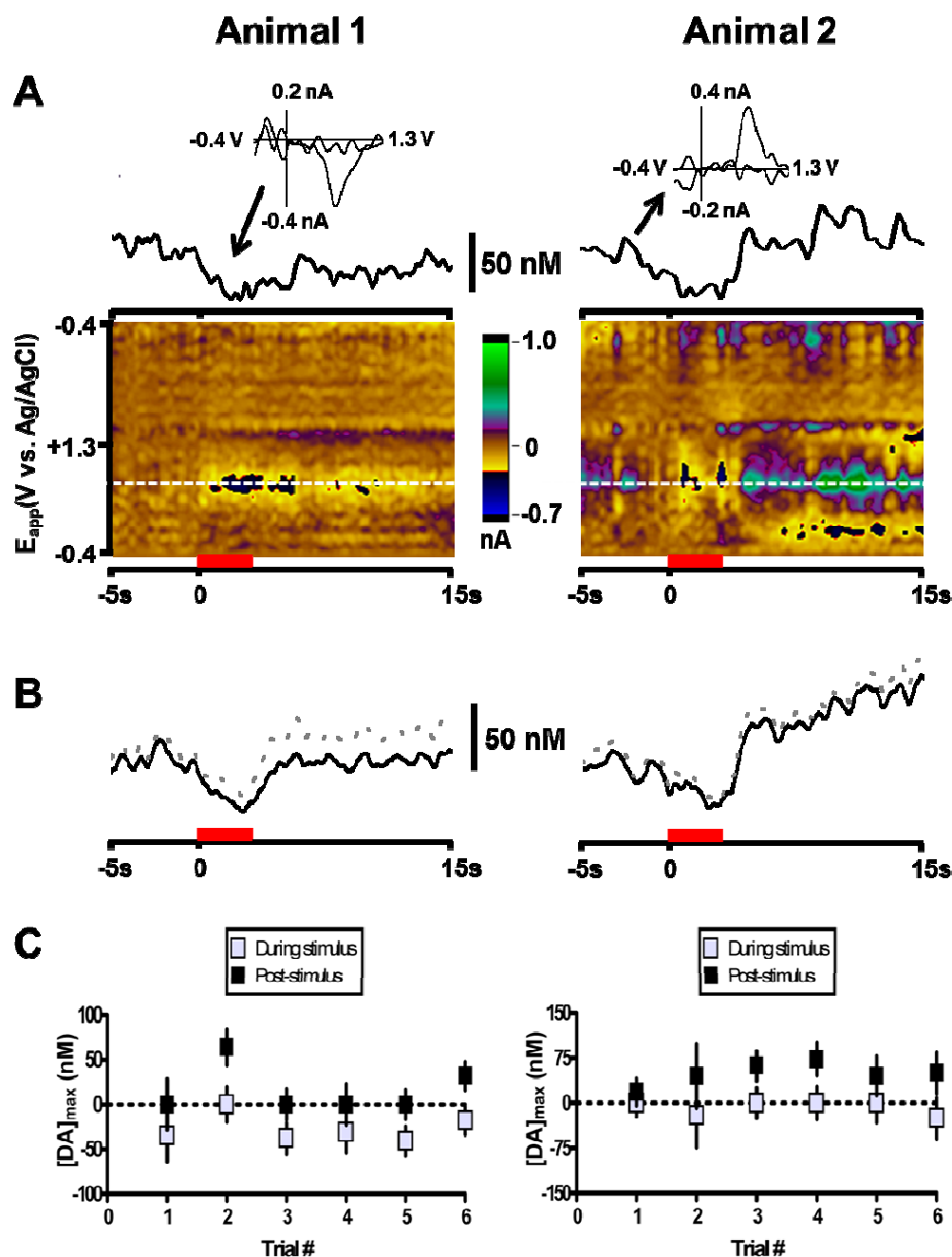


Figure 3.2. Dopamine signaling in the NAc shell in response to tail pinch. (A) Example dopamine responses to tail-pinch for two separate animals. Single trial electrochemical data is shown. The white dashed lines in the color plots indicate the potential of dopamine oxidation (~ 0.65 V). Current features at this potential become apparent with the administration of the tail-pinch stimulus (time denoted by red bars) and are converted to concentration by a post-calibration factor to produce the traces above the color plots. Representative cyclic voltammograms are provided for the times marked by the arrows. Negative oxidation currents at $+0.65$ V are representative of a decrease in dopamine concentrations. (B) Average dopamine concentration changes for the same animals and same recording locations ($n = 6$ trials each). The time of tail pinch is indicated by the red bars. Error bars are S.E.M. (C) Peak dopamine changes by trial for the same animals and same recording locations in response to tail pinch. The vertical lines through the data points indicate the noise levels (3σ) at the dopamine oxidation potential for each trial.

was obtained from the oxidation peak of the voltammograms ($\sim +0.65$ V). The dopamine responses to tail-pinch were much smaller than the concentration changes that occurred with electrical stimulation. At each recording depth tail pinch (at $t = 0$, 3 s duration, denoted as red bar) was repeated at least 3 times. In the example animal extracellular dopamine levels rapidly decreased on average during the tail pinch ($t = 0$ to 3 s). Once the stimulus ceased dopamine concentrations returned or, in some locations, spiked above pre-stimulus basal levels ($t = 3$ s). Apparent variation in the initial time of a dopamine response is most likely due to human error as the tail pinch was administered manually. At the end of each experiment electrical stimulation of the VTA was used to confirm dopamine release in each location. Tail pinch data are only presented for depths that exhibited dopamine release with electrical stimulation.

Three dopamine response types were observed with tail pinch among locations in the NAc shell, and these changes were observable even in individual trials (Fig. 3.2). During the tail pinch dopamine levels remained constant in some locations while decreased in others. At the offset of the stimulus dopamine levels either returned to baseline or transiently increased. Figure 3.2A provides example individual trial data for a monophasic decrease and a biphasic decrease-increase dopamine response to the stimulus. The dopamine response pattern was clearer when data was averaged for a recording location (Fig. 3.2B) as not all components of a response were observable ($S/N \geq 3$) in individual trials (Fig. 3.2C). It is important to note that many recording sites in the NAc shell exhibited no measurable dopamine response to tail pinch even though release could be evoked by electrical stimulation, which is likely due in part to the sedative effects of urethane anesthesia. Of 53 recording locations ($n=7$ animals), 12 sites exhibited a monophasic dopamine decrease during the tail pinch, 10 sites exhibited a monophasic dopamine increase to the cessation of the pinch, and 5 sites responded with the biphasic dopamine

decrease-increase pattern. No response was discernable in the other 26 recording locations.

Effects of dopamine autoreceptor and transporter inhibition on tail-pinch induced responses in the NAc shell

Effects of the selective dopamine uptake inhibitor GBR 12909 (GBR, 15 mg/kg), and the D2 autoreceptor antagonist raclopride (Rac, 2 mg/kg), on dopamine signaling in response to the tail pinch were investigated. Figure 3.3 shows dopamine responses to tail pinch before (control) and after drug administration (Rac+GBR) for different recording locations in the NAc shell. Under each dopamine concentration profile, voltammetric data is shown in a false-color plot. The oxidation and reduction potentials for dopamine are indicated by dashed and solid white lines, respectively. The time course of dopamine concentration changes was obtained from the oxidation peak ($\sim +0.65$ V) of the voltammograms.

Consistent with previous studies in the NAc shell of anesthetized animals, combined administration (5 min apart) of Rac and GBR enhanced dopamine overflow dynamics and induced spontaneous dopamine transients (Park *et al.*, 2010; Park *et al.*, 2011). These transients are clearly visible in Figure 3.3A, where tail-pinch did not induce measurable dopamine changes ($S/N < 3$) even after Rac and GBR. However, many initially unresponsive recording depths exhibited measurable tail-pinch induced dopamine responses after pharmacological manipulation (Fig 3.3B). When dopamine responses were observed in any animal, they were always time-locked to the duration of the stimulus even when its timing was extended (Fig 3.3B). Of 21 sites that showed no dopamine response pre-drug, only 6 remained unresponsive after administration of Rac and GBR.

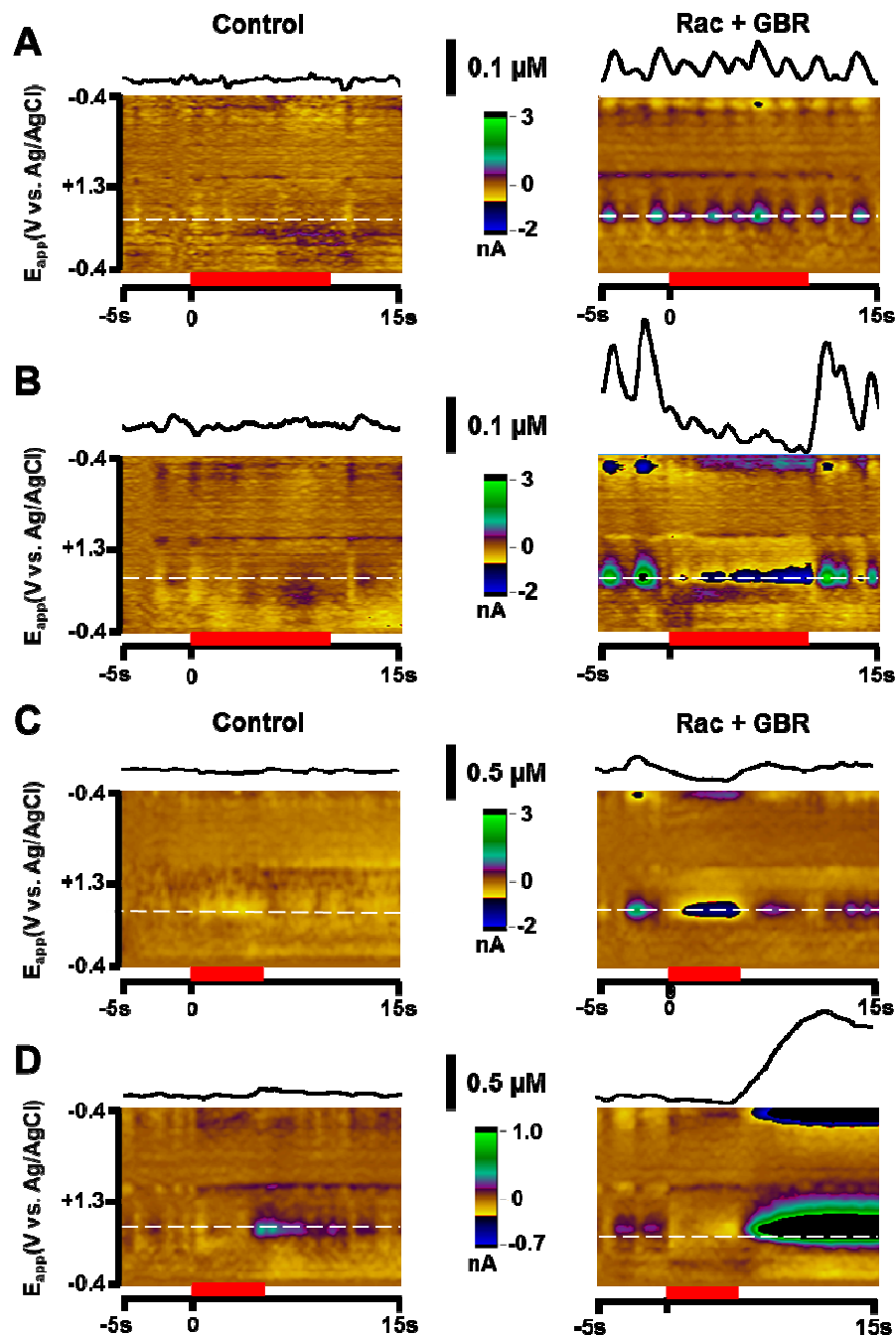


Figure 3.3. Dopamine signaling in the NAc shell in response to tail pinch after transporter and autoreceptor inhibition. Changes in extracellular dopamine were more clearly observed after administration of the selective dopamine drugs, raclopride (Rac, 2 mg/kg) and GBR 12909 (GBR, 15 mg/kg). (A and B) Tail-pinch induced dopamine responses for a single animal at two recording depths before (left) and after (right) pharmacological manipulation. Electrochemical data is provided in the color plots where the potential of dopamine oxidation (~ 0.65 V) is indicated by the white dashed lined. Dopamine concentration changes over time are provided above the color plots. The time of tail pinch (10 s duration) is indicated by the red bars. (C and D) Tail-pinch induced dopamine responses for a separate animal at two recording depths before (left) and after (right) pharmacological manipulation. The time of tail pinch (3 s duration) is indicated by the red bars.

In the second of the two animals shown, changes in dopamine concentration during tail pinch were small, but measurable before drug administration (Fig. 3.3C and D, left panels). In this animal, extracellular dopamine levels monophasically decreased to the stimulus at one location (Fig. 3.3C) and changed in a biphasic manner at another (Fig. 3.3D). Once dopamine transients were induced through autoreceptor and transporter inhibition, these dopamine responses became pronounced (Fig. 3.3C and D, right panels). Overall pre-drug dopamine responses to tail pinch ($\Delta[\text{DA}] = -46.9 \pm 3.9$ nM during stimulus; $\Delta[\text{DA}] = 63.1 \pm 7.0$ nM post stimulus, $n = 7$) were significantly enhanced after dopamine drug administration (Rac + GBR: $\Delta[\text{DA}] = -89.4 \pm 12.9$ nM during stimulus, $P < 0.05$; $\Delta[\text{DA}] = 630 \pm 145$ nM, $P < 0.01$ post-stimulus, $n = 7$).

Rapid extracellular norepinephrine changes in the vBNST elicited by tail pinch

A second set of experiments was conducted to investigate extracellular norepinephrine concentration changes in the vBNST in response to noxious stimulation. Figure 3.4A displays the electrode tract (left) for norepinephrine measurements in vBNST (shaded red), and a histological image of the vBNST (right) with the recording site marked by electrolytic lesion indicated by the dashed white circle. Only signals that were verified by histology to be recorded in the vBNST were used in this study ($n = 7$). Within the vBNST (DV ~ 7.3 mm – 7.7 mm from the skull) electrically-stimulated norepinephrine release reached a maximum at a depth of ~7.5 mm as described previously (Park *et al.*, 2009; Herr *et al.*, 2012). Figure 3.4B displays norepinephrine release evoked by electrical stimulation and tail pinch (left and right panels respectively, denoted by red bar) at different depths in the vBNST. As norepinephrine release is confined to a narrow range of depths in the vBNST (Park *et al.*, 2009; Park *et al.*, 2012), data from only one recording depth was obtained for each animal.

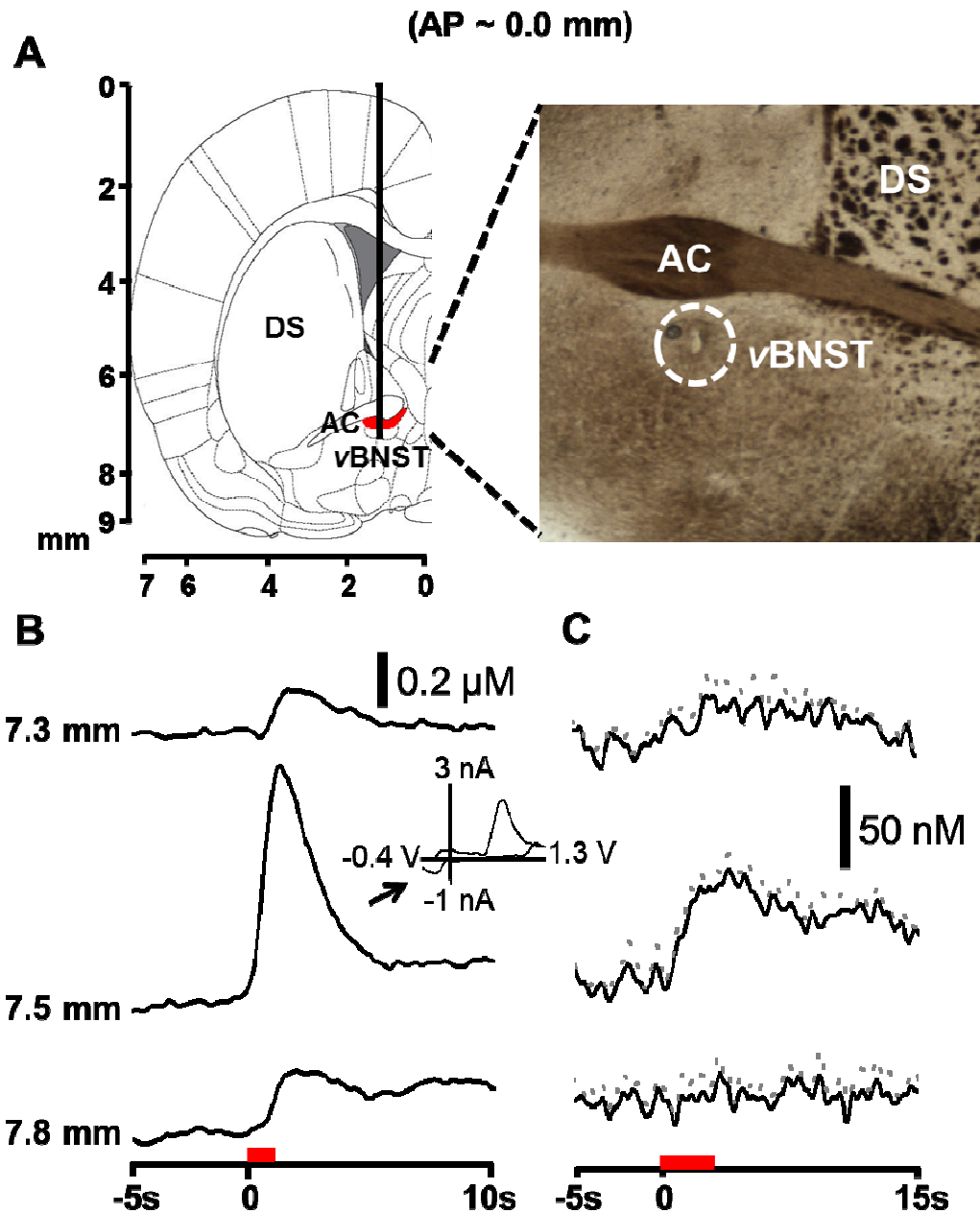


Figure 3.4. Anatomical mapping of tail pinch induced and electrically evoked norepinephrine responses in the vBNST. (A) Solid line in the schematic diagram illustrates the approximate path of the carbon-fiber microelectrodes in the vBNST (shaded red, left). The coronal section was taken from the atlas of Paxinos and Watson [43]. The placement of the carbon-fiber microelectrode tip is indicated by the dotted white circle, which provides histological evidence that the electrode was positioned in the vBNST (right). AP, anterior-posterior; AC, anterior commissure; CPu, caudate-putamen; vBNST, ventral bed nucleus of the stria terminalis. (B) Mapping of electrically evoked (60 Hz, 60 pulses, $\pm 300 \mu\text{A}$) norepinephrine release in the vBNST recorded at the depth indicated. The red bars under the current trace show the electrical stimulation time. (C) Average norepinephrine concentration changes to tail-pinch at the recording depth indicated ($n = 3$ trials each). The time of tail pinch is indicated by the red bar. The dashed lines represent error as S.E.M.

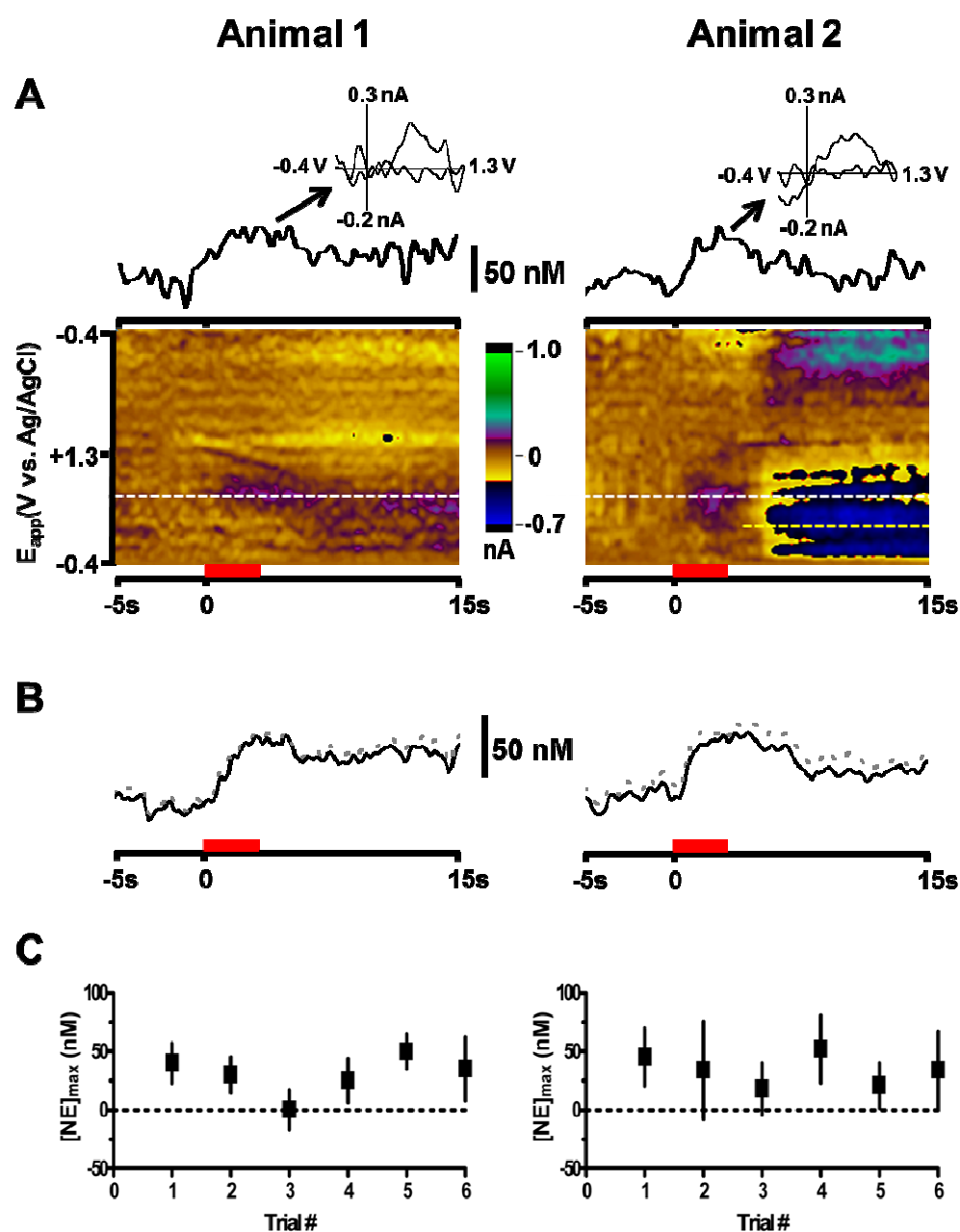


Figure 3.5. Norepinephrine signaling in the vBNST in response to tail pinch. (A) Example dopamine responses to tail-pinch for two separate animals. Single trial electrochemical data is shown. The white dashed lines in the color plots indicate the potential of norepinephrine oxidation (~ 0.7 V). Current features at this potential become apparent with the administration of the tail-pinch stimulus (time denoted by red bars) and are converted to concentration by a post-calibration factor to produce the traces above the color plots. Representative cyclic voltammograms are provided for the times marked by the arrows. (B) Average norepinephrine concentration changes for the same animals and same recording locations ($n = 6$ trials each). The time of tail pinch is indicated by the red bars. Error bars are S.E.M. (C) Peak norepinephrine changes by trial for the same animals and same recording locations in response to tail pinch. The vertical lines through the data points indicate the noise levels (3σ) at the norepinephrine oxidation potential for each trial.

In contrast to dopamine trials in the NAc shell, norepinephrine concentrations in the vBNST consistently increased during tail pinch and remained elevated briefly even after the stimulus ended (Fig. 3.4C). Again, apparent variation in the initial time of norepinephrine response is due to the fact that the tail pinch was administered manually. Similar to dopamine in the NAc shell, the norepinephrine changes observed during tail pinch were smaller than that elicited by the electrical stimulation (Fig. 3.4B and C), but were still detectable in single trial data (Fig. 3.5). Clear norepinephrine responses were found after data was averaged for multiple trials at a single location (Fig. 3.5B). The magnitude of individual responses did not significantly change after multiple noxious stimulations (Fig. 3.5C).

Effects of norepinephrine autoreceptor and transporter inhibition on tail-pinch induced responses in the vBNST

As in dopamine experiments, the effects of the selective norepinephrine uptake inhibitor, desipramine (15 mg/kg), and α_2 receptor antagonist, idazoxan (5 mg/kg), on norepinephrine transmission in response to tail pinch were investigated. Pre- and post-drug norepinephrine concentration changes are shown for two animals in Figure 3.6. Under each norepinephrine concentration profile, data is shown in a false-color plot of voltammetric current. The time course of norepinephrine concentration changes was obtained from oxidation potential of norepinephrine denoted on the color plots by the dashed white lines. For some anesthetized animals prominent pH shifts coincided with changes in norepinephrine concentration in the vBNST (Fig. 3.6B, pH features indicated by yellow dashed lines) (Takmakov *et al.*, 2010). Concentration data for such trials were obtained through the use of principle component analysis (see, **Data Analysis**).

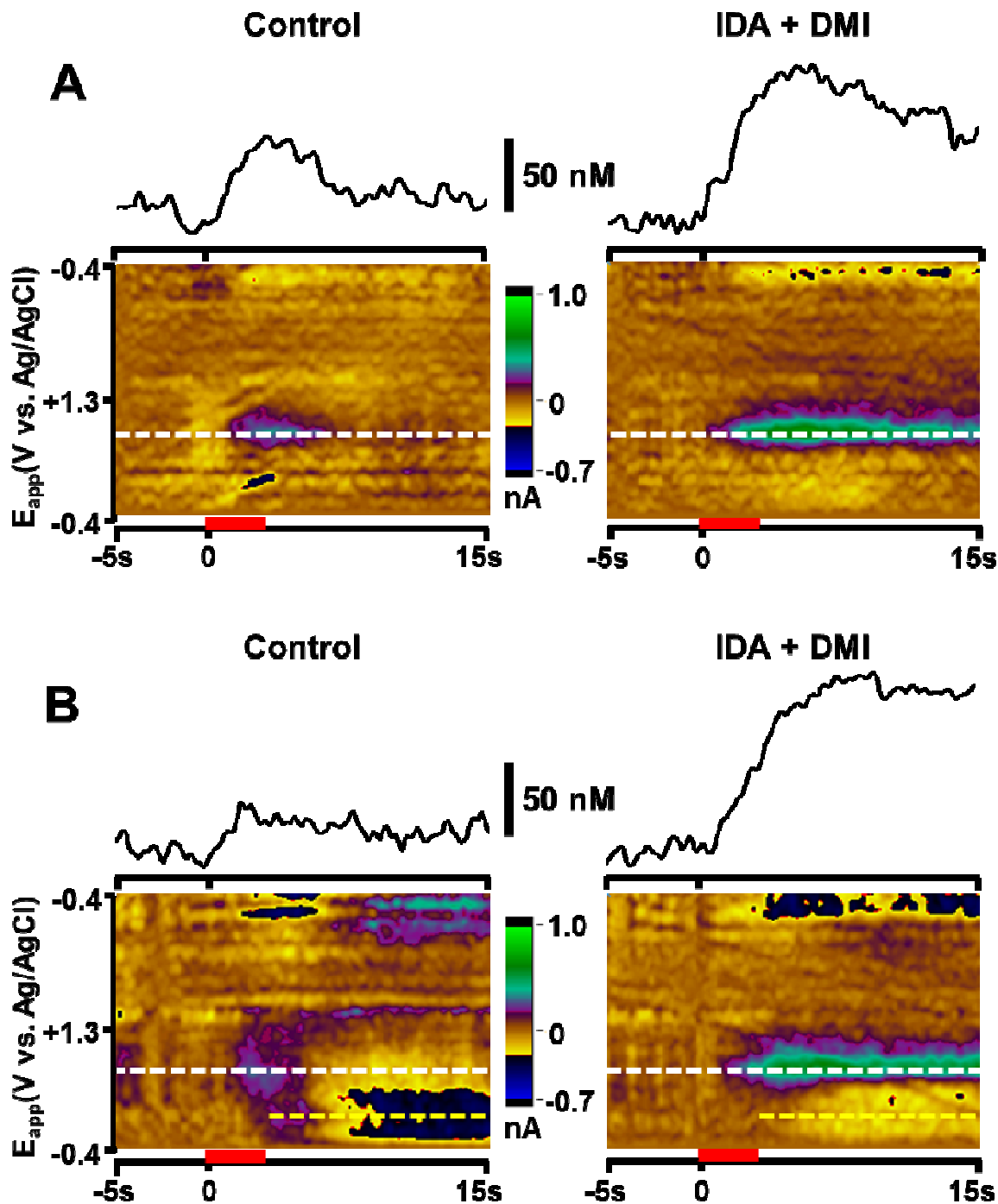


Figure 3.6. Norepinephrine signaling in the vBNST in response to tail pinch after transporter and autoreceptor inhibition. Norepinephrine signaling patterns were more clearly observed after administration of the selective norepinephrine drugs, idazoxan (IDA, 5 mg/kg) and desipramine (DMI, 15 mg/kg). (A and B) Tail-pinch induced norepinephrine responses two separate animals before (left) and after (right) pharmacological manipulation. Electrochemical data is provided in the color plots where the potential of norepinephrine oxidation (~ 0.65 V) is indicated by the white dashed lined. Norepinephrine concentration changes over time are provided above the color plots. The time of tail pinch (3 s duration) is indicated by the red bars.

Unlike dopamine, the combined effects of autoreceptor/transporter inhibition do not induce transient norepinephrine release (Park *et al.*, 2011), but did significantly increase the magnitude and duration of extracellular norepinephrine elevation with tail pinch in this study. Norepinephrine transmission continued to display the same response pattern to the tail pinch even after norepinephrine drug administration (Pre-drug $\Delta[NE] = 47.1 \pm 3.8$ nM, $n = 7$), Post IDA +DMI $\Delta[NE] = 119.8 \pm 17$ nM, $P < 0.01$, $n = 7$).

Discussion

Tail pinch is a classic noxious stimulus, which may result in pain depending on its intensity [20]. In rodents this mild stressor generates a state of arousal that can facilitate motivated behaviors as varied as feeding, copulation and maternal behaviors (Antelman & Szechtman, 1975; Szechtman *et al.*, 1977; Leyton & Stewart, 1996). In anesthetized animals where affective and cognitive aspects of pain are dampened, noxious sensory input can still evoke measurable alterations in the neurons underlying these behaviors, including those of the central catecholamine systems (Grant *et al.*, 1988; Brischoux *et al.*, 2009).

Here we investigated the effects of a brief tail-pinch on catecholamine neurotransmission in two limbic terminal regions of the anesthetized rat brain, the NAc shell and the vBNST. Using FSCV and pharmacological agents to enhance release dynamics, we report new features in dopamine transmission for the NAc shell during tail pinch and, moreover, find that norepinephrine transmission in the BNST is oppositely regulated by noxious stimulation. While some intertrial variation was apparent at each recording site, neither dopamine nor norepinephrine responses showed sensitization over repeated stimulations.

Tail-pinch induced dopamine transmission in the NAc shell

As an important limbic-motor interface, the NAc has received considerable attention regarding its role during appetitive behaviors, where dopamine overflow increases during the presentation, seeking and anticipation of food reward, drugs of abuse, and intracranial self-stimulation (Phillips *et al.*, 2003; Roitman *et al.*, 2008; Park *et al.*, 2013a). While not as extensively characterized, accumbal dopamine also responds to various states of aversion (Roitman *et al.*, 2008; Badrinarayan *et al.*, 2012; Park *et al.*, 2012; Oleson & Cheer, 2013), and can inhibit pain (Altier & Stewart, 1999; Taylor *et al.*, 2003; Wood, 2006). However, in contrast to the general excitation of dopamine neurons by reward, electrophysiological recordings have established that the effects of noxious stimuli on VTA dopamine neurons are variable. Subpopulations of VTA dopamine neurons are excited, inhibited or unaffected by noxious stimuli such as electrical foot-shock and tail-pinch (Mantz *et al.*, 1989; Ungless *et al.*, 2004; Brischoux *et al.*, 2009; Zweifel *et al.*, 2011). Moreover, an additional subset of dopamine neurons exhibits a transient surge of activity at the offset of aversive stimuli (Brischoux *et al.*, 2009; Wang & Tsien, 2011).

These diverse firing patterns are thought to be due to a functional separation of VTA dopamine neurons into populations that encode motivational salience versus motivational value (Matsumoto & Hikosaka, 2009; Bromberg-Martin *et al.*, 2010). Dopamine neurons associated with motivational salience increase firing to signify the relative importance of a stimulus. In contrast, the activity of dopamine neurons relaying motivational value directly correlates to the hedonic aspects of a stimulus. Though it is often difficult to discriminate between these two signaling modalities during reward—where salience and value are highly correlated—aversive stimuli are both salient and of negative valence, and therefore affect the activities of these neuronal populations inversely.

This dichotomy in motivational processing is maintained in the NAc, where the NAc core is more associated with salience and attentional-orientation while the NAc shell

mediates valuation of external stimuli to drive approach-avoidance behaviors (Bromberg-Martin *et al.*, 2010; Saddoris *et al.*, 2013). Supporting this idea, we previously found regional differences in accumbal dopamine transmission to acute tail pinch (Budygin *et al.*, 2011). During the tail pinch, a salient noxious event, dopamine increased in the NAc core. At the cessation of the tail pinch, which unarguably has rewarding attributes (Tanimoto *et al.*, 2004), dopamine transiently increased in the NAc shell.

Oddly, we did not observe a response during the tail-pinch in the NAc shell, where one would expect the aversiveness of the stimulus to be signaled by decreased dopamine release. Here we proposed that the absence of this dopamine response in our past study was due an insufficient limit of detection. To increase signal strength, we pharmacologically blocked the D2 autoreceptor and the dopamine transporter (DAT) respectively with raclopride and GBR12909. These drugs act to increase the amount and duration of dopamine release that occurs with neuronal activation, and, when administered in combination, cause high-frequency dopamine transients within the NAc of anesthetized animals (Venton & Wightman, 2007; Park *et al.*, 2010). These dopamine transients are of measurable amplitude and provide background activity by which to clearly resolve decreases in release.

With pharmacological enhancement, we confirmed that tail pinch does suppress dopamine transmission in the shell, but not at all locations. Instead, we observed that tail-pinch induced dopamine signaling varies within the shell, which was not evident in our previous study as data was averaged for each animal. Within this accumbal region, dopamine either decreased at the onset of the noxious stimulus or increased at the stimulus offset, and, at some locations, exhibited both of these responses. Other locations, however, showed no discernible dopamine change to tail-pinch even after pharmacological manipulation. The type of response observed was unlikely due to differences in synaptic

proximity as all of the locations reported here exhibited similar electrically-stimulated dopamine release and drug-induced transient activity.

Together three distinct release patterns were identified, corresponding to the activities reported for VTA dopamine neurons during noxious stimulation (Ungless *et al.*, 2004; Brischoux *et al.*, 2009). Our data suggests that the NAc shell is innervated by VTA dopamine neurons that differentially encode noxious input, in contrast to the NAc core where dopamine uniformly increased during tail pinch. Variation in dopamine signaling is not unexpected for this region given that appetitive and aversive processing are believed to be confined to subdomains of the NAc shell (Reynolds & Berridge, 2002). The temporo-spatial aspects of these responses may underlie the controversial results observed in past studies.

Tail-pinch induced norepinephrine transmission in the vBNST

The BNST, a major limbic target of the central norepinephrine system, integrates descending cortico-limbic and ascending sensory information to modulate HPA axis activity and, in turn, glucocorticoid secretion in response to stress (Dumont, 2009). In general norepinephrine transmission in the brain is considered a major component of the central stress response, where it acts to heighten arousal and behavioral responsivity (Aston-Jones & Cohen, 2005; Morilak *et al.*, 2005). Norepinephrine in the BNST, which is densely concentrated in the ventral region, specifically acts to facilitate HPA axis output during negative emotional states (Forray & Gysling, 2004).

The noradrenergic innervation of the BNST originates principally from the NST and A1 cell groups, though a small contribution does arise from the LC through the dorsal noradrenergic bundle (Lindvall & Stenevi, 1978; Forray *et al.*, 2000). The medullar (NST and A1) populations are positioned to relay sensory, visceral, cardiorespiratory and, though not as extensively characterized, nociceptive information between the peripheral and central nervous systems (Pertovaara, 2006; Rinaman, 2011). Studies have found a role for the

NST in the baroreflex to noxious thermal stimulation (Gau *et al.*, 2009) and in the tonic control of nociceptive thresholds (Marques-Lopes *et al.*, 2012). Furthermore, catecholamine neurons in this area are activated by visceral pain (Gallas *et al.*, 2011). The LC, a dense population of norepinephrine neurons located in the hindbrain, is also excited by a wide-range of sensory stimuli including those that present physical or psychological threat including nociception (Svensson, 1987; Chapman & Nakamura, 1999), and in the case of persistent pain provides feedback inhibition (Pertovaara, 2006).

Consistent with electrophysiological work, norepinephrine release within the BNST is enhanced by a variety of stressors such as restraint, bitter taste, reward-omission and morphine withdraw (Pacak *et al.*, 1995; Van Bockstaele *et al.*, 2008; Park *et al.*, 2012; Park *et al.*, 2013a). Pain can of course be a particularly potent form of stress and, accordingly, somatic and visceral nociception also stimulates BNST norepinephrine release (Deyama *et al.*, 2009; Deyama *et al.*, 2011). Functionally, increased BNST norepinephrine transmission through β adrenergic receptors is associated with the negative affective component of pain and is required for pain-induced conditioned-place aversion (Deyama *et al.*, 2008) .

Together these reports describe a positive correlation between noradrenergic cell activity and states of aversion. Congruently, we found extracellular norepinephrine concentration in the vBNST transiently increased to acute tail-pinch (Fig. 3.5). Though it was not possible to map different recording depths within the vBNST due to its size, similar norepinephrine responses were observed across all animals. Unlike for dopamine in the NAc, no new features in vBNST norepinephrine responses were revealed after pharmacological enhancement of norepinephrine release with administration of the α_2 autoreceptor antagonist idazoxan and the NET inhibitor desipramine.

Interestingly, extracellular norepinephrine remained elevated briefly after the noxious stimulation ceased, and the duration of the response became further extended after transporter blockade. While few non-voltammetric studies have considered extracellular

norepinephrine responses to a single, brief noxious stimulation as we have done here, microdialysis measurements have recorded basal changes in BNST norepinephrine in awake animals lasting minutes to hours beyond the presentation of a stressor (Morilak *et al.*, 2005). This may suggest that BNST norepinephrine plays a limited role in transmitting information regarding the temporal aspects of external stimuli, and rather promotes a general change in affective state to generate the appropriate coping response to environmental challenge.

Conclusions

In summary, we demonstrated that tail pinch, an acute noxious stimulus, triggers transient changes in extracellular catecholamine levels in the NAc shell and the vBNST of anesthetized rats. Throughout the NAc shell, a region associated with value-driven motivational behavior, dopamine transmission was overall attenuated by the stimulation and increased by its cessation. In the BNST, a key upstream regulator of adrenal stress hormone secretion, tail pinch caused an extended increase in extracellular norepinephrine levels. The opposing effects of tail pinch we observed align with the respective roles of accumbal dopamine and BNST norepinephrine as reward and stress neurotransmitters. Moreover, the temporal differences between their responses are in agreement with the respective involvement of these two limbic structures in motor versus hormonal aspects of pain processing. Together these data demonstrate that limbic catecholamine systems are divergently recruited during a physically threatening stimulation, and may be crucial in the expression of pain-related responses.

REFERENCES

- Abercrombie, E.D., Keefe, K.A., DiFrischia, D.S. & Zigmond, M.J. (1989) Differential effect of stress on in vivo dopamine release in striatum, nucleus accumbens, and medial frontal cortex. *J Neurochem.*, **52**, 1655-1658.
- Altier, N. & Stewart, J. (1999) The role of dopamine in the nucleus accumbens in analgesia. *Life Sci.*, **65**, 2269-2287.
- Amato, D., Natesan, S., Yavich, L., Kapur, S. & Muller, C.P. (2011) Dynamic regulation of dopamine and serotonin responses to salient stimuli during chronic haloperidol treatment. *Int J Neuropsychopharmacol*, **14**, 1327-1339.
- Antelman, S.M. & Szechtman, H. (1975) Tail pinch induces eating in sated rats which appears to depend on nigrostriatal dopamine. *Science.*, **189**, 731-733.
- Aston-Jones, G. & Cohen, J.D. (2005) An integrative theory of locus coeruleus-norepinephrine function: adaptive gain and optimal performance. *Annu Rev Neurosci*, **28**, 403-450.
- Badrinarayan, A., Wescott, S.A., Vander Weele, C.M., Saunders, B.T., Couturier, B.E., Maren, S. & Aragona, B.J. (2012) Aversive stimuli differentially modulate real-time dopamine transmission dynamics within the nucleus accumbens core and shell. *J Neurosci*, **32**, 15779-15790.
- Brischoux, F., Chakraborty, S., Brierley, D.I. & Ungless, M.A. (2009) Phasic excitation of dopamine neurons in ventral VTA by noxious stimuli. *Proc Natl Acad Sci U S A.*, **106**, 4894-4899. Epub 2009 Mar 4894.
- Bromberg-Martin, E.S., Matsumoto, M. & Hikosaka, O. (2010) Dopamine in motivational control: rewarding, aversive, and alerting. *Neuron*, **68**, 815-834.
- Budygin, E.A., Park, J., Bass, C.E., Grinevich, V.P., Bonin, K.D. & Wightman, R.M. (2011) Aversive stimulus differentially triggers subsecond dopamine release in reward regions. *Neuroscience*, **7**.
- Cahill, P.S., Walker, Q.D., Finnegan, J.M., Mickelson, G.E., Travis, E.R. & Wightman, R.M. (1996) Microelectrodes for the measurement of catecholamines in biological systems. *Anal Chem.*, **68**, 3180-3186.
- Chapman, C.R. & Nakamura, Y. (1999) A passion of the soul: an introduction to pain for consciousness researchers. *Conscious Cogn.*, **8**, 391-422.

- Delgado, P.L. (2004) Common pathways of depression and pain. *J Clin Psychiatry*, **65 Suppl 12**, 16-19.
- Deyama, S., Ide, S., Kondoh, N., Yamaguchi, T., Yoshioka, M. & Minami, M. (2011) Inhibition of noradrenaline release by clonidine in the ventral bed nucleus of the stria terminalis attenuates pain-induced aversion in rats. *Neuropharmacology*, **61**, 156-160.
- Deyama, S., Katayama, T., Kondoh, N., Nakagawa, T., Kaneko, S., Yamaguchi, T., Yoshioka, M. & Minami, M. (2009) Role of enhanced noradrenergic transmission within the ventral bed nucleus of the stria terminalis in visceral pain-induced aversion in rats. *Behav Brain Res.*, **197**, 279-283.
- Deyama, S., Katayama, T., Ohno, A., Nakagawa, T., Kaneko, S., Yamaguchi, T., Yoshioka, M. & Minami, M. (2008) Activation of the beta-adrenoceptor-protein kinase A signaling pathway within the ventral bed nucleus of the stria terminalis mediates the negative affective component of pain in rats. *J Neurosci*, **28**, 7728-7736.
- Dumont, E.C. (2009) What is the bed nucleus of the stria terminalis? *Prog Neuropsychopharmacol Biol Psychiatry.*, **33**, 1289-1290. Epub 2009 Jul 1212.
- Elman, I., Borsook, D. & Volkow, N.D. (2013) Pain and suicidality: insights from reward and addiction neuroscience. *Prog Neurobiol*, **109**, 1-27.
- Forray, M.I. & Gysling, K. (2004) Role of noradrenergic projections to the bed nucleus of the stria terminalis in the regulation of the hypothalamic-pituitary-adrenal axis. *Brain Res Brain Res Rev*, **47**, 145-160.
- Forray, M.I., Gysling, K., Andres, M.E., Bustos, G. & Araneda, S. (2000) Medullary noradrenergic neurons projecting to the bed nucleus of the stria terminalis express mRNA for the NMDA-NR1 receptor. *Brain Res Bull*, **52**, 163-169.
- Gallas, S., Sinno, M.H., Boukhettala, N., Coeffier, M., Dourmap, N., Gourcerol, G., Ducrotte, P., Dechelotte, P., Leroi, A.M. & Fetissov, S.O. (2011) Gastric electrical stimulation increases ghrelin production and inhibits catecholaminergic brainstem neurons in rats. *Eur J Neurosci*, **33**, 276-284.
- Gau, R., Sevoz-Couche, C., Laguzzi, R., Hamon, M. & Bernard, J.F. (2009) Inhibition of cardiac baroreflex by noxious thermal stimuli: a key role for lateral paragigantocellular serotonergic cells. *Pain*, **146**, 315-324.

- Grant, S.J., Aston-Jones, G. & Redmond, D.E., Jr. (1988) Responses of primate locus coeruleus neurons to simple and complex sensory stimuli. *Brain Res Bull.*, **21**, 401-410.
- Hasue, R.H. & Shammah-Lagnado, S.J. (2002) Origin of the dopaminergic innervation of the central extended amygdala and accumbens shell: a combined retrograde tracing and immunohistochemical study in the rat. *J Comp Neurol*, **454**, 15-33.
- Heien, M.L., Phillips, P.E., Stuber, G.D., Seipel, A.T. & Wightman, R.M. (2003) Overoxidation of carbon-fiber microelectrodes enhances dopamine adsorption and increases sensitivity. *Analyst.*, **128**, 1413-1419.
- Herr, N.R., Park, J., McElligott, Z.A., Belle, A.M., Carelli, R.M. & Wightman, R.M. (2012) In Vivo Voltammetry Monitoring of Electrically Evoked Extracellular Norepinephrine in Subregions of the Bed Nucleus of the Stria Terminalis. *J Neurophysiol*, **107**, 1731-1737.
- Kalivas, P.W. & Duffy, P. (1995) Selective activation of dopamine transmission in the shell of the nucleus accumbens by stress. *Brain research*, **675**, 325-328.
- Keithley, R.B. & Wightman, R.M. (2011) Assessing principal component regression prediction of neurochemicals detected with fast-scan cyclic voltammetry. *ACS Chem Neurosci.*, doi: 10.1021/cn200035u.
- Leyton, M. & Stewart, J. (1996) Acute and repeated activation of male sexual behavior by tail pinch: opioid and dopaminergic mechanisms. *Physiol Behav*, **60**, 77-85.
- Lindvall, O. & Stenevi, U. (1978) Dopamine and noradrenaline neurons projecting to the septal area in the rat. *Cell Tissue Res*, **190**, 383-407.
- Mantz, J., Thierry, A.M. & Glowinski, J. (1989) Effect of noxious tail pinch on the discharge rate of mesocortical and mesolimbic dopamine neurons: selective activation of the mesocortical system. *Brain research*, **476**, 377-381.
- Marques-Lopes, J., Martins, I., Pinho, D., Morato, M., Wilson, S.P., Albino-Teixeira, A. & Tavares, I. (2012) Decrease in the expression of N-methyl-D-aspartate receptors in the nucleus tractus solitarius induces antinociception and increases blood pressure. *J Neurosci Res*, **90**, 356-366.
- Matsumoto, M. & Hikosaka, O. (2009) Two types of dopamine neuron distinctly convey positive and negative motivational signals. *Nature*, **459**, 837-841.

- Michael, D., Travis, E.R. & Wightman, R.M. (1998) Color images for fast-scan CV measurements in biological systems. *Anal.Chem.*, **70**, 586A-592A.
- Morilak, D.A., Barrera, G., Echevarria, D.J., Garcia, A.S., Hernandez, A., Ma, S. & Petre, C.O. (2005) Role of brain norepinephrine in the behavioral response to stress. *Prog Neuropsychopharmacol Biol Psychiatry*, **29**, 1214-1224.
- Oleson, E.B. & Cheer, J.F. (2013) On the role of subsecond dopamine release in conditioned avoidance. *Front Neurosci*, **7**, 96.
- Pacak, K., McCarty, R., Palkovits, M., Kopin, I.J. & Goldstein, D.S. (1995) Effects of immobilization on in vivo release of norepinephrine in the bed nucleus of the stria terminalis in conscious rats. *Brain Res.*, **688**, 242-246.
- Park, J., Aragona, B.J., Kile, B.M., Carelli, R.M. & Wightman, R.M. (2010) In vivo voltammetric monitoring of catecholamine release in subterritories of the nucleus accumbens shell. *Neuroscience*, **169**, 132-142.
- Park, J., Bucher, E.S., Fontillas, K., Owesson-White, C., Ariansen, J.L., Carelli, R.M. & Wightman, R.M. (2013a) Opposing catecholamine changes in the bed nucleus of the stria terminalis during intracranial self-stimulation and its extinction. *Biol Psychiatry*, **74**, 69-76.
- Park, J., Bucher, E.S. & Wightman, R.M. (2013b) Opposing Regulation of Norepinephrine and Dopamine in Rat Limbic Brain Regions in Response to Aversive Stimuli. In Eiden, L.E. (ed) *Catecholamine Research in the 21st Century* Academic Press, New York pp. 159.
- Park, J., Kile, B.M. & Wightman, R.M. (2009) *In vivo* voltammetric monitoring of norepinephrine release in the rat ventral bed nucleus of the stria terminalis and anteroventral thalamic nucleus. *Eur J Neurosci.*, **30**, 2121-2133.
- Park, J., Takmakov, P. & Wightman, R.M. (2011) In vivo comparison of norepinephrine and dopamine release in rat brain by simultaneous measurements with fast-scan cyclic voltammetry. *J Neurochem*, **119**, 932-944.
- Park, J., Wheeler, R.A., Fontillas, K., Keithley, R.B., Carelli, R.M. & Wightman, R.M. (2012) Catecholamines in the bed nucleus of the stria terminalis reciprocally respond to reward and aversion. *Biol Psychiatry*, **71**, 327-334.
- Paxinos, G. & Watson, C. (2007) *The Rat Brain in Stereotaxic Coordinates*. Academic Press, New York.

- Pei, Q., Zetterstrom, T. & Fillenz, M. (1990) Tail pinch-induced changes in the turnover and release of dopamine and 5-hydroxytryptamine in different brain regions of the rat. *Neuroscience*, **35**, 133-138.
- Pertovaara, A. (2006) Noradrenergic pain modulation. *Prog Neurobiol.*, **80**, 53-83.
- Phillips, P.E., Stuber, G.D., Heien, M.L., Wightman, R.M. & Carelli, R.M. (2003) Subsecond dopamine release promotes cocaine seeking. *Nature*, **422**, 614-618.
- Reynolds, S.M. & Berridge, K.C. (2002) Positive and negative motivation in nucleus accumbens shell: bivalent rostrocaudal gradients for GABA-elicited eating, taste "liking"/"disliking" reactions, place preference/avoidance, and fear. *J Neurosci*, **22**, 7308-7320.
- Rinaman, L. (2011) Hindbrain noradrenergic A2 neurons: diverse roles in autonomic, endocrine, cognitive, and behavioral functions. *Am J Physiol Regul Integr Comp Physiol*, **300**, R222-235.
- Robinson, D.L., Hermans, A., Seipel, A.T. & Wightman, R.M. (2008) Monitoring rapid chemical communication in the brain. *Chem Rev.*, **108**, 2554-2584. .
- Roitman, M.F., Wheeler, R.A., Wightman, R.M. & Carelli, R.M. (2008) Real-time chemical responses in the nucleus accumbens differentiate rewarding and aversive stimuli. *Nat Neurosci*, **11**, 1376-1377.
- Saddoris, M.P., Sugam, J.A., Cacciapaglia, F. & Carelli, R.M. (2013) Rapid dopamine dynamics in the accumbens core and shell: learning and action. *Front Biosci (Elite Ed)*, **5**, 273-288.
- Svensson, T.H. (1987) Peripheral, autonomic regulation of locus coeruleus noradrenergic neurons in brain: putative implications for psychiatry and psychopharmacology. *Psychopharmacology (Berl)*. **92**, 1-7.
- Swanson, L.W. (1982) The projections of the ventral tegmental area and adjacent regions: a combined fluorescent retrograde tracer and immunofluorescence study in the rat. *Brain Res Bull.*, **9**, 321-353.
- Szechtman, H., Siegel, H.I., Roseblatt, J.S. & Komisaruk, B.R. (1977) Tail-pinch facilitates onset of maternal behavior in rats. *Physiol Behav*, **19**, 807-809.

- Takmakov, P., Zachek, M.K., Keithley, R.B., Bucher, E.S., McCarty, G.S. & Wightman, R.M. (2010) Characterization of local pH changes in brain using fast-scan cyclic voltammetry with carbon microelectrodes. *Anal Chem*, **82**, 9892-9900.
- Tanimoto, H., Heisenberg, M. & Gerber, B. (2004) Experimental psychology: event timing turns punishment to reward. *Nature*, **430**, 983.
- Taylor, B.K., Joshi, C. & Uppal, H. (2003) Stimulation of dopamine D2 receptors in the nucleus accumbens inhibits inflammatory pain. *Brain research*, **987**, 135-143.
- Ungless, M.A., Magill, P.J. & Bolam, J.P. (2004) Uniform inhibition of dopamine neurons in the ventral tegmental area by aversive stimuli. *Science*, **303**, 2040-2042.
- Van Bockstaele, E.J., Qian, Y., Sterling, R.C. & Page, M.E. (2008) Low dose naltrexone administration in morphine dependent rats attenuates withdrawal-induced norepinephrine efflux in forebrain. *Prog Neuropsychopharmacol Biol Psychiatry*, **32**, 1048-1056.
- Venton, B.J. & Wightman, R.M. (2007) Pharmacologically induced, subsecond dopamine transients in the caudate-putamen of the anesthetized rat. *Synapse*, **61**, 37-39.
- Wang, D.V. & Tsien, J.Z. (2011) Convergent processing of both positive and negative motivational signals by the VTA dopamine neuronal populations. *PLoS One*, **6**, e17047.
- Wood, P.B. (2006) Mesolimbic dopaminergic mechanisms and pain control. *Pain*, **120**, 230-234.
- Zhang, D., Zhang, H., Jin, G.Z., Zhang, K. & Zhen, X. (2008) Single dose of morphine produced a prolonged effect on dopamine neuron activities. *Mol Pain*, **4**, 57.
- Zweifel, L.S., Fadok, J.P., Argilli, E., Garelick, M.G., Jones, G.L., Dickerson, T.M., Allen, J.M., Mizumori, S.J., Bonci, A. & Palmiter, R.D. (2011) Activation of dopamine neurons is critical for aversive conditioning and prevention of generalized anxiety. *Nat Neurosci*, **14**, 620-626.

CHAPTER 4: OPPOSING CATECHOLAMINE CHANGES IN THE BED NUCLEUS OF THE STRIA TERMINALIS DURING INTRACRANIAL SELF-STIMULATION AND ITS EXTINCTION

Introduction

Intracranial self-stimulation (ICSS) is an operant behavior in which animals are conditioned to press a lever to deliver an electrical stimulation to specific brain regions (Olds & Milner, 1954; Wise, 1996; Wise, 2002). Early research suggested that norepinephrine was a critical neurotransmitter involved in ICSS (reviewed in (Weinshenker & Schroeder, 2007)). Anatomical sites that supported ICSS were found near norepinephrine processes (Ritter & Stein, 1974), and radioactive norepinephrine and its metabolites were released during ICSS (Stein & Wise, 1969). However, subsequent research found evidence to the contrary (Roll, 1970; Clavier *et al.*, 1976; Corbett *et al.*, 1977; Corbett & Wise, 1979), and supported a more important role for dopamine in ICSS reward (Fibiger, 1978). Norepinephrine has also been suggested to be involved in the extinction of reward based behaviors, although this role has also been disputed (Mason, 1979; Tombaugh *et al.*, 1983; Lucki & Frazer, 1985).

ICSS studies have shown that mesolimbic dopamine neurons projecting from the ventral tegmental area (VTA) are important in the neural circuitry mediating reward (Hernandez & Shizgal, 2009). Indeed, dopamine has been viewed as the primary neurotransmitter involved in the rewarding aspects of ICSS (Wise, 1996). Our previous studies demonstrated that reward learning can be investigated by quantifying dopamine changes in the nucleus accumbens (NAc) with carbon-fiber microelectrodes using fast-scan

cyclic voltammetry (Owesson-White *et al.*, 2008). Transient surges of extracellular dopamine become time-locked to cues that predict ICSS reward and coincide with cues

associated with cocaine or food reward (Phillips *et al.*, 2003b; Day *et al.*, 2007). Since dopamine transients are a direct result of burst firing of dopaminergic neurons (Somers *et al.*, 2009), these results concur with electrophysiological recordings that demonstrated that the firing rate of dopamine neurons encode for a reward prediction error (Schultz *et al.*, 1997; Pan *et al.*, 2005).

In this work we measure the roles of dopamine and norepinephrine during ICSS in the bed nucleus of the stria terminalis (BNST) and compare them to dopamine responses in the NAc. The BNST is part of the extended amygdala and serves as a relay center between limbic brain regions and the hypothalamic paraventricular nucleus (Cullinan *et al.*, 1993). The anterior portion of the BNST receives both dopaminergic and noradrenergic inputs, but they are differentially distributed (Park *et al.*, 2012). The ventral (v) BNST has the highest noradrenergic innervation in the brain (Kilts & Anderson, 1986) but has little dopamine content (Delfs *et al.*, 2000; Park *et al.*, 2009a). In contrast, the dorsolateral (d) BNST receives dopaminergic innervation from the VTA and periaqueductal gray but contains negligible norepinephrine (Phelix *et al.*, 1992; 1994; Carboni *et al.*, 2000; Meloni *et al.*, 2006; McElligott & Winder, 2009). The research reported here provides three new insights into the role of catecholamines in ICSS. First, dopaminergic responses in the dBNST were found to resemble dopaminergic responses in the NAc. Second, unlike dopamine, norepinephrine in the vBNST was not released in response to cues that predicted lever availability. Third, during extinction, norepinephrine release occurred at the time of the anticipated electrical stimulation whereas there was a suppression of extracellular dopamine.

Experimental

Animals

Male Sprague-Dawley rats (n = 24, Charles River, NC), aged 90-120 d and weighing 280-380 g, were used. They were individually housed in a controlled temperature

environment with a 12:12 light:dark cycle. Food and water were available *ad libitum*. All procedures were approved by the Institutional Animal Care and Use Committee of the University of North Carolina.

Surgery

Rats were anesthetized with ketamine hydrochloride (100 mg/kg) and xylazine hydrochloride (20 mg/kg) administered intraperitoneally and placed in a stereotaxic frame. A guide cannula (Bioanalytical Systems, West Lafayette, IL) was positioned above the *d*/BNST (anteroposterior (AP) -0.1 mm, mediolateral (ML) +1.6 mm), the *v*BNST (AP 0.0 mm, ML +1.2 mm), or the NAc (AP 1.7 mm, ML 0.8 mm). Coordinates were from a stereotaxic atlas (Paxinos & Watson, 2007). An Ag/AgCl reference electrode was implanted contralateral to the guide cannula in the left forebrain. A bipolar stimulating electrode was implanted in the VTA/substantia nigra (VTA/SN) (AP -5.2 mm, ML +1.2 mm, dorsoventral (DV) -8.0 to -9.0 mm). Stimulation at these coordinates also activates the ventral noradrenergic bundle (VNB) (Park *et al.*, 2009a). Stainless steel skull screws and dental cement secured all items.

Intracranial self-stimulation (ICSS) training

After each animal recovered to their presurgery weight, ICSS training commenced as previously described (Owesson-White *et al.*, 2008). During recording sessions, an audiovisual cue was followed 2 s later by lever extension. Depression of the lever by the rat delivered an electrical stimulation to the animal.

On the day of recording, some animals also underwent ICSS extinction where the lever-press did not deliver the electrical stimulation. When the cue no longer elicited lever-press behavior, ICSS was reinstated with 1-2 operator-delivered stimulations.

Fast-scan cyclic voltammetry

Following successful training, a fresh, glass-sealed carbon-fiber microelectrode (75–100 μm exposed tip length, 7 μm diameter, T-650; Amoco, Greenville, SC (Cahill & Wightman, 1995; Phillips *et al.*, 2003a)) was lowered into the brain with a micromanipulator inserted into the guide cannula. The microelectrode was lowered to the *d*/BNST (DV -6.0 to -7.0 mm), the *v*BNST (DV -7.2 to -7.7 mm) or the NAc shell (DV -6.4 to -7.4 mm (Owesson-White *et al.*, 2008)). The carbon-fiber and Ag/AgCl reference electrodes were connected to a head-mounted amplifier attached to a commutator (Med-Associates, St. Albans, VT). Fast-scan cyclic voltammetry was computer-controlled (Heien *et al.*, 2003). A triangular scan (-0.4 to +1.3 V, 400 V/s) was repeated every 100 ms. Data were digitized and stored on a computer using software written in LABVIEW (National Instruments).

Histology

At the end of the experiment, electrode placements were verified by electrolytic lesions made with the carbon-fiber microelectrodes (Fig. 4.1) (Park *et al.*, 2009a). Rats were euthanized with an overdose of urethane (2.0 g/kg) and a lesion was made at the recording site by applying constant current (20 μA for 10 s). Brains were removed and stored in 10 % formalin solution for a week before being sectioned into 40 μm coronal slices. The sections were mounted on slides and viewed with an optical microscope.

Chemicals and drugs

Chemicals and drugs were reagent-quality and used without further purification. Drugs were obtained from Sigma-Aldrich (St. Louis, MO, USA). Calibration of the carbon-fiber microelectrodes with standards for pH, dopamine, and norepinephrine were made in a buffer (pH 7.4 containing 15 mM Tris, 140 mM NaCl, 3.25 mM KCl, 1.2 mM CaCl_2 , 1.25 mM NaH_2PO_4 , 1.2 mM MgCl_2 , and 2.0 mM Na_2SO_4).

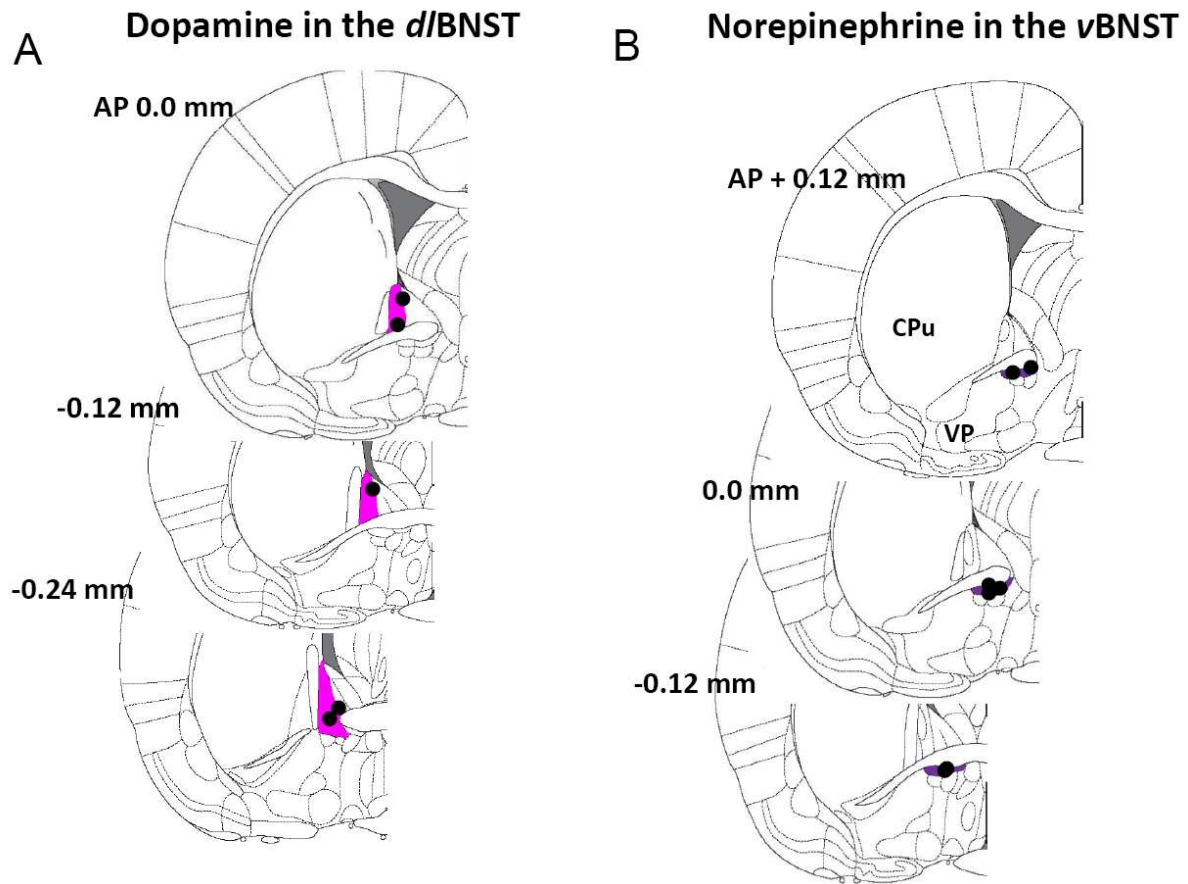


Figure 4.1. Representative histological verification of recording sites in the NAc and the vBNST. Electrolytic lesions confirmed that recording sites () were within the subregions of the BNST. The locations of the carbon-fiber microelectrode tips in (A) the dBNST and (B) the vBNST were visualized by the electrolytic lesion. The coronal sections are adapted from the atlas of Paxinos and Watson (Paxinos and Watson, 2007). The numbers on individual sections indicate distance, in millimeters, anterior to posterior from bregma.

At least one pharmacological agent selective for each catecholamine was administered intraperitoneally (i.p.) at the end of every experiment (0.6 mL volume) to verify the identity of the electrochemical signal (Park *et al.*, 2009a). Cyclic voltammetry cannot be used to distinguish dopamine from norepinephrine and thus the pharmacological distinction is required (Park *et al.*, 2011). Desipramine-HCl (DMI, 15 mg/kg), raclopride-HCl (Rac, 2 mg/kg), and idazoxan-HCl (IDA, 5 mg/kg) were dissolved in saline. GBR 12909 (GBR, 15 mg/kg) was dissolved in water and diluted in saline. For sites reported in the *d*/BNST positive responses were obtained to dopaminergic drugs (GBR, Rac) but not noradrenergic drugs (DMI, IDA) whereas the opposite was true in the *v*BNST (Fig. 4.2) as described in a previous study (Park *et al.*, 2012). The limited chemical selectivity of cyclic voltammetry precludes its use in brain regions that employ both catecholamines as neurotransmitters.

Data analysis

Catecholamine concentration changes were quantified using principal component regression (Heien *et al.*, 2005; Keithley *et al.*, 2010). The post-calibration factors were from the average responses obtained with multiple electrodes in our previous studies (Park *et al.*, 2010; Park *et al.*, 2012) (6.9 ± 0.3 pA/($\mu\text{M} \cdot \mu\text{m}^2$) for dopamine, and 4.5 ± 0.2 pA/($\mu\text{M} \cdot \mu\text{m}^2$) for norepinephrine). A residual analysis procedure was used to verify that the cyclic voltammograms of the trials being predicted were consistent with the cyclic voltammograms used for calibration (Keithley *et al.*, 2009).

Clampfit 8.1 (Axon Instruments, Foster City, CA, USA) was used to analyze maximal catecholamine concentration evoked by the cue or lever-press. The half-life ($t_{1/2}$) for catecholamine clearance was taken as the time to descend from its maximum to half of that value (Park *et al.*, 2007). Only catecholamine concentrations with signal to noise (S/N) > 3 were considered as cue- or lever-press evoked catecholamine release. Concentration changes were evaluated by subtracting the average baseline (-2.0 to 0 s relative to cue or

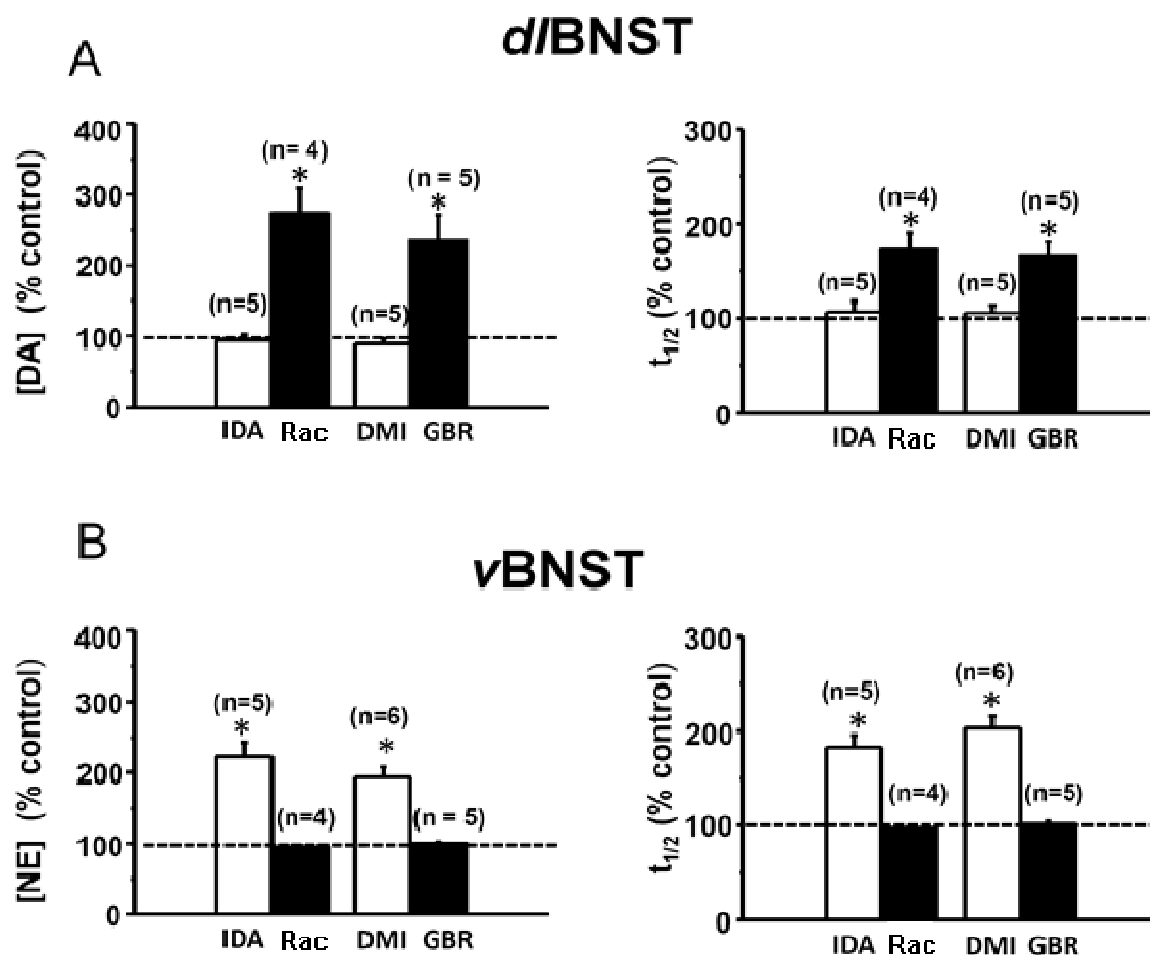


Figure 4.2. Effects of selective autoreceptor and uptake inhibitors on electrically-evoked catecholamine release and clearance in subregions of the BNST. Abbreviations: [CA], maximal catecholamine release; $t_{1/2}$, clearance half-life; IDA, idazoxan (5 mg/kg); DMI, desipramine (15 mg/kg); Rac, raclopride (2 mg/kg); GBR, GBR 12909 (15 mg/kg); *d*l, dorsal lateral; *v*, ventral. * Indicates significantly different from control values ($P < 0.05$).

lever-press) from events after the cue (0.1-2.0 s) or lever-press (2-15 s). Mean values were compared with the two-tailed Student's *t*-test to calculate the level of significance. The coefficient of variation (CV, the ratio of the standard deviation of the mean) was used to characterize the catecholamine maximum concentrations. Statistical analysis employed GraphPad Software version 4.0 (San Diego, CA, USA). Data are represented as mean \pm S.E.M. and 'n' values indicate the number of rats.

Results

Cue-evoked dopamine concentration changes in the *d*/BNST during ICSS

Following ICSS training, catecholamine release was measured in the *d*/BNST. During training, the animal learned that a tone and house light were followed 2 s later by lever extension, and that a lever-press delivered ICSS stimulation to its brain (timing diagram in Fig. 4.3A). As shown for a single trial (Fig. 4.3B), dopamine release occurs both following the cues and the lever-press. The color plot shows the cyclic voltammograms recorded with the applied voltage as the ordinate and the abscissa as the acquisition time of the cyclic voltammogram. The current is encoded in color. The trace above the color plot is the dopamine concentration extracted from these data by principal component regression. The low residual confirms that the training set used to extract the dopamine concentrations describes the data appropriately (Fig. 4.3C).

were allowed multiple ICSS trials. As shown in this animal, the cue-evoked maximal dopamine concentration ($[DA]_{cue}$) was similar with each trial ($[DA]_{cue} = 36.7 \pm 2.6$ nM from the first 30 trials and 30.9 ± 1.8 nM from the last 30 trials, $t_{29} = 1.87$, $P > 0.05$, Fig. 4.3D). In contrast, lever-press-evoked dopamine ($[DA]_{stim.}$) decreased significantly over trials and fit to a parabolic curve ($r^2 = 0.81$, $[DA]_{stim.} = 278 \pm 11$ nM from the first 30 trials and 182 ± 3 nM from the last 30 trials, $t_{29} = 9.87$, $P < 0.0001$, Fig. 4.3D). In both respects, the responses of

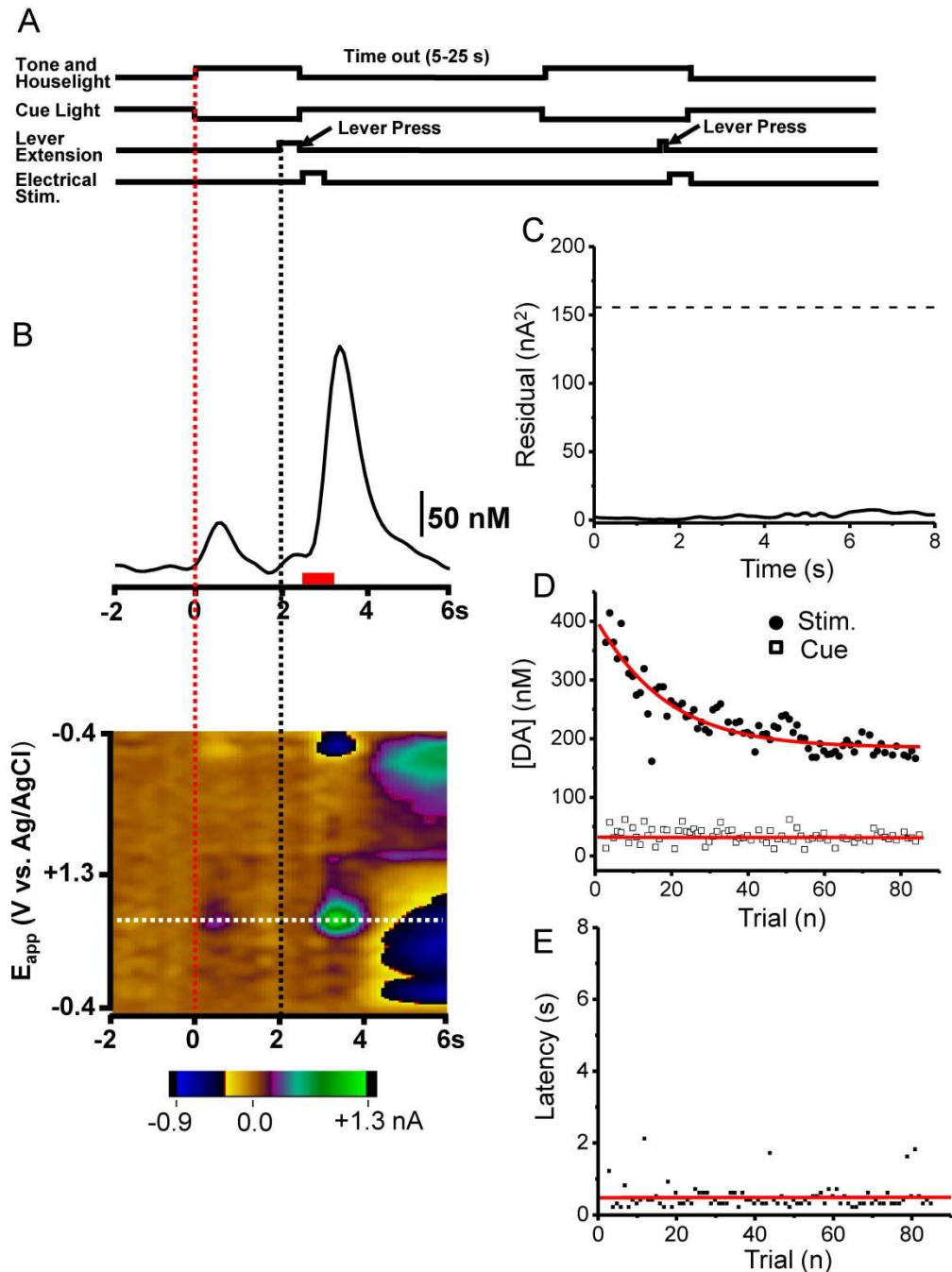


Figure 4.3. Dopamine changes in the *d*/BNST during maintenance-delay ICSS. (A) Temporal sequence of task. (B) Upper; a representative temporal dopamine concentration trace from a single trial during maintenance-delay ICSS. Principal component regression was used to extract the time course of the dopamine concentration transients. Dopamine release occurs immediately following the cue ($t = 0$, red dotted line) and again after the lever-press (lever out at 2 s, black dotted line). Red bar shows the stimulus duration. Lower: two-dimensional color plot representation of the background subtracted cyclic voltammograms collected 2 s before cue and 6 s after the lever extension. Catecholamine concentration changes are apparent in color plots at the potential for its oxidation (~0.65 V, white dashed line) and its reduction (~-0.2 V). (C) Residual from principal component analysis. (D) Cue- and lever-press-evoked dopamine release across trials. (E) Latency to press the lever across trials. Stimulus parameters: 60 Hz, 40 biphasic pulses, 2 ms pulse width.

dopamine were similar to our findings in the NAc (Owesson-White *et al.*, 2008). The latency to press after lever extension was essentially constant indicating that the animal had learned the behavior (Fig. 4.3E). Similar results were obtained in the *d*/BNST in 6 animals undergoing identical ICSS training. The average value of $[DA]_{cue}$ was 27.8 ± 5.3 nM and for $[DA]_{stim.}$ was 216 ± 51 nM.

Pharmacological effects on dopamine in the *d*/BNST

For some animals, dopamine release during ICSS was also monitored following administration of inhibitors of dopamine uptake (GBR 12909) and norepinephrine uptake (DMI) ($n = 5$ animals). When examined 20 minutes after GBR ($n = 2$), both cue- and lever-press-evoked dopamine concentrations significantly increased ($[DA]_{cue} = 34.8 \pm 1.1$ nM before and 63.3 ± 2.0 nM after GBR, $t_{49} = 8.85$, $P < 0.0001$; $[DA]_{stim.} = 118 \pm 7$ nM before and 427 ± 6 nM after GBR, $t_{49} = 78.05$, $P < 0.0001$, Fig. 4.4, data recorded when both responses had stabilized in amplitude). Interestingly, the maximal cue evoked dopamine shows greater relative variation than do the stimulus-evoked changes. The CV was found to be 0.281 for cue-evoked dopamine release and 0.109 during electrically-stimulated dopamine release. The latency to lever-press decreased (but not significantly) after administration of GBR (predrug = 0.64 ± 0.07 s, after GBR = 0.47 ± 0.05 s, $t_{49} = 1.98$, $P > 0.05$).

In contrast, DMI ($n = 3$) did not significantly change cue-evoked dopamine concentration in the *d*/BNST ($[DA]_{cue} = 45.1 \pm 2.5$ nM before and 41.6 ± 2.0 after DMI, $t_{49} = 0.98$, $P > 0.05$, representative example in Fig. 4.5A). There was also no significant change in stimulated dopamine release ($[DA]_{stim.} = 299 \pm 4$ nM predrug and $[DA]_{stim.} = 303 \pm 8$ nM after DMI, $t_{49} = 0.583$, $P > 0.05$, Fig. 4.5B). DMI did significantly increase the latency to lever-press (0.47 ± 0.05 s before and 0.76 ± 0.06 s after DMI, $t_{49} = 3.736$, $P < 0.001$).

Following DMI, this animal was administered GBR. As with GBR alone, cue and

Dopamine in *d*/BNST

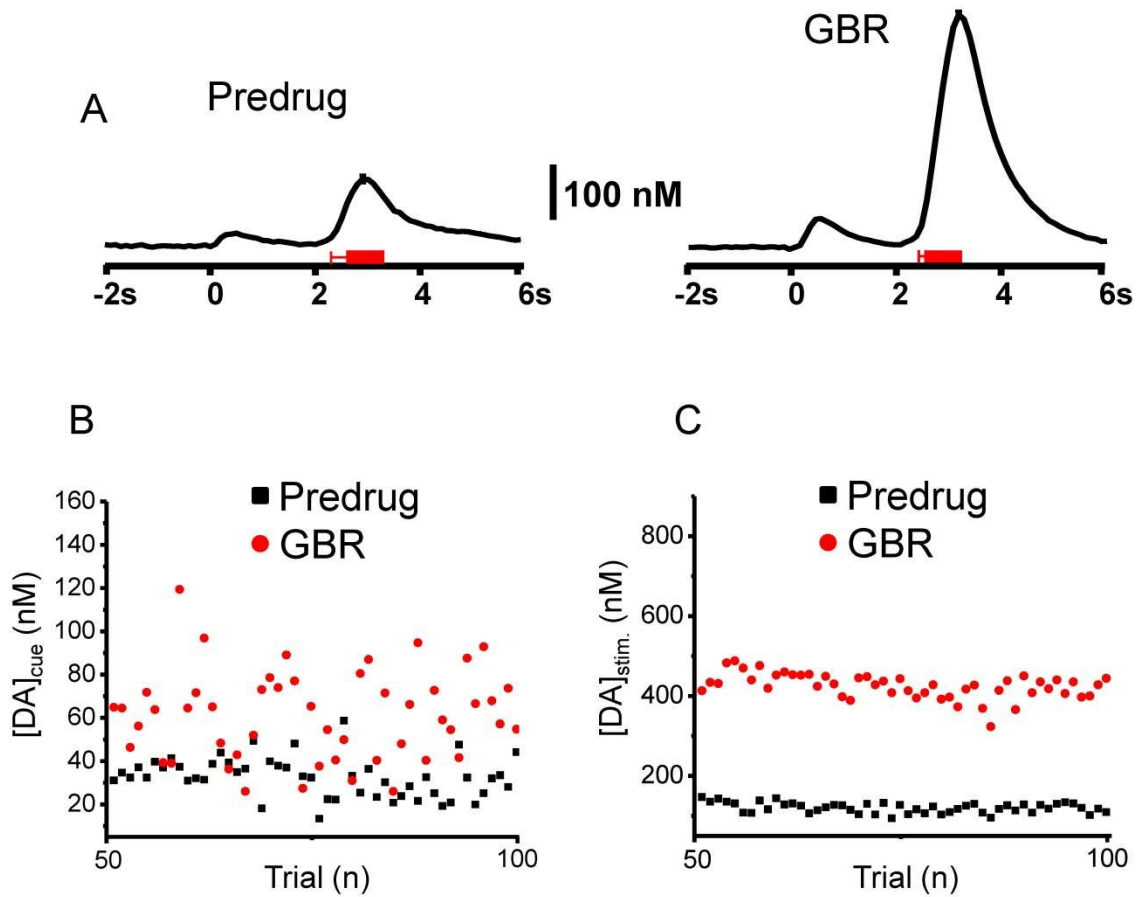


Figure 4.4. Dopamine increase in the *d*/BNST during maintenance-delay ICSS after administration of GBR. (A) Average dopamine concentration traces with a representative \pm S.E.M. and two-dimensional color plots from 50 trials before drug session (predrug, left) and 20 min after the administration of GBR (15 mg/kg, i.p., right). Principal component regression was used to extract time course of the dopamine concentration traces. The red bars under the current traces denote the average onset and duration of electrical stimulation. (B) Cue- and (C) lever-press-evoked dopamine concentration changes across trials.

Dopamine in *d*/BNST

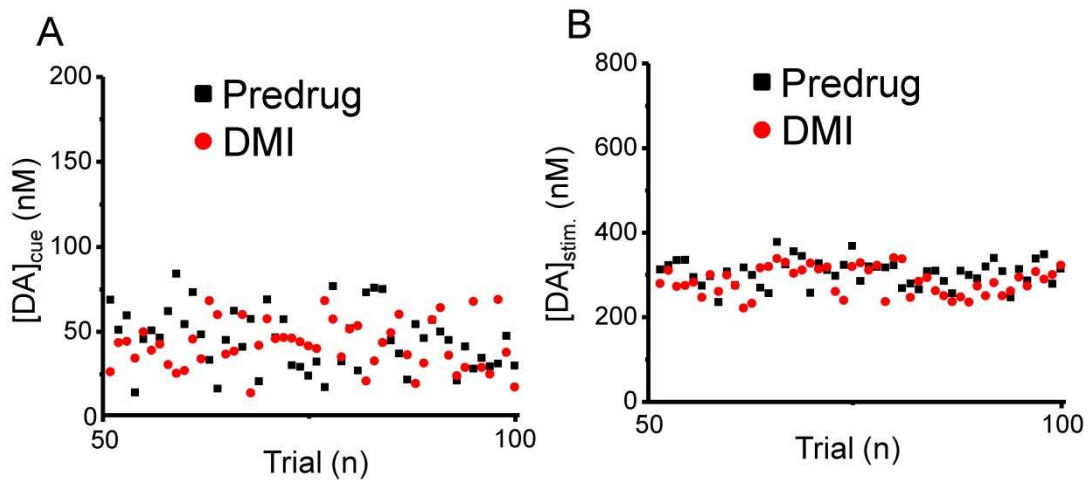


Figure 4.5. Dopamine concentration changes in the *d*/BNST and latency to lever-press during maintenance-delay ICSS before and after administration of DMI. Responses are only shown for 50 trials after the initial decay in stimulated release had occurred. Maximum dopamine concentrations following (A) the cue and (B) the lever-press as a function of trial number.

lever-press-evoked dopamine concentrations were increased ($[DA]_{\text{cue}} = 99.4 \pm 4.8 \text{ nM}$, $t_{49} = 10.52$, $P < 0.0001$ and $[DA]_{\text{stim.}} = 1226 \pm 64 \text{ nM}$, $t_{49} = 14.55$, $P < 0.0001$) and the latency to lever-press was restored to its original value ($0.49 \pm 0.06 \text{ s}$).

Norepinephrine responses during maintenance-delay trials

In a different group of animals, measurements were made in the vBNST to evaluate changes in extracellular norepinephrine concentration during an identical ICSS task. There was no response to the cue but norepinephrine increased during the electrical stimulation (Fig. 4.6A) that followed the lever-press. The residual (Fig. 4.6B) was below that predicted for 95 % of the noise from the training set. In this animal, maximum lever-press-evoked norepinephrine concentration ($[NE]_{\text{stim.}}$) decreased with subsequent trials ($[NE]_{\text{stim.}} = 288 \pm 8 \text{ nM}$ from the first 30 trials and $213 \pm 4 \text{ nM}$ from the last 30 trials, $t_{29} = 8.160$, $P < 0.0001$, Fig. 4.6C), although the latency to lever-press did not significantly change with trials (Fig. 4.6D). Similar results were obtained in 6 other animals. The average value across all trials of $[NE]_{\text{stim}}$ was $135 \pm 25 \text{ nM}$. The average latency to lever-press from these animals over 100 trials was $1.25 \pm 0.27 \text{ s}$. Norepinephrine release in response to the cue was never observed, even with extended training (Fig. 4.7).

Pharmacological effects on norepinephrine in the vBNST

In some animals norepinephrine changes during ICSS were evaluated after uptake inhibitors ($n = 3$ for GBR and $n = 4$ for DMI, example in Figure 4.8). DMI significantly increased stimulated release following the lever-press (from $[NE]_{\text{stim}} = 213 \pm 3 \text{ nM}$ to $[NE]_{\text{stim}} = 269 \pm 8 \text{ nM}$ after DMI, $t_{49} = 6.57$, $P < 0.0001$, 50 trials) and the evoked signal gradually declined to predrug levels (Fig. 4.8A and B). Even following DMI, cue-evoked norepinephrine did not occur. The latency to lever-press following DMI increased significantly (latency was $0.97 \pm 0.16 \text{ s}$ before drug and $1.96 \pm 0.42 \text{ s}$ after drug, $t_{49} = 2.609$,

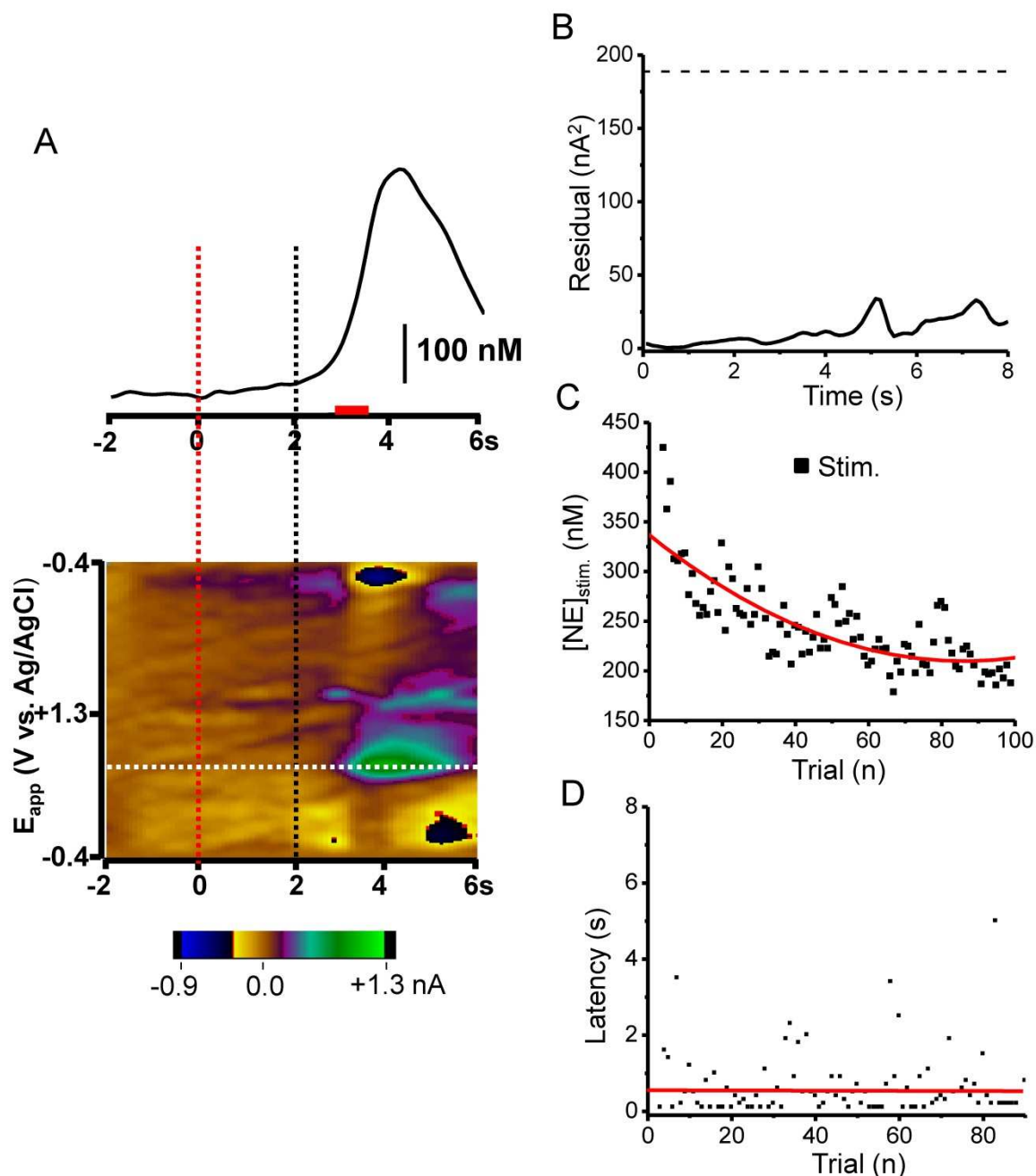


Figure 4.6. Norepinephrine changes in the vBNST during maintenance-delay ICSS. (A) Upper; a representative temporal norepinephrine concentration trace from a single trial during the task. Principal component regression was used to extract time course of the norepinephrine concentration transients. Norepinephrine was evoked after the lever-press (lever out at 2 s, black dotted line) but not after the cue ($t = 0$, red dotted line). Red bar shows the stimulus duration. Lower; Two-dimensional color plot representation of the background subtracted cyclic voltammograms collected 2 s before cue and 6 s after the lever extension. Catecholamine concentration changes are apparent in color plots at the potential for its oxidation (~ 0.65 V) and its reduction (~ -0.23 V). (B) Residual from principal component regression. The dashed line shows the level where 95% of the noise is anticipated. (C) Norepinephrine concentration changes evoked by self-delivered stimulation in consecutive trials. (D) Latency to press the lever in consecutive trials.

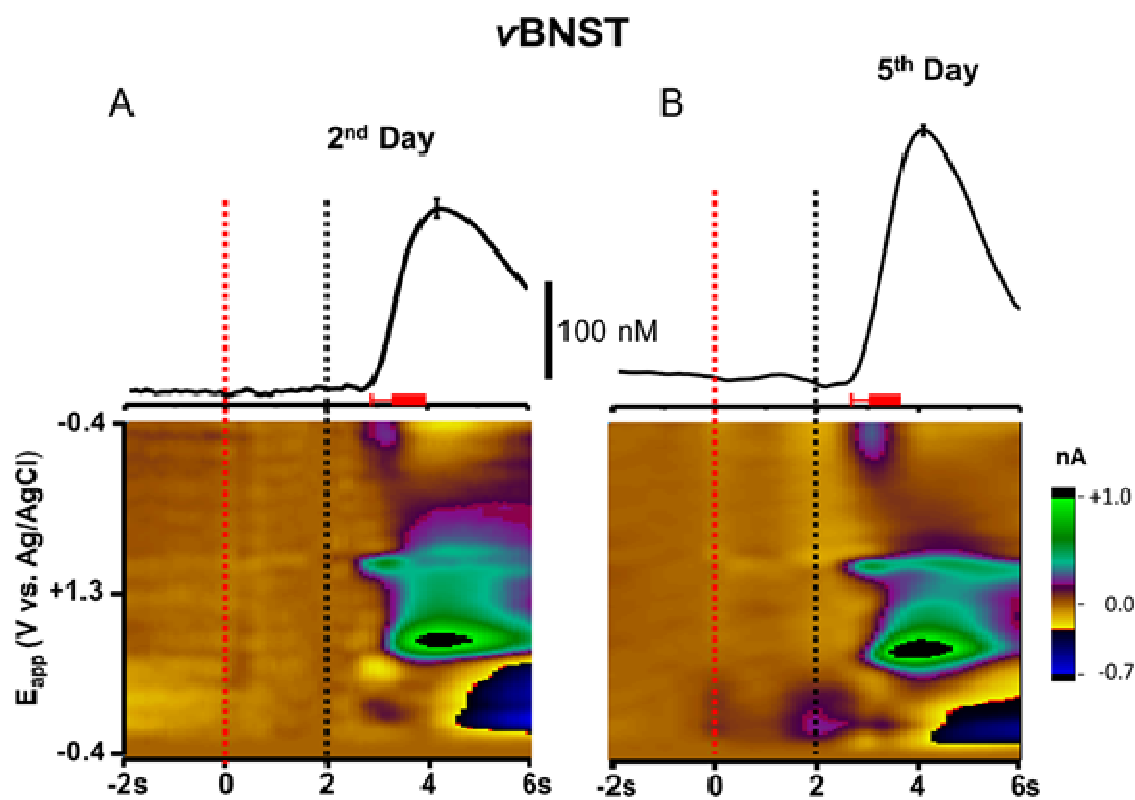


Figure 4.7. Average norepinephrine concentration traces in the vBNST during phase 2 of ICSS at (A) 2nd day and (B) 5th day of training. The onset of the audiovisual cue and lever extension are indicated by the red and black dotted lines respectively. Red bars under the concentration traces denote the average onset and duration of the stimulation. Lever-press was rewarded with electrical stimulation of the VTA/SN and VNB. Stimulus parameters: 60 Hz, 40 pulses, 2 ms pulse width. Principal component regression was used to extract time course of the catecholamine concentration traces. Data is shown as mean + S.E.M.

Norepinephrine in vBNST

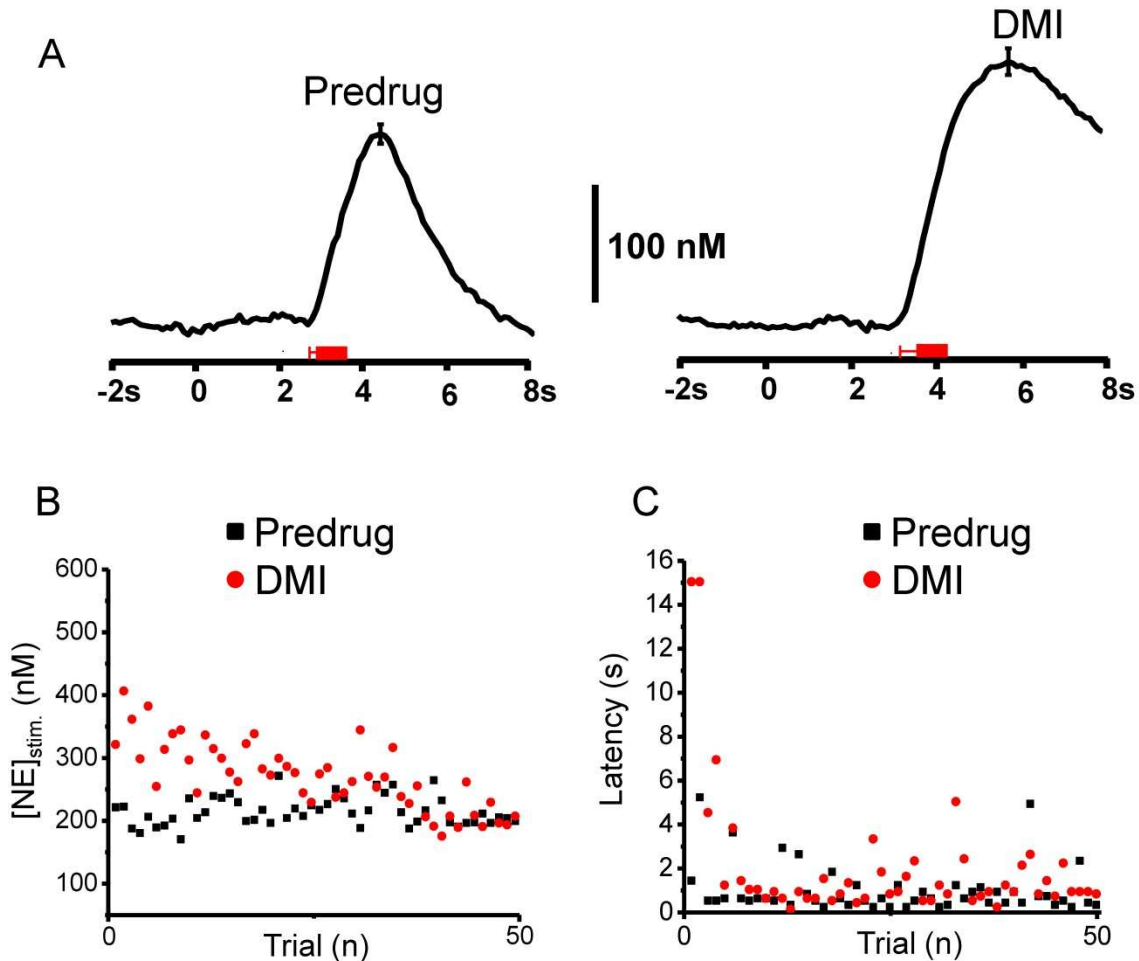


Figure 4.8. Norepinephrine increase in the vBNST during maintenance-delay ICSS after administration of DMI. (A) Average norepinephrine concentration traces with a representative \pm S.E.M. from ~ 50 trials before drug session (predrug, left) and 20 min after the administration of DMI (DMI, 15 mg/kg, i.p., right). The red bars under the current traces denote the average onset and duration of electrical stimulation. Principal component regression was used to extract the time course of the norepinephrine concentration traces. (B) Lever-press-evoked norepinephrine concentration change and (C) the latency of lever-press across trials.

$P < 0.05$, Fig. 4.5C). In a single animal that was administered GBR following DMI, the latency to lever-press was restored to its original value (0.85 ± 0.02 s). Administration of GBR alone had a slight effect on the norepinephrine responses to stimulation ($[NE]_{stim} = 105 \pm 3$ nM predrug and $[NE]_{stim} = 99 \pm 2$ nM after GBR, $t_{37} = 2.044$, $P < 0.05$, Fig. 4.9A and B), however it did shorten the latency to lever-press (1.74 ± 0.26 s before and 0.86 ± 0.19 s after GBR, $t_{37} = 2.801$, $P < 0.01$, Fig 4.9C).

Extracellular changes of dopamine and norepinephrine during extinction of ICSS

During extinction, the sequence of cues and lever extension was unchanged; however, depression of the lever had no consequence. Previous studies have demonstrated that cue-evoked dopamine release in the NAc decreased across extinction trials and this was accompanied by a decline in goal-directed behavior (Owesson-White *et al.*, 2008). In addition we found that dopamine in the NAc decreased during extinction at the time where the stimulation should have occurred by 18.3 ± 1.4 nM ($n = 5$, individual example in Figure 4.10A, lever press indicated by dashed red line). Identical behavior was observed in the *d*/BNST in one animal (Figure 4.10B). However, due to the low success rate of *d*/BNST experiments, we primarily compare the behavior of norepinephrine in the *v*BNST with that of dopamine in the NAc shell (implantation success was approximately 17 % in the *d*/BNST versus 80 % in the NAc).

During extinction, norepinephrine was still unresponsive to the cue but it increased following the unrewarded lever-presses (example after the lever-press in one animal is shown in Fig. 4.10C). Data that was averaged and analyzed by principal component regression reveal an increase in norepinephrine concentration ($n = 5$ rats, 32.3 ± 3.5 nM) following the lever-press during extinction trials. In two animals, norepinephrine changes during extinction were examined after administration of DMI. The norepinephrine response to extinction following the lever-press was significantly enhanced

Norepinephrine in vBNST

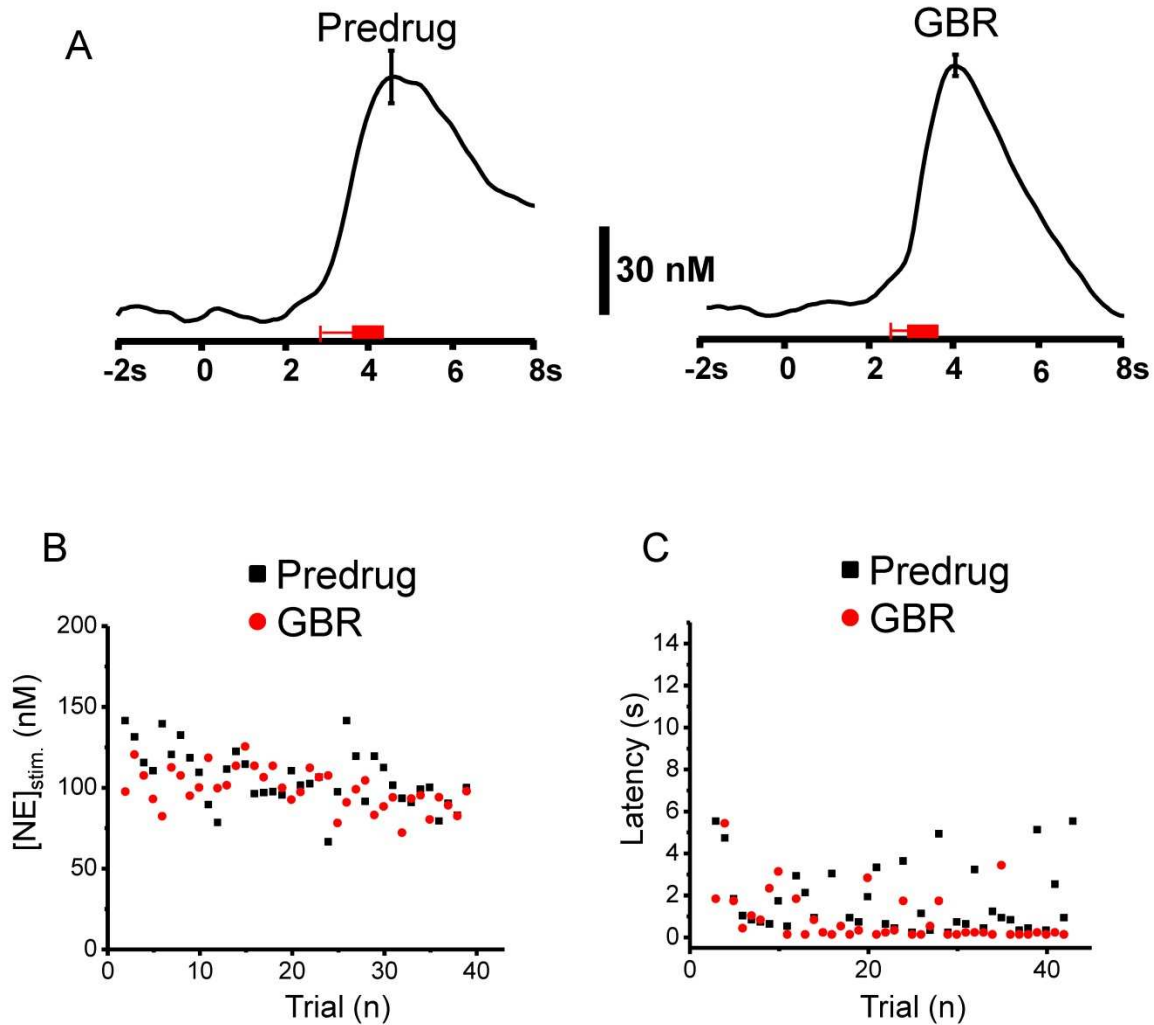


Figure 4.9. Norepinephrine concentration change in the vBNST and latency of the lever-press during maintenance-delay ICSS after administration of GBR. (A) Average norepinephrine concentration traces with a representative \pm S.E.M. and from ~ 50 trials 20 min after the administration GBR (15 mg/kg, i.p.). The red bars under the current traces denote the average onset and duration of electrical stimulation. Principal component regression was used to extract time course of the norepinephrine concentration traces. (B) Lever press-evoked norepinephrine concentration change and (C) the latency of lever-press across trials.

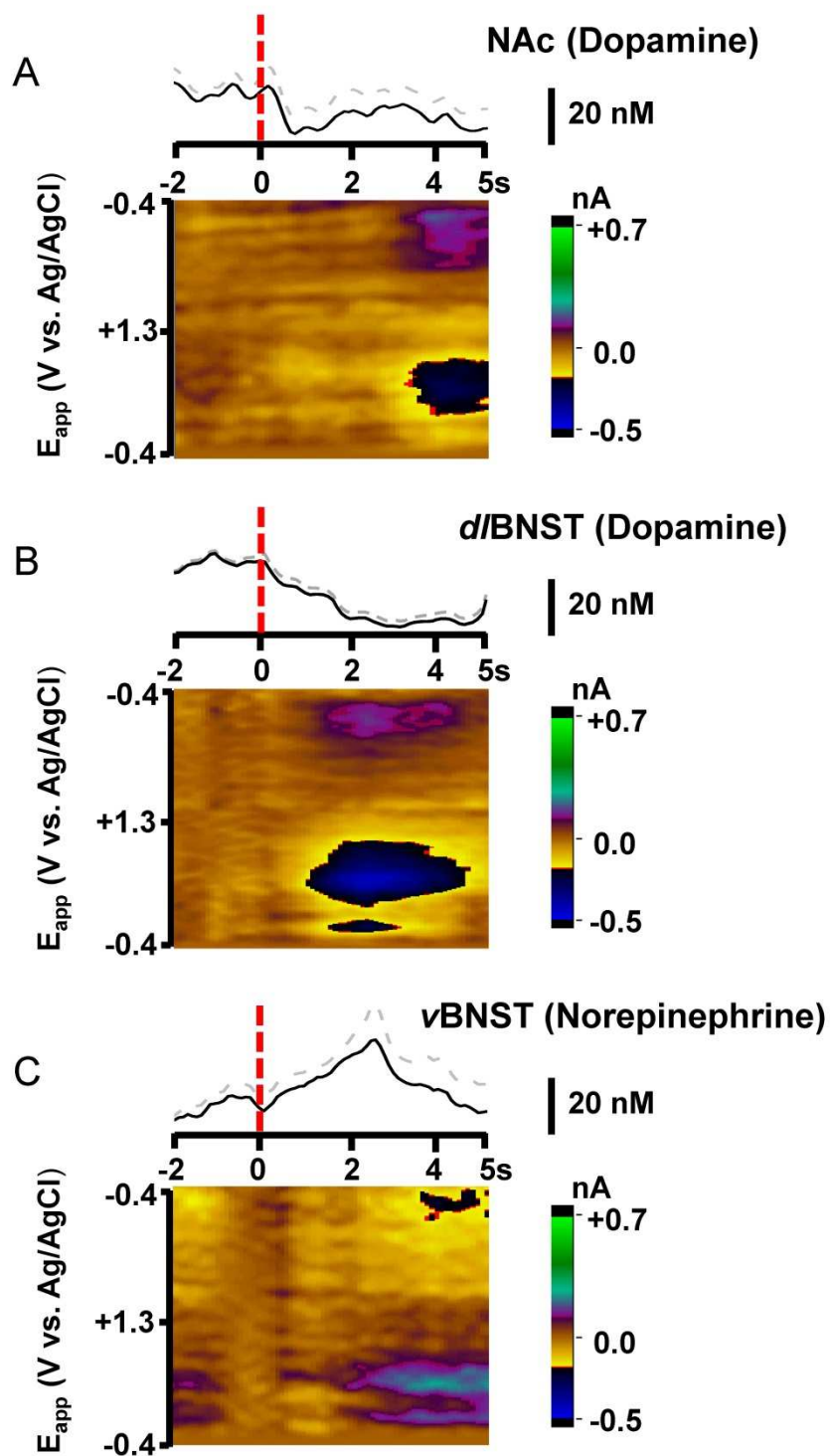


Figure 4.10. Catecholamine responses in the NAc (A), d/BNST (B) and vBNST (C) during ICSS extinction. Each data set is averaged from a single animal. The concentration profiles (displayed as mean and S.E.M.) above the 2D color plots were extracted using principal component analysis. Time of lever-press is indicated by the red dotted line. In extinction trials lever-press was not rewarded with electrical stimulation.

(from 38.0 ± 3.6 to 85.6 ± 13.1 nM following DMI, $t_5 = 4.01$, $P < 0.01$, example in Fig. 4.11), but there was still no change to the cue. Electrically evoked norepinephrine and ICSS behavior were restored during subsequent reinstatement trials.

Discussion

Here we found that dopamine release in the *d*/BNST in response to cues that predict lever availability closely resembles dopamine changes in the NAc (Owesson-White *et al.*, 2008; Beyene *et al.*, 2010). In contrast, norepinephrine in the *v*BNST does not respond to the cue, even after prolonged training. However, both catecholamines are released after the lever-press as a consequence of the VNB and VTA/SN electrical stimulation. During ICSS extinction, cue-evoked dopamine disappears in the *d*/BNST just as in the NAc shell (Owesson-White *et al.*, 2008). As shown here, extracellular dopamine actually decreases at the time of the lever-press when electrical stimulation is expected but not delivered. Remarkably, during extinction, norepinephrine increases at the expected time of electrical stimulation. The opposite responses of these two catecholamines in the extended amygdala are in accord with a proposed role of this system in distinct aspects of the addiction cycle that includes both positive and negative reinforcement mechanisms (Solomon & Corbit, 1974; Koob & Volkow, 2010). Dopamine relays information concerning positive hedonic states whereas the negative hedonic responses are mediated by norepinephrine (Park *et al.*, 2012).

Different roles for each catecholamine in subregions of the BNST during ICSS

Since the BNST is involved in the regulation of stress, homeostasis, and reward (Delfs *et al.*, 2000; Erb *et al.*, 2000; Cecchi *et al.*, 2002; Sullivan *et al.*, 2004; Fendt *et al.*, 2005; McElligott & Winder, 2009), activated catecholamine neurotransmission in this region during ICSS was anticipated. Indeed, previous experiments have demonstrated that dopamine

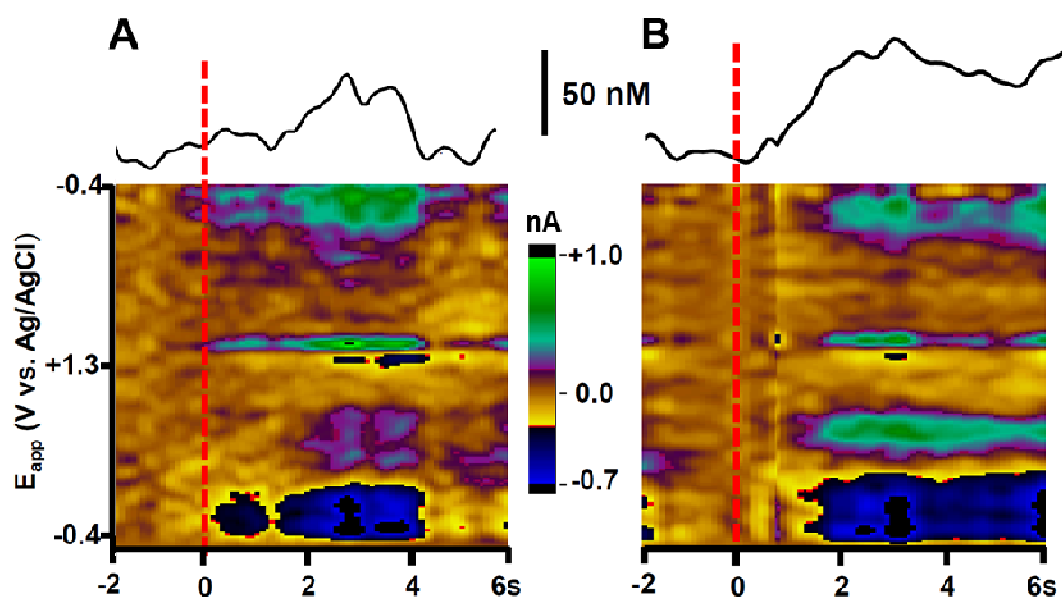


Figure 4.11. Norepinephrine concentration changes during ICSS extinction before (A) and after (B) the administration of the norepinephrine uptake inhibitor DMI (15 mg/kg). Data shown are representative single trial responses from one animal. Principal component regression was used to extract time course of the concentration traces. The red dotted line indicates the time of lever-press, which did not elicit the rewarding stimulation during the extinction trials.

neurotransmission is promoted in the *d*/BNST during reward-based behaviors (Epping-Jordan *et al.*, 1998; Eiler *et al.*, 2003), including ICSS (Jonkman & Markou, 2006). The temporal resolution provided by fast-scan cyclic voltammetry allowed us to distinguish catecholamine changes associated with the cues from those associated with the electrical stimulation. In the *d*/BNST dopamine was found to increase both in response to the cues that predict lever availability and during the self-administered (electrical) stimulation. The cue-evoked responses are similar to those observed in other dopaminergic regions during reward-based operant behaviors (Stuber *et al.*, 2005; Day *et al.*, 2007; Day *et al.*, 2010; Jones *et al.*, 2010). The greater variability of cue-induced dopamine transients when compared to stimulated release has been reported before (Owesson-White *et al.*, 2008). While the stimulation activates a uniform population of terminals on each trial, cue-induced dopamine appears to arise from a more variable activation of terminals.

This is the first time rapid recordings have been applied to norepinephrine during ICSS, and it has allowed us to reinvestigate the decades-old question of the role of norepinephrine in ICSS and extinction. Early studies suggested that the norepinephrine release was associated with reward function (Stein & Wise, 1969; Ritter & Stein, 1974). Although our work confirms that norepinephrine release is evoked by a site that supports ICSS, it is not evoked by the predictive cue. Thus it clearly plays a different role than dopamine during ICSS.

When an animal acquires cue-reward associations, burst firing of midbrain dopaminergic neurons occurs at the onset of the cue (Schultz *et al.*, 1997; Pan *et al.*, 2005). Previously, we have shown that time-locked dopamine concentration transients also occur in terminal regions at such times (Cheer *et al.*, 2007; Owesson-White *et al.*, 2008). Thus, dopamine release at the cue is one of the neurochemical responses that immediately elicits a goal-directed behavior (Wise, 2004; Weinshenker & Schroeder, 2007). In contrast, cue-evoked norepinephrine was not observed in the *v*BNST. This is unlikely to be a

consequence of norepinephrine transmission restricted to a synaptic compartment because considerable evidence indicates that it communicates extrasynaptically in the BNST (Phelix *et al.*, 1992; Miles *et al.*, 2002). Indeed, electrophysiological studies have shown that noradrenergic neurons in the LC respond to novelty but lack a sustained response to stimuli (Sara *et al.*, 1994; Bouret & Sara, 2004).

To investigate whether selective uptake inhibitors affect ICSS, latency to press following DMI (NET inhibitor) or GBR 12909 (DAT inhibitor) was examined. In the absence of drug, the latency to lever-press was quite short because the animals were well trained. Overall, DMI significantly increased the latency to lever-press (Fig. 4.8C), consistent with the finding that acute DMI causes a decrement in ICSS reward (Hall *et al.*, 1990). Following GBR administration, the latency to lever-press decreased but not significantly ($P > 0.05$, $n = 5$ animals), presumably because of a ceiling effect. Supporting this assumption, in rats with an average latency to press of more than 1.0 s (example in Fig. 4.9) or who had previously received DMI, the latency was significantly decreased after GBR. Consistent with this finding, GBR has been shown to increase responding for ICSS reward (Maldonado-Irizarry *et al.*, 1994).

Opposing catecholamine changes during extinction of ICSS

Since identical dopamine responses were obtained during ICSS in the *d*/BNST as previously obtained in the NAc (Owesson-White *et al.*, 2008), we compared our previous dopamine results to those for norepinephrine in the *v*BNST. During ICSS extinction, the decrease in lever-pressing was accompanied by a significant decrease in cue-evoked phasic dopamine in the NAc shell across trials (Owesson-White *et al.*, 2008), similar to that seen during extinction of cocaine self-administration (Stuber *et al.*, 2005). In addition, extracellular dopamine decreased at the time when the electrical stimulation should have

occurred, consistent with electrophysiological data demonstrating reward prediction error (Mirenowicz & Schultz, 1996; Ungless *et al.*, 2004).

A role for norepinephrine in the behavior observed during extinction of ICSS has long been suspected. During extinction of ICSS, animals with lesions of the locus coeruleus pressed the lever with more vigor and over a prolonged period compared to intact animals (Mason & Iversen, 1979). This response was attributed to a failure of locus coeruleus-lesioned rats to pay attention to relevant cues. Subsequent research employing lesioned animals have provided support for this hypothesis (Selden *et al.*, 1990), consistent with the view from electrophysiological studies in intact animals that norepinephrine neuronal systems are important in paying attention to the surrounding environment (Aston-Jones & Cohen, 2005). Further, norepinephrine acting at central β -adrenergic receptors has been suggested to be important in the retrieval of drug-associated memories following extinction (Fricks-Gleason & Marshall, 2008; Otis & Mueller, 2011). Regardless, our data supports a role for norepinephrine during extinction. During ICSS, the 2 s cue predicts impending reward availability and results in a dopamine concentration transient without a change in norepinephrine. However, during extinction animals now learn that the 2 s cue predicts the absence of reward following a lever-press. This is associated with a norepinephrine surge. It is unlikely that this surge acts as a cue-associated signal since it occurs after the 2 s cue and any cues associated with the press itself (e.g., lever depression, click of the lever etc). A signal at the lever press is critical so that it can trigger a decline in goal-directed behavior; this requires new learning concerning the prediction of non-reward, a process that has been linked to norepinephrine (Mason, 1983; Janak & Corbit, 2011).

Alternative hypotheses must also be considered. For example, the vBNST receives noradrenergic input from the nucleus of the solitary tract as well as the locus coeruleus (Park *et al.*, 2009b). These two nuclei have been shown to have quite different responses during aversive events such as opiate withdrawal (Delfs *et al.*, 2000), and, in the present

experiments, we cannot distinguish which nuclei is the primary contributor to the measured norepinephrine release. In addition to its role in attention, norepinephrine release has also been associated with aversive stimuli. Using the same measurement approach, we previously showed that norepinephrine release was evoked by intraoral quinine infusion, an aversive tastant (Park *et al.*, 2012). Because the omission of reward can be considered aversive, this may also be the origin of the norepinephrine surge during ICSS extinction. In the prefrontal cortex, extracellular norepinephrine increases following both aversive and rewarding stimuli (Ventura *et al.*, 2007). However, those changes last for longer than an hour and it is unclear whether the rapid changes we report here have a similar origin.

Conclusions

Subsecond recordings of catecholamines in subregions of the BNST during ICSS reveal that time-locked catecholamine changes occur during this reward-seeking behavior. In a manner quite similar to events in the NAc shell, phasic dopamine release in the *d*/BNST was evoked by a cue that had become associated with ICSS. In contrast, there was no evidence of cue-evoked, phasic norepinephrine in the *v*BNST during ICSS. Both catecholamines were released by the stimulation as a consequence of the positioning of the stimulating electrode in the VTA/SN/VNB. During extinction, the activity of both catecholamines was dramatically altered. Dopamine release to the cue diminished during ICSS extinction and the dopamine concentration actually decreased following the lever-press. At this time, when the cue no longer predicts impending ICSS availability and there is new learning about the consequence of the lever-press, extracellular norepinephrine increased. These data support the hypothesis that norepinephrine plays a central role in responses to extinction. Furthermore, the data demonstrate that catecholamine neurons in subregions of the BNST encode opposite aspects of learning during goal-directed behavior.

REFERENCES

- Aston-Jones, G. & Cohen, J.D. (2005) An integrative theory of locus coeruleus-norepinephrine function: adaptive gain and optimal performance. *Annual review of neuroscience*, **28**, 403-450.
- Beyene, M., Carelli, R.M. & Wightman, R.M. (2010) Cue-evoked dopamine release in the nucleus accumbens shell tracks reinforcer magnitude during intracranial self-stimulation. *Neuroscience*, **169**, 1682-1688.
- Bouret, S. & Sara, S.J. (2004) Reward expectation, orientation of attention and locus coeruleus-medial frontal cortex interplay during learning. *Eur J Neurosci.*, **20**, 791-802.
- Cahill, P.S. & Wightman, R.M. (1995) Simultaneous amperometric measurement of ascorbate and catecholamine secretion from individual bovine adrenal medullary cells. *Anal Chem.*, **67**, 2599-2605.
- Carboni, E., Silvagni, A., Rolando, M.T. & Di Chiara, G. (2000) Stimulation of in vivo dopamine transmission in the bed nucleus of stria terminalis by reinforcing drugs. *J Neurosci.*, **20**, RC102.
- Cecchi, M., Khoshbouei, H., Javors, M. & Morilak, D.A. (2002) Modulatory effects of norepinephrine in the lateral bed nucleus of the stria terminalis on behavioral and neuroendocrine responses to acute stress. *Neuroscience*, **112**, 13-21.
- Cheer, J.F., Aragona, B.J., Heien, M.L., Seipel, A.T., Carelli, R.M. & Wightman, R.M. (2007) Coordinated accumbal dopamine release and neural activity drive goal-directed behavior. *Neuron.*, **54**, 237-244.
- Clavier, R.M., Fibiger, H.C. & Phillips, A.G. (1976) Evidence that self-stimulation of the region of the locus coeruleus in rats does not depend upon noradrenergic projections to telencephalon. *Brain res*, **113**, 71-81.
- Corbett, D., Skelton, R.W. & Wise, R.A. (1977) Dorsal noradrenergic bundle lesions fail to disrupt self-stimulation from the region of locus coeruleus. *Brain res*, **133**, 37-44.
- Corbett, D. & Wise, R.A. (1979) Intracranial self-stimulation in relation to the ascending noradrenergic fiber systems of the pontine tegmentum and caudal midbrain: a moveable electrode mapping study. *Brain res*, **177**, 423-436.
- Cullinan, W.E., Herman, J.P. & Watson, S.J. (1993) Ventral subicular interaction with the hypothalamic paraventricular nucleus: evidence for a relay in the bed nucleus of the stria terminalis. *J Comp Neurol*, **332**, 1-20.
- Day, J.J., Jones, J.L., Wightman, R.M. & Carelli, R.M. (2010) Phasic nucleus accumbens dopamine release encodes effort- and delay-related costs. *Biological psychiatry*, **68**, 306-309.
- Day, J.J., Roitman, M.F., Wightman, R.M. & Carelli, R.M. (2007) Associative learning mediates dynamic shifts in dopamine signaling in the nucleus accumbens. *Nat Neurosci*, **10**, 1020-1028.

- Delfs, J.M., Zhu, Y., Druhan, J.P. & Aston-Jones, G. (2000) Noradrenaline in the ventral forebrain is critical for opiate withdrawal-induced aversion. *Nature.*, **403**, 430-434.
- Eiler, W.J., 2nd, Seyoum, R., Foster, K.L., Mailey, C. & June, H.L. (2003) D1 dopamine receptor regulates alcohol-motivated behaviors in the bed nucleus of the stria terminalis in alcohol-preferring (P) rats. *Synapse*, **48**, 45-56.
- Epping-Jordan, M.P., Markou, A. & Koob, G.F. (1998) The dopamine D-1 receptor antagonist SCH 23390 injected into the dorsolateral bed nucleus of the stria terminalis decreased cocaine reinforcement in the rat. *Brain Res*, **784**, 105-115.
- Erb, S., Hitchcott, P.K., Rajabi, H., Mueller, D., Shaham, Y. & Stewart, J. (2000) Alpha-2 adrenergic receptor agonists block stress-induced reinstatement of cocaine seeking. *Neuropsychopharmacology*, **23**, 138-150.
- Fendt, M., Siegl, S. & Steiniger-Brach, B. (2005) Noradrenaline transmission within the ventral bed nucleus of the stria terminalis is critical for fear behavior induced by trimethylthiazoline, a component of fox odor. *J Neurosci.*, **25**, 5998-6004.
- Fibiger, H.C. (1978) Drugs and reinforcement mechanisms: a critical review of the catecholamine theory. *Annu Rev Pharmacol Toxicol.*, **18**, 37-56.
- Fricks-Gleason, A.N. & Marshall, J.F. (2008) Post-retrieval beta-adrenergic receptor blockade: effects on extinction and reconsolidation of cocaine-cue memories. *Learning & memory*, **15**, 643-648.
- Hall, F.S., Stellar, J.R. & Kelley, A.E. (1990) Acute and chronic desipramine treatment effects on rewarding electrical stimulation of the lateral hypothalamus. *Pharmacol Biochem Behav.*, **37**, 277-281.
- Heien, M.L., Khan, A.S., Ariansen, J.L., Cheer, J.F., Phillips, P.E., Wassum, K.M. & Wightman, R.M. (2005) Real-time measurement of dopamine fluctuations after cocaine in the brain of behaving rats. *Proc Natl Acad Sci U S A*, **102**, 10023-10028.
- Heien, M.L., Phillips, P.E., Stuber, G.D., Seipel, A.T. & Wightman, R.M. (2003) Overoxidation of carbon-fiber microelectrodes enhances dopamine adsorption and increases sensitivity. *Analyst.*, **128**, 1413-1419.
- Hernandez, G. & Shizgal, P. (2009) Dynamic changes in dopamine tone during self-stimulation of the ventral tegmental area in rats. *Behav Brain Res*, **198**, 91-97.
- Janak, P.H. & Corbit, L.H. (2011) Deepened extinction following compound stimulus presentation: noradrenergic modulation. *Learning & memory (Cold Spring Harbor, N. Y.)*, **18**, 1-10.
- Jones, J.L., Day, J.J., Aragona, B.J., Wheeler, R.A., Wightman, R.M. & Carelli, R.M. (2010) Basolateral amygdala modulates terminal dopamine release in the nucleus accumbens and conditioned responding. *Biological psychiatry*, **67**, 737-744.

- Jonkman, S. & Markou, A. (2006) Blockade of nicotinic acetylcholine or dopamine D1-like receptors in the central nucleus of the amygdala or the bed nucleus of the stria terminalis does not precipitate nicotine withdrawal in nicotine-dependent rats. *Neurosci Lett*, **400**, 140-145.
- Keithley, R.B., Carelli, R.M. & Wightman, R.M. (2010) Rank estimation and the multivariate analysis of in vivo fast-scan cyclic voltammetric data. *Anal Chem*, **82**, 5541-5551.
- Keithley, R.B., Heien, M.L. & Wightman, R.M. (2009) Multivariate concentration determination using principal component regression with residual analysis. *Trends Analyt Chem*, **28**, 1127-1136.
- Kilts, C.D. & Anderson, C.M. (1986) The simultaneous quantification of dopamine, norepinephrine and epinephrine in micropunched rat brain nuclei by on-line trace enrichment HPLC with electrochemical detection: Distribution of catecholamines in the limbic system. *Neurochem Int*, **9**, 437-445
- Koob, G.F. & Volkow, N.D. (2010) Neurocircuitry of addiction. *Neuropsychopharmacology*, **35**, 217-238.
- Lucki, I. & Frazer, A. (1985) Performance and extinction of lever press behavior following chronic administration of desipramine to rats. *Psychopharmacology (Berl)*, **85**, 253-259.
- Maldonado-Irizarry, C.S., Stellar, J.R. & Kelley, A.E. (1994) Effects of cocaine and GBR-12909 on brain stimulation reward. *Pharmacol Biochem Behav*, **48**, 915-920.
- Mason, S.T. (1979) Noradrenaline: reward or extinction ? *Neurosci. Biobehav. Rev.*, **3**, 1-10.
- Mason, S.T. (1983) The neurochemistry and pharmacology of extinction behavior. *Neurosci. Biobehav. Rev.*, **7**, 325-347.
- Mason, S.T. & Iversen, S.D. (1979) Theories of the dorsal bundle extinction effect. *Brain res*, **180**, 107-137.
- McElligott, Z.A. & Winder, D.G. (2009) Modulation of glutamatergic synaptic transmission in the bed nucleus of the stria terminalis. *Prog Neuropsychopharmacol Biol Psychiatry*, **33**, 1329-1335.
- Meloni, E.G., Gerety, L.P., Knoll, A.T., Cohen, B.M. & Carlezon, W.A., Jr. (2006) Behavioral and anatomical interactions between dopamine and corticotropin-releasing factor in the rat. *J Neurosci.*, **26**, 3855-3863.
- Miles, P.R., Mundorf, M.L. & Wightman, R.M. (2002) Release and uptake of catecholamines in the bed nucleus of the stria terminalis measured in the mouse brain slice. *Synapse*, **44**, 188-197.
- Mirenowicz, J. & Schultz, W. (1996) Preferential activation of midbrain dopamine neurons by appetitive rather than aversive stimuli. *Nature*, **379**, 449-451.
- Olds, J. & Milner, P. (1954) Positive reinforcement produced by electrical stimulation of septal area and other regions of rat brain. *Journal of comparative and physiological psychology*, **47**, 419-427.

- Otis, J.M. & Mueller, D. (2011) Inhibition of beta-adrenergic receptors induces a persistent deficit in retrieval of a cocaine-associated memory providing protection against reinstatement. *Neuropsychopharmacology : official publication of the American College of Neuropsychopharmacology*, **36**, 1912-1920.
- Owesson-White, C.A., Cheer, J.F., Beyene, M., Carelli, R.M. & Wightman, R.M. (2008) Dynamic changes in accumbens dopamine correlate with learning during intracranial self-stimulation. *Proc Natl Acad Sci U S A*, **105**, 11957-11962.
- Pan, W.X., Schmidt, R., Wickens, J.R. & Hyland, B.I. (2005) Dopamine cells respond to predicted events during classical conditioning: evidence for eligibility traces in the reward-learning network. *J Neurosci*, **25**, 6235-6242.
- Park, J., Aragona, B.J., Kile, B.M., Carelli, R.M. & Wightman, R.M. (2010) In vivo voltammetric monitoring of catecholamine release in subterritories of the nucleus accumbens shell. *Neuroscience*, **169**, 132-142.
- Park, J., Galligan, J.J., Fink, G.D. & Swain, G.M. (2007) Differences in sympathetic neuroeffector transmission to rat mesenteric arteries and veins as probed by in vitro continuous amperometry and video imaging. *J Physiol.*, **584**, 819-834. .
- Park, J., Kile, B.M. & Wightman, R.M. (2009a) *In vivo* voltammetric monitoring of norepinephrine release in the rat ventral bed nucleus of the stria terminalis and anteroventral thalamic nucleus. *Eur J Neurosci.*, **30**, 2121-2133.
- Park, J., Kile, B.M. & Wightman, R.M. (2009b) In vivo voltammetric monitoring of norepinephrine release in the rat ventral bed nucleus of the stria terminalis and anteroventral thalamic nucleus. *Eur J Neurosci*, **30**, 2121-2133.
- Park, J., Wheeler, R.A., Fontillas, K., Keithley, R.B., Carelli, R.M. & Wightman, R.M. (2011) Catecholamines in the Bed Nucleus of the Stria Terminalis Reciprocally Respond to Reward and Aversion. *Biological psychiatry*.
- Park, J., Wheeler, R.A., Fontillas, K., Keithley, R.B., Carelli, R.M. & Wightman, R.M. (2012) Catecholamines in the bed nucleus of the stria terminalis reciprocally respond to reward and aversion. *Biol Psychiatry*, **71**, 327-334.
- Paxinos, G. & Watson, C. (2007) *The Rat Brain in Stereotaxic Coordinates*. Elsevier Inc., Burlington.
- Phelix, C.F., Liposits, Z. & Paull, W.K. (1992) Monoamine innervation of bed nucleus of stria terminalis: an electron microscopic investigation. *Brain Res Bull*, **28**, 949-965.
- Phelix, C.F., Liposits, Z. & Paull, W.K. (1994) Catecholamine-CRF synaptic interaction in a septal bed nucleus: afferents of neurons in the bed nucleus of the stria terminalis. *Brain Res Bull.*, **33**, 109-119.
- Phillips, P.E., Robinson, D.L., Stuber, G.D., Carelli, R.M. & Wightman, R.M. (2003a) Real-time measurements of phasic changes in extracellular dopamine concentration in freely moving rats by fast-scan cyclic voltammetry. *Methods Mol Med.*, **79**, 443-464.

- Phillips, P.E., Stuber, G.D., Heien, M.L., Wightman, R.M. & Carelli, R.M. (2003b) Subsecond dopamine release promotes cocaine seeking. *Nature*, **422**, 614-618.
- Ritter, S. & Stein, L. (1974) Self-stimulation in the mesencephalic trajectory of the ventral noradrenergic bundle. *Brain Res*, **81**, 145-157.
- Roll, S.K. (1970) Intracranial self-stimulation and wakefulness: effect of manipulating ambient brain catecholamines. *Science*, **168**, 1370-1372.
- Sara, S.J., Vankov, A. & Herve, A. (1994) Locus coeruleus-evoked responses in behaving rats: a clue to the role of noradrenaline in memory. *Brain Res Bull.*, **35**, 457-465.
- Schultz, W., Dayan, P. & Montague, P.R. (1997) A neural substrate of prediction and reward. *Science.*, **275**, 1593-1599.
- Selden, N.R., Robbins, T.W. & Everitt, B.J. (1990) Enhanced behavioral conditioning to context and impaired behavioral and neuroendocrine responses to conditioned stimuli following ceruleocortical noradrenergic lesions: support for an attentional hypothesis of central noradrenergic function. *J Neurosci*, **10**, 531-539.
- Solomon, R.L. & Corbit, J.D. (1974) An opponent-process theory of motivation. I. Temporal dynamics of affect. *Psychol Rev*, **81**, 119-145.
- Somers, L.A., Beyene, M., Carelli, R.M. & Wightman, R.M. (2009) Synaptic overflow of dopamine in the nucleus accumbens arises from neuronal activity in the ventral tegmental area. *J Neurosci*, **29**, 1735-1742.
- Stein, L. & Wise, C.D. (1969) Release of norepinephrine from hypothalamus and amygdala by rewarding medial forebrain bundle stimulation and amphetamine. *Journal of comparative and physiological psychology*, **67**, 189-198.
- Stuber, G.D., Wightman, R.M. & Carelli, R.M. (2005) Extinction of cocaine self-administration reveals functionally and temporally distinct dopaminergic signals in the nucleus accumbens. *Neuron*, **46**, 661-669.
- Sullivan, G.M., Apergis, J., Bush, D.E., Johnson, L.R., Hou, M. & Ledoux, J.E. (2004) Lesions in the bed nucleus of the stria terminalis disrupt corticosterone and freezing responses elicited by a contextual but not by a specific cue-conditioned fear stimulus. *Neuroscience*, **128**, 7-14.
- Tombaugh, T.N., Pappas, B.A., Roberts, D.C., Vickers, G.J. & Szostak, C. (1983) Failure to replicate the dorsal bundle extinction effect: telencephalic norepinephrine depletion does not reliably increase resistance to extinction but does augment gustatory neophobia. *Brain Res*, **261**, 231-242.
- Ungless, M.A., Magill, P.J. & Bolam, J.P. (2004) Uniform inhibition of dopamine neurons in the ventral tegmental area by aversive stimuli. *Science*, **303**, 2040-2042.
- Ventura, R., Morrone, C. & Puglisi-Allegra, S. (2007) Prefrontal/accumbal catecholamine system determines motivational salience attribution to both reward- and aversion-related stimuli. *Proceedings of the National Academy of Sciences of the United States of America*, **104**, 5181-5186.

- Weinshenker, D. & Schroeder, J.P. (2007) There and back again: a tale of norepinephrine and drug addiction. *Neuropsychopharmacology*, **32**, 1433-1451.
- Wise, R.A. (1996) Addictive drugs and brain stimulation reward. *Annual review of neuroscience*, **19**, 319-340.
- Wise, R.A. (2002) Brain reward circuitry: insights from unsensed incentives. *Neuron*, **36**, 229-240.
- Wise, R.A. (2004) Dopamine, learning and motivation. *Nat Rev Neurosci.*, **5**, 483-494.

CHAPTER 5: MEDULLARY NOREPINEPHRINE NEURONS MODULATE LOCAL OXYGEN CONCENTRATIONS IN THE BED NUCLEUS OF THE STRIA TERMINALIS

Introduction

The neurovascular unit, composed of neuronal, glial, and vascular elements, serves to support brain function by matching O₂-rich blood flow with the metabolic demands of regional activity. It is understood that the products of local neurotransmission trigger this response, known as functional hyperemia; however, much remains to be learned regarding the actions and mechanisms of the chemical messengers involved (Cauli & Hamel, 2010). This information is crucial to understanding disease pathologies that involve dysregulation of cerebral blood flow (CBF)—including cerebral ischemia (Baker *et al.*, 2013) and many forms of dementia (Bell & Zlokovic, 2009)—as well as to interpreting data from brain imaging techniques such as blood O₂ level dependent (BOLD) fMRI.

The catecholamine norepinephrine is one major neurotransmitter implicated in this hemodynamic process. Its neurons lie in several nuclei, designated A1-7, scattered along the hindbrain and brainstem. These cell populations diffusely project throughout the brain and terminate primarily as non-junctional varicosities (Latsari *et al.*, 2002), allowing their activity to exert a broad field of influence. The noradrenergic neurons of the locus coeruleus (LC, A6) are typically associated with the neurovascular unit. These neurons provide the majority of cortical noradrenergic input, and they terminate proximal to both astrocytes and microvessels (Cohen *et al.*, 1997; Aoki *et al.*, 1998). The presence of adrenoceptors on these neurovascular targets (Hertz *et al.*, 2010), which are sensitive to LC denervation (Kalaria *et al.*, 1989; Cohen *et al.*, 1997), provides further evidence that the LC norepinephrine system is positioned to influence their activities. Indeed, studies have

established that noradrenergic signaling can influence energy metabolism (Obel *et al.*, 2012), vascular permeability (Raichle *et al.*, 1975), ionic fluctuations in astrocytes (Muyderman *et al.*, 1997), as well as glutamate signaling by modulation of its synthesis (Gibbs *et al.*, 2008) and uptake (Alexander *et al.*, 1997). Other reports have demonstrated that CBF responses coincide with altered LC activity (Raichle *et al.*, 1975; Goadsby & Duckworth, 1989; Toussay *et al.*, 2013).

Here we consider the vasoactivity of norepinephrine in a region weakly innervated by the LC: the ventral bed nucleus of the stria terminalis (vBNST). The vBNST is a structure of the extended amygdala involved in the autonomic and behavioral responses to stress (Drolet, 2009). We targeted this deep brain region as it receives the densest norepinephrine input in the brain (Kilts & Anderson, 1986). Its noradrenergic innervation arises primarily from the nucleus of the solitary tract (NST, A2) and the A1 cell group through the ventral noradrenergic bundle (Forray & Gysling, 2004). These cell groups are located in the medulla oblongata, and receive cardiovascular, respiratory, gastrointestinal and other visceral information from peripheral afferents. Though these norepinephrine populations have not been formally associated with cerebral hemodynamic function, their terminals are associated with the perivascular space in regions such as the paraventricular nucleus (Swanson *et al.*, 1977). In addition, non-specific chemical stimulation of NST neurons attenuates CBF, and this effect is believed to be neurogenic in origin (Maeda *et al.*, 1998).

In this study, norepinephrine concentrations were transiently increased within the vBNST by electrical stimulation of the ventral noradrenergic bundle (VNB) and by local application through iontophoresis. Fast-scan cyclic voltammetry (FSCV) at a carbon-fiber microelectrode was employed to simultaneously detect norepinephrine transients and changes in extracellular O₂ with subsecond and micrometer resolution. Extracellular O₂ is a function of ongoing metabolism and local blood flow. We found that surges of norepinephrine in the vBNST are accompanied by an increase in O₂ that is followed by a

transient decrease below baseline levels. This response is due to the local actions of norepinephrine at its receptors and does not depend on LC functionality. In a brain slice that lacks CBF, iontophoresis of norepinephrine had no effect on measured O₂ concentrations whereas electrical stimulation caused O₂ concentration to decrease, supporting a role for functional hyperemia as the origin of our *in vivo* results.

Experimental

Chemicals and drugs

All chemicals and drugs were used as received from Sigma Aldrich (St. Louis, MO, USA), unless otherwise noted.

Electrode fabrication

Two electrode types were employed in this study. Experiments without iontophoresis used single barrel carbon-fiber microelectrodes (Cahill *et al.*, 1996). Each electrode was cut under a light microscope to an exposed length of 100 µm. For iontophoresis experiments, voltammetric recordings were made with four-barrel probes (Herr *et al.*, 2008). One barrel housed a carbon-fiber electrode while the other three barrels contained the desired solutions.

Fast-scan cyclic voltammetry

FSCV was computer-controlled using a data acquisition program (HDCV, UNC-Chapel Hill, NC)(Bucher *et al.*, 2013) programmed in LabVIEW (National Instruments, Austin, TX). A single PCIe-6363 card (National Instruments, Austin, TX) generated the voltammetric and stimulation waveforms and simultaneously collected cyclic voltammograms. The voltammetric waveform was applied to the carbon-fiber microelectrode and its current response transduced through a locally-constructed UEI potentiostat (UNC Department of Chemistry Electronics Design Facility).

Voltammetric recordings employed two waveforms. For electrode placement, iontophoresis barrel priming, and post-experiment signal verification, a triangular waveform designed specifically for catecholamine detection was used. This waveform scanned between -0.4 V and 1.3 V at 400 V/s (Heien *et al.*, 2003). For combined measurements of O₂ and norepinephrine the voltage ramp scanned at 400 V/S between 0.8 V and -1.4 V with a holding potential of 0 V (Venton *et al.*, 2003). Before use of either waveform the electrode was conditioned with the voltage ramp for 15 min at 60 Hz and 15 min at 10 Hz. Recordings were made at a 10 Hz application frequency.

Calibrations

Electrode responses to norepinephrine, O₂, and 4-methylcatecholamine were determined through an air-impermeable flow-injection analysis system with glass syringes and PEEKTM tubing. All standards were prepared in TRIS buffer (15 mM TRIS, 126 mM NaCl, 2.5 mM KCl, 25 mM NaHCO₃, 2.4 mM CaCl₂, 1.2 mM NaH₂PO₄, 1.2 mM MgCl₂, 2.0 mM Na₂SO₄) adjusted to pH 7.4 with NaOH. O₂ calibrations employed a N₂-purged solution, an air-saturated solution, and an O₂-saturated solution. Peak reduction currents were taken for O₂ calibrations, while peak oxidation currents were used for the catecholamines. The average calibration factors were as follows: 16.4 nA/ μ M norepinephrine (+1.3 V waveform), -0.3 nA/ μ M O₂ and 8.9 nA/ μ M 4-methylcatechol (O₂-sensitive waveform).

Voltammetric data presentation and analysis

FSCV data were processed through the HDCV analysis program. Each file was digitally-filtered (4th order low pass Bessel, 2 KHz cutoff) and background-subtracted from baseline currents. Data are presented as color plots, with the waveform plotted along the ordinate and the acquisition time shown along the abscissa. Currents are mapped in false-

color in a 3: -2 ratio. Principal component regression, a multivariate chemometric algorithm, was used to determine concentrations for data collected on the -0.4 V/ +1.3 V waveform (Keithley *et al.*, 2009).

Unless otherwise indicated data are shown as mean \pm standard error. All n values represent number of animals. Data were considered statistically significant when $P < 0.05$.

Surgery

All animal procedures were approved by the Institutional Animal Care and Use Committee of the University of North Carolina at Chapel Hill in accordance with the Public Health Service (PHS) policy on Humane Care and Use of Laboratory Animals and the Amended Animal Welfare Act of 1985. Care was taken to minimize the number of animals used in this study and their suffering. Adult male Sprague-Dawley rats (300 – 400 g) were purchased from Charles River (Wilmington, MA). Animals were anesthetized with urethane (1.5 g/kg) and placed in a stereotaxic frame (Kopf, Tujunga, CA). Surgical procedures were as described previously (Park *et al.*, 2009) with anterior-posterior (AP), medial-lateral (ML), and dorsal-ventral (DV) coordinates referenced from bregma according to Paxinos and Watson (2007). A fresh carbon-fiber microelectrode was lowered into the ventral bed nucleus of the stria terminalis (vBNST, AP +0.0 mm, ML +1.2 mm, DV -7.0 to -7.8 mm), and a Ag/AgCl reference was implanted in the contralateral hemisphere. A bipolar stimulating electrode (Plastics One, West Lafayette, IN) was placed in the VNB (AP -5.2 mm, ML +1.2 mm, DV -8.0 to 8.6 mm) ipsilaterally to the recording electrode. Electrical stimulations (10 - 80 biphasic pulses, 60 Hz, $\pm 300 \mu\text{A}$, 2 ms per pulse) were delivered via an optically isolated stimulator (NL 800A, Neurolog, Digitimer Ltd, Hertfordshire, UK). The depths of the carbon fiber and stimulating electrodes were adjusted to achieve maximal measured norepinephrine release.

In vitro procedure

Brain slices containing the vBNST were prepared from Sprague-Dawley rats (300 – 400 g) anesthetized with urethane (1.5 g/kg). Brains were quickly removed after decapitation and submerged in ice-cold, oxygenated (95% O₂/5%CO₂) bicarbonate buffer solution (87 mM NaCl, 2.5 mM KCl, 1.2 mM NaH₂PO₄, 25 mM NaHCO₃, 7 mM MgCl₂, 0.5 mM CaCl₂, 75 mM Sucrose) adjusted to pH 7.4. A Vibroslice NVSL (World Precision Instruments, Sarasota, FL) was used to cut 300 µm coronal sections. BNST slices were transferred to a perfusion chamber (RC-22, Warner Instruments, Hamden, CT) fitted with a microscope (Nikon Fv-, Gibraltar Stage) and maintained under a flow (2 ml/min) of oxygenated bicarbonate buffer (126 mM NaCl, 2.5 mM KCl, 1 mM NaH₂PO₄, 26 mM NaHCO₃, 1.2 mM MgCl₂, 2.4 mM CaCl₂, 11 mM Glucose) heated to 37°C. For electrochemical recordings a carbon fiber electrode was lowered 75 µm into the tissue underneath the anterior commissure. A tungsten bipolar stimulating electrode (Frederick Haer Co., Bowdoinham, ME) was placed on the surface of the slice proximal to the recording electrode.

Pharmacological investigations

In the first set of experiments pharmacological agents were introduced systemically by intraperitoneal (i.p.) injection. First, a 30 min baseline was established by repeating a 60 pulse electrical stimulus every 5 min. Next, sterile saline (1 mL) was administered as a vehicle control, followed by a selective norepinephrine drug. These included idazoxan (α_2 antagonist, 5 mg/kg), desipramine HCl (transporter inhibitor, 15 mg/kg), propranolol HCl (non-selective β antagonist, 20 mg/kg), and terazosin (α_1 antagonist, 5 mg/kg, Tocris Bioscience, Bristol, UK). Doses were chosen to identify receptor contributions, not to quantitatively assess their relative effects. All drugs were dissolved in 0.5 mL saline, except for terazosin, which was dissolved in 1.0 mL saline with gentle heat. Data were collected for at least 45 min following drug administration to allow maximum effects.

A second set of experiments used iontophoresis to introduce the adrenoceptor antagonists as well as *N*-nitro-L-arginine methyl ester (L-NAME, nitric oxide synthase inhibitor) and 1-aminobenzotriazole (ABT, cytochrome P450 inhibitor, Tocris Bioscience, Bristol, UK) directly at the recording electrode. Iontophoresis solutions were prepared as 5 mM drug, 5 mM 4-methylcatechol and 5 mM NaCl, adjusted to pH 5.6. 4-Methylcatechol provided an electroactive marker to monitor ejections with FSCV (Herr *et al.*, 2008). Drug concentrations were calculated from the relative mobility of each pharmacological agent relative to 4-methylcatechol. Ejections were induced by positive current (5 – 400 nA) generated by a constant-current source (Neurophore, Harvard Apparatus, Holliston, MA). Each iontophoresis barrel was primed at a depth dorsal to the vBNST (-5 mm – -6 mm) to ensure reproducible ejection profiles, and a negative retaining current (-1 – -10 nA) was applied to any leaking barrels. After baseline measurements were taken as described for the I.P. protocol, drugs were applied through a 30 s ejection. Ejection of 4-methylcatechol did not evoke O₂ changes (*vide infra*) and so it served as a control. Ejected drug concentrations were between 5 – 35 μ M at the carbon fiber. Measured ejections currents were allowed to return to baseline before stimulation data were collected.

A third type of pharmacological manipulation involved local introduction of norepinephrine-selective agonists through iontophoresis. Drugs were prepared as described for the antagonist ejections. Methoxamine (α_1 agonist) and clonidine (α_2 agonist) solutions contained 4-methylcatechol to monitor their ejections electrochemically. Norepinephrine and isoproterenol (non-selective β agonist) were prepared without 4-methylcatechol as both are electroactive. Each was ejected in the vBNST for 1 s (3 – 5 min apart) to reproduce the duration of the electrical stimulation used in other portions of this study. Based on the capabilities of the iontophoresis barrel, a range of concentrations (between 1 – 20 μ M) was tested for each agonist. For some experiments antagonists were loaded into the remaining iontophoresis barrels. In these experiments baseline

norepinephrine responses were recorded for 30 min before an antagonist was administered following the protocol of the electrical stimulation experiments.

Signal verification

The placement of the stimulating electrode also activates the dopaminergic neurons of the ventral tegmental area (Park *et al.*, 2011). To ensure that the voltammetric catecholamine signal was due to norepinephrine, and not structurally-similar dopamine, each experiment ended with *i.p.* administration of raclopride (dopamine D2 autoreceptor antagonist) followed by either idazoxan (α_2 autoreceptor antagonist) or desipramine (norepinephrine transporter inhibitor). Only locations that selectively responded to the norepinephrine drugs were used in this study (Park *et al.*, 2011).

Histology

At the end of data collection a constant potential (10 V, 30 s) was applied to the carbon-fiber to lesion the recording site. Animals were then sacrificed with an overdose of urethane. Brains were promptly removed and fixed with 10% formalin and post-fixed for at least 3 days before coronal slices (40 – 50 μ m) were prepared on a freezing microtome (Leica, Germany), mounted on a glass slide, coverslipped, and viewed under a light microscope.

LC lesioning with DSP-4

The LC-selective neurotoxin DSP-4 (N-(2-chloroethyl)-N-ethyl-2-bromobenzylamine) (Fritschy & Grzanna, 1989) was administered to rats ($n = 5$, 150 – 200 g) in two doses (0.5 mL, 50 mg/kg, I.P.) three days apart. DSP-4 was dissolved in saline immediately before use. Measurements commenced 9 days after the last dose to allow peripheral effects to diminish. Untreated rats were used as a control in both experiments.

Immunohistochemistry

Rats were anaesthetized with urethane and transcardially perfused with 0.1M phosphate buffered saline (PBS) at pH 7.4, followed by 4% paraformaldehyde in PBS. Brains were removed, post-fixed for >24 hours, then cryoprotected in 30% sucrose for >48 hours. Sections (40 μ m) were cut with a freezing microtome (Leica, Germany) and collected in 0.1 M PBS.

Immunofluorescence procedures were adapted from elsewhere (Hartig *et al.*, 2009). Briefly, sections were washed in 0.1 M Tris-buffered saline, pH 7.4 (TBS), then blocked with 5% normal donkey serum in TBS with 0.3% Triton-X-100 (NDS-TBS-T) for 1 hr. Tissue was incubated overnight at 4 °C in primary cocktail prepared in NDS-TBS-T, which contained mouse-anti-GFAP (1:300, Sigma), rabbit-anti-DBH (1:500, Immunostar), and biotinylated solanum tuberosum lectin (20 μ g/mL, Vector). After 3 rinses in TBS-T, sections were incubated in secondary cocktail for 2 hr at room temperature. Secondary cocktail was prepared in TBS with 2% bovine serum albumin and contained AlexaFluor 488-conjugated goat-anti-rabbit IgG (1:500, Life Technologies), Alex Fluor 633-conjugated goat-anti-mouse IgG (1:500, Life Technologies), and streptavidin-DyLight 405 (20 μ g/mL, Fisher). Sections were rinsed extensively in TBS, mounted and coverslipped with Fluoromount (Sigma) before visualization on a confocal microscope.

Sections were analyzed with a FV1000 microscope (Olympus) equipped with a diode laser, argon laser, and helium-neon laser for the excitations of DyLight 405, AlexaFluor 488, and Alexa Fluor 633, respectively. Images are based on a single optical section of <1 μ m thickness, and captured using FV1000ASW software (Olympus). DBH quantification employed constant acquisition parameters and three sections (-0.05 mm to +0.05 mm AP from bregma) were analyzed for each animal. Mean pixel intensity was analyzed using image J software in a 9000 square pixel area. For the vBNST, a rectangle of 450 by 200

pixels was drawn directly beneath the anterior commissure, and cortical sections were analyzed in a 300 by 300 pixel square.

Cardiorespiratory measurements

The cardiorespiratory effects of anesthesia and systemic adrenergic antagonism were determined in a separate group of rats (300 – 400g). A MouseOx pulse oximeter system equipped with a collar sensor (Starr Life Sciences, Oakmont, PA) was used to monitor heart rate (beats per min) and respiratory rate (breaths per min). Pre-urethane measurements were taken with the animal at rest. Anesthetized data were collected 3 hr after administration of urethane (1.5 g/kg). Thereafter, one of four adrenergic antagonists (terazosin, idazoxan, propranolol or desipramine) was delivered (i.p.) at the dose listed under *Pharmacological Investigations*. Post-drug cardiorespiratory values were recorded 35 min after injection.

Results

Immunohistochemistry of recording environment

Immunohistochemistry was employed to provide an overview of the neurovascular environment of the vBNST on the spatial scale of our recording electrode. Three major neurovascular components were targeted: microvessels (STL), glial cells (GFAP), and norepinephrine terminals (DBH). Their distribution is shown in Figure 5.1. At these coordinates, the ventral portion of the BNST is located underneath the anterior commissure (AC). A range of vessel sizes (~3 to 15 μm) were found within the vBNST confirming the presence of both arterioles and capillaries. Astrocytes were highly associated with the larger microvessels as well as with the myelinated axon fibers composing the AC.

Consistent with our previous work (Park *et al.*, 2009) the densest region of noradrenergic innervation was located within the vBNST. At higher magnifications these

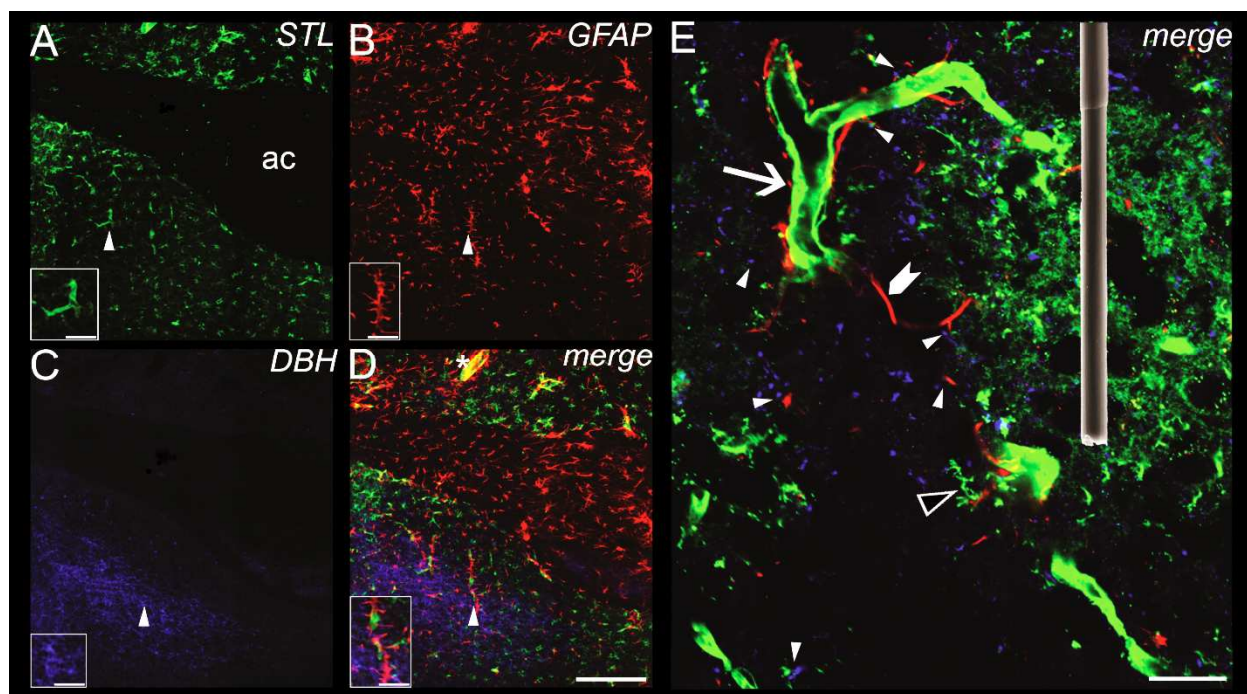


Figure 5.1. Confocal laser scanning images of triple-fluorescence labeling in the rat vBNST. (A) Lectin staining of vasculature and microglia with biotinylated *Solanum tuberosum* agglutinin (STL) and DyLight-405 conjugated streptavidin, color coded in green (ac= anterior commissure). Simultaneously labeled astroglia are shown in (B) with mouse anti-glial fibrillary acidic protein (GFAP) and Alexa Fluor-633 tagged goat anti-mouse IgG, color-coded in red. Concomitantly revealed norepinephrine terminals were color coded in blue, and visualized in (C) using rabbit anti-dopamine beta hydroxylase (DBH) and Alexa Fluor-488 goat anti-rabbit IgG. (D) A merge of A, B, and C. An example of glial-vessel colocalization is indicated by an asterisk and appears yellow. Terminal-glial colocalization is seen in pink. Scale bar = 200 μ m. Insets demonstrate the triangle labeled features at higher magnification. Scale bar = 50 μ m. (E) Further magnification in a different slice revealed the diverse architecture of blood vessels (arrow), microglia (open triangle), astrocytes (chevron), and norepinephrine terminals (blue) within the vBNST. Sites where norepinephrine terminals interact with vessels and/or astroglia are indicated by closed triangles. An electronmicrograph of a 100 μ m long carbon-fiber microelectrode is superimposed to demonstrate the electrochemical sampling environment. Scale bar = 20 μ m.

terminals appeared scattered within the perivascular space in proximity to both microvessels and astrocytes, as has been reported for cortical regions. Within the areas of highest terminal density, spanning only ~1 mm along the medial-lateral plane, vascular heterogeneity is apparent. The dimensions of the carbon-fiber microelectrode (100 μ m length, 5 μ m diameter, superimposed in Fig 5.1E) are small enough to probe these microenvironments. In these experiments the placement of the carbon-fiber electrode was optimized for the detection of norepinephrine, not for the detection of O₂ changes. Therefore, the immediate neurovascular landscape likely varied between recording locations.

O₂ response with electrical stimulation

To investigate whether norepinephrine release in the vBNST coincides with O₂ changes, electrical stimulation of the ventral noradrenergic bundle (VNB) was used to induce norepinephrine overflow while extracellular O₂ and norepinephrine changes were monitored simultaneously. Norepinephrine has a peak-oxidation potential of 0.75 V and a peak for reduction of its electroformed o-quinone at -0.2 V on the negative going scan. O₂ is reduced at -1.35 V on the negative going scan (Fig 5.2). We found that O₂ changes accompanied VNB stimulation and that the responses were variable between animals (Fig 5.3). Minor adjustment of the recording and stimulating electrode depths did not have a significant effect on the measured O₂ signal (Fig 5.4). This suggests signal variability may be a result of anterior-posterior/medial-lateral positioning.

One stimulated O₂ response predominated in our studies (~65% of locations) and thus was chosen for pharmacological characterization. In this response, O₂ levels rose after the stimulation and reached a maximum (6.98 ± 0.93 μ M) on average 1.9 ± 0.1 s after stimulation onset. This increase was subsequently followed by a transient dip below

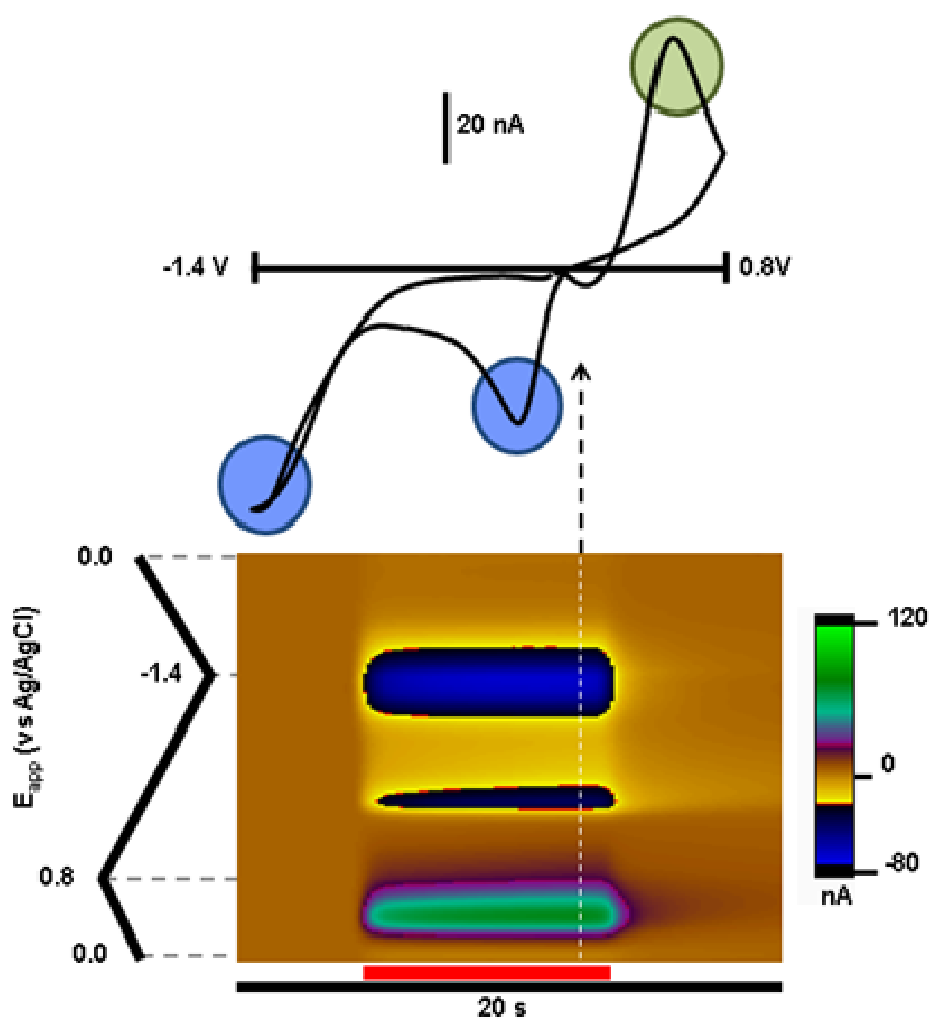
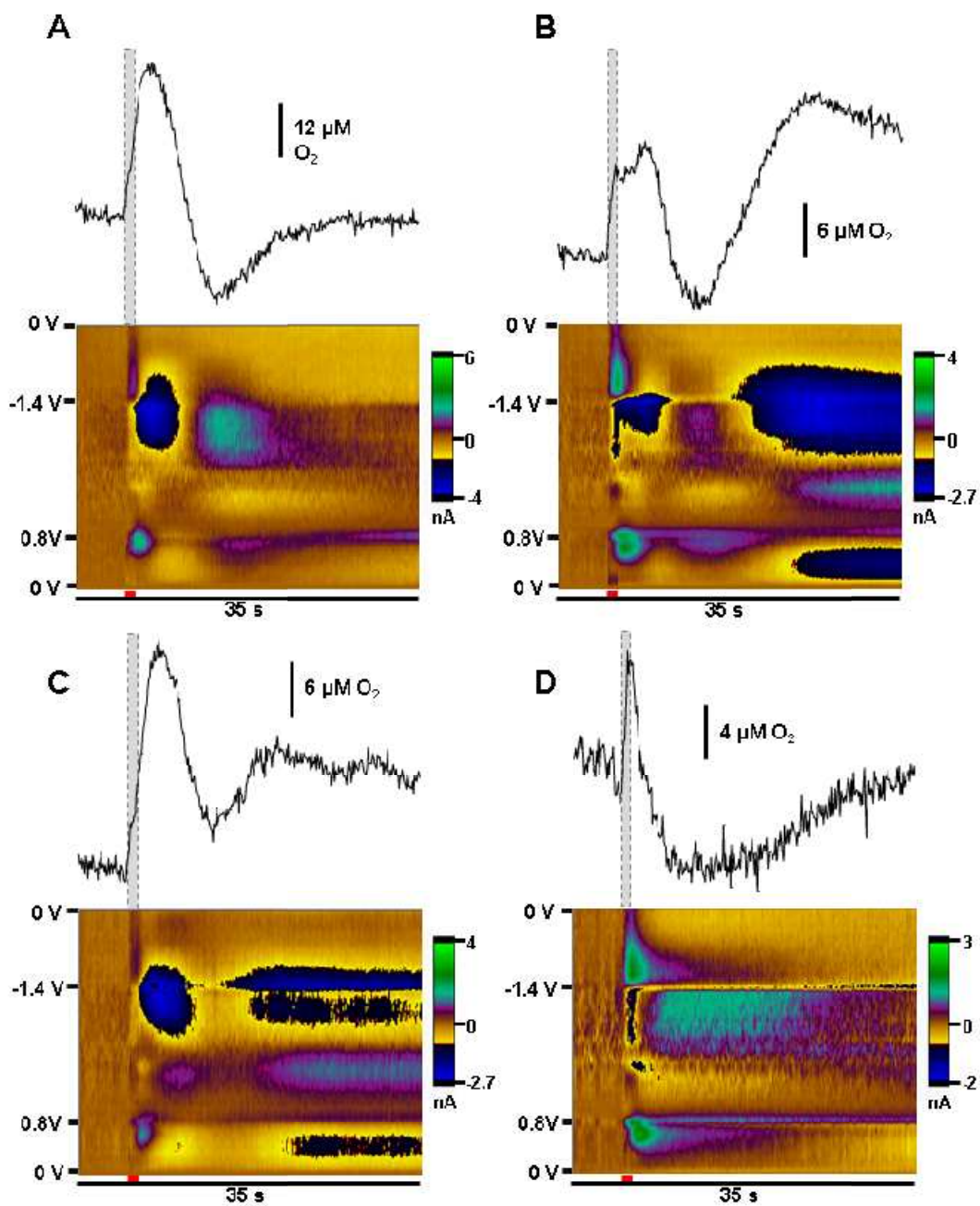
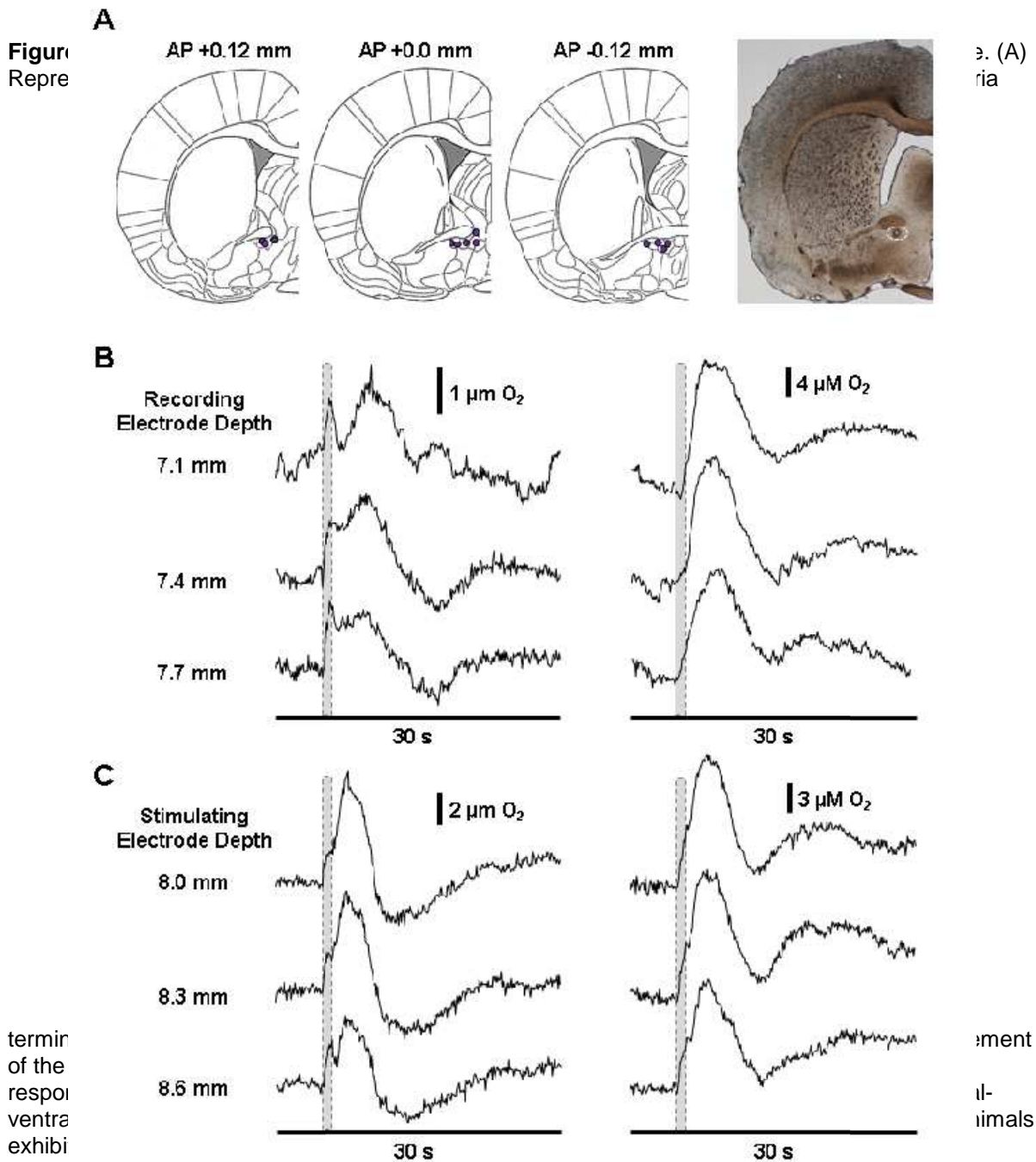


Figure 5.2. Simultaneous detection of 250 μM O_2 and 8 μM norepinephrine in an air-impermeable flow injection system. Redox currents are displayed in a color plot with the time of injection indicated by the red bar. The oxidation of norepinephrine and the reduction of its *o*-quinone produce currents at +0.75 V (anodic scan) and -0.2 V (cathodic scan) respectively. The reduction of molecular O_2 generates currents which peak at the -1.4 V switching potential. These features are readily apparent in a cyclic voltammogram exacted from the time of sample injection.

Figure



(C). In a small number of animals ($\sim 5\%$), the stimulation resulted in a monophasic O_2 decrease (D). Only responses that resembled (A) and (B) were characterized for the purposes of this study.



baseline concentrations ($-3.98 \pm 0.74 \mu\text{M}$), peaking 9.6 ± 0.2 s after the stimulation. We termed the initial O_2 increase as event 1 and the subsequent decrease as event 2. In many animals a second, prolonged increase in extracellular O_2 was measured after the initial response long after clearance of norepinephrine, similar to our previous recordings in the

striatum (Venton *et al.*, 2003). The second O₂ increase was unaffected by local adrenoceptor pharmacology (Fig 5.5). Thus, our discussion focuses on events 1 and 2.

Example data averaged over multiple trials from a single animal are provided in Figure 5.6A. Multiple chemical fluctuations are visible in the color plot. Immediately after the stimulation norepinephrine release is apparent as positive current at its oxidation potential. Concurrent O₂ fluctuations appear at -1.35 V on the forward voltage scan. As O₂ is detected through its reduction, negative currents correspond to increases in concentration, while positive currents indicate decreases. These O₂ events are accompanied by pH changes (Venton *et al.*, 2003) that overlap with the oxidation potential of norepinephrine at later times in the recording. A positive current feature occurs after the -1.4 V switching potential during the stimulation. It is due to adsorption of ions such as Ca²⁺ (Takmakov *et al.*, 2010). The amplitude of each O₂ event was compared with the amount of released norepinephrine evoked by the electrical stimulation. While both responses correlated with peak norepinephrine concentration across animals, Event 2 exhibited a better linear fit ($r^2 = 0.61$) in comparison to Event 1 ($r^2 = 0.27$). To vary the amount of norepinephrine released in one location the duration of the electrical stimulation was varied (0.17 – 1.33 s) by changing the number of electrical pulses applied. Norepinephrine release and the O₂ changes increased linearly with pulse number within this range. The response of event 1 to stimulation duration was significantly different from that of norepinephrine ($P < 0.01$) and of event 2 ($P < 0.05$). The pulse dependence of event 2, however, closely resembled the norepinephrine response ($P > 0.05$).

We also examined the effects of electrically stimulated norepinephrine release in a

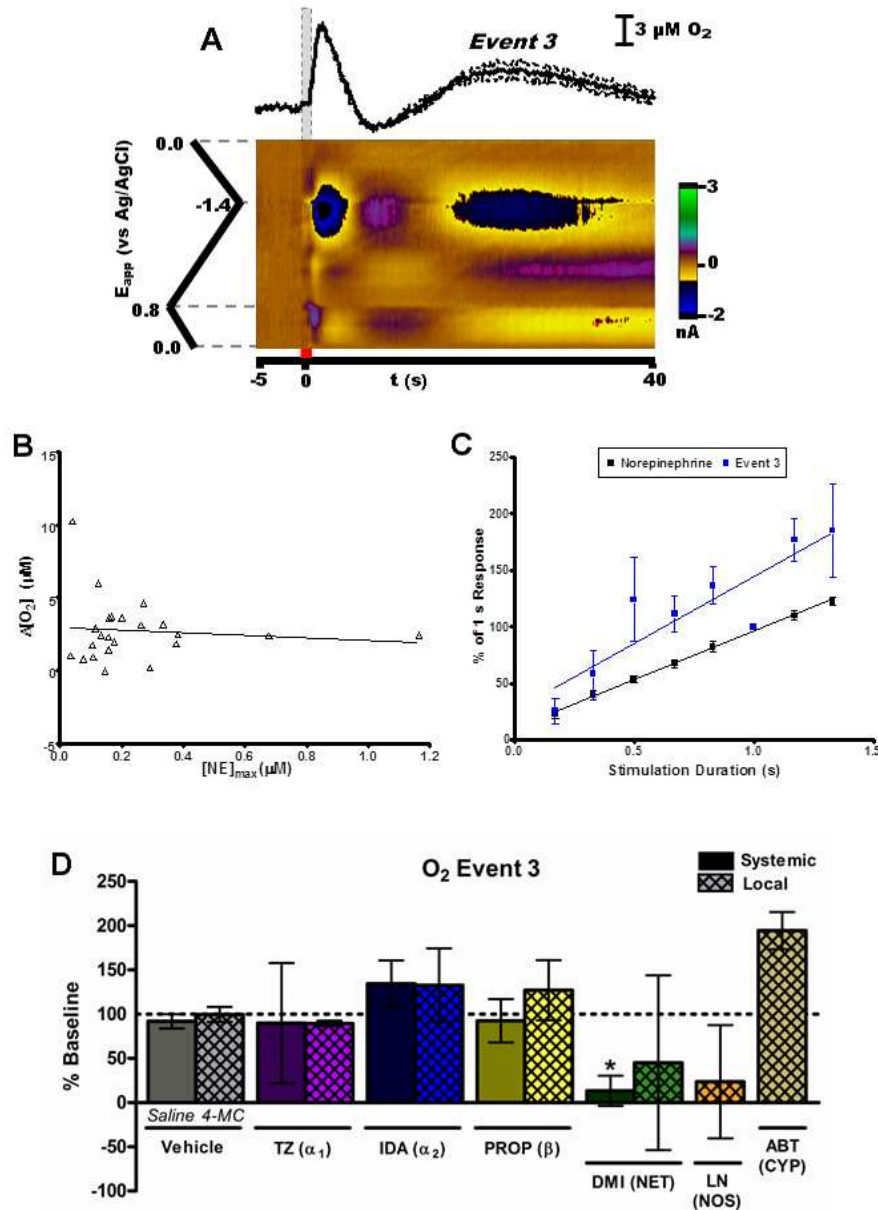


Figure 5.5. Characterization of the second O_2 increase induced by electrical-stimulation of the VNB. (A) The second O_2 increase, denoted as event 3, is observable in an extended time view of the electrically-stimulation response. (B) The magnitude of the event 3 is poorly correlated with the concentration of norepinephrine released by stimulation ($n = 23$, $r^2 = 0.01$). (C) Average peak amplitudes for norepinephrine and event 3 as a function of stimulation pulse number ($n = 5, 10$ to 80 pulses). Each data set is normalized to the 60 pulse response. Event 3 increased linearly within this pulse range ($r^2 = 0.31$). The slope of its response was not significantly different than that of norepinephrine. (D) Pharmacology of event 3. Systemic drug administration (solid) was performed through *i.p.* injection. Local drug administration (crosshatch) was accomplished through iontophoretic ejection. Saline ($n = 21$), 4-methylcatechol (4-MC, $n = 4$), terazosin (TZ, $n = 5$ systemic, $n = 4$ local), idazoxan (IDA, $n = 5$ systemic, $n = 4$ local), propranolol (PROP, $n = 4$ systemic, $n = 5$ local), local desipramine (DMI, $n = 4$), L-NAME (LN, $n = 4$) and ABT ($n = 3$) did not statistically affect event 3. Systemic desipramine (DMI) significantly decreased the amplitude this event ($P < 0.05$, $n = 4$). Significance was determined by a one-way ANOVA with a Bonferroni post hoc test comparing drug to its vehicle control (saline or 4-MC).

coronal brain slice that contained the vBNST. The stimulation (60 pulses, 60 Hz) was evoked with a bipolar electrode placed 100 - 200 μm from the carbon-fiber electrode. Following the stimulation, O_2 decreased by $36.1 \pm 6.2 \mu\text{M}$ in a monotonic fashion, reaching a minima $17.9 \pm 3.1 \text{ s}$ after the stimulation ($n = 3$ animals, 2 slices from each animal).

Effect of DSP-4 on electrically-stimulated O_2 response

To ascertain whether the stimulated O_2 changes were dependent on LC activity a subset of animals in this study was treated with the neurotoxin DSP-4. DSP-4 causes selective degradation of LC norepinephrine axons, leaving the norepinephrine neurons of the brainstem nuclei intact (Fritschy & Grzanna, 1989). DSP-4 significantly reduced norepinephrine terminal density in the cortical region above the BNST ($P < 0.001$, $n = 5$), which receives its innervation solely from LC neurons (Fritschy & Grzanna, 1989). DSP-4 did not, however, exert a significant effect on the terminal density within vBNST (Fig 5.7). Responses to VNB stimulation also remained intact after DSP-4. In treated animals, no significant differences in peak times and magnitudes were found for norepinephrine release and the O_2 response (Table 1).

O_2 response with adrenoceptor blockade

While electrical stimulation is an effective means to depolarize proximal neurons its effects are relatively non-selective, causing release of other neuromodulators. We therefore employed selective antagonists to determine the involvement of noradrenergic receptors in the electrically-stimulated O_2 response. Drugs were introduced both systemically (*i.p.* injection) and locally at the recording site (iontophoresis ejection). Because systemic administration of adrenergic drugs and anesthesia can influence cardiorespiratory function we also monitored heart rate and breathing rate after their systemic application (Fig 5.8).

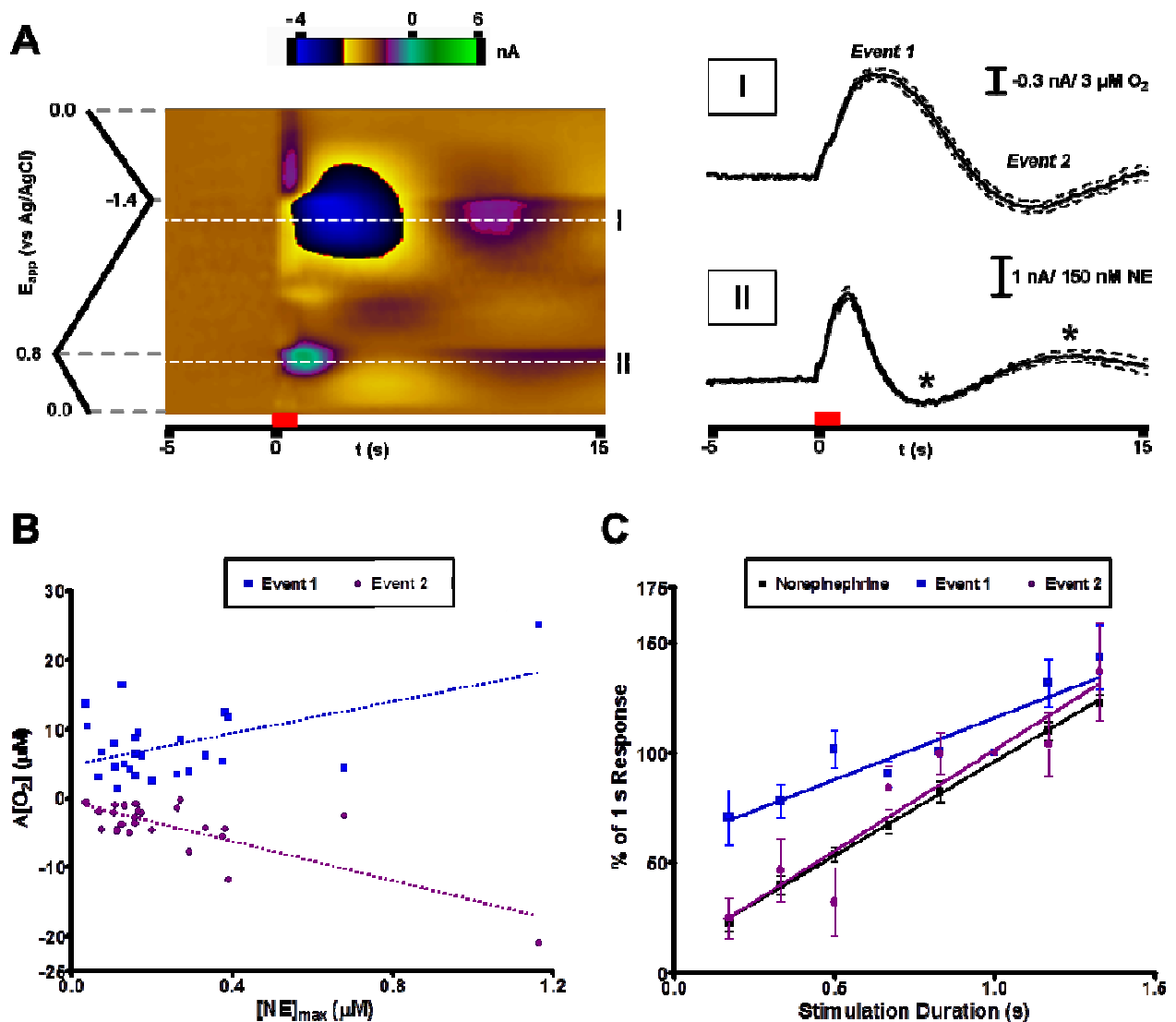


Figure 5.6. Predominant O₂ response recorded in the vBNST with electrical stimulation of the VNB. (A) Representative data averaged from 10 consecutive stimulations in a single animal. Current at all applied potentials is visualized in a false-color display (left) with the stimulation time denoted by the red bar. Extracellular O₂ is monitored at its reduction potential (-1.35 V, I). Current extracted from this potential reveals a biphasic O₂ response following electrical stimulation. Norepinephrine release is simultaneously measured at its oxidation potential (+0.75 V, II) and is visible shortly after the stimulation onset. Changes in extracellular pH also generate current at this potential later in the recording (asterisks). Dashed lines indicate the standard error of the mean for these measurements. (B) Magnitude of the O₂ response compared to stimulated norepinephrine release across multiple animals (n=25). Both O₂ events showed linear responses to the concentration of evoked norepinephrine (Event 1: $11.46 \pm 3.90 \mu\text{M O}_2/\mu\text{M NE}$, $r^2 = 0.27$; Event 2: $-14.20 \pm 2.37 \mu\text{M O}_2/\mu\text{M NE}$,

$r^2 = 0.61$). (C) Average peak amplitudes for norepinephrine and O_2 as a function of stimulation pulse number ($n = 5, 10$ to 80 pulses). Each data set is normalized to the 60 pulse response. Responses for O_2 (Event 1: $r^2 = 0.849$; Event 2: $r^2 = 0.895$) and norepinephrine ($r^2 = 0.997$) were linear within this pulse range.

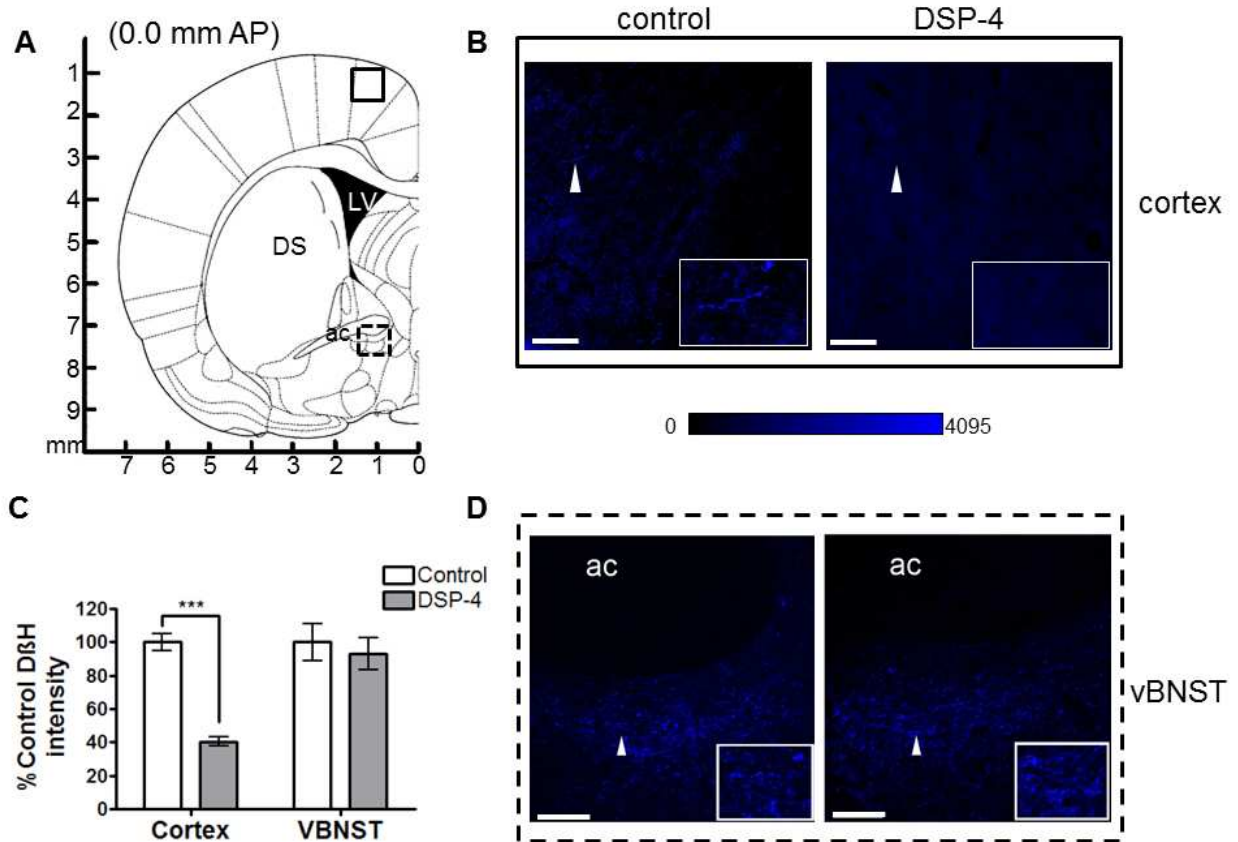


Figure 5.7. The effect of DSP-4 lesioning on DBH immunoreactivity. (A) Locations in the cortex (solid box) and the ventral bed nucleus of the stria terminalis (dashed box) used to obtain the fluorescence data in B - D. Diagram adapted from the atlas of Paxinos and Watson. (C) Identical acquisition parameters were employed to detect changes in DBH immunoreactivity between control and DSP-4 treated animals. Significant changes were noted in cortical but not vBNST sections. Intensity is in arbitrary units, and represents a ratio of Alexa Fluor-488 conjugated goat anti-rabbit fluorescence emission in treated compared to untreated animals. Representative images are shown for cortical (B) and vBNST (D) sections. Scale bar = $100\mu\text{m}$, $35\mu\text{m}$ for inset images.

Group	Norepinephrine		Event 1		Event 2	
	[NE] _{max} (μM)	t _{max} (s)	[O ₂] _{max} (μM)	t _{max} (s)	[O ₂] _{max} (μM)	t _{max} (s)
Control	0.22 ± 0.04	1.9 ± 0.1	6.98 ± 0.93	2.7 ± 0.1	-3.98 ± 0.74	9.6 ± 0.2
DSP-4	0.24 ± 0.10	2.0 ± 0.1	6.50 ± 1.95	3.2 ± 0.5	-5.59 ± 1.27	10.6 ± 1.3

Table 5.1. Average norepinephrine and O₂ responses to VNB stimulation. No statistical difference between control and DSP-4 treated animals, t-test with Welch's correction for unequal variance. Control n=25, DSP-4 treatment n=5.

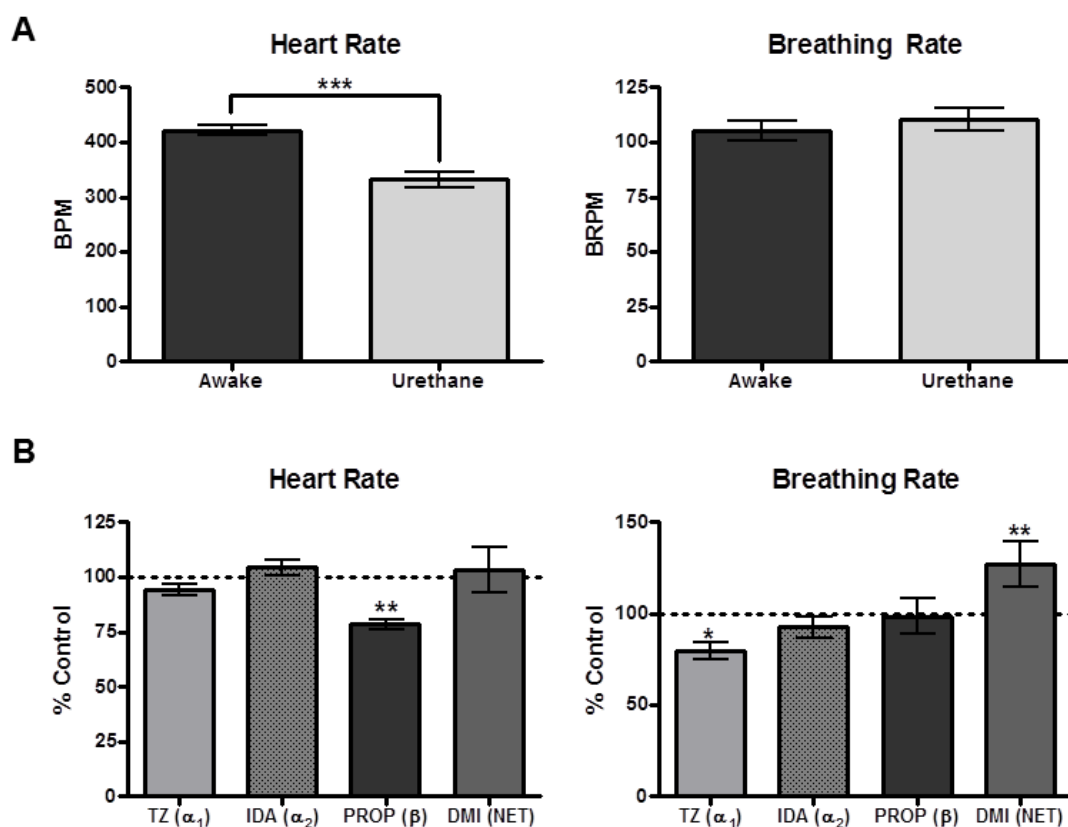


Figure 5.8. Cardiorespiratory responses to anesthesia and adrenoceptor antagonists. (A) Effect of 1.5 g/kg urethane on heart and breathing rate. At this dose, there was a significant reduction in heart rate ($n=16$, $P<0.001$, two-tailed paired student's t -test), but no change in breathing rate. effect on breathing rate. (B) Heart and breathing rates after i.p. administration of terazosin (TZ), idazoxan (IDA), propranolol (PROP) and desipramine (DMI). Significance determine by a Dunnet's post hoc test following a one-way ANOVA, $n=4$ for each. * $P<0.05$, ** $P<0.01$, *** $P<0.001$. BPM: beats per minute, BRPM: breaths per minute

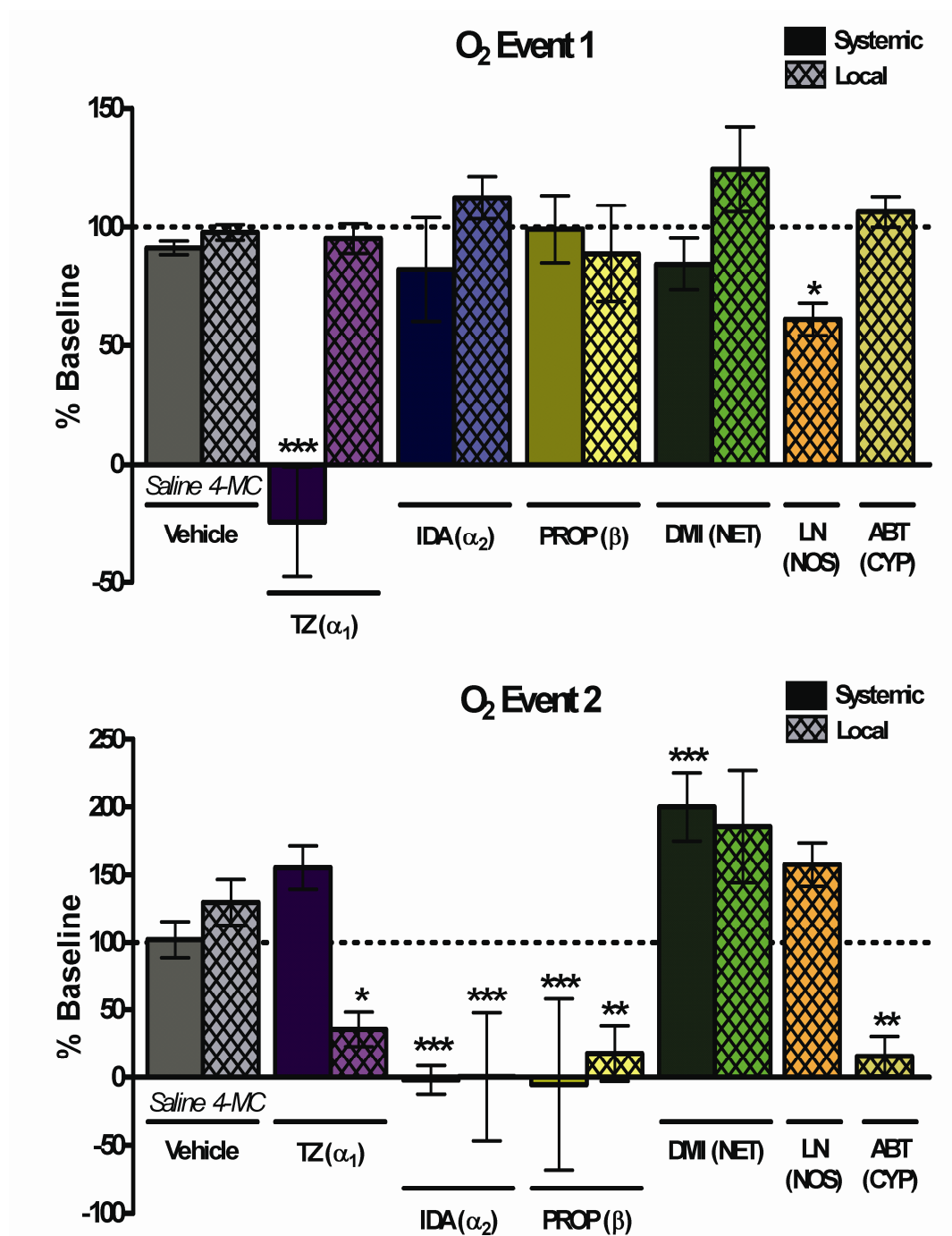
Urethane had no effect on breathing rate but did suppress heart rate. The adrenergic drugs exerted minor effects on these parameters.

Pharmacology of the VNB-stimulated O_2 changes is summarized in Figure 5.9. The average baseline peak amplitudes of event 1 and 2 were taken as 100% and compared to post-drug values. Vehicle treatments (local or systemic) did not affect either event. Event 1 was only affected by systemic administration of terazosin, an α_1 antagonist, and local administration of L-NAME, a nitric oxide synthesis inhibitor. Event 2 was attenuated by local administration of ABT, a cytochrome P450/20-HETE synthesis inhibitor. Interestingly, event 2 was also sensitive to local blockade of all adrenoceptor types, decreasing with administration of terazosin, idazoxan (α_2 antagonist), propranolol (β antagonist). Systemic administration of the adrenergic drugs produced matching results except for terazosin, probably due to its competing effect on event 1. To assess the effect of increasing stimulated norepinephrine release without influencing presynaptic α_2 activity, which controls autoinhibition of release, the norepinephrine transporter blocker desipramine was administered. Desipramine increased the magnitude of event 2, though the effect was only significant with systemic administration. As this result opposes the effects of α_2 inhibition, the effect of idazoxan on the O_2 response is most likely due to post-synaptic actions, not increased norepinephrine overflow.

Local iontophoresis of norepinephrine

To preclude the confounding effects of corelease with electrical stimulation, we used iontophoresis to directly apply norepinephrine at the site of the recording electrode within the vBNST (Fig 5.10). Iontophoresis of 4-methylcatechol, the electroactive marker for the drug solutions, did not produce current changes at the reduction potential for O_2 (Fig 5.10B),

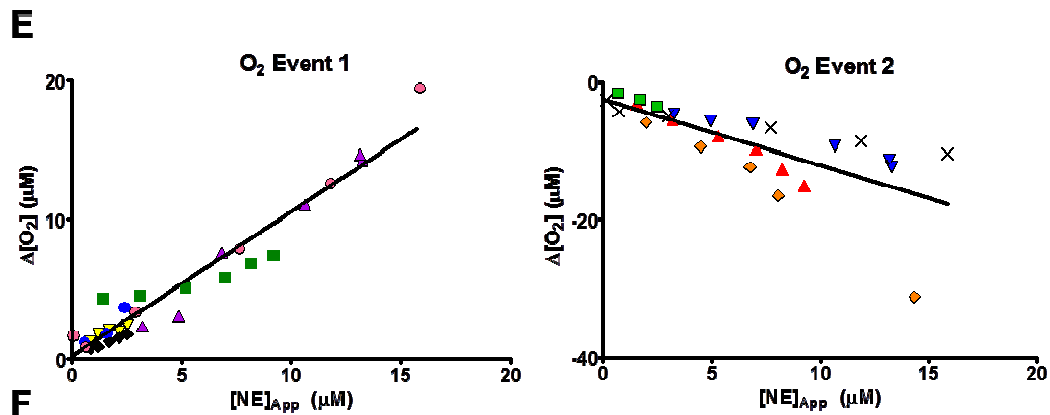
confirming the absence of vehicle effects. Administration of norepinephrine (1 s ejections),



however, induced O₂ fluctuations that mimicked those following VNB stimulation (Fig 5.10C).

Figure 5.9. Pharmacology of the VNB-stimulated O₂ response recorded in the vBNST. The substrate inhibited is indicated underneath the data columns. Systemic drug administration (solid) was

Figure 5.10 O_2 changes induced by direct delivery of norepinephrine with iontophoresis. (A-D) Example responses from a single recording location. Iontophoresis of 4 μM norepinephrine *in vivo* (C) evokes a biphasic O_2 response that is not an artifact of natural activity (A) or vehicle (B; ejection of 4



When this experiment was repeated in brain slice preparations, no O₂ response was observed with iontophoresis of norepinephrine (Fig 5.10D, n = 4 animals, 2 slices from each animal).

Using the carbon-fiber microelectrode to monitor iontophoretic ejections, a range of norepinephrine concentrations (1 s ejections) were delivered at each recording location. Both the increase (event 1) and decrease (event 2) phases of the O₂ response showed dose-dependence to the amount of norepinephrine ejected (Fig 5.10E). Neither event saturated within the range of norepinephrine concentrations assayed (50 nM - 15 μ M). The absolute ratio of event 1 to event 2 (0.81 ± 0.07 , n = 12 animals, 27 concentrations) was lower than for electrical stimulation (4.87 ± 1.52 , n = 25 animals). As with electrical stimulation the peak time of event 1 closely tracked the ejection, while the peak time of event 2 was more delayed with increased norepinephrine output ($t_p = 11.2 - 23.2$ s after ejection, Fig 5.11). There was some variability in the O₂ response between animals. In a few locations (16.7%) only event 1 was evoked, while in others (16.7%) only event 2 was produced.

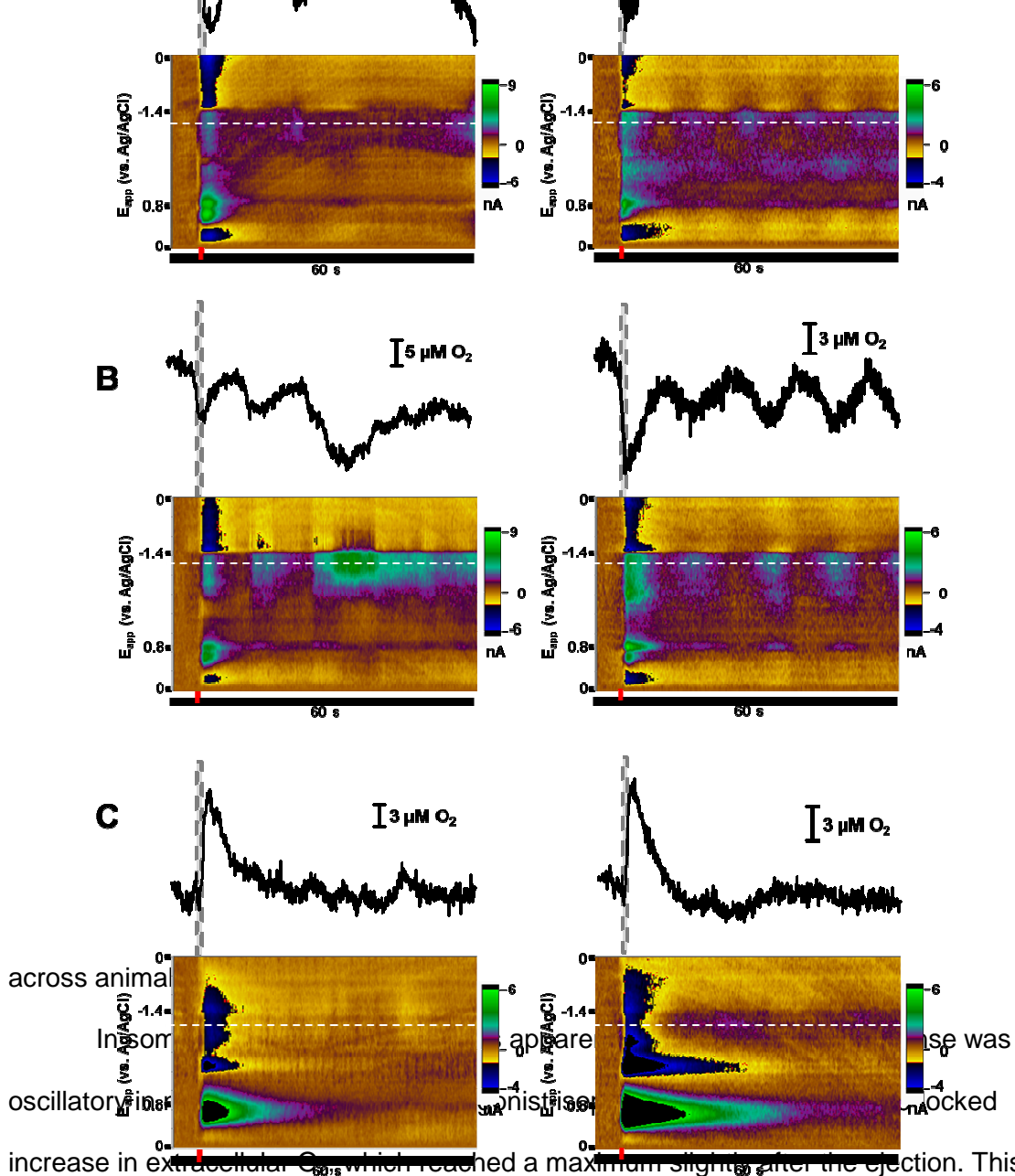
Local response pharmacology was investigated by using the remaining iontophoresis barrels to apply norepinephrine receptor antagonists. Event 1 was sensitive to β receptor antagonism by propranolol ($P < 0.05$, n = 5). Similar to the VNB-stimulated response, Event 2 could be attenuated by inhibition of all receptor types ($P < 0.01$ for terazosin, n = 3, idazoxan, n = 4, and propranolol, n = 5, Fig 5.10F).

Local iontophoresis of selective adrenoceptor agonists

Methoxamine (α_1 agonist), clonidine (α_2 agonist) and isoproterenol (β agonist) were delivered iontophoretically (1s ejections, 1 - 15 μ M) to assess whether any portion of the O₂ response could be triggered by activation of a single adrenoceptor type. Example responses are provided in Figure 5.12. Agonism of α_1 and α_2 receptors induced transient O₂ decreases (Fig 5.12A-B). The timing and number of these decreases varied from trial-to-trial and

Figure 5.11. Effect of norepinephrine concentration applied by iontophoresis (NE_{app}) on the peak time (t_p) for the second O_2 event. The minima for event 2 became more delayed with greater norepinephrine concentrations ($n=5$, slope = 0.50 ± 0.10 s/ μ M norepinephrine, $r^2 = 0.54$).

Figure 5.12. O_2 changes induced by local delivery of adrenoceptor agonists with iontophoresis. Example responses to methoxamine (α_1 agonist, panel A), clonidine (α_2 agonist, panel B), and isoproterenol (non-selective β agonist, panel C) are shown for different recording locations. The recording potential for O_2 is indicated by the white dashed lines. Ejection times (1 s in duration) are denoted by the gray opening bars and the red bars.



increase in extracellular O_2 , which reached a maximum slightly after the ejection. This response was found in all vBNST locations assayed (Fig 5.12C). In many animals (63.6%) the O_2 increase was again followed by a transient decrease event (Fig 15.2C, right).

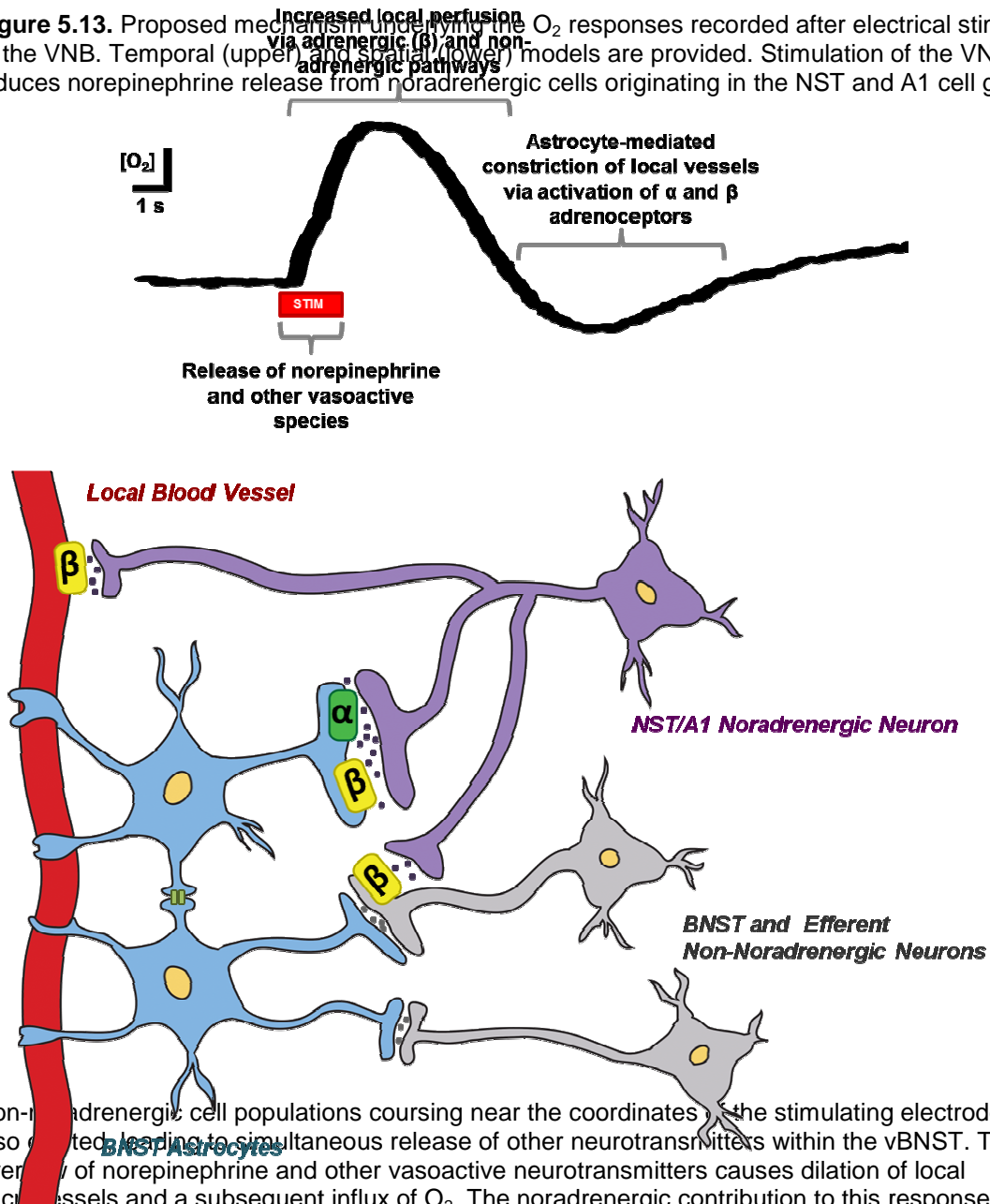
Compared to the responses observed after iontophoresis of norepinephrine, the absolute

ratio of event 1 to event 2 was much larger for isoproterenol (5.40 ± 0.87 , $n = 11$ animals, 22 concentrations).

Discussion

A vast collection of literature supports a role for noradrenergic neurotransmission in functional hyperemia (Raichle *et al.*, 1975; Bekar *et al.*, 2012). The simultaneous detection of norepinephrine and O_2 with high temporal resolution permitted us to directly probe local noradrenergic mechanisms. Moreover, the micrometer dimensions of the carbon-fiber electrode allowed us to target the vBNST, a deep brain region innervated by non-coerulean norepinephrine neurons. We found both electrically evoked and iontophoretically applied norepinephrine induced similar O_2 responses in this region. Norepinephrine was found to play opposing roles in these responses. The initial O_2 increase involved a β component, but principally originated from release of other substances including NO. At later times synergistic activation of α and β adrenoceptors induced an O_2 decrease. These results reveal the complex control of O_2 levels by norepinephrine in the vBNST that originates from the multicellular locations of its receptors and their modulation of other chemical messengers (Fig. 5.13). In a slice preparation, where blood flow is absent but metabolic activity can be evoked thereby increasing O_2 consumption, electrical stimulation caused prolonged O_2 decreases. O_2 changes were not detectable after iontophoresis of

Figure 5.13. Proposed mechanism underlying the O_2 responses recorded after electrical stimulation of the VNB. Temporal (upper) and spatial (lower) models are provided. Stimulation of the VNB induces norepinephrine release from noradrenergic cells originating in the NST and A1 cell groups.



Non-noradrenergic cell populations coursing near the coordinates of the stimulating electrode are also excited, leading to simultaneous release of other neurotransmitters within the vBNST. This overflow of norepinephrine and other vasoactive neurotransmitters causes dilation of local microvessels and a subsequent influx of O_2 . The noradrenergic contribution to this response is mediated through activation of β adrenoceptors either indirectly, by modulating local cell activity, or directly, by relaxation of vascular smooth muscle. Local O_2 concentrations continue to rise shortly after the stimulation ceases. Thereafter, a signaling cascade initiated by the synergistic activation of adrenoceptors on astrocytes results in the release of secondary messengers from astrocytic endfeet. These messengers act upon vessels to cause their constriction, and in turn, provide an active termination of the hyperemic response. As a result, O_2 levels transiently decrease before returning to baseline concentrations.

norepinephrine in slices. These results support a hyperemic origin of the *in vivo* O_2 responses.

The vasoactions of central norepinephrine are usually attributed to LC neurons (Raichle *et al.*, 1975; Kalaria *et al.*, 1989; Cohen *et al.*, 1997; Bekar *et al.*, 2012; Toussay *et al.*, 2013). In our preparation, the placement of the stimulating electrode activates other noradrenergic neurons, including the NST and A1 cell groups. However, electrical stimulations are non-specific, and may result in off-target depolarizations. Since the vBNST receives a small percentage of its noradrenergic innervation from the LC (McNaughton & Mason, 1980), and electrical stimulation of the LC elicits release (Park *et al.*, 2009), we needed to assess coerulean influence on O₂ dynamics in the vBNST. To achieve this, we lesioned LC fibers with a selective neurotoxin. Electrically evoked O₂ responses were unchanged after LC lesioning, suggesting the noradrenergic contribution arose from the NST and A1 innervation, and not indirect LC stimulation. As DSP-4 does affect hemodynamics in cortical regions (Bekar *et al.*, 2012; Toussay *et al.*, 2013), it is unlikely that our results are skewed by compensatory mechanisms that evolved between administration of the neurotoxin and the recordings. To our knowledge, this data is the first to implicate norepinephrine release from these medullary cell populations in functional hyperemia.

Variation in O₂ fluctuations was witnessed across animals, which was likely due in part to the ability of our sensor to capture neurovascular heterogeneity that exists at sub-millimeter scales within the vBNST. However, in the majority of animals, electrical stimulation evoked an O₂ increase, which closely resembled the temporal dynamics of norepinephrine release and uptake, followed by an O₂ decrease. We observed similar effects following iontophoretic application of norepinephrine, affirming that norepinephrine's effects were mediated in the local terminal field and not by activity in other brain regions. In both stimulation and iontophoresis paradigms the magnitude of each O₂ event increased with the norepinephrine output, but did not saturate within the concentration ranges assayed.

Taken together these data support the notion that norepinephrine release affects a vascular area proportional to presynaptic activity, consistent with restricted volume neurotransmission.

Adrenoceptors are expressed in neurons, astrocytes, endothelial cells, pericytes and smooth muscle (Elfont *et al.*, 1989; Hertz *et al.*, 2010)—the major constituents of the neurovascular system. Indeed, 8% of noradrenergic terminals in the cortex are located in the perivascular space, and are not proximal to neuronal targets (Cohen *et al.*, 1997). Through receptor activation, norepinephrine likely influences the concerted actions of these components to support metabolic needs. The data here demonstrate that each event of the O₂ response had distinct signaling pathways. In the vBNST we found event 1 to be partially dependent on local β receptor activity. When evoked by direct application of norepinephrine, event 1 could be blocked by the non-selective β antagonist, propranolol, and was reproduced by the β agonist, isoproterenol. This pharmacology is consistent with the well-documented dilatory effect of β receptors on vascular smooth muscle. As β receptors are expressed on rat cerebral microvessels (Kobayashi *et al.*, 1981), a transient surge of norepinephrine in the vBNST may directly induce local vasodilation, thereby increasing the inflow of O₂-rich blood and giving rise to event 1. Indirect mechanisms cannot be discounted, however. Stimulation of β receptors in this region may influence local cell activity and, in turn, the release of vasodilators dependent on this activity. A study by Winder and coworkers found β pharmacology to have no effect on glutamatergic transmission in the vBNST (Egli *et al.*, 2004). Therefore, if event 1 is produced by an indirect noradrenergic mechanism it is unlikely due to the alteration of glutamatergic activity.

In apparent contradiction, electrically evoked O₂ changes only responded to peripheral blockade of α_1 receptors. Adrenergic α_1 receptors are known to constrict superficial cerebral arteries and arterioles in the rat (Bekar *et al.*, 2012), and their dilation may blunt the redirection of blood flow to the BNST. Consistent with a remote location of α_1 modulation, Event 1 was not produced or inhibited by local application of α_1 pharmacology.

While iontophoresis of the β agonist produced an O_2 increase, its contribution to Event 1 appears to be masked when evoked through electrical stimulation. This is likely due to the actions of co-released neuromodulators initiated by non-selective neuronal activation. VNB stimulation also depolarizes neurons in the ventral tegmental area/ substantia nigra that could release vasodilators such as acetylcholine (Venton *et al.*, 2003), which cannot be detected by our technique. Consistent with this view, we found that event 1 could be attenuated by inhibiting the synthesis of NO locally in the vBNST.

During the second O_2 event, concentrations transiently decreased below baseline levels. This observed decrease required local activation of both α and β adrenoceptors. Though it is not possible to comment on their relative contributions, inhibition of each adrenoceptor attenuated the decrease. Interestingly when selective agonists were applied, only activation of β receptors with isoproterenol produced a time-locked response that resembled event 2. In contrast, iontophoresis of the α agonists methoxamine and clonidine was followed by O_2 decrease events. It is possible that α_1 and α_2 receptors, which have higher affinity than β types, are partially occupied by tonic concentrations within the norepinephrine-rich vBNST. Baseline α activity therefore may be enough to permit the O_2 response when low affinity β receptors are stimulated. As expected in this scenario, the ratio of event 1 to 2 is much larger for isoproterenol in comparison to norepinephrine, which binds to both α and β receptor types.

Though reported less frequently, cerebral O_2 decreases have been cited in the literature (Wade, 2002). For a healthy organism, it is unlikely that these occurrences are due to an imbalance of metabolic demand. More accepted are the theories that O_2 decreases arise from reduced blood flow due to either 'vascular steal' from other activated brain regions or local neuronal inactivation. The timing and pharmacology of event 2 in our study supports the possibility of a constriction-mediated termination of the initial O_2 increase, a function that has been associated with noradrenergic signaling in the somatosensory cortex

(Bekar *et al.*, 2012). Norepinephrine-mediated constrictions are canonically produced by vascular α adrenoceptor activation. However, the β sensitivity of event 2 and the temporal delay of its onset following norepinephrine clearance indicate that the O_2 decrease arises from noradrenergic activation of other chemical messengers that subsequently act at the vascular wall.

Astrocytes present a potential intermediary. These glial cells express all adrenoceptor types and are well-documented to respond to norepinephrine (Stone & Ariano, 1989; Hertz *et al.*, 2010). Of its many effects, noradrenergic stimulation is reported to induce intracellular Ca^{2+} waves, which can propagate over entire astrocyte populations. One study demonstrated that norepinephrine-evoked Ca^{2+} events are followed by constriction of nearby vessels, theorized to be due to generation of 20-HETE (Mulligan & MacVicar, 2004). In agreement with their observations, the magnitude of event 2 was reduced with ABT, which blocks formation of 20-HETE through inhibition of cytochrome P450. Additionally, we observed transient decreases in O_2 with α adrenoceptor activation that were often oscillatory in nature, much like astrocyte Ca^{2+} fluctuations. Supporting the additional involvement of β signaling in event 2, both α and β receptors can stimulate astrocyte Ca^{2+} responses *in vivo* (Bekar *et al.*, 2008) (Ding *et al.*, 2013), and synergistic activation of these receptors potentiates Ca^{2+} responses *in vitro* (Espallergues *et al.*, 2007). While it is not possible to dismiss indirect vascular effects through altered neuronal activity (Egli *et al.*, 2004), the reported effects of norepinephrine on astrocytes are overall consistent with the temporal and pharmacological characteristics of event 2.

Conclusions

In summary, we have established a role for brainstem norepinephrine neurons in the control of extracellular O_2 in a terminal region. When activated, these cells increased norepinephrine overflow in the vBNST, locally triggering a biphasic O_2 response. This

response was absent in a preparation that lacked CBF and had distinct receptor mechanisms. The initial increase involved a small β receptor component and was also due to NO formation. The subsequent decrease was induced by the synergistic actions of α and β receptor types. The delayed temporal characteristics of this decrease indicate that adrenergic activation induced a chemical cascade resulting in the formation of 20-HETE, a known vasoconstrictor. Oscillatory O_2 responses to selective agonists suggest astrocytes may mediate this cascade. These data support the view that norepinephrine is one of many substances that can match energy demands and supply in the brain.

REFERENCES

- Alexander, G.M., Grothusen, J.R., Gordon, S.W. & Schwartzman, R.J. (1997) Intracerebral microdialysis study of glutamate reuptake in awake, behaving rats. *Brain Res*, 766, 1-10.
- Aoki, C., Venkatesan, C., Go, C.G., Forman, R. & Kurose, H. (1998) Cellular and subcellular sites for noradrenergic action in the monkey dorsolateral prefrontal cortex as revealed by the immunocytochemical localization of noradrenergic receptors and axons. *Cereb Cortex*, 8, 269-277.
- Baker, W.B., Sun, Z., Hiraki, T., Putt, M.E., Durduran, T., Reivich, M., Yodh, A.G. & Greenberg, J.H. (2013) Neurovascular coupling varies with level of global cerebral ischemia in a rat model. *J Cereb Blood Flow Metab*, 33, 97-105.
- Bekar, L.K., He, W. & Nedergaard, M. (2008) Locus coeruleus alpha-adrenergic-mediated activation of cortical astrocytes in vivo. *Cereb Cortex*, 18, 2789-2795.
- Bekar, L.K., Wei, H.S. & Nedergaard, M. (2012) The locus coeruleus-norepinephrine network optimizes coupling of cerebral blood volume with oxygen demand. *J Cereb Blood Flow Metab*, 32, 2135-2145.
- Bell, R.D. & Zlokovic, B.V. (2009) Neurovascular mechanisms and blood-brain barrier disorder in Alzheimer's disease. *Acta Neuropathol*, 118, 103-113.
- Bucher, E.S., Brooks, K., Verber, M.D., Keithley, R.B., Owesson-White, C., Carroll, S., Takmakov, P., McKinney, C.J. & Wightman, R.M. (2013) Flexible software platform for fast-scan cyclic voltammetry data acquisition and analysis. *Anal Chem*, 85, 10344-10353.
- Cahill, P.S., Walker, Q.D., Finnegan, J.M., Mickelson, G.E., Travis, E.R. & Wightman, R.M. (1996) Microelectrodes for the measurement of catecholamines in biological systems. *Anal Chem*, 68, 3180-3186.
- Cauli, B. & Hamel, E. (2010) Revisiting the role of neurons in neurovascular coupling. *Front Neuroenergetics*, 2, 9.
- Cohen, Z., Molinatti, G. & Hamel, E. (1997) Astroglial and vascular interactions of noradrenaline terminals in the rat cerebral cortex. *J Cereb Blood Flow Metab*, 17, 894-904.
- Ding, F., O'Donnell, J., Thrane, A.S., Zeppenfeld, D., Kang, H., Xie, L., Wang, F. & Nedergaard, M. (2013) α 1-Adrenergic receptors mediate coordinated Ca²⁺ signaling of cortical astrocytes in awake, behaving mice. *Cell Calcium*, 54, 387-394.

- Drolet, G. (ed) (2009) *Progress in Neuro-Psychopharmacology & Biological Psychiatry* Elsevier, Inc., Amsterdam.
- Egli, R.E., Kash, T.L., Choo, K., Savchenko, V., Matthews, R.T., Blakely, R.D. & Winder, D.G. (2004) Norepinephrine Modulates Glutamatergic Transmission in the Bed Nucleus of the Stria Terminalis. *Neuropsychopharmacology*, 30, 657-668.
- Elfont, R.M., Sundaresan, P.R. & Sladek, C.D. (1989) Adrenergic receptors on cerebral microvessels: pericyte contribution. *American Journal of Physiology - Regulatory, Integrative and Comparative Physiology*, 256, R224-R230.
- Espallergues, J., Solovieva, O., Técher, V., Bauer, K., Alonso, G., Vincent, A. & Hussy, N. (2007) Synergistic activation of astrocytes by ATP and norepinephrine in the rat supraoptic nucleus. *Neuroscience*, 148, 712-723.
- Forray, M.I. & Gysling, K. (2004) Role of noradrenergic projections to the bed nucleus of the stria terminalis in the regulation of the hypothalamic-pituitary-adrenal axis. *Brain Res Brain Res Rev*, 47, 145-160.
- Fritschy, J.M. & Grzanna, R. (1989) Immunohistochemical analysis of the neurotoxic effects of DSP-4 identifies two populations of noradrenergic axon terminals. *Neuroscience*, 30, 181-197.
- Gibbs, M.E., Hutchinson, D. & Hertz, L. (2008) Astrocytic involvement in learning and memory consolidation. *Neurosci Biobehav Rev*, 32, 927-944.
- Goadsby, P.J. & Duckworth, J.W. (1989) Low frequency stimulation of the locus coeruleus reduces regional cerebral blood flow in the spinalized cat. *Brain Res*, 476, 71-77.
- Hartig, W., Reichenbach, A., Voigt, C., Boltze, J., Bulavina, L., Schuhmann, M.U., Seeger, J., Schusser, G.F., Freytag, C. & Grosche, J. (2009) Triple fluorescence labelling of neuronal, glial and vascular markers revealing pathological alterations in various animal models. *J Chem Neuroanat*, 37, 128-138.
- Heien, M.L., Phillips, P.E., Stuber, G.D., Seipel, A.T. & Wightman, R.M. (2003) Overoxidation of carbon-fiber microelectrodes enhances dopamine adsorption and increases sensitivity. *Analyst*, 128, 1413-1419.
- Herr, N.R., Kile, B.M., Carelli, R.M. & Wightman, R.M. (2008) Electroosmotic flow and its contribution to iontophoretic delivery. *Anal Chem*, 80, 8635-8641.

- Hertz, L., Lovatt, D., Goldman, S.A. & Nedergaard, M. (2010) Adrenoceptors in brain: Cellular gene expression and effects on astrocytic metabolism and $[Ca^{2+}]_i$. *Neurochemistry International*, 57, 411-420.
- Kalaria, R.N., Stockmeier, C.A. & Harik, S.I. (1989) Brain microvessels are innervated by locus ceruleus noradrenergic neurons. *Neurosci Lett*, 97, 203-208.
- Keithley, R.B., Heien, M.L. & Wightman, R.M. (2009) Multivariate concentration determination using principal component regression with residual analysis. *Trends Analyt Chem*, 28, 1127-1136.
- Kilts, C.D. & Anderson, C.M. (1986) The simultaneous quantification of dopamine, norepinephrine and epinephrine in micropunched rat brain nuclei by on-line trace enrichment HPLC with electrochemical detection: Distribution of catecholamines in the limbic system. *Neurochem Int*, 9, 437-445.
- Kobayashi, H., Maoret, T., Ferrante, M., Spano, P. & Trabucchi, M. (1981) Subtypes of β -adrenergic receptors in rat cerebral microvessels. *Brain Research*, 220, 194-198.
- Latsari, M., Dori, I., Antonopoulos, J., Chiotelli, M. & Dinopoulos, A. (2002) Noradrenergic innervation of the developing and mature visual and motor cortex of the rat brain: a light and electron microscopic immunocytochemical analysis. *J Comp Neurol*, 445, 145-158.
- Maeda, M., Duelli, R., Schrock, H. & Kuschinsky, W. (1998) Autoradiographic determination of local cerebral blood flow and local cerebral glucose utilization during chemical stimulation of the nucleus tractus solitarii of anesthetized rats. *J Auton Nerv Syst*, 69, 132-140.
- McNaughton, N. & Mason, S.T. (1980) The neuropsychology and neuropharmacology of the dorsal ascending noradrenergic bundle--a review. *Prog Neurobiol*, 14, 157-219.
- Mulligan, S.J. & MacVicar, B.A. (2004) Calcium transients in astrocyte endfeet cause cerebrovascular constrictions. *Nature*, 431, 195-199.
- Muyderman, H., Hansson, E. & Nilsson, M. (1997) Adrenoceptor-induced changes of intracellular K^+ and Ca^{2+} in astrocytes and neurons in rat cortical primary cultures. *Neuroscience Letters*, 238, 33-36.
- Obel, L.F., Andersen, K.M., Bak, L.K., Schousboe, A. & Waagepetersen, H.S. (2012) Effects of adrenergic agents on intracellular Ca^{2+} homeostasis and metabolism of glucose in astrocytes with an emphasis on pyruvate carboxylation, oxidative decarboxylation

- and recycling: implications for glutamate neurotransmission and excitotoxicity. *Neurotox Res*, 21, 405-417.
- Park, J., Kile, B.M. & Wightman, R.M. (2009) In vivo voltammetric monitoring of norepinephrine release in the rat ventral bed nucleus of the stria terminalis and anteroventral thalamic nucleus. *Eur J Neurosci*, 30, 2121-2133.
- Park, J., Takmakov, P. & Wightman, R.M. (2011) In vivo comparison of norepinephrine and dopamine release in rat brain by simultaneous measurements with fast-scan cyclic voltammetry. *J Neurochem*, 119, 932-944.
- Raichle, M.E., Hartman, B.K., Eichling, J.O. & Sharpe, L.G. (1975) Central noradrenergic regulation of cerebral blood flow and vascular permeability. *Proc Natl Acad Sci U S A*, 72, 3726-3730.
- Stone, E.A. & Ariano, M.A. (1989) Are glial cells targets of the central noradrenergic system? A review of the evidence. *Brain Res Brain Res Rev*, 14, 297-309.
- Swanson, L.W., Connelly, M.A. & Hartman, B.K. (1977) Ultrastructural evidence for central monoaminergic innervation of blood vessels in the paraventricular nucleus of the hypothalamus. *Brain Res*, 136, 166-173.
- Takmakov, P., Zachek, M.K., Keithley, R.B., Bucher, E.S., McCarty, G.S. & Wightman, R.M. (2010) Characterization of local pH changes in brain using fast-scan cyclic voltammetry with carbon microelectrodes. *Anal Chem*, 82, 9892-9900.
- Toussay, X., Basu, K., Lacoste, B. & Hamel, E. (2013) Locus coeruleus stimulation recruits a broad cortical neuronal network and increases cortical perfusion. *J Neurosci*, 33, 3390-3401.
- Venton, B.J., Michael, D.J. & Wightman, R.M. (2003) Correlation of local changes in extracellular oxygen and pH that accompany dopaminergic terminal activity in the rat caudate-putamen. *J Neurochem*, 84, 373-381.
- Wade, A.R. (2002) The negative BOLD signal unmasked. *Neuron*, 36, 993-995.

CHAPTER 6: FLEXIBLE SOFTWARE PLATFORM FOR FAST-SCAN CYCLIC VOLTAMMETRY DATA ACQUISITION AND ANALYSIS

Introduction

Electrochemistry is widely employed for the detection of neurotransmitters at single biological cells, in brain slices, and *in vivo* (Robinson *et al.*, 2008). The original impetus for the development of *in vivo* measurements of neurotransmitters was the detection of dopamine (Adams, 1976; Millar *et al.*, 1985). Today, however, this approach is used not only for the detection of catecholamines but also for compounds as diverse as adenosine (Swamy & Venton, 2007), oxygen (Venton *et al.*, 2003), histamine, and 5-hydroxytryptamine (Hashemi *et al.*, 2011). Although several voltammetric techniques have been evaluated for *in vivo* use, fast-scan cyclic voltammetry (FSCV) is particularly useful because it combines high sensitivity (nanomolar range) with sufficient features to identify the substances detected. To follow the rapid concentration fluctuations of neurotransmitters, cyclic voltammograms are generated at high scan rates (>100 V/s), allowing data collection on the millisecond time scale. At these high rates, very large background currents are generated. This charging current can be removed by analog or digital background subtraction, yielding cyclic voltammograms of the analytes of interest (Hermans *et al.*, 2008).

The rapid scan rates and the large number of data points that are collected both require a computer for waveform generation and data acquisition. Typically, at least 10 cyclic voltammograms (CVs) are recorded per second with each containing 1000 scanned potentials within the voltammetric sweep. Furthermore, multiple electrodes can also be

used, and the electrochemical experiments may be combined with other electrical measurements (ionselective electrodes, amperometry, electrophysiology, etc.) (Armstrong-James *et al.*, 1980; Venton *et al.*, 2003; Zachek *et al.*, 2009). Multifunctional data acquisition systems from several vendors that include analog and digital inputs and outputs and clocks are readily available and allow such measurements. Thus, electrochemical instrumentation has advanced considerably from 1983 when one of the first commercially available computer controlled potentiostats, the BAS 100, was introduced (He *et al.*, 1982). Our own lab (Michael *et al.*, 1999), as well as others (Yorgason *et al.*, 2011), have generated a series of programs for neurotransmitter measurements as documented elsewhere (Michael & Wightman, 1999).

Here we describe some of the features of our HDCV ('High Definition Cyclic Voltammetry'), our latest software package for high speed acquisition and analysis of electrochemical data. HDCV serves as an upgrade and replacement for TarHeelCV, the previous program distributed by our group for FSCV data acquisition and analysis (Robinson & Wightman, 2007). These new programs incorporate features that were not previously present. The data acquisition program enables simultaneous collection from up to 16 electrodes, allowing use with arrays (Zachek *et al.*, 2010). Multiple waveforms, optimized for each analyte, can be used simultaneously, and the waveforms can have any shape. Data is digitally background subtracted and displayed in real time as it is collected. The program allows concurrent electrochemical and electrophysiological recording at a single electrode. In the electrophysiological recordings, the firing of individual neurons is measured in the form of single units. Importantly, it allows continuous data collection for several hours. Moreover, the program is compatible with behavioral experiments in which items such as levers, tone generators, or other binary output devices, can be connected to digital input signal lines and user-mapped into the data flow. All of the analog and digital data are clocked in lockstep with a common hardware clock. The data analysis program streamlines

the analysis of large amounts of data, facilitates signal-averaging of events marked by the digital signals, performs current artifact removal, and provides digital filtering. Principal component regression is incorporated to extract signals of specific analytes. In this manuscript we illustrate several of these capabilities with examples from ongoing experiments.

Experimental

Hardware

All events configured through HDCV employ a single PCIe-6363 X-series data acquisition card (National Instruments, Austin, TX) rather than the three required with TarheelCV. (It is expected that future versions of HDCV will allow the use of USB-connected DAQ hardware.) A custom-built breakout box (UNC Department of Chemistry Electronics Design Facility) provides access to 4 analog outputs, 16 differential analog inputs, and 40 digital I/O lines. For single electrode experiments, the maximum sampling rate is 2 MHz. For multiple electrodes, the acquisition card's single instrumentation amplifier limits the maximum sampling rate to 1 MHz divided by the number of channels. Another digital line (Port2/Line 0) gates output signals through the breakout box. This line is held high when HDCV is initialized. Signal routing is otherwise fully configurable through the acquisition program.

Software

The HDCV electrochemical software suite was written in LabVIEW (National Instruments, Austin, TX). HDCV consists of two independent executable programs for data acquisition and analysis.

HDCV data acquisition

HDCV Data Acquisition controls the hardware, while also collecting and displaying data in real-time. Low-level hardware control is achieved through an interface that allows the selection of a device and the assignment of its analog and digital lines to specific functions in the software. The interface allows the user to customize analog and digital input/output (I/O) parameters, adjust analog input gain settings, and assign names to the I/O lines. Analog and digital lines are synchronized via a signal generated by the DAQ hardware clock. The timing of this clocking signal is defined by the CV frequency.

Analog outputs can be assigned to one of three functions: waveform generation, electrical stimulation, or analog background subtraction. For waveform generation, the shape of the applied voltage can be designed from preset options (triangle, sine, square and sawtooth), designed arbitrarily by piecewise mathematical construction, or loaded from a text file. Additional inputs provide control over the voltage limits, scan-rate, application frequency and sampling rate. Stimulation trains are defined by pulse duration, polarity (mono and biphasic), frequency, and number. The stimulus onset is delayed from the beginning of the voltage waveform by a user-defined time to prevent overlap. These trains can be triggered internally at a user-defined time or externally by a digital input. For analog background subtraction, an inverted voltage proportional to the electrode charging current is output. In a manner similar to noise-cancelling headphones, this signal is applied to the inverting input of the headstage amplifier decreasing the amount of background recorded. This prevents saturation of the headstage amplifier and allows the data acquisition card voltage range to be reduced to decrease quantization noise (Hermans *et al.*, 2008).

Bidirectional digital lines are used to control and monitor binary output external devices. Two digital lines are reserved to output the CV frequency signal and the timing signal for electrochemistry/electrophysiology experiments so that other instruments can be synchronized with HDCV. Other digital outputs can be set to change state once per file or

once per waveform application. Other ports can be specified as digital inputs, which the program will record.

Data are collected and saved as files in single run, multiple run, or continuous modes. Single run mode is designed for short duration (seconds to several minutes) collection periods. Multiple run mode allows automatic collection of multiple experiments (separated by a specified rest time) that are saved in one file. Continuous mode allows for minutes to hours of data acquisition and is designed for recordings during behavioral experiments.

Acquired data are stored in two files. The main file, with a .hdcv extension, contains a header with the operating parameters and the current values for each cyclic voltammogram. The transition times of digital input lines are recorded in a companion text file with a .dig extension.

HDCV analysis

HDCV Analysis is used for post-processing data (including files generated by TarheelCV). Data are displayed in a color plot with currents at all potentials shown as a function of acquisition time (Michael *et al.*, 1998). Current at each potential is background subtracted from a user-defined time point and is visualized in false color. At a user-selected time and potential, two supporting plots display current versus time and its corresponding cyclic voltammogram. These representations are controlled by the main cursor placement within the color plot. An additional display maps the timing of digital input signals. (For backward compatibility with TarheelCV, the electrochemical and digital data files are concatenated into HDCV format using the Data Converter program included in the executable package).

HDCV analysis offers several digital filtering and smoothing options including a two dimensional Fast Fourier Transform (FFT) algorithm. On-screen deglitching tools allow for

easy removal of undesired electrical artifacts (glitches). If digital inputs are recorded, they serve as time points to clip periods of data into time bins. Such changes are saved in an analysis work file, preserving the original data.

Concentration information can be extracted from files in one of two ways. If the data represent the response of a single analyte, the user may input a calibration factor to convert currents into concentrations. Principal component regression (PCR) is used for more complex *in vivo* experiments (Keithley *et al.*, 2009; 2010). HDCV performs PCR analysis on data based on a user-built training set of CV standards. Concentrations determined by either of these methods can be averaged across multiple files, runs, or time bins.

Experimental setup

Four major components are required for combined electrochemical/electrophysiological (echem/ephys) experiments during behavior (Fig 6.1). These include two computer stations for separate acquisition of echem/ephys data, a custom-built headstage amplifier that interfaces with a universal electrochemical instrument (UEI) mainframe (UNC Department of Chemistry Electronics Shop), and a commercially available operant conditioning system (Med. Associates, Inc., St. Albans, VT). HDCV software controls the voltammetric acquisition parameters, collects current responses, and synchronizes experimental timing through the PCIe-6363 in the electrochemistry computer. The output waveform is reduced to one third to utilize the full DAC bit depth and low-pass filtered to reduce quantization noise before application via a swivel commutator (Med. Associates, Inc.) to the headstage amplifier. Stimulation waveforms are configured within HDCV, converted to current by a pair of optically isolated stimulators (Digitimer Ltd., Letchworth, U.K.) and routed to the headstage. The Med Associates operant conditioning system generates digital time stamps indicating behavioral events such as a lever press. These are delivered to the PCIe-6363 via an 8 bit interface, synchronizing the echem/ephys

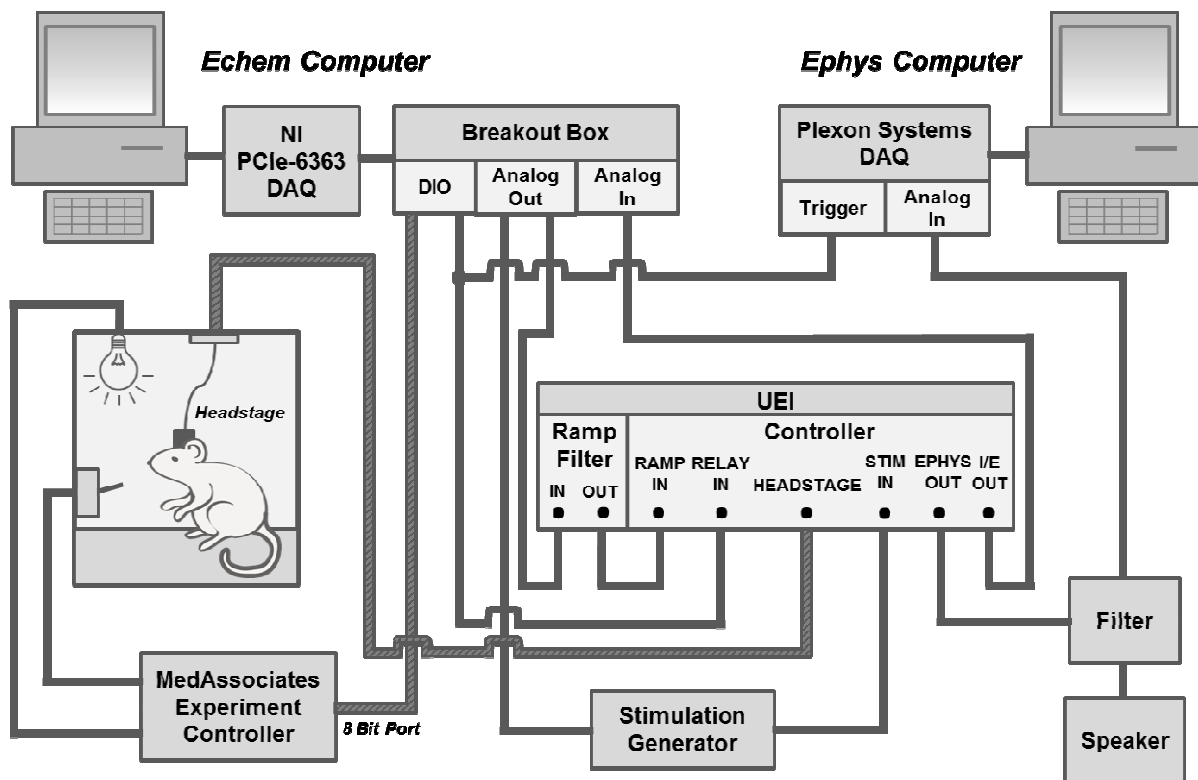


Figure 6.1. Block diagram of hardware for combined electrochemical/electrophysiological (echem/ephys) recordings during behavior. During these experiments an animal in a behavioral chamber responds to the presentation of visual/auditory stimuli and electrical stimulation via an implanted electrode. Signals from the implanted carbon-fiber electrode are recorded. Electrical signals are routed to the headstage through a custom breakout box and control instrumentation (UEI). The echem computer controls the voltammetry parameters, records digital signals generated by the Med Associates Operant Conditioning System, and times the switch between recording modes via a digital relay signal. Stimulation waveforms are converted to current by an optically isolated device. The ephys computer (Plexon) records cell firing. The firing due to cell activity is transduced into an audio signal via an external speaker. DIO: digital input-output port; I/E port: output of current to voltage converter; Stim In: port for electrical stimulation signal.

measurements with behavioral events. In combined echem/ephys experiments, the voltage of the electrode floats between voltammetric recordings to allow recording of electrical activity from nearby cells. This is controlled by a digital output that triggers a CMOS analog switch on a modified headstage (UNC Department of Chemistry Electronics Design Facility) that alternates between a current-to-voltage amplifier for FSCV, and a voltage-follower for single unit recordings, circuitry described previously (Takmakov *et al.*, 2011). Electrophysiology is collected on a computer with *Plexon* Neurosurgery Workstation software (Plexon Inc., Dallas, TX).

Experimental procedures

Experiments shown here are used to illustrate the features of HDCV. The experimental details have been described in detail elsewhere (Owesson-White *et al.*, 2008; Park *et al.*, 2009).

Results and Discussion

Programming techniques

LabVIEW is a programming language optimized for data acquisition and processing. The data acquisition program of HDCV, in particular, involves several interesting coding techniques. The main program is written as four loops operating in parallel. The data acquisition loop has the highest priority, and runs once per CV. The data collected are fed through queues to two separate processing loops that run at lower priority so data acquisition is not delayed. The analog data loop trims away unwanted data points (the interval between voltammograms), maintains real-time graphs, and stores the data to a file. The digital data loop runs only once per transition on any digital input line, and likewise

maintains graphs and stores the data to a second file. The fourth loop, the event loop, handles user interactions.

Timing control

Traditional LabVIEW programming provides a way for an input task to clock an output task so that the two proceed in lockstep, data point by data point. This technique was extended to maintain four tasks in parallel: analog input (the master) clocking analog output, digital input, and digital output. This provides far higher temporal resolution for the digital input lines than TarHeelCV, which sampled them only once per CV scan. It also provided a useful organizing principle for the entire program.

Active/passive configuration routines

HDCV has extensive configuration screens, because numerous parameters for experiment control are provided to the user. Each of these is implemented as a LabVIEW VI (virtual instrument), an interaction screen with associated code. The full process entails: read a configuration file, display its parameters, allow the user to change them, post-process the parameters into a form more useful for program operation, and update the configuration file. In some cases postprocessing reveals errors that could only have been revealed by configuring the hardware. Reading the configuration file and postprocessing its contents needs to be done on every startup whether or not the user intends to make any changes.

To implement this scheme, we used an approach we term Active/Passive routines in which each configuration VI can be called in either mode. In active mode, it opens and waits for the user to change and confirm the settings. In passive mode, it invisibly loads and postprocesses the configuration file. When encountering certain errors that would prevent meaningful operation, it can become active, displaying a message and waiting for the user

to resolve the problem. These VIs are called in active mode when the program is first run, or upon user request.

Setup control structure

The experiment setup VI, in particular, presented interesting problems. It uses an interface with nine tabs, many of which lead to complex, full-screen pages that display many parameters and graphs. Several of these pages have internal states (useful for maintaining graphs) that need to be "unpacked" from the raw parameters when the page is presented, and "packed away" when the page is closed. A natural program structure would be to have a Case structure with a separate case for each page in the user interface, and within each, an Event structure to handle events relevant to that page (an Event structure is a Case-like control structure that waits for a user interface event and then executes the appropriate case when an event takes place).

In HDCV the program structure was designed in the following way. A single Event structure in a loop fields all events for the entire VI. It translates each event type into a textual code. Each event is passed via queue to the main operating loop. The main operating loop consists of a primary Case structure, with a case for each page in the user interface. Within each case is an inner Case structure, with a case for each event relevant to that page. The Event structure takes special action when the user switches tabs, and generates two event codes. The first, "Leaving", is directed to the page that has been open, and allows its code to pack away any data for that page as needed. The second, "Entering", is directed to the page that is being opened, and allows its code to make preparations. This last feature alone was so powerful as to make the entire technique worthwhile. The code organization that resulted from allowing each page to "own" a case in the primary Case structure has proved vastly useful for the understanding and readability of the code.

Data storage

HDCV uses the binary data file format provided by LabVIEW. Data are organized into "chunks", one per run of a Multiple run experiment, one per experiment otherwise. Each chunk is stored as a three-dimensional array, indexed by CV, channel (for multichannel data collection experiments), and data point. Writing the 3-D array after data collection is vulnerable to data loss in case of system failure during long experiments. To avoid this problem, the 3-D array is written into the file piecemeal, one "slice" per CV, as it is collected. Each slice can be viewed as a two-dimensional array, indexed by channel and data point. At the end of the experiment, the number of CVs is plugged into the 3-D array header, completing the file.

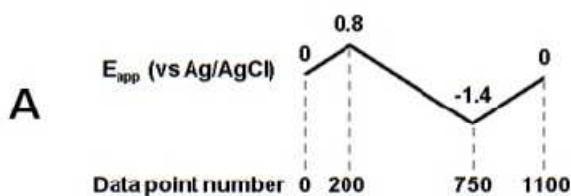
The same technique is used when reading the data for long experiments. No portion of the analysis process could handle all the data for a multiple hour experiment at once without exceeding available memory. The user specifies the time region of interest (up to 5 minutes long), and analysis reads the data only for that time region.

Real-time data analysis and acquisition

The HDCV acquisition program has several live data displays that provide immediate user feedback. These include oscilloscopes for the analog and digital signals, a current-time chart, and a live color chart. These run continuously during waveform application and are active even when data storage is not occurring.

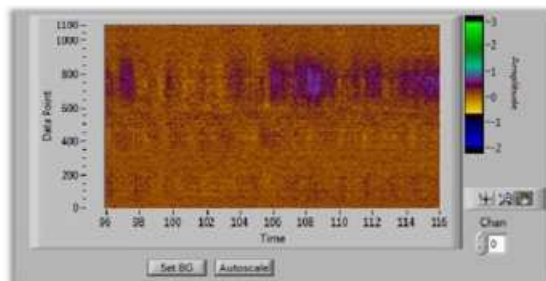
The live color chart is particularly useful since the entire experiment can be viewed with the voltage scan mapped along the ordinate, and the time of CV acquisition shown along the abscissa. Oxidation and reduction currents are shown in a 3: -2 false color scale to enhance peak contrast. (Michael *et al.*, 1998) Hence, the color chart provides both qualitative and quantitative data assessment. The flux of multiple analytes, potential-dependent noise, and electrode stability can be monitored continuously. This type of

Figure 6.2. Results
accumbens of an an
dopamine. (A) Volta
applied at 400 V/s e

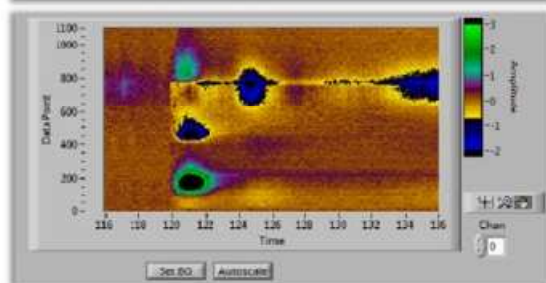


implanted in the nucleus
accumbens of an anesthetized rat.
FSCV studies employ various
waveforms optimized for different
target analytes. This particular
waveform (Fig. 6.2A) allowed
simultaneous dopamine and oxygen
measurements (Venton *et al.*,
2003).

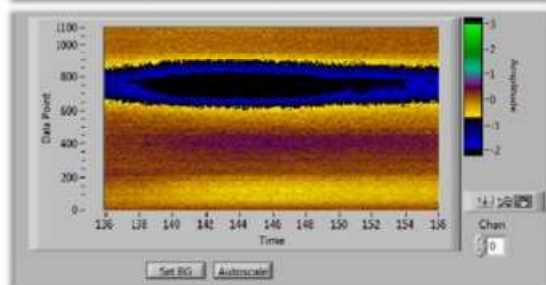
B



C



D



consecutive time intervals
shown on the abscissa. Oxygen
decreases as dopamine is
released (data points 100-120).
next 20 s time window.

ordinate and time (s) is
before the present view. (B)
stimulation evokes dopamine
change continues into the

immediate feedback assists with trouble-shooting and experimental optimization.

To illustrate this feature, Figure 6.2 shows data obtained during acquisition with a carbon-fiber electrode in the nucleus accumbens of an anesthetized rat. FSCV studies employ various waveforms optimized for different target analytes. This particular waveform (Fig. 6.2A) allowed simultaneous dopamine and oxygen measurements (Venton *et al.*, 2003).

During the experiment, the color chart scrolls to the left as each CV is collected. Controls allow the user to choose an input channel, select the most recent CV as the basis for background subtraction, and adjust the color scale. Figure 6.2B-D display screen shots captured during three sequential 20 s periods. In Figure 6.2B (where the waveform is applied but data storage was not initiated) transient decreases in oxygen resulting from natural activity appear as positive currents centered on -1.4 V (data point 750). In the next interval, file collection was initiated and an electrical stimulation occurs (Fig 6.2C). Stimulated dopamine release is evidenced by positive peaks (oxidation) at 0.6 V (data point 160) and negative peaks (reduction) at -0.2 V (data point 450). Uncharacterized extracellular changes induced by the stimulation result in a positive, non-faradaic current artifact at the cathodic switching potential. A biphasic increase in oxygen follows generating negative (reduction) current fluctuations at -1.4 V, which peak at 124 s (Fig 6.2C) and 144 s (Fig 6.2D). In Figure 6.2D, features at 0.2 V (data point 50) and 0 V (data point 400) show a prolonged alkaline pH shift accompanying the oxygen fluctuations. These data enable evaluation of neurotransmitters in the regulation of cerebral blood flow (Venton *et al.*, 2003).

Simultaneous detection of neurotransmitter release and single unit activity

Neuronal communication involves electrical impulses and chemical messengers. The combined echem/ephys technique provides a unique opportunity to study these interdependent processes simultaneously with high spatial and temporal resolution. The combined echem/ephys technique has seen significant advancement since Millar and coworkers initiated its development over thirty years ago (Millar *et al.*, 1981). In the last decade, a miniaturized switching headstage enabled experiments in freely-moving animals (Takmakov *et al.*, 2011), allowing combined echem/ephys measurements for delineating the neuronal circuitry involved in behavior (Cheer *et al.*, 2005; Owesson-White *et al.*, 2009; Cacciapaglia *et al.*, 2011). This technique has been paired to iontophoretic drug delivery

(Armstrong-James *et al.*, 1980) to identify the receptors that locally gate dopamine neurotransmission (Belle *et al.*, 2013).

As described in the Experimental Section, combined echem/ephys experiments are complex and require coordination between several instruments (Fig 6.1). During combined measurements, a digital relay output from the PCIe-6363 triggers a solid-state switch in the headstage that controls acquisition modes. The timing scheme during an experiment with behavioral DIOs is shown in Figure 6.3A. When the digital output from HDCV goes low, the headstage current-to-voltage amplifier circuit connects to the carbon-fiber electrode and the waveform is applied. When the digital output goes high, the current-to-voltage amplifier disconnects and a voltage-follower amplifier connects to the carbon-fiber electrode to measure the spiking activity of proximal neurons. Typically these modes alternate at 5 Hz to allow adequate time to detect single unit activity. HDCV concurrently records any digital inputs, and these time stamps can be used to align data to the appropriate behavioral event.

Figure 6.3B shows an example of simultaneous echem/ephys data collected during intracranial self-stimulation (ICSS) with the waveform scanning from -0.4 V to +1.3 V at 400 V/s for the detection of dopamine (Phillips *et al.*, 2003). ICSS is a paradigm in which an animal depresses a lever to deliver an electrical stimulation to its own brain. With the stimulating electrode implanted in select brain regions, animals find this rewarding. In our design, lever extension into the behavioral chamber is preceded by a tone and light cue

Undesirable current artifacts can occur during the transitions between free-floating and applied potentials. Although the headstage amplifier uses a state-of-the-art CMOS

\

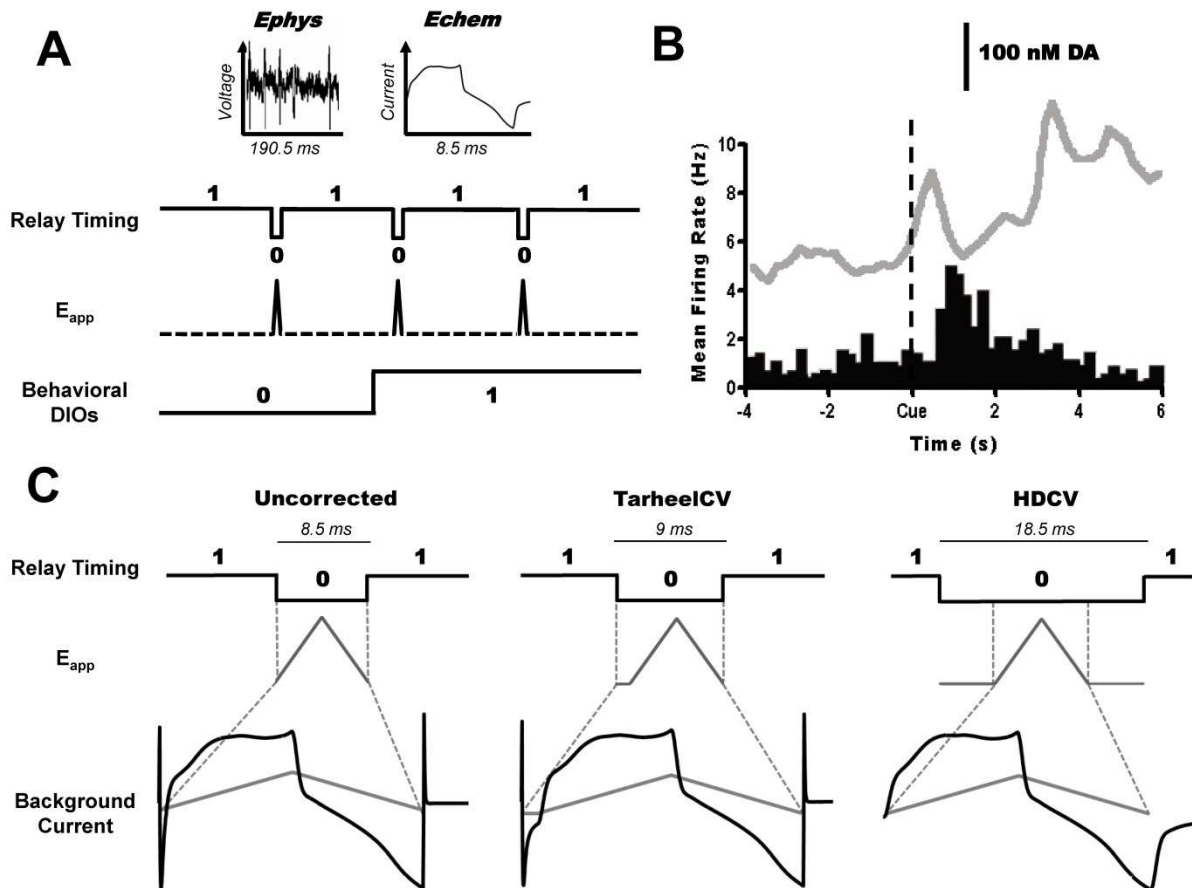


Figure 6.3. Simultaneous electrochemistry/electrophysiology (echem/ephys) measurements. (A) Basic timing diagram during behavioral experiments. The state of the digital relay timing line controls when the potential of the electrodes floats (E_{app} dotted) and the waveform is applied (E_{app} solid). Behavioral events are recorded as digital transitions. (B) Example average ($n = 30$ trials) of dopamine concentration (grey trace) and average single unit firing rate (histogram) during ICSS recorded in the nucleus accumbens of an awake rat. The stimulating electrode in this study was implanted in the dopaminergic neurons of the ventral tegmental area. Data are aligned to the audiovisual cue. (C) Current response during waveform application. Voltage is applied to the electrode when the relay state is low while the recording window, defined by the CV application frequency, is denoted by the grey dashed lines. When the relay is in sync with the CV frequency clock (uncorrected, left) current spikes occur at the beginning and end of the voltage ramp. The CV frequency clock also triggers the relay in TarheelCV (middle), but the recording window is increased to add holding time before the voltage sweep. In HDCV (right) a line distinct from the CV frequency clock is configured to hold low 5 ms before and after the recording window.

(Owesson-White *et al.*, 2008). The data here are aligned to the onset of this cue and reveal that extracellular dopamine and cell firing increase in this location following the cue.

switch between the voltage and current amplifiers, a small amount of charge injection and input capacitance occurs when switching, and artifacts appear in the data (Fig 6.3C, right). In older approaches, this was minimized by adding extra data points preceding the voltage ramp that produced a buffer for current stabilization. Extra data points were then removed during post-collection analysis. In HDCV the change of state of the digital relay line does not

have to be synchronized to the CV frequency clock. This allows for a wider voltage application window without changing the time frame of echem collection. The current artifact occurs at a set time before and after voltammetry acquisition, and no post collection correction is needed during analysis.

Two dimensional data filtering

FSCV is useful for the detection of rapid chemical fluctuations of nanomolar concentrations (Wightman *et al.*, 2007). To resolve these small signals, digital filtering strategies are employed to remove high-frequency noise. Previously, TarheelCV filtered each cyclic voltammogram with a 4th order low-pass Bessel filter (cutoff frequency of 2 kHz for a 400 V/s scan rate) (Wiedemann *et al.*, 1991), an option that is also available in HDCV. For further noise removal, users previously employed an 8-point nearest neighbor smoothing kernel. This filter generates a two-dimensional moving-point average that smooths differences within the CV domain and across consecutive CV scans and can be repeated multiple times. The disadvantages of this nearest-neighbor smoothing kernel are that it executes slowly and that the frequency effects are not intuitive. In contrast, HDCV offers a more rational two-dimensional Fast-Fourier transform (2D-FFT) filter for noise reduction. With a 2D-FFT filter the color plot is transformed into the frequency domain before a filtering

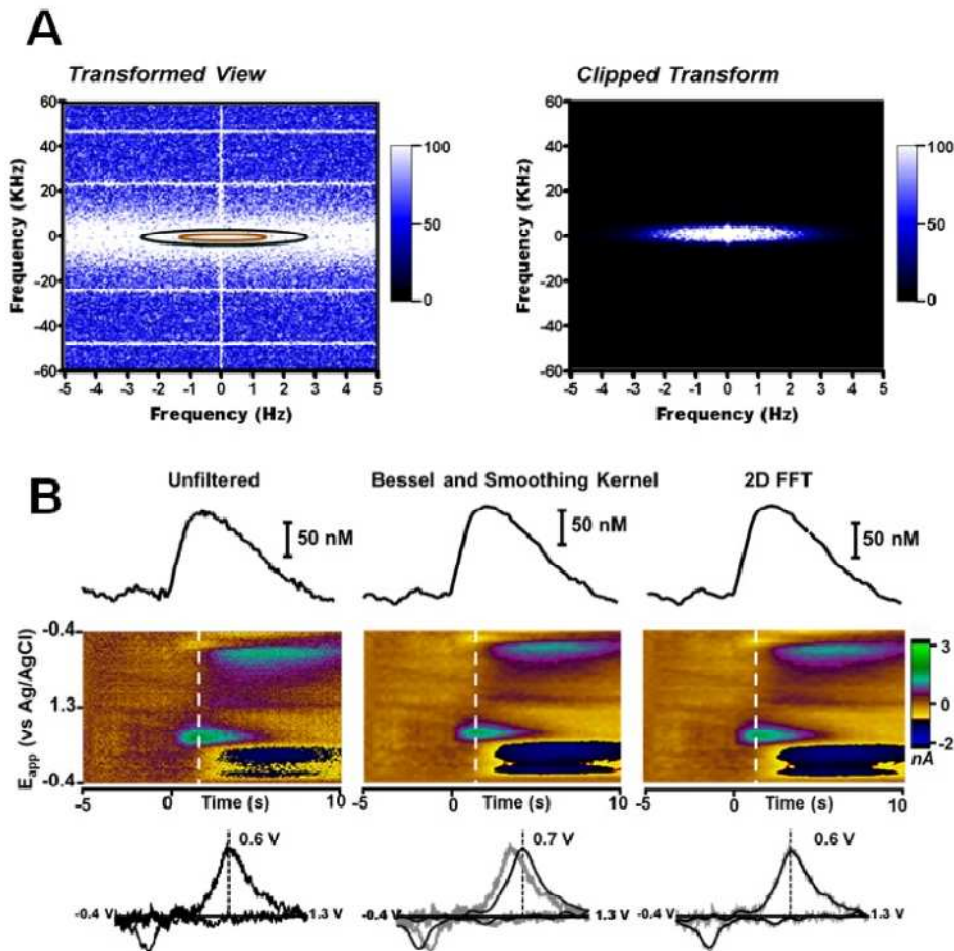


Figure 6.4. Use of the 2D FFT filter in HDCV. (A) Transformed view of the original and filtered (clipped) data. Signal intensity at each frequency is shown for the CV domain (ordinate) and the time domain (abscissa). Both axes are centered at 0 Hz and extend from $-f_s/2$ to $f_s/2$, where f_s is the sampling frequency. The -3 dB and -50 dB cutoffs are shown by the orange and black ellipses respectively. A Bessel roll-off is applied to smooth the transition between the -3 dB point and -50 dB point. Cutoff frequencies (time domain: 1.35 Hz, CV domain: 2 kHz) were chosen to resemble application of a 2 kHz low pass Bessel filter and an 8 point nearest neighbor smoothing kernel. (B) Comparison of filtering methodologies on data taken during *in vivo* norepinephrine release in the bed nucleus of the stria terminalis of an anesthetized rat. Release was evoked by electrical stimulation of the ventral noradrenergic bundle. The original unfiltered data is shown to the right. Stimulation onset is denoted at time 0. Norepinephrine concentration extracted by PCR is shown as a trace above the color plot. The CV below is taken from the time point indicated by the white dotted line. The middle panel shows this data after filtering with the 2 KHz low pass Bessel filter and smoothing kernel. The right panel shows the data after the 2D FFT filter with the parameters shown in part (A).

mask is applied. The retained frequencies are then transformed back into the spatial domain by the inverse Fourier transform. The effects of a low-pass 2D-FFT filter are analogous to a smoothing kernel, removing high frequency-noise components in the CV and time

dimensions. However, the 2D-FFT approach is preferred because it is rapidly calculated while maintaining the temporal resolution in the CV and the CV frequency domains. In the 2D-FFT filtering menu, the transformed signal and noise components of the data are viewed (Fig 6.4A). Cutoff frequencies are defined by an ellipse representing the -3dB point across both domains (inner orange ellipse). The outer ellipse (shown in black) indicates the -50 dB boundaries where increased signal attenuation occurs. The clipped transform displays the intensities of the retained frequencies.

Figure 6.4B shows the results of different filtering methods on data collected during electrically stimulated norepinephrine release in an anesthetized rat. (Park *et al.*, 2009) The original unfiltered data are shown on the left. The oxidation of norepinephrine is visible in the color plot at 0.6 V on the forward scan. An alkaline shift in pH produces the features around -0.2 V on the forward and backward scans. The trace above the color plot represents norepinephrine concentration extracted with PCR and the dotted line in the color plot represents the time of the CV shown below. The middle panels show these data after filtering with a 2 kHz Bessel function in the cyclic voltammetry domain and an 8-point smoothing kernel. Noise is significantly reduced but the oxidation peak potential for norepinephrine is offset by 100 mV. The right panes illustrate the same data after use of the 2D-FFT filter in HDCV. The 2D-FFT filter removes noise similarly, while retaining the peak position of the CV.

Analysis of continuous data

FSCV is well suited to capture subsecond changes in neurotransmitter concentrations that naturally occur. However, FSCV also has the ability to measure slower concentration changes, although this feature has been less frequently used (Heien *et al.*, 2005; Hermans *et al.*, 2008). Traditional approaches collected data in 15, 30, or 60 second epochs so the data could be easily read. Data sets were then reorganized after the

experiment into several more files that were time-locked around specific behavioral events. This approach was both tedious and created redundancies.

HDCV facilitates the collection and analysis of large amounts of data. Unlike TarheelCV, 'continuous' data ranging from minutes to hours can be stored within an HDCV file. Experimental progress is viewed with live displays while the file is written. Afterwards, the file can be reviewed in the analysis program. Memory limitations are avoided by recalling a portion of the binary file at a time. CVs used for digital background subtraction can be taken from any point in the file, while zoom and pan controls allow the user to navigate through time in the file.

The utility of HDCV's extended time views was demonstrated while analyzing dopamine release following intravenous drug administration (Owesson-White *et al.*, 2012). Here we show a prolonged dopamine response triggered by presentation of audio noise to an awake rat. Figure 6.5 shows data from a multi-minute experiment, where data were collected in separate 30 s files using TarheelCV. Noise begins shortly into the first file and continues for the remaining time. When viewing this data in TarheelCV, each 30 s period must be individually background subtracted (Fig 6.5A, background at yellow line). This can lead to discontinuous data sets (Keithley & Wightman, 2011). A concatenated version of the data viewed in HDCV is shown below (Fig 6.5B). One set of CVs from the beginning of the file is used for background subtraction. Both representations of the data reveal a decrease in dopamine (negative current at 0.6 V) when the white noise begins. A CV captured at 75 s in Panel 4A shows little change because of the background subtraction method. However, a CV taken at the same time point in the continuous version of the data reveals continuation of the negative dopamine transition (Fig 6.5C).

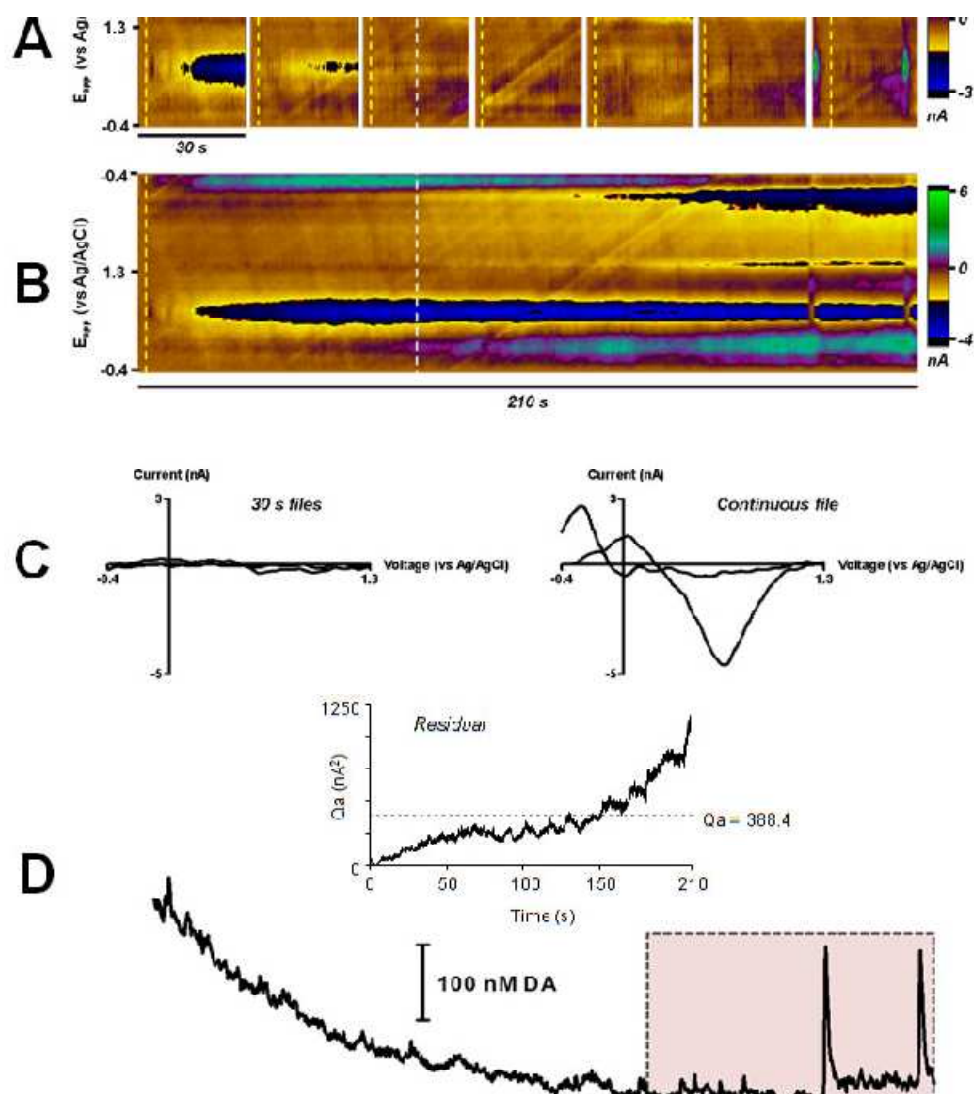


Figure 6.5. Continuous data analysis in HDCV. (A) Electrochemical recording of dopamine with the carbon-fiber electrode implanted in the nucleus accumbens of a freely-moving animal. Data is shown in 30 s file segments, as originally collected with the TarheelCV acquisition program. White audio noise begins at the bar above the color plots. Each file is background subtracted at the time indicated by the yellow dotted line. (B) Data from part (A) concatenated into a continuous HDCV file through a data convertor program. Unlike TarheelCV, HDCV reads only the requested portion of the data file at a single time permitting long periods of data to be analyzed with a single background subtraction time point (yellow dotted line). (C) Background-subtracted CVs taken from the 30 s and continuous files at the same time point (white dotted lines in A and B). (D) PCR of the continuous data reveals a decrease in dopamine concentration over time. Based on the residual analysis (inset) the concentrations in the shaded box are statistically unreliable.

Continuous analysis of FSCV experiments is limited by the signal-to-drift ratio, with the drift arising from the background current. Principal component regression (PCR) is one method of assessing this limitation. In Figure 6.5D, the dopamine concentrations from the continuous file were extracted with PCR utilizing dopamine and pH training sets. In this example analysis, an extraordinary large decrease in extracellular dopamine is apparent

after the onset of the noise. Positive concentration spikes at the end of the trace are due to electrical stimulations. However, the residual, which represents signals not accounted for by PCR analysis, surpasses the expected noise levels (shown as Q_a , Fig 6.5D inset) at 135 s. This indicates that the components of the training set do not accurately describe all significant sources contributing to the current signal, most likely due to drift in this example. Therefore, concentrations determined by PCR past this time point are statistically unreliable (Keithley *et al.*, 2009; 2010). If the unknown current source is identified and added as a component of the training set even longer analysis is possible (Hermans *et al.*, 2008).

Time bin generation and signal averaging

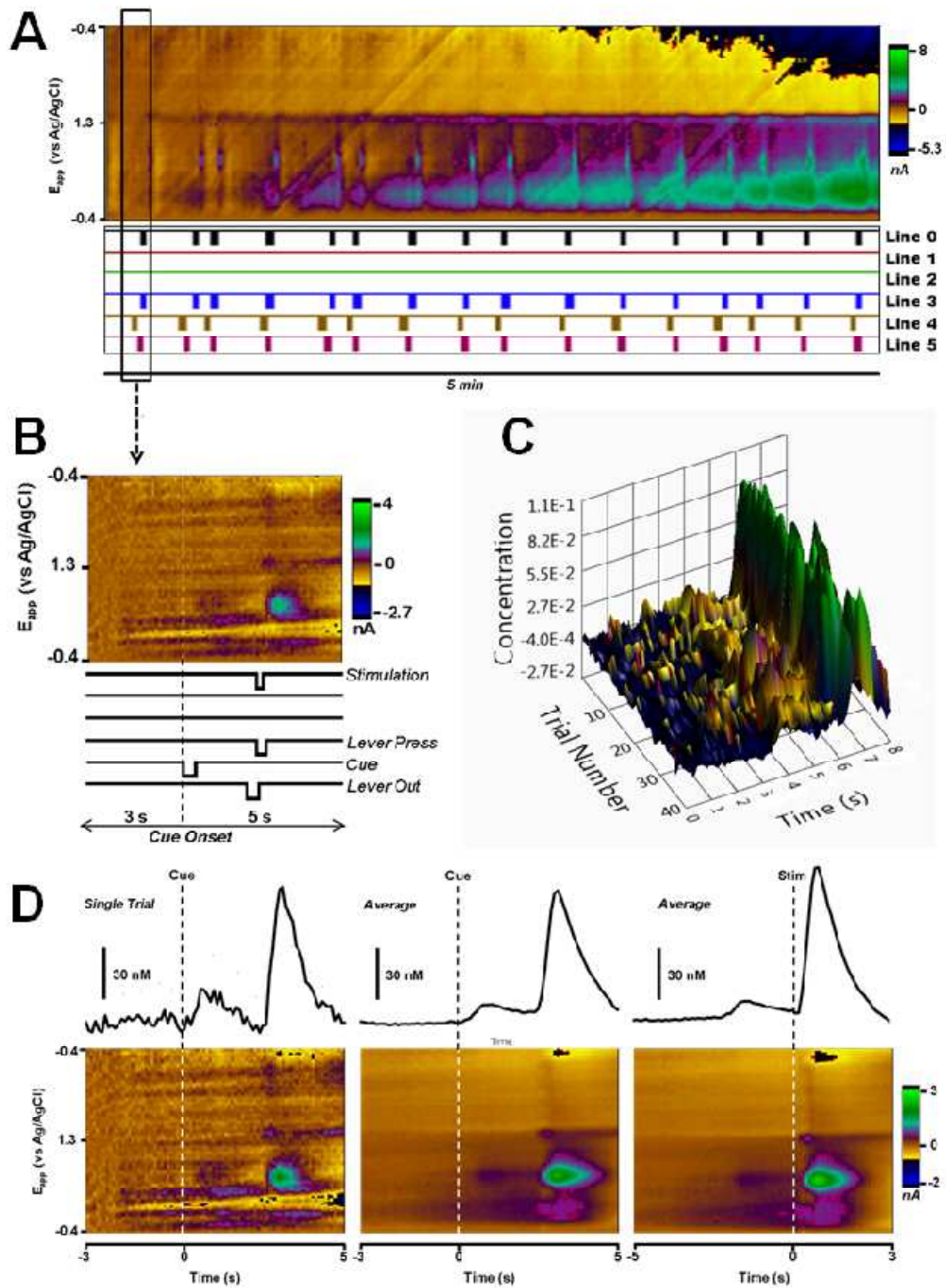
The application of FSCV in behavioral neuroscience has provided a greater understanding of dopamine in reward, learning and addiction (Phillips *et al.*, 2003; Robinson *et al.*, 2003; Day *et al.*, 2007; Owesson-White *et al.*, 2009; Park *et al.*, 2011). Behavioral paradigms often involve a series of events that are repeated at random intervals. In these experiments data are continuously recorded while events of interest, such as a cue or lever press, are marked by digital transitions produced by an operant conditioning system. Both electrochemical and digital data can be viewed simultaneously in HDCV Analysis (Fig 6.6A). The analysis of such data requires breakdown into smaller time bins, usually aligned to a given digital event. Each time bin is separately viewed, electrical artifacts are removed, and concentrations of different analytes are extracted with PCR. Finally, signal-to-noise is improved by averaging multiple time bins from similar events. The analysis routine in TarheelCV was disjointed and time-consuming, requiring an individual file per time bin, and externally generated training sets for PCR. Now, HDCV streamlines this analysis by incorporating the entire process and providing a greater degree of feedback. After opening a continuous file, the user indicates the digital line of interest, the direction of the transition and the time frame surrounding the event. HDCV allows visualization of each time bin. An

option on the main screen allows removal of electrical artifacts by replacing them with an average of CVs taken before and after the artifact. All of this work can be saved in a file that is separate from the original data, which avoids storage of redundant information.

An example time bin recorded during an ICSS experiment is shown in Figure 6.6B. The data in Figure 6.6A was recorded during multiple ICSS trials, each one beginning with the audiovisual cue (digital line 4). The time bin shown in Figure 6.6B was aligned to this cue. The user can select the set of voltammograms for digital background subtraction for each time bin.

HDCV supports each step of PCR by making it easy to capture and save standards from many files. Tools that aid in the construction of a valid training set include a principal component score plot used to evaluate linearity of training set cyclic voltammograms, a K-matrix plot which evaluates the predictive ability of the calibration model for each analyte, and a Cook's Distance calculation which is used to identify improper training set samples. All of these approaches are described elsewhere (Keithley & Wightman, 2011). HDCV integrates these tools into the user interface, whereas before users were forced to use multiple programs for calculations including Microsoft Excel and MATLAB. The user-constructed training set is then applied to a data file or set of time bins. A new window displays concentration and residual information for each time bin, and the user can further refine which time bins to keep for averaging. Figure 6.6D shows results obtained from this process. The dopamine concentration for the time bin aligned to the ICSS cue

Figure 6.6 Time bin analysis procedure in HPCV. (A) A five minute view of continuous data collected during its recording period. (B) A zoomed-in view of the data from the time bin indicated in (A). (C) A 3D surface plot of the data from (B). (D) A series of plots showing the time course of the data from (B). The top row shows the raw data for a single trial, the middle row shows the average of 40 trials, and the bottom row shows the average of 40 trials with a color scale for current (nA).



Proc
align
show
timir
sho

; set
1

n in

response to the cue at time 0. A second increase appears approximately 3 s later when the animal receives an electrical stimulation for pressing the extended lever. The central panel in Figure 6.6D shows the average from 40 similar time bins revealing the same features but with an increased signal-to-noise ratio.

Proper time bin alignment is crucial when interpreting data from such paradigms. In the averaged data (Fig 6.6D, middle), the alignment provides an attenuated view of the stimulation response because the animal pressed the lever at variable times after the cue. Averaged time bins are easily realigned to another digital line in HDCV, a process that required reanalysis of the entire data set in TarheelCV. In Figure 6.6D (right) the same time bins are averaged to the stimulus onset to provide an accurate response profile. All of these analysis features reduce the amount of time required to analyze the results of such experiments (from days to hours).

Conclusions

HDCV is a reliable, established program for FSCV. It has multiple features that enable flexible data acquisition and facilitate data analysis. The program retains features of previous programs while adding improvements in signal processing, data interpretation, and alignment with external events. The program was designed to enable future experiments that enhance the information obtained concerning neuronal processing during behavioral activities. The software is freely available for non-profit use on the website of the UNC Chemistry Electronics Facility.

REFERENCES

- Adams, R.N. (1976) Probing brain chemistry with electroanalytical techniques. *Anal Chem*, 48, 1126A-1138A.
- Armstrong-James, M., Millar, J. & Kruk, Z.L. (1980) Quantification of noradrenaline iontophoresis. *Nature*, 288, 181-183.

- Belle, A.M., Owesson-White, C., Herr, N.R., Carelli, R.M. & Wightman, R.M. (2013) Controlled Iontophoresis Coupled with Fast-Scan Cyclic Voltammetry/Electrophysiology in Awake, Freely Moving Animals. *ACS Chem Neurosci*.
- Cacciapaglia, F., Wightman, R.M. & Carelli, R.M. (2011) Rapid dopamine signaling differentially modulates distinct microcircuits within the nucleus accumbens during sucrose-directed behavior. *J Neurosci*, 31, 13860-13869.
- Cheer, J.F., Heien, M.L., Garris, P.A., Carelli, R.M. & Wightman, R.M. (2005) Simultaneous dopamine and single-unit recordings reveal accumbens GABAergic responses: implications for intracranial self-stimulation. *Proc Natl Acad Sci U S A*, 102, 19150-19155.
- Day, J.J., Roitman, M.F., Wightman, R.M. & Carelli, R.M. (2007) Associative learning mediates dynamic shifts in dopamine signaling in the nucleus accumbens. *Nat Neurosci*, 10, 1020-1028.
- Hashemi, P., Dankoski, E.C., Wood, K.M., Ambrose, R.E. & Wightman, R.M. (2011) In vivo electrochemical evidence for simultaneous 5-HT and histamine release in the rat substantia nigra pars reticulata following medial forebrain bundle stimulation. *J Neurochem*, 118, 749-759.
- He, P., Avery, J.P. & Faulkner, L.R. (1982) Cybernetic Control of an Electrochemical Repertoire. *Analytical chemistry*, 54, A313-&.
- Heien, M.L., Khan, A.S., Ariansen, J.L., Cheer, J.F., Phillips, P.E., Wassum, K.M. & Wightman, R.M. (2005) Real-time measurement of dopamine fluctuations after cocaine in the brain of behaving rats. *Proc Natl Acad Sci U S A*, 102, 10023-10028.
- Hermans, A., Keithley, R.B., Kita, J.M., Sombers, L.A. & Wightman, R.M. (2008) Dopamine detection with fast-scan cyclic voltammetry used with analog background subtraction. *Anal Chem*, 80, 4040-4048.
- Keithley, R.B., Heien, M.L. & Wightman, R.M. (2009) Multivariate concentration determination using principal component regression with residual analysis. *Trends Analyt Chem*, 28, 1127-1136.
- Keithley, R.B., Heien, M.L. & Wightman, R.M. (2010) Erratum to "Multivariate concentration determination using principal component regression with residual analysis" *Trends Anal. Chem.*, 29, 110.
- Keithley, R.B. & Wightman, R.M. (2011) Assessing principal component regression prediction of neurochemicals detected with fast-scan cyclic voltammetry. *ACS Chem Neurosci*, 2, 514-525.
- Michael, D., Travis, E.R. & Wightman, R.M. (1998) Color images for fast-scan CV measurements in biological systems. *Anal Chem*, 70, 586A-592A.

- Michael, D.J., Joseph, J.D., Kilpatrick, M.R., Travis, E.R. & Wightman, R.M. (1999) Improving data acquisition for fast-scan cyclic voltammetry. *Anal Chem*, 71, 3941-3947.
- Michael, D.J. & Wightman, R.M. (1999) Electrochemical monitoring of biogenic amine neurotransmission in real time. *J Pharm Biomed Anal*, 19, 33-46.
- Millar, J., Armstrong-James, M. & Kruk, Z.L. (1981) Polarographic assay of iontophoretically applied dopamine and low-noise unit recording using a multibarrel carbon fibre microelectrode. *Brain Research*, 205, 419-424.
- Millar, J., Stamford, J.A., Kruk, Z.L. & Wightman, R.M. (1985) Electrochemical, pharmacological and electrophysiological evidence of rapid dopamine release and removal in the rat caudate nucleus following electrical stimulation of the median forebrain bundle. *Eur J Pharmacol*, 109, 341-348.
- Owesson-White, C.A., Ariansen, J., Stuber, G.D., Cleaveland, N.A., Cheer, J.F., Wightman, R.M. & Carelli, R.M. (2009) Neural encoding of cocaine-seeking behavior is coincident with phasic dopamine release in the accumbens core and shell. *Eur J Neurosci*, 30, 1117-1127.
- Owesson-White, C.A., Cheer, J.F., Beyene, M., Carelli, R.M. & Wightman, R.M. (2008) Dynamic changes in accumbens dopamine correlate with learning during intracranial self-stimulation. *Proc Natl Acad Sci U S A*, 105, 11957-11962.
- Owesson-White, C.A., Roitman, M.F., Sombers, L.A., Belle, A.M., Keithley, R.B., Peele, J.L., Carelli, R.M. & Wightman, R.M. (2012) Sources contributing to the average extracellular concentration of dopamine in the nucleus accumbens. *J Neurochem*, 121, 252-262.
- Park, J., Kile, B.M. & Wightman, R.M. (2009) In vivo voltammetric monitoring of norepinephrine release in the rat ventral bed nucleus of the stria terminalis and anteroventral thalamic nucleus. *Eur J Neurosci*, 30, 2121-2133.
- Park, J., Wheeler, R.A., Fontillas, K., Keithley, R.B., Carelli, R.M. & Wightman, R.M. (2011) Catecholamines in the Bed Nucleus of the Stria Terminalis Reciprocally Respond to Reward and Aversion. *Biological psychiatry*.
- Phillips, P.E., Stuber, G.D., Heien, M.L., Wightman, R.M. & Carelli, R.M. (2003) Subsecond dopamine release promotes cocaine seeking. *Nature*, 422, 614-618.
- Robinson, D.L., Hermans, A., Seipel, A.T. & Wightman, R.M. (2008) Monitoring rapid chemical communication in the brain. *Chem Rev*, 108, 2554-2584.
- Robinson, D.L., Venton, B.J., Heien, M.L. & Wightman, R.M. (2003) Detecting subsecond dopamine release with fast-scan cyclic voltammetry in vivo. *Clin Chem*, 49, 1763-1773.
- Robinson, D.L. & Wightman, R.M. (2007) Rapid Dopamine Release in Freely Moving Rats. In Michael, A.C., Borland, L.M. (eds) *Electrochemical Methods for Neuroscience* CRC Press, Boca Raton pp. 17-34.

- Swamy, B.E. & Venton, B.J. (2007) Subsecond detection of physiological adenosine concentrations using fast-scan cyclic voltammetry. *Anal Chem*, 79, 744-750.
- Takmakov, P., McKinney, C.J., Carelli, R.M. & Wightman, R.M. (2011) Instrumentation for fast-scan cyclic voltammetry combined with electrophysiology for behavioral experiments in freely moving animals. *Rev Sci Instrum*, 82, 074302.
- Venton, B.J., Michael, D.J. & Wightman, R.M. (2003) Correlation of local changes in extracellular oxygen and pH that accompany dopaminergic terminal activity in the rat caudate-putamen. *J Neurochem*, 84, 373-381.
- Wiedemann, D.J., Kawagoe, K.T., Kennedy, R.T., Ciolkowski, E.L. & Wightman, R.M. (1991) Strategies for low detection limit measurements with cyclic voltammetry. *Anal Chem*, 63, 2965-2970.
- Wightman, R.M., Heien, M.L., Wassum, K.M., Sombers, L.A., Aragona, B.J., Khan, A.S., Ariansen, J.L., Cheer, J.F., Phillips, P.E. & Carelli, R.M. (2007) Dopamine release is heterogeneous within microenvironments of the rat nucleus accumbens. *Eur J Neurosci*, 26, 2046-2054.
- Yorgason, J.T., Espana, R.A. & Jones, S.R. (2011) Demon voltammetry and analysis software: analysis of cocaine-induced alterations in dopamine signaling using multiple kinetic measures. *Journal of neuroscience methods*, 202, 158-164.
- Zachek, M.K., Park, J., Takmakov, P., Wightman, R.M. & McCarty, G.S. (2010) Microfabricated FSCV-compatible microelectrode array for real-time monitoring of heterogeneous dopamine release. *Analyst*, 135, 1556-1563.
- Zachek, M.K., Takmakov, P., Moody, B., Wightman, R.M. & McCarty, G.S. (2009) Simultaneous decoupled detection of dopamine and oxygen using pyrolyzed carbon microarrays and fast-scan cyclic voltammetry. *Anal Chem*, 81, 6258-6265.

CHAPTER 7: EVALUATION OF FUSED-SILICA INSULATED CARBON-FIBER MICROELECTRODES FOR LONGITUDINAL NEUROCHEMICAL STUDIES

Introduction

Dopamine signaling in the basal ganglia has a critical role in motor-coordination and motivational behavior (Carelli, 2004; Schultz, 2013; Calabresi *et al.*, 2014). Among existing analytical techniques, fast-scan cyclic voltammetry (FSCV) at carbon-fiber microelectrodes has proven particularly valuable in the study of rapid dopamine release in anesthetized and behaving rodents (Robinson *et al.*, 2008; Willuhn *et al.*, 2010). Indeed, FSCV measurements have provided insight into how this catecholamine neurotransmitter modulates learned behaviors and how its dysregulation contributes to the pathology of disorders as varied as drug addiction (Aragona *et al.*, 2008; Wheeler *et al.*, 2011; Ehrich *et al.*, 2014) and Parkinson's disease (Cragg *et al.*, 2000; Janezic *et al.*, 2013; Lohr *et al.*, 2014).

As our knowledge of the midbrain dopamine system has grown it has become increasingly apparent that it is a complex, dynamic neuronal network that is capable of adaption (Robinson *et al.*, 2011; Ferris *et al.*, 2013; Park *et al.*, 2013; Crowley *et al.*, 2014) and spatially heterogeneous on a micrometer scale (Garris *et al.*, 1994; Wightman *et al.*, 2007; Park *et al.*, 2010). With this in mind, the ability to conduct FSCV measurements over multiple days or months would provide valuable information on how dopamine signaling changes during learning and disease progression. Traditionally such studies are carried out in one of two ways, either by sacrificing animals at different time points of the experiment (Addy *et al.*, 2010; McElligott *et al.*, 2013) or by implanting a fresh carbon-fiber microelectrode on each day of testing via a microdrive attached to the skull

(Garris *et al.*, 1997). Both of these strategies notably fail to maintain the exact same neurochemical environment between sampling points.

Chronic sensor implantation, however, would allow longitudinal data to be collected from the same dopamine terminal population. While early attempts at chronic electrochemical measurements found little success (Duff & O'Neill, 1994; Kruk *et al.*, 1998), Phillips and coworkers recently reported of a new type of carbon-fiber microelectrode that can function after several months of implantation (Clark *et al.*, 2010). Their initial work demonstrated that this chronic FSCV sensor can measure naturally-evoked dopamine transients up to four-months after implantation and over a period of 25 days. Overall, the survival and performance of Phillips' chronic electrode has been attributed to its size; in contrast to the conventional 0.6 mm borosilicate glass that is used to insulate conventional FSCV electrodes, the carbon-fiber of the chronic electrode is housed in 90 μ m diameter fused-silica tubing. This results in little tissue damage during implantation and, in turn, little immune reactivity even after several months of implantation.

Although this chronic carbon-fiber microelectrode presents the first viable sensor for long-term measurement of rapid dopamine neurotransmission, there is still question as to how they can be used. For instance, comparison of measurements over multiple days requires a stable electrode response and, while implantation itself does not deteriorate the sensitivity of the sensor for dopamine, no one has considered the potential effects of extended waveform application. Previous work by our lab has demonstrated that the carbon fiber is altered by the voltammetric scan through an oxidative etching process, which continuously cleans the surface while enhancing dopamine sensitivity through increased adsorption (Heien *et al.*, 2003; Takmakov *et al.*, 2010; Keithley *et al.*, 2011). In the short term this process is stable; however, at longer times this etching process could result in significant loss of electrode area or even degradation of the seal.

In attempt to address such concerns, our lab has initiated a number of experiments to more clearly define the limitations of chronic FSCV measurements. This chapter describes construction of the chronic probes and the results of our preliminary investigations.

Experimental

Chronic electrode construction

Chronic electrode fabrication was a four day process, consisting of the following steps.

(1) Threading:

Polyimide-fused silica tubing (90 μm o.d., 20 μm i.d., Polymicrotechnologies, Phoenix, AZ) was cut into 10 mm pieces using a fresh scalpel blade so that the edges were free from perforation. Single carbon fibers (~ 2 in length, 5 μm diameter, T-650 type, Amoco, Greenville, SC) were then guided through the cut capillaries in a bath of ethanol, using cotton applicators and a stereoscope (Wild M3Z, Leica, Buffalo Grove, IL). The carbon fibers were positioned so that approximately half extended from each end of the capillaries. Filled capillaries were set aside to dry overnight.

(2) Forming the seal:

Once dry, the filled capillaries were suspended 1-2 mm over a cut piece of paper using an arched strip ($\frac{1}{8}$ x 1 in) of label tape. Each piece of paper was secured to a petri dish using additional tape. Next, quick setting epoxy (Part No. TQS-2, Super Glue Corp., Rancho Cucamonga, CA) was applied to one end of each carbon fiber in a dabbing motion with a small gauge need tip under the stereoscope. The epoxy was then drawn through the capillaries by pulling the opposite end of the carbon fibers with a finger. This process was repeated until the epoxy had wicked several millimeters into the capillaries and formed hemispheric seals. The applied epoxy was allowed to dry overnight.

(3) Trimming the fiber and adding a connection pin:

After the epoxy had 24 h to harden, the carbon fibers at the end of the seals were cut with a pair of Vannas scissors (3 mm blades, 0.1 mm tips) to an exposed length of ~150 μm . Following this step, silver epoxy (Part No. 8331-14G, MG Chemicals, Surrey, B.C., Canada) was applied to rectangular areas (~3 x 1 mm) of Parafilm®. The uncut side of each fused-silica electrode was placed into a silver epoxy deposit using forceps. Connector pins (Part No. 0667-0-15-01-30-27-10-0, Mill Max Mfg. Corp., Oyster Bay, NY) were positioned on top of the silver-epoxy submerged fibers and allowed to dry overnight.

(4) Insulating the connection:

The electrodes were secured onto a handheld mount via the connection pin. Quick setting epoxy was applied around the carbon-fiber-pin area and a portion of the capillary to secure the connection and to provide a degree of electrical insulation. The epoxy insulation was allowed to dry overnight before the electrodes were used. A schematic diagram of the assembled components is shown in Figure 7.1.

Acute electrode construction

Carbon-fibers (~ 2 in length, 5 μm diameter, T-650 type, Amoco, Greenville, SC) were aspirated into borosilicate capillaries (0.6 mm x 0.4 mm diameter, 4 in length) using a vacuum pump. Each capillary was then pulled into two separate electrodes sealed to a fine tip using a micropipette puller (Narishige, East Meadow, NY). The exposed carbon fibers were cut to a 150 μm length with a surgical scalpel under a light microscope. Electrical connections were made to wires with gold pin connectors by silver paint. The wires were secured to the capillaries with shrink wrap. Comparison of the acute and chronic electrode types is provided in Figures 7.2 and 7.3.

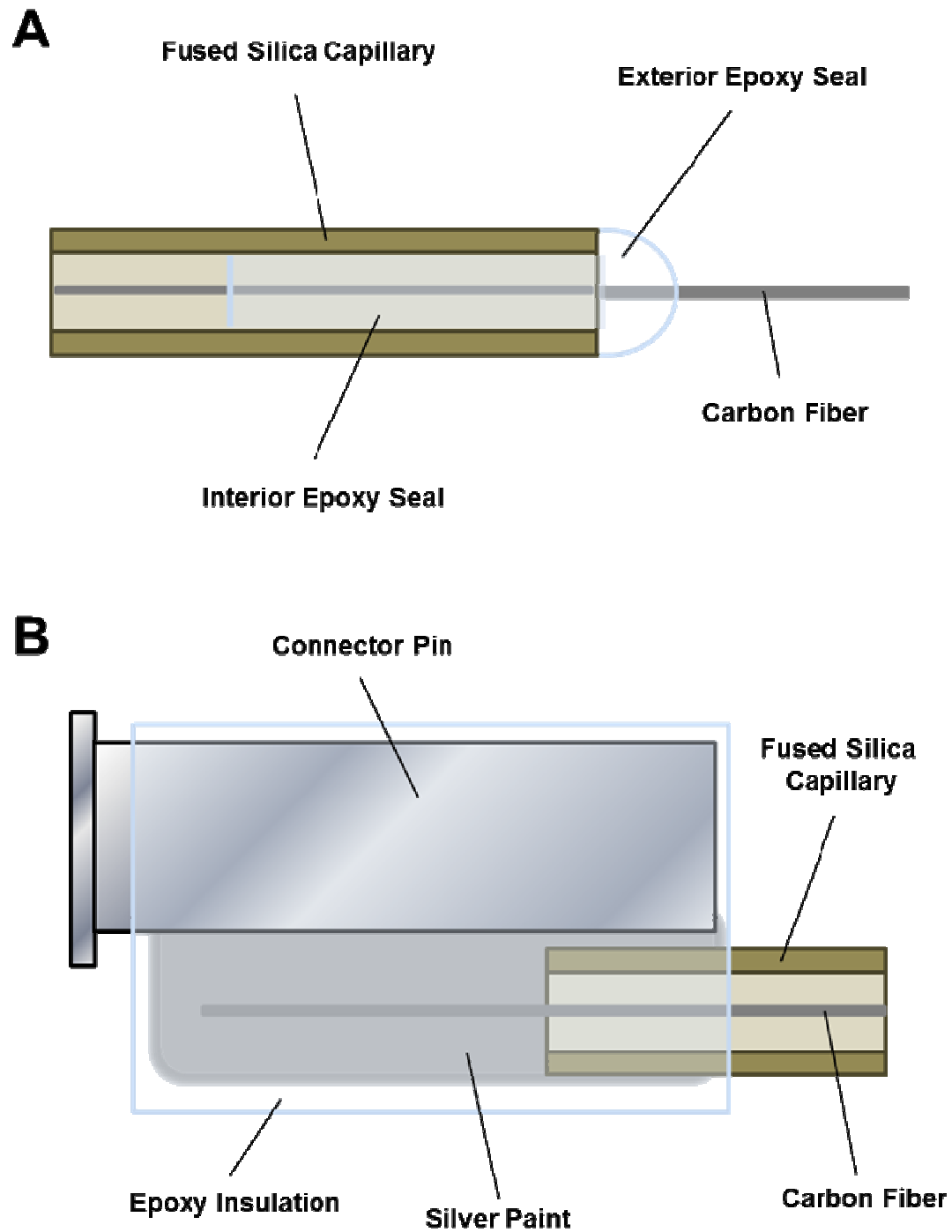


Figure 7.1. Schematic of the chronic type microelectrode. (A) Components at the sensor tip. (B) Components at the sensor connection.

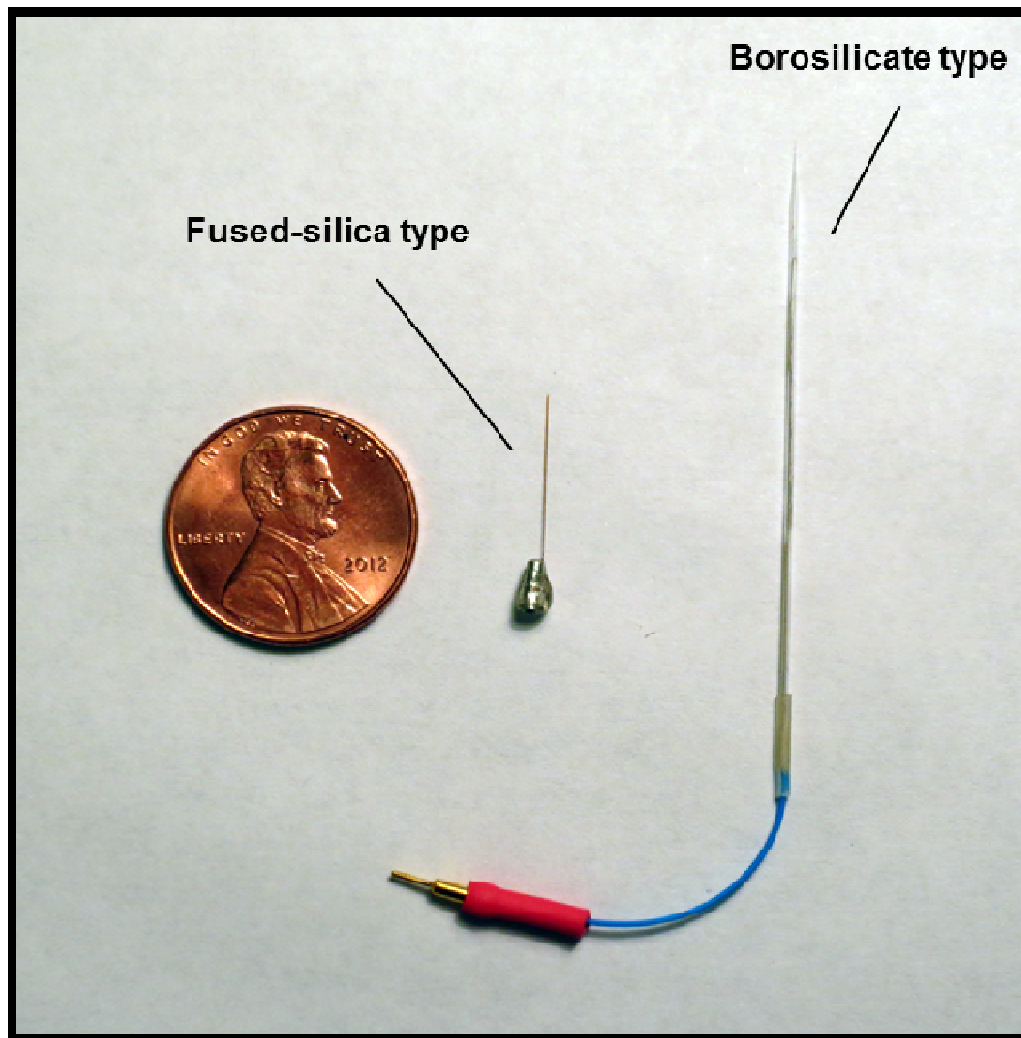


Figure 7.2 Size comparison between acute and chronic microelectrode types

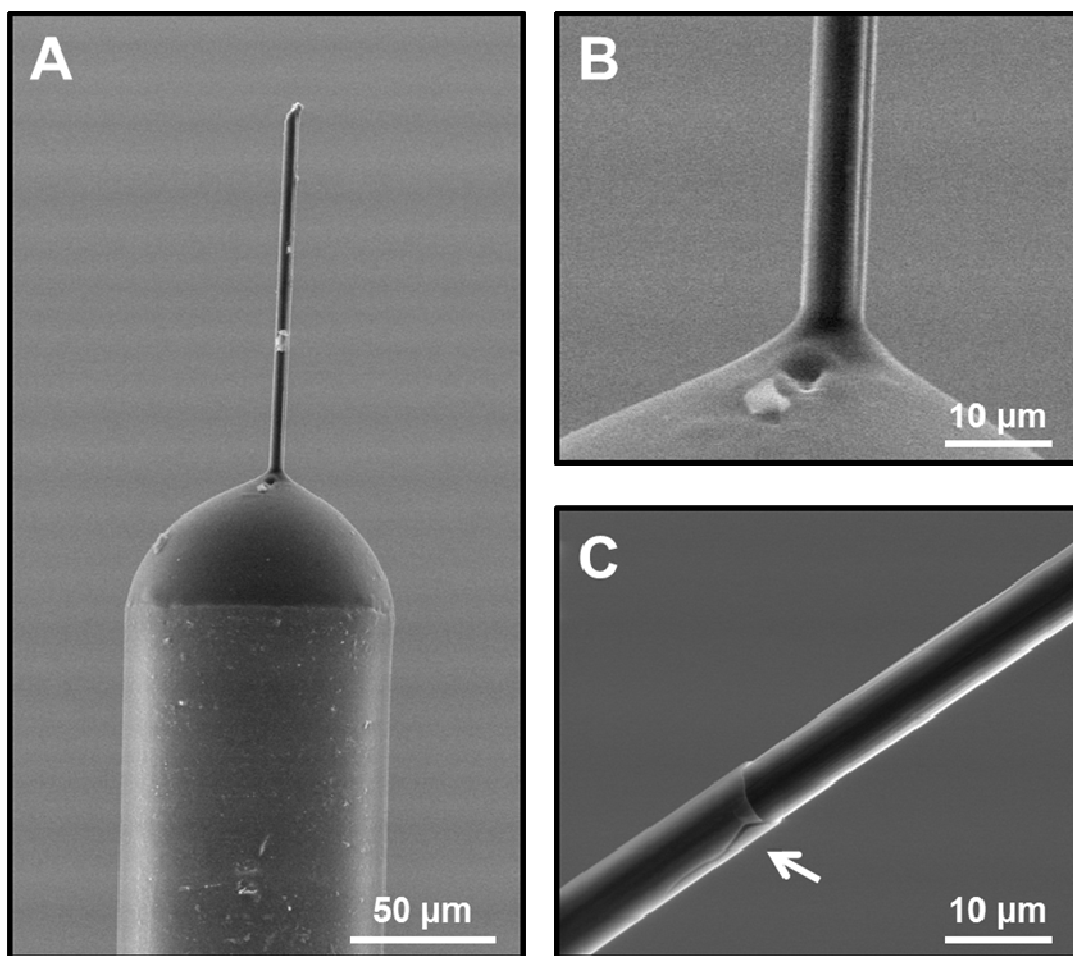


Figure 7.3. Electron micrographs of acute and chronic carbon-fiber microelectrodes. (A) A chronic microelectrode. The fused silica capillary, epoxy seal and carbon-fiber are visible. (B) The seal of the chronic electrode shown in panel A. (C) The seal of an acute microelectrode. The arrow indicates a hairline fracture along the glass seal.

Electrochemical measurements

FSCV was performed with TarheelCV, a program written in LabVIEW (National Instruments, Austin, TX), and a locally-constructed macro head-stage amplifier (UNC Electronics Facility, Chapel Hill, NC). Reference electrodes were Ag/AgCl. Measurements were made using a triangular sweep scanning from -0.4 V to 1.3 V at rate of 400 V/s. The waveform was applied at 10 Hz with a -0.4 V holding potential. Carbon-fiber electrodes were preconditioned with the waveform for 30 min (15 min at 60 Hz, 15 min at 10 Hz) before each use.

Flow injection analysis

The sensitivity, temporal response, and limit of detection for each electrode were determined using a submerged flow injection analysis system fitted with a 6-port rotary valve controlled by a pneumatic actuator. Dopamine solutions were prepared in Tris buffer (15 mM Tris, 126 mM NaCl, 2.5 mM KCl, 25 mM NaHCO₃, 2.4 mM CaCl₂, 1.2 mM NaH₂PO₄, 1.2 mM MgCl₂, 2.0 mM Na₂SO₄) adjusted to pH 7.4 with NaOH. All standards were introduced as 5 s injections at a flow rate of 2 mL/min.

Peak currents, noise levels and response times were determined for flow injection data using the data analysis component of TarheelCV (Figure 7.4). All data were filtered using a low-pass Bessel filter with a 2 KHz cutoff frequency. Peak oxidation currents were used to generate dopamine calibration curves. Response time was measured as the amount of time necessary for the peak current to rise from 10% to 90% of its maximum value. Limit of detection was calculated as three times the standard deviation of the noise at the potential of dopamine oxidation during the 5 s before each injection. Statistical analysis was accomplished using GraphPad Prism software. P values less than 0.05 were considered statistically significant.

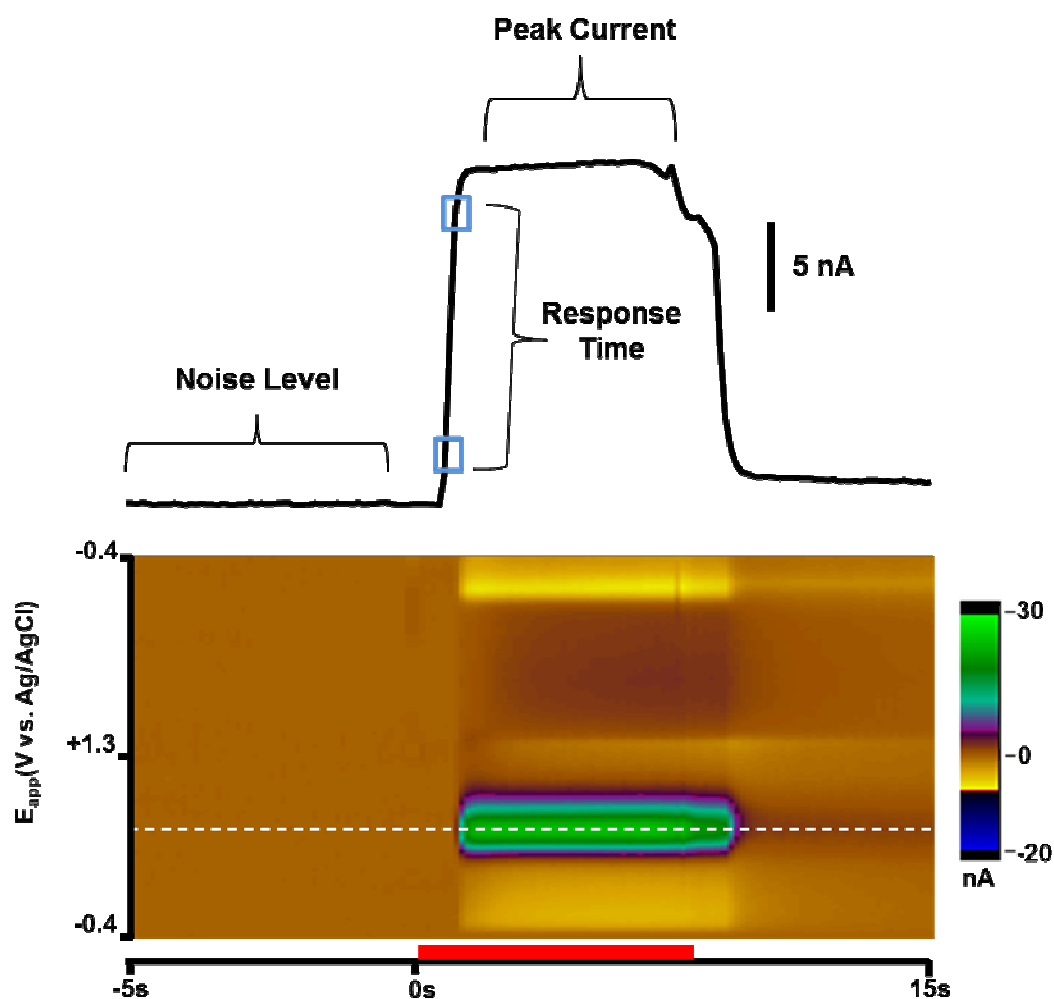


Figure 7.4. Example data collected during a flow injection analysis experiment. Voltammetric data is displayed as a color plot with the voltage applied mapped along the ordinate, the time of voltammogram acquisition along the abscissa and current in false color. Features corresponding to the oxidation (+0.6 V, dashed white line) and reduction (-0.4 V) of dopamine (2 μM) appear slightly after the time of injection (denoted by the red bar). The trace above the color plot represents the current at the dopamine oxidation potential during data collection. Peak current, response time and noise levels were determined from the indicated areas on the current

In vivo measurements

All animal procedures were approved by the Institutional Animal Care and Use Committee of the University of North Carolina at Chapel Hill. Male Sprague-Dawley rats (250 – 350 g, Charles Rivers, Wilmington, MA) were paired-houses in a 12:12 h light-dark cycle temperature and humidity controlled environment with food and water available *ad libitum*. On the day of electrode implantation, animals were anesthetized with isoflurane (1.5–2.0%) and mounted in a stereotaxic frame. The dorsal skull was exposed and holes were drilled for placement of a chronic type carbon-fiber microelectrode, a stainless steel bipolar stimulating electrode, an acutely implantable reference and support screws. Anterior-posterior (AP), medial-lateral (ML) and dorsal-ventral (DV) coordinates were reference from bregma based on the atlas of Paxinos and Watson.

The hole for the carbon-fiber microelectrode targeted the dorsal striatum (AP +1.2 mm, ML +2.0 mm, DV -4.0 – -5.5 mm). A guide cannula for implantation of a Ag/AgCl reference was positioned above a hole at similar anterior-posterior coordinates in the contralateral hemisphere and secured with dental cement. During the surgery a stimulating electrode was lowered into the ventral tegmental area (AP -5.2 mm, ML +1.2 mm, DV -8.0 – -9.0 mm). Stimulation of these coordinates ($\pm 300 \mu\text{A}$, 60 biphasic pulses, 2 ms/pulse, 60 Hz, NL 800□A, Neurolog, Digitimer, Hertfordshire, UK) was used with voltammetric measurements to guide placement of the carbon-fiber microelectrode during the surgery. Once the carbon-fiber electrode was placed at a depth with optimal stimulated catecholamine release it was secured to the skull with dental cement. The stimulating electrode was then completely removed and the skin was sutured with Vet Bond Adhesive to seal the remaining exposed portion of the skull. Animals were closely monitored closely after surgical procedures and allowed to recover on a heating pad. Once animals awoke they were administered Children's Tylenol (0.4 mL, 12.8 mg acetaminophen) and maintained for 6-8 weeks post op before voltammetric experiments were conducted.

On the day of recording, the animals were anesthetized with urethane (1.5 mg/kg) and placed in a stereotaxic frame. The posterior portion of the skull was re-exposed with a scalpel. A drill was used to removed bone growth over the ventral tegmental area hole so that a new stimulating electrode could be implanted. A fresh Ag/AgCl reference electrode was inserted through the guide cannula and the depth of stimulation was adjusted to maximize the amount of dopamine release recorded at the carbon-fiber microelectrode.

Results

Comparison of acute and chronic type electrode performance

Acute (borosilicate) and chronic (fused-silica) electrode types were characterized using flow injection analysis. The effect of prolonged use was examined using the chronic electrodes types by recalibrating each electrode after several periods of waveform application. During each period the waveform was applied at 60 Hz for 2 h to mimic 12 h of recording at the conventional 10 Hz frequency.

Results are summarized in Figure 7.5 and Table 7.1. Acute electrodes had a higher sensitivity and a lower limit of detection for dopamine than chronic electrodes (unpaired student's t-test, $P < 0.001$). No differences were found between their time responses.

During prolonged waveform application experiments, the calibration factor of the chronic electrodes was different for every time interval assayed. Through the first two periods of waveform application (equivalent to 24 h of use) the sensitivity of the electrodes increased to 160% of its initial value. The sensitivity of the electrodes then fell to 79% of this peak value over the two periods of waveform application (between 24 h to 48 h of equivalent use). Analysis of this data by one-way ANOVA with a Bonferoni post-hoc test revealed significant differences in sensitivity and limit of detection after each period of cycling ($P < 0.001$), except between the second (12 h) and fourth (36 h) time points. No significant differences were found between time responses.

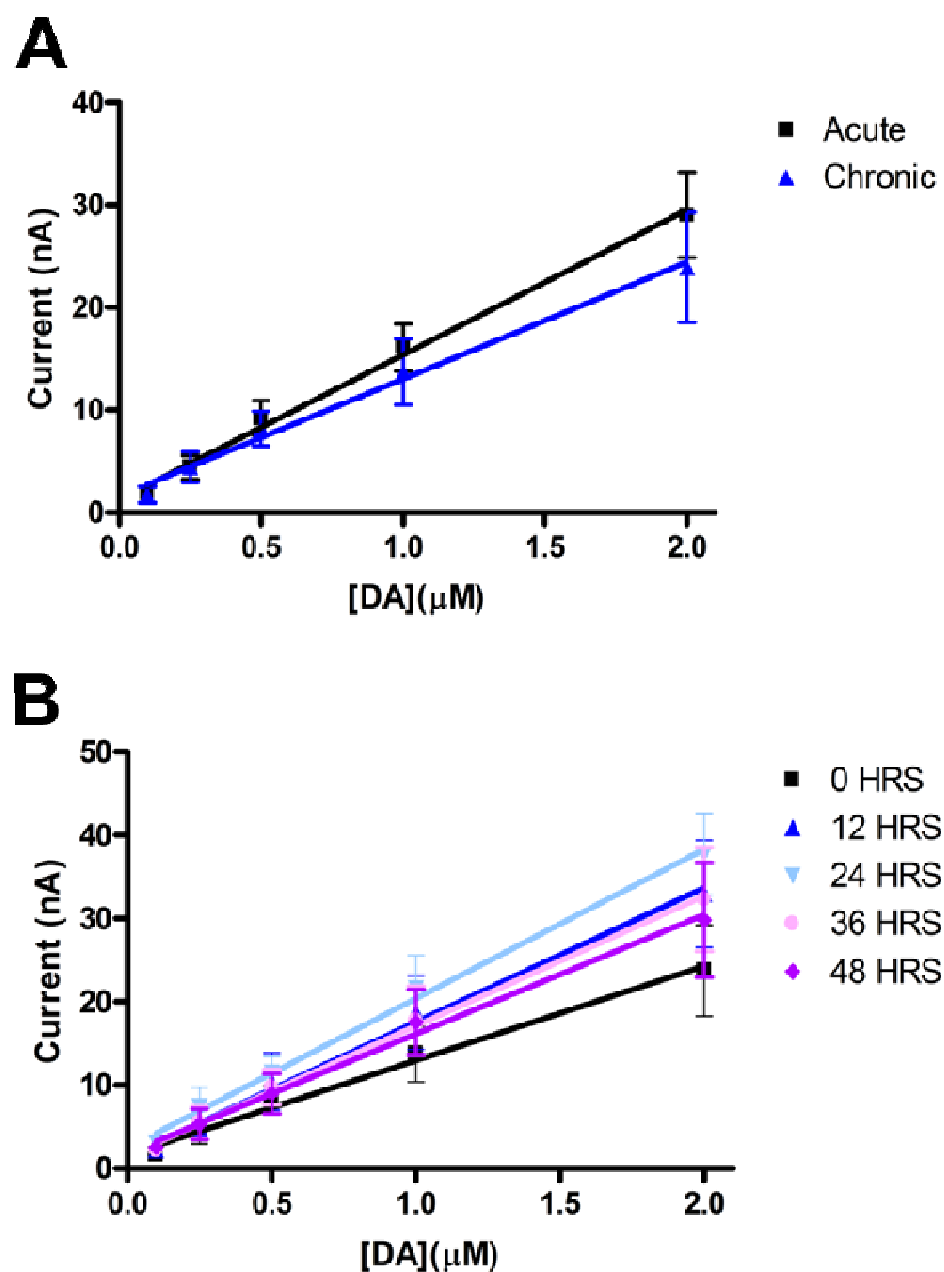


Figure 7.5. Dopamine calibration curves for 150 μ m carbon fiber microelectrodes. Error is shown as standard deviation for the number of electrodes indicated in Table 1. (A) Comparison of acute and chronic electrode responses. (B) Effect of prolonged waveform application on chronic electrode responses

Electrode Type	n	Cycle Time (h)	Sensitivity (nA/ μ M)	LOD (nM)	Temporal Response (s)
Acute	15	0	14.2 \pm 0.4	11.2 \pm 0.5	1.1 \pm 0.3
Chronic	22	0	11.3 \pm 0.4 [§]	14.2 \pm 0.8 [§]	1.0 \pm 0.3
	14	12	16.2 \pm 0.7*	11.6 \pm 1.2*	0.9 \pm 0.5
	12	24	18.0 \pm 0.6*	19.8 \pm 3.2*	0.8 \pm 0.4
	12	36	15.6 \pm 0.7*	9.9 \pm 0.3*	0.9 \pm 0.4
	12	48	14.3 \pm 0.7*	17.9 \pm 2.2*	0.9 \pm 0.2

Table 7.1. Chronic and acute electrode responses to dopamine with flow injection analysis. Cycle time indicates the length of waveform application (at a 10 Hz recording frequency) before the calibration was obtained. LOD, limit of detection; n, number of electrodes. [§]Significantly different from acute electrodes as determined by student's t-test, P < 0.001. *Significantly different from chronic electrodes with 0 h of waveform application as determined by student's t-test, P < 0.001

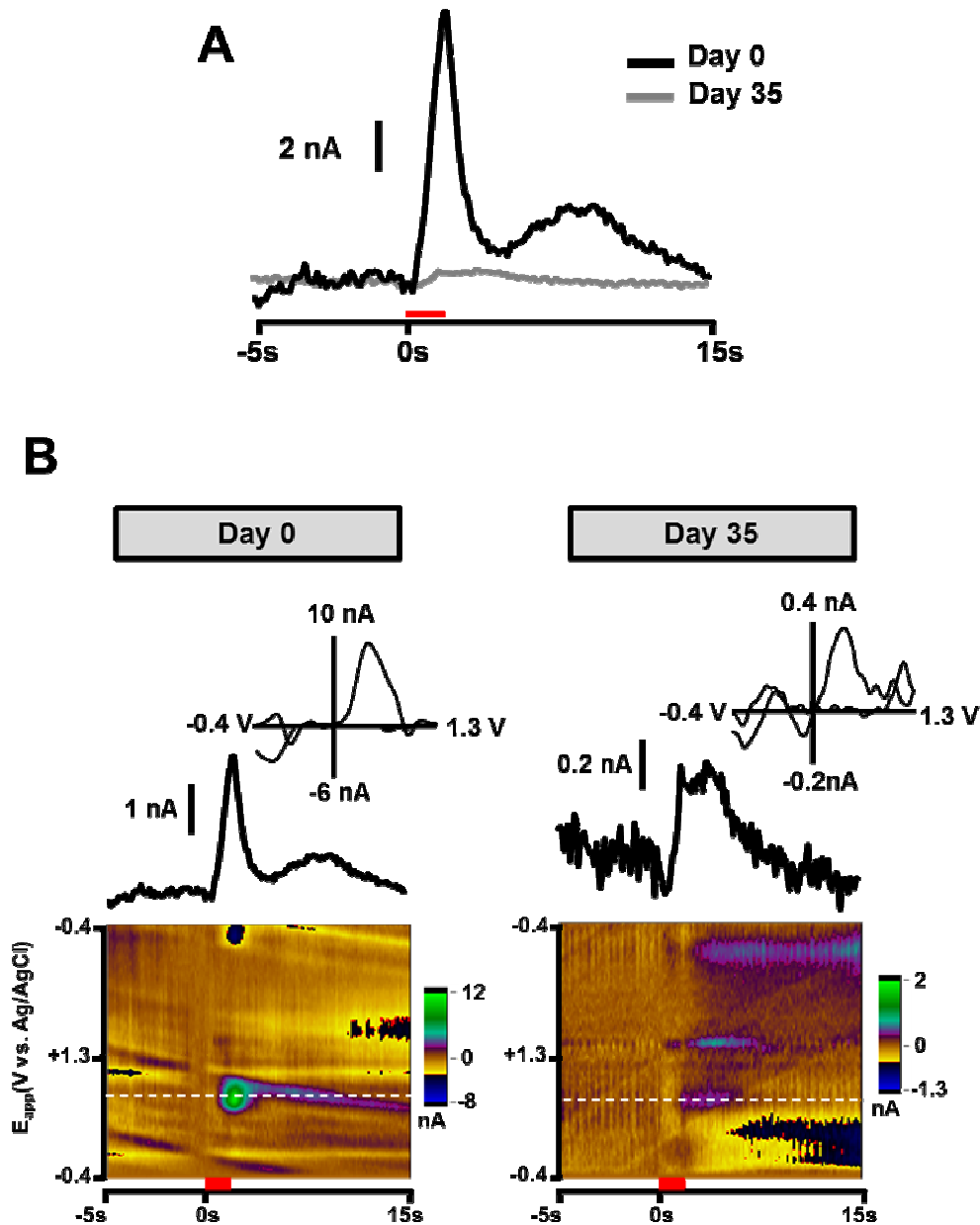


Figure 7.6 In vivo performance of chronically implanted carbon-fiber microelectrode. (A) Electrically-stimulated dopamine release at the same location in the dorsal striatum immediately after the electrode was secured with dental cement (Day 0) and after chronic implantation (Day 35). The second peak in the Day 0 trace is due to 60 Hz noise as measurements on the day of the surgery were made outside of a Faraday cage. The time of stimulation is denoted by the red bar. (B) More detailed view of voltammetric data shown in A. Oxidation potential for dopamine is indicated by the white dashed lines in the color plots. Inset cyclic voltammograms are taken at the times of peak dopamine current.

Carbon-fiber electrode performance after chronic implantation

Only one electrode (of 3 attempted surgeries) survived chronic implantation (Figure 6). However, for this single electrode the peak dopamine signal had diminished to 4% of its original value between the day of surgery and the day of the experiment (a 35 day period). In addition, the temporal aspects of the stimulated dopamine response appeared to be slower than observed on the day of implantation.

Discussion

There are several notable points of discussion in this initial work. First, we found that the acute electrodes were more sensitive to dopamine than the chronic electrodes. This was surprising as both types were made using the same stock of T-650 carbon fibers, and therefore should exhibit the same adsorption and electron-transfer kinetics. There are however other factors that could influence sensitivity such as in mass transport and surface area. Though most of the voltammetric signal for dopamine is due to its adsorption between scans (Bath *et al.*, 2000), it is possible that the geometry of the chronic electrode could hinder mass transport to the carbon fiber near the seal (Figure 3B). Furthermore, environmental scanning electrode microscopy revealed hairline cracks in the seals of many of the acute electrodes (Figure 3C). Taking this into consideration, it is reasonable to assume that the exposed carbon-fiber area was underestimated for the acute electrodes. This would in turn lead to a higher apparent sensitivity.

Of particular relevance to longitudinal studies, we found that the electrochemical response to physiological concentrations of dopamine changed with prolonged use. These changes were consistent with the oxidative etching process reported to occur with this waveform, (Heien *et al.*, 2003; Takmakov *et al.*, 2010) which is the predominant waveform used in behavioral dopamine studies. Over the first two periods of waveform cycling the sensitivity to dopamine increased, probably due to continued generation of adsorption-

mediating oxides. This was followed by a decrease in sensitivity over the last two periods of cycling, where the effects of surface etching likely overcame those of surface oxidation. Regardless of the actual mechanisms mediating these changes, these data clearly demonstrate that the sensitivity of the electrode is time dependent and changes at an inconstant rate.

In our single successful animal experiment, we found that dopamine release was attenuated and temporally distorted after 35 days of electrode implantation. While the work of Phillips and coworkers also observed a loss in temporal response—which can theoretically be accounted for by deconvolution techniques (Venton *et al.*, 2002)—they did not report any differences in electrode sensitivity after chronic implantation (Clark *et al.*, 2010). Therefore, the large attenuation of dopamine release in our experiment suggests that the position of the electrode shifted from the day of surgery or that significant tissue damage had occurred around the carbon-fiber. This is at odds with the previous report, which found little glial reactivity or terminal degradation at the site of implantation.

Conclusions

Together these preliminary results suggest that caution is needed in the use of chronically implanted electrodes. Importantly, our observations from flow injection analysis experiments warn against data interpretations that are based on signal amplitude comparison across multiple days. Future work is needed and will continue to explore the performance of the chronic FSCV sensors *in vivo*.

REFERENCES

- Addy, N.A., Daberkow, D.P., Ford, J.N., Garriss, P.A. & Wightman, R.M. (2010) Sensitization of rapid dopamine signaling in the nucleus accumbens core and shell after repeated cocaine in rats. *J Neurophysiol*, 104, 922-931.
- Aragona, B.J., Cleaveland, N.A., Stuber, G.D., Day, J.J., Carelli, R.M. & Wightman, R.M. (2008) Preferential enhancement of dopamine transmission within the nucleus accumbens shell by cocaine is attributable to a direct increase in phasic dopamine release events. *J Neurosci*, 28, 8821-8831.
- Bath, B.D., Michael, D.J., Trafton, B.J., Joseph, J.D., Runnels, P.L. & Wightman, R.M. (2000) Subsecond adsorption and desorption of dopamine at carbon-fiber microelectrodes. *Anal Chem*, 72, 5994-6002.
- Calabresi, P., Picconi, B., Tozzi, A., Ghiglieri, V. & Di Filippo, M. (2014) Direct and indirect pathways of basal ganglia: a critical reappraisal. *Nat Neurosci*, 17, 1022-1030.
- Carelli, R.M. (2004) Nucleus accumbens cell firing and rapid dopamine signaling during goal-directed behaviors in rats. *Neuropharmacology*, 47 Suppl 1, 180-189.
- Clark, J.J., Sandberg, S.G., Wanat, M.J., Gan, J.O., Horne, E.A., Hart, A.S., Akers, C.A., Parker, J.G., Willuhn, I., Martinez, V., Evans, S.B., Stella, N. & Phillips, P.E. (2010) Chronic microensors for longitudinal, subsecond dopamine detection in behaving animals. *Nat Methods*, 7, 126-129.
- Cragg, S.J., Clarke, D.J. & Greenfield, S.A. (2000) Real-time dynamics of dopamine released from neuronal transplants in experimental Parkinson's disease. *Exp Neurol*, 164, 145-153.
- Crowley, N.A., Cody, P.A., Davis, M.I., Lovinger, D.M. & Mateo, Y. (2014) Chronic methylphenidate exposure during adolescence reduces striatal synaptic responses to ethanol. *Eur J Neurosci*, 39, 548-556.
- Duff, A. & O'Neill, R.D. (1994) Effect of probe size on the concentration of brain extracellular uric acid monitored with carbon paste electrodes. *J Neurochem*, 62, 1496-1502.
- Ehrich, J.M., Phillips, P.E. & Chavkin, C. (2014) Kappa Opioid Receptor Activation Potentiates the Cocaine-Induced Increase in Evoked Dopamine Release Recorded In Vivo in the Mouse Nucleus Accumbens. *Neuropsychopharmacology*.

- Ferris, M.J., Calipari, E.S., Yorgason, J.T. & Jones, S.R. (2013) Examining the complex regulation and drug-induced plasticity of dopamine release and uptake using voltammetry in brain slices. *ACS Chem Neurosci*, 4, 693-703.
- Garris, P.A., Christensen, J.R., Rebec, G.V. & Wightman, R.M. (1997) Real-time measurement of electrically evoked extracellular dopamine in the striatum of freely moving rats. *J Neurochem*, 68, 152-161.
- Garris, P.A., Ciolkowski, E.L. & Wightman, R.M. (1994) Heterogeneity of evoked dopamine overflow within the striatal and striatoamygdaloid regions. *Neuroscience*, 59, 417-427.
- Heien, M.L., Phillips, P.E., Stuber, G.D., Seipel, A.T. & Wightman, R.M. (2003) Overoxidation of carbon-fiber microelectrodes enhances dopamine adsorption and increases sensitivity. *Analyst*, 128, 1413-1419.
- Janezic, S., Threlfell, S., Dodson, P.D., Dowie, M.J., Taylor, T.N., Potgieter, D., Parkkinen, L., Senior, S.L., Anwar, S., Ryan, B., Deltheil, T., Kosillo, P., Cioroch, M., Wagner, K., Ansorge, O., Bannerman, D.M., Bolam, J.P., Magill, P.J., Cragg, S.J. & Wade-Martins, R. (2013) Deficits in dopaminergic transmission precede neuron loss and dysfunction in a new Parkinson model. *Proc Natl Acad Sci U S A*, 110, E4016-4025.
- Keithley, R.B., Takmakov, P., Bucher, E.S., Belle, A.M., Owesson-White, C.A., Park, J. & Wightman, R.M. (2011) Higher sensitivity dopamine measurements with faster-scan cyclic voltammetry. *Anal Chem*, 83, 3563-3571.
- Kruk, Z.L., Cheeta, S., Milla, J., Muscat, R., Williams, J.E. & Willner, P. (1998) Real time measurement of stimulated dopamine release in the conscious rat using fast cyclic voltammetry: dopamine release is not observed during intracranial self stimulation. *J Neurosci Methods*, 79, 9-19.
- Lohr, K.M., Bernstein, A.I., Stout, K.A., Dunn, A.R., Lazo, C.R., Alter, S.P., Wang, M., Li, Y., Fan, X., Hess, E.J., Yi, H., Vecchio, L.M., Goldstein, D.S., Guillot, T.S., Salahpour, A. & Miller, G.W. (2014) Increased vesicular monoamine transporter enhances dopamine release and opposes Parkinson disease-related neurodegeneration in vivo. *Proc Natl Acad Sci U S A*, 111, 9977-9982.
- McElligott, Z.A., Fox, M.E., Walsh, P.L., Urban, D.J., Ferrel, M.S., Roth, B.L. & Wightman, R.M. (2013) Noradrenergic synaptic function in the bed nucleus of the stria terminalis varies in animal models of anxiety and addiction. *Neuropsychopharmacology*, 38, 1665-1673.
- Park, J., Aragona, B.J., Kile, B.M., Carelli, R.M. & Wightman, R.M. (2010) In vivo voltammetric monitoring of catecholamine release in subterritories of the nucleus accumbens shell. *Neuroscience*, 169, 132-142.

- Park, J., Bucher, E.S., Fontillas, K., Owesson-White, C., Ariansen, J.L., Carelli, R.M. & Wightman, R.M. (2013) Opposing catecholamine changes in the bed nucleus of the stria terminalis during intracranial self-stimulation and its extinction. *Biol Psychiatry*, 74, 69-76.
- Robinson, D.L., Hermans, A., Seipel, A.T. & Wightman, R.M. (2008) Monitoring rapid chemical communication in the brain. *Chem Rev*, 108, 2554-2584.
- Robinson, D.L., Zitzman, D.L., Smith, K.J. & Spear, L.P. (2011) Fast dopamine release events in the nucleus accumbens of early adolescent rats. *Neuroscience*, 176, 296-307.
- Schultz, W. (2013) Updating dopamine reward signals. *Curr Opin Neurobiol*, 23, 229-238.
- Takmakov, P., Zachek, M.K., Keithley, R.B., Walsh, P.L., Donley, C., McCarty, G.S. & Wightman, R.M. (2010) Carbon microelectrodes with a renewable surface. *Anal Chem*, 82, 2020-2028.
- Venton, B.J., Troyer, K.P. & Wightman, R.M. (2002) Response times of carbon fiber microelectrodes to dynamic changes in catecholamine concentration. *Anal Chem*, 74, 539-546.
- Wheeler, R.A., Aragona, B.J., Fuhrmann, K.A., Jones, J.L., Day, J.J., Cacciapaglia, F., Wightman, R.M. & Carelli, R.M. (2011) Cocaine cues drive opposing context-dependent shifts in reward processing and emotional state. *Biol Psychiatry*, 69, 1067-1074.
- Wightman, R.M., Heien, M.L., Wassum, K.M., Sombers, L.A., Aragona, B.J., Khan, A.S., Ariansen, J.L., Cheer, J.F., Phillips, P.E. & Carelli, R.M. (2007) Dopamine release is heterogeneous within microenvironments of the rat nucleus accumbens. *Eur J Neurosci*, 26, 2046-2054.
- Willuhn, I., Wanat, M.J., Clark, J.J. & Phillips, P.E. (2010) Dopamine signaling in the nucleus accumbens of animals self-administering drugs of abuse. *Curr Top Behav Neurosci*, 3, 29-71.